

Manufacturing of Low-Dosed Pharmaceutical Filament Sticks and its Analytical Challenges

Inaugural-Dissertation

zur Erlangung des Doktorgrades der Mathematisch-Naturwissenschaftlichen Fakultät der
Heinrich-Heine-Universität Düsseldorf

vorgelegt von

Rebecca Chamberlain

geb. Peters

aus Essen

Düsseldorf, März 2024

Aus dem Institut für Pharmazeutische Technologie und Biopharmazie
der Heinrich-Heine-Universität Düsseldorf

Gedruckt mit der Genehmigung der
Mathematisch-Naturwissenschaftlichen Fakultät der
Heinrich-Heine-Universität Düsseldorf

Berichterstatter:

1. Prof. Dr. Jörg Breitzkreutz

2. Jun.- Prof. Dr. Michael Hacker

Tag der mündlichen Prüfung: 13.03.2024

Für meine liebste Familie

Table of contents

TABLE OF CONTENTS	I
LIST OF ABBREVIATIONS	II
PUBLICATIONS	III
1 Introduction	1
1.1 Hot-melt Extrusion	1
1.1.1 Processing considerations and critical process parameters (CPPs)	2
1.1.1.1 Material properties	2
1.1.1.2 Process parameters	6
1.1.1.3 CPPs for the process-formulation interplay	9
1.1.2 Process and product analyzers	11
1.1.3 Application in therapeutics	13
1.1.4 Fused deposition modeling (FDM) three-dimensional (3d) printing and alternative manufacturing processes	15
1.2 Characterization and Quality Control of CQA of Pharmaceutical Filaments	17
1.2.1 Diameter of filaments	18
1.2.2 Content uniformity in filaments	19
1.2.3 Color of filaments	22
1.2.4 Intermediate filament sticks	23
1.3 The Potential of 3d Printing for the Pharmacotherapy of Parkinson Patients	25
1.3.1 Recent drug therapy of Morbus Parkinson	25
1.3.2 Adaption of administration route, dosing, and dosing intervals	27
1.3.3 Combination drug product	28
1.3.4 Relevance of 3d printed medicine for large- and small-scale production	30
1.3.5 Market authorization status for 3d printed medicines	32
1.4 Aims of the Thesis / Outline of the Thesis	34
1.5 References	37
2 Filament Intermediates for Pharmaceutical FDM 3d Printing	53
2.1 Quality of FDM 3d Printed Medicines for Pediatrics: Considerations for Formulation Development, Filament Extrusion, Printing Process and Printer Design	53
2.2 Patent: Filament Cutting Device	74
3 Characterization and Quality Control of Drug-loaded Filaments	87
3.1 Precise Dosing of Pramipexole for Low-Dosed Filament Production by Hot Melt Extrusion Applying Various Feeding Methods	87
3.2 Drug Content Determination of Low-Dosed Hot-Melt Extruded Filaments using Raman Spectroscopy	105
3.3 Introducing Fiber-Assisted Colorimetric Measurements as a Quality Control Tool of Hot Melt Extruded Filaments	107
4 Development and Characterization of Combination Drug Product	123
4.1 Dose-independent drug release from 3d printed oral medicines for patient-specific dosing to improve therapy safety	144
4.2 Embedding a Sensitive Liquid-Core Waveguide UV Detector into an HPLC-UV System for Simultaneous Quantification of Differently Dosed APIs during Drug Release	130
4.3 3d Printed Mini-Floating-Polypill for Parkinson's Disease: Combination of Levodopa, Benserazide, and Pramipexole in Various Dosing for Personalized Therapy	145
5 Summary and Outlook	168
6 Acknowledgements / Danksagung	172
7 Eidesstattliche Erklärung	174

List of abbreviations

Abbreviation	
3d	<i>Three-dimensional</i>
API(s)	<i>Active pharmaceutical ingredient(s)</i>
AV	<i>Acceptance value</i>
BCS	<i>Biopharmaceutics Classification System</i>
BMBF	<i>Federal Ministry of Education and Research</i>
CDD	<i>Charge-coupled device</i>
CIELAB	<i>Commission Internationale de l'Eclairage L*a*b*</i>
COMT	<i>Catechol-O-methyltransferase</i>
CPP(s)	<i>Critical process parameters</i>
CQA(s)	<i>Critical product quality attribute(s)</i>
CV	<i>Coefficient of variation</i>
D1	<i>Dopamine 1</i>
D2	<i>Dopamine 2</i>
DA	<i>Dopamine</i>
DDS(s)	<i>Drug delivery system(s)</i>
DSC	<i>Differential Scanning Calorimetry</i>
EMA	<i>European Medicines Agency</i>
FDA	<i>Food and Drug Administration</i>
FDM	<i>Fused Deposition Modeling</i>
HBS(s)	<i>Hydrodynamically balanced system(s)</i>
HME	<i>Hot-melt extrusion</i>
HPLC	<i>High-performance liquid chromatography</i>
IPS	<i>Idiopathic Parkinson syndrome</i>
LCM	<i>Life cycle management</i>
L/D	<i>Length to diameter</i>
LDR	<i>Long-duration response</i>
LTP	<i>Long-term potentiation</i>
MAO-B	<i>Monoamine oxidase B</i>
NCE	<i>New chemical entities</i>
PAT	<i>Process analytical technology</i>
Pharm. Eur.	<i>European Pharmacopoeia</i>
RSD	<i>Relative standard deviation</i>
SA/V	<i>Surface area to volume ratio</i>
t_g	<i>Glass transition temperature</i>
t_m	<i>Melt temperature</i>
USP	<i>United States Pharmacopeia</i>

Publications

Published manuscripts:

1) Hellen Windolf, Rebecca Chamberlain, Julian Quodbach. *"Predicting Drug Release from 3d Printed Oral Medicines Based on the Surface Area to Volume Ratio of Tablet Geometry."* *Pharmaceutics* 13(9): 1453, 2021.

- Own contribution: 8%
- RC performed extrusions and filament characteristic measurements. She provided the intermediates for 3d printing. RC reviewed the manuscript. HW wrote the manuscript.

2) Julian Quodbach, Malte Bogdahn, Jörg Breitzkreutz, Rebecca Chamberlain, Karin Eggenreich, Alessandro Giuseppe Elia, Nadine Gottschalk, Gesine Gunkel-Grabole, Lena Hoffmann, Dnyaneshwar Kapote, Thomas Kipping, Stefan Klinken, Fabian Loose, Tristan Marquetant, Hellen Windolf, Simon Geißler, Tilmann Spitz. *"Quality of FDM 3d Printed Medicines for Pediatrics: Considerations for Formulation Development, Filament Extrusion, Printing Process and Printer Design."* *Therapeutic Innovation & Regulatory Science*, 56(6): 910-928, 2022.

- Own contribution: 24%
- This review was written on the basis of an invitation by the publisher. RC performed extrusions and filament characteristic measurements. RC participated in the authorship of the chapter: *"Hot-Melt Extrusion of Intermediates for Pediatric 3d Printing"*. RC helped with the revision of the texts.

3) Rebecca Chamberlain, Hellen Windolf, Simon Geissler, Julian Quodbach, Jörg Breitzkreutz. *"Precise Dosing of Pramipexole for Low-Dosed Filament Production by Hot Melt Extrusion Applying Various Feeding Methods."* *Pharmaceutics*, 14(1): 216, 2022.

- Own contribution: 80%
- RC performed extrusions, dry granulation, filament characteristic measurements. She evaluated the data herself and provided them for the manuscript. RC wrote the manuscript. HW, SG, JQ and JB reviewed the manuscript.

4) Hellen Windolf, Rebecca Chamberlain, Julian Quodbach. *"Dose-independent Drug Release from 3d Printed Oral Medicines for Patient-specific Dosing to Improve Therapy Safety."* International Journal of Pharmaceutics, 616(9): 121555, 2022.

- Own contribution: 18%
- RC performed extrusions and filament characteristic measurements. She provided the intermediates for 3d Printing. RC reviewed the manuscript. HW wrote the manuscript.

5) Hellen Windolf, Rebecca Chamberlain, Arnold Delmotte, Julian Quodbach. *"Blind-Watermarking—Proof-of-Concept of a Novel Approach to Ensure Batch Traceability for 3d Printed Tablets."* Pharmaceutics 14(2): 432, 2022.

- Own contribution: 5%
- RC performed extrusions and filament characteristic measurements. She provided the intermediates for 3d Printing. RC reviewed the manuscript. HW wrote the manuscript.

6) Rebecca Chamberlain, Hellen Windolf, Bjoern B. Burckhardt, Jörg Breitzkreutz, Björn Fischer. *"Embedding a Sensitive Liquid-Core Waveguide UV Detector into an HPLC-UV System for Simultaneous Quantification of Differently Dosed Active Ingredients during Drug Release."* Pharmaceutics 14(3): 639, 2022.

- Own contribution: 54%
- RC performed analytical measurements, extrusions, and dissolutions. She evaluated the data herself and provided them for the manuscript. RC wrote the manuscript. HW, BBB, JB and BF reviewed the manuscript.

7) Rebecca Chamberlain, Hellen Windolf, Jörg Breitzkreutz. *„Arzneizubereitungen für die Therapie des idiopathischen Parkinson-Syndroms“* Pharmakon 10(3): 216-226, 2022.

- Own contribution: 45%
- This review was written on the basis of an invitation by the publisher. RC and HW conducted the literature research. RC, HW and JB determined the structure

of the article. RC and HW wrote the manuscript and JB reviewed the manuscript.

8) Hellen Windolf, Rebecca Chamberlain, Jörg Breitzkreutz, Julian Quodbach. " *3d Printed Mini-Floating-Polypill for Parkinson's Disease: Combination of Levodopa, Benserazide, and Pramipexole in Various Dosing for Personalized Therapy Quality of FDM 3d Printed Medicines for Pediatrics: Considerations for Formulation Development, Filament Extrusion, Printing Process and Printer Design.*" *Pharmaceutics* 14(5): 931, 2022.

- Own contribution: 36%
- RC performed extrusions and filament characteristic measurements. She provided the intermediates for 3d Printing. RC reviewed the manuscript. HW wrote the manuscript.

9) Rebecca Chamberlain, Eirini Mangiorou, Björn Fischer. " *Introducing Fiber-Assisted Colorimetric Measurements as a Quality Control Tool of Hot Melt Extruded Filaments.*" *Pharmaceutics* 14(5): 1055, 2022.

- Own contribution: 80%
- RC performed extrusion runs. She evaluated the data herself and provided it for the manuscript. RC and EM wrote the manuscript. BF reviewed the manuscript.

10) Rebecca Chamberlain, Jörg Breitzkreutz, Björn Fischer. " *Drug Content Determination of Low-Dosed Hot-Melt Extruded Filaments using Raman Spectroscopy.*" *Pharmaceutical Development and Technology*, submitted on 30.10.2023, in review.

- Own contribution: 80 %
- RC performed analytical measurements and extrusions. She evaluated the data herself and provided it for the manuscript. RC wrote the manuscript. JB and BF reviewed the manuscript.

11) Rebecca Chamberlain, Stefan Stich, Correl Spöringer, Jörg Breitzkreutz. Patent application. Submitted to German Patent and Trademark Office: D-2021/756.

- Own contribution: 40%

- RC has identified the need for an optimized cutting unit to be able to cut filament sticks. She performed preliminary experiments. She worked on a prototype of this invention, which was optimized by SS and CS in the fine mechanics department of the university. RC wrote the submission for the patent application and provided support in the writing of the filing document. JB reviewed the manuscript.

Oral presentations:

- R. Chamberlain (Presenter), H. Windolf, L. Hoffmann, N. Gottschalk. *"Polyprint-vom Polymer zur 3d gedruckten Arzneiform."*
First PhD students and post-doc conference of the program „ProMatLeben“, September 3 - 4, 2019, Berlin, Germany

Poster presentations:

- R. Chamberlain (Presenter), H. Windolf, L. Hoffmann, A. Michel, S. Klinken, J. Breitreutz, J. Quodbach. *"Prozessoptimierung der Filamentherstellung mittels Schmelzextrusion mit einem niedrigdosierten Arzneistoff."*
First PhD students and post-doc conference of the program „ProMatLeben“, September 3 - 4, 2019, Berlin, Germany
- R. Chamberlain (Presenter), H. Windolf, B. Fischer, J. Breitreutz, J. Quodbach. *"Raman microscopy of low-dose filaments for 3d printing."* 12th World Meeting on Pharmaceutics, Biopharmaceutics and Pharmaceutical Technology (PBP), May 11-14, 2021, online
- H. Windolf, R. Chamberlain, J. Breitreutz, J. Quodbach. *"Vergleich der Druckpräzision von zwei 3d Druckern."* First PhD students and post-doc conference of the program „ProMatLeben“, September 3-4, 2019, Berlin, Germany
- H. Windolf, R. Chamberlain, J. Quodbach. *"3d gedruckte orale Darreichungsformen mit dosisunabhängiger Freisetzung."*
Second PhD students and post-doc conference of the program „ProMatLeben“, May 18-19, 2021, online, (2nd place poster award)

- H. Windolf, R. Chamberlain, J. Quodbach. “*Dose-independent drug release from 3d printed oral dosage forms.*”
12th World Meeting on Pharmaceutics, Biopharmaceutics and Pharmaceutical Technology (PBP), May 11-14, 2021, online

1 Introduction

1.1 Hot-melt Extrusion

Research and development in the pharmaceutical industry have advanced hot-melt extrusion (HME) as an alternative "platform technology" for the development of solid dosage forms [1]. With the help of the HME process, the active pharmaceutical ingredient is embedded in a carrier system and is fabricated into pharmaceutical dosage forms, such as (intermediate) granules, tablets, implants, and transdermal/ transmucosal/ transungual drug delivery systems (DDSs). The selection of raw material and the instrument process-formulation interplay are of interest since critical quality attributes (CQAs) of hot melt extruded material are directly dependent on both formulation and manufacturing process [2]. To produce an extrudate, powders or granules are added to the extruder barrel via powder feeder systems (volumetrically or gravimetrically) and liquid excipients by liquid feeders (pump systems). The extruder barrel is recessed for the screw(s), which are inserted in the barrel and are driven by the engine. The screws may orient on varying configuration depending on the desired level of sheer and the speed of mixing or operation. The rotation of the screws conveys the metered material to the die. The heating of the barrel takes place electrically: in some extruders, heating takes place only from below, in other extruders around the entire barrel shell. Heat transfer occurs by conduction as the barrel material is heated and transfers the energy into the material being processed. In addition, the conveying of the material through the screw causes friction of the material, which generates energy. A constant barrel temperature is ensured by a cooling unit usually driven by water cooling. The molten material is mixed and conveyed to the die. A die plate is attached to the end of the screw, from which the material is pushed through and leaves the extruder barrel. To avoid air entrapment during melting, the barrel can be opened at certain positions, or a vacuum pump can be connected for degassing/venting. If the molten mass is not continuously fed through the die, the flow can be regulated by adding a melt pump between the barrel and the die. After the melt exits the die, the extrudate can be shaped and cut. Cooling of the extrudate takes place either passively at room temperature or actively by water- or air-cooling systems. Consequently, the subprocesses of the manufacturing of extrudates via HME include material feeding, conveying, melting, and mixing, melt conveying, degassing/venting, pumping, shaping, cutting, and cooling [1].

A schematic representation of a typical pharmaceutical twin-screw extrusion process is illustrated in Fig. 1.

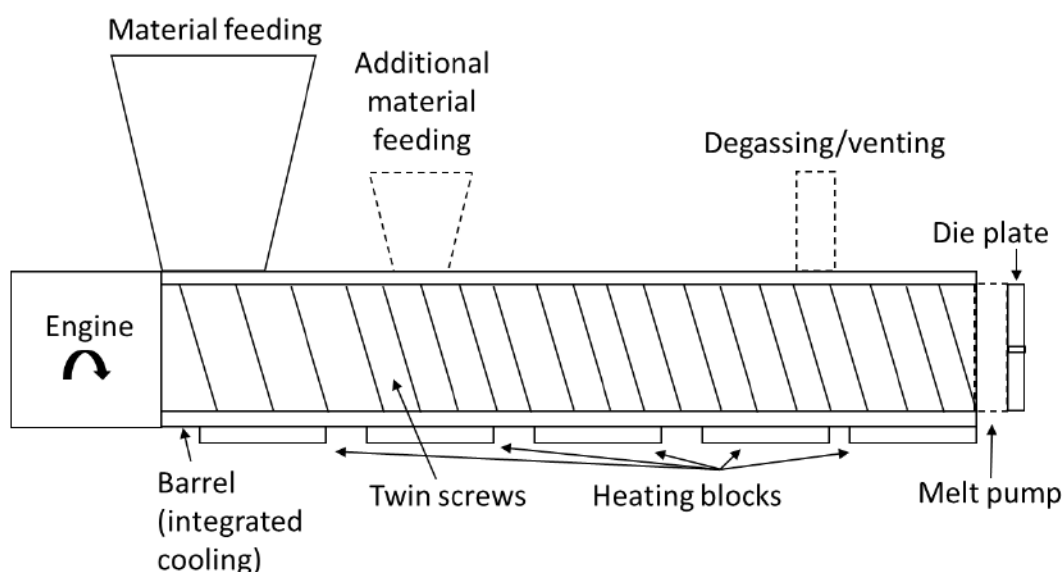


Fig 1. Schematic representation of a typical pharmaceutical twin-screw extrusion set-up (dashed elements are optional and not mandatory for the assembly of the extruder).

1.1.1 Processing considerations and critical process parameters (CPPs)

When considering HME as the manufacturing technique for DDS, the relevant material properties, adjustable/resulting extrusion parameters, and CPPs for the process-formulation interplay must be evaluated since critical product quality attributes (CQA) are directly dependent on all three categories [3].

1.1.1.1 Material properties

HME for manufacturing of DDS may involve the use of active pharmaceutical ingredients (APIs), matrix carriers, bulking agents, plasticizers, lubricants, processing aids, release modifiers, disintegration aids, antioxidants, and other miscellaneous additives [2,4]. All these materials must be approved by authorities (e.g., Food and Drug Administration (FDA), European Medicines Agency (EMA)) and must meet pharmaceutical criteria defined by the monographs in the relevant pharmacopeias (United States Pharmacopeia (USP), European Pharmacopoeia (Pharm. Eur.)) [5]. International Conference on Harmonization-guidelines should be consulted to meet the requirements for a pharmaceutical DDS [6].

The following material properties are important for the extrusion process:

- **Thermal stability**

Thermal stability of the API(s) and the excipient(s) is a prerequisite for the HME process. The decomposition temperature must not be exceeded to avoid degradation products [7]. This includes depolymerization, chain scission, elimination of water, elimination of functional groups, pyrolysis, pH change, interactions between API and excipients and other thermal degradation processes [8,9]. Since the application of HME involves heat and shear stress to generate a melt, it must be ensured that the efficacy and safety of all materials remain unchanged [10].

- **Melt viscosity**

The melt viscosity [Pa·s] of a polymer at a given temperature is the rate at which chains can move relative to each other [11]. This is controlled by the ease of rotation of the backbone bonds and the degree of entanglement, which depends on the chain length (molar mass), chain flexibility and interaction between functional groups. For a specific polymer, the melt viscosity is considerably dependent on the weight average molar mass. The higher the molar mass, the greater the entanglements and the melt viscosity. Chain branching also influences the melt viscosity. Generally, the greater the amount of long chain branching at constant weight average molar mass, the lower the melt viscosity [12].

The dependence of the polymer melt viscosity on temperature at a given shear rate follows the Arrhenius equation (Eq. 1) [13]:

$$\eta = K' \cdot e^{\frac{E_a}{R \cdot T}} \quad (1)$$

In Equation 1, η is the melt viscosity, K' represents a constant depending on the structure and the molecular weight of the polymer; E_a is the activation energy, R is the gas constant and T is the temperature. As a thumb of rule, HME is carried out at temperatures of 20-40°C above glass transition temperature (t_g) of the polymer carrier system [14]. Since the temperature T is not only generated by heat conduction of the barrel from electrical bands but also generated from shearing of the melt, the energy of the shear must be considered when analyzing additional mechanical energy applied to the melt per unit mass of processed material as specific mechanical energy [15]. The process of transforming mechanical energy from shearing into thermal energy is called viscous heat generation.

The generated energy per unit volume (E) due to viscous heat dissipation follows Equation 2 [24]:

$$E = m \cdot \gamma^{n+1} \quad (2)$$

In Equation 2, m is a material constant, γ is the shear rate and n is the power law constant. The combination of the thermal energy and energy evoked by shearing influences the melt viscosity. The operating extrusion range for melt viscosity of the polymer is between 800 and 10,000 Pa·s [16]. For processability, the melt viscosity of a polymer must not be too high to avoid an increase of the torque resulting in an overloading of the engine and the screw since the torque is directly proportional to melt viscosity [17]. If the melt viscosity is too low, the processing to the desired DDS is not possible [18].

If the required processing energy cannot be provided, for example, because the degradation temperature is exceeded, additives (plasticizer) can lower the melt viscosity and therefore lower the required energy input [19]. Plasticization of the polymer is generally attributed to the inter-molecular secondary valence forces between the plasticizer and the polymer. Plasticizers can decrease the t_g and the melt viscosity of a polymer by increasing the free volume between polymer chains. Solid plasticizers are recommended because they exhibit a lower degree of mobility of the polymer and provide greater stability [20]. The miscibility of the plasticizer with the polymer is guaranteed if there is only one t_g noticeable in the thermogram of the blend obtained by differential scanning calorimetry (DSC) [21].

- **Viscoelasticity**

Viscoelasticity is the property of materials that implicates elastic and viscous behavior when undergoing deformation [22]. Exiting the extrusion die, the diameter increase of a molten thermoplastic extrudate shows viscoelastic behavior of different magnitude [23]. The swelling phenomenon at different temperatures is correlated with shear stress in the die. Not only the diameter of the die, but also the length of the die has an impact on the viscoelastic behavior of the thermoplastic carrier as it represents a flow through a capillary. The ratio of the extrudate diameter to the orifice diameter represents the swelling index and can be calculated for the melt [24]. The ovality of the extrudate is also dependent on the melt viscoelasticity [25].

- **Solid state properties**

All materials can undergo a change in the physical properties through the HME process [26]. Liquid components can either evaporate or vaporize, solidify, or remain as liquid components in the filament [1,26]. The carrier hardens while cooling and represents the matrix of the DDS. Partially crystalline polymers lead to the disadvantage that a high process temperature must be applied since the crystalline regions are immobile until the melt temperature (T_m) is reached and may lead to an increase of the torque. The polymer matrix might have changed its solid property during/after melting (Fig. 2A), which can influence for instance the API solubility in the polymer or the drug release from the polymer matrix [57,28]. The incorporated API (liquid or solid fed) may also change its properties compared to the starting material, whose solid-state property, in some cases, must be preserved by additive stabilizers [29]. This is particularly decisive for the drug release, but may also influence e.g., melt viscosity [30], viscoelastic behavior [31], and the color of the melt [32]. As mentioned above, the API can remain in its initial form (crystalline, amorphous) or change its solid-state property. In Fig. 2B, the three types of solid dispersions are described namely the amorphous solid solution, the dispersed amorphous API in the polymer and the dispersed crystalline API in the polymer matrix.

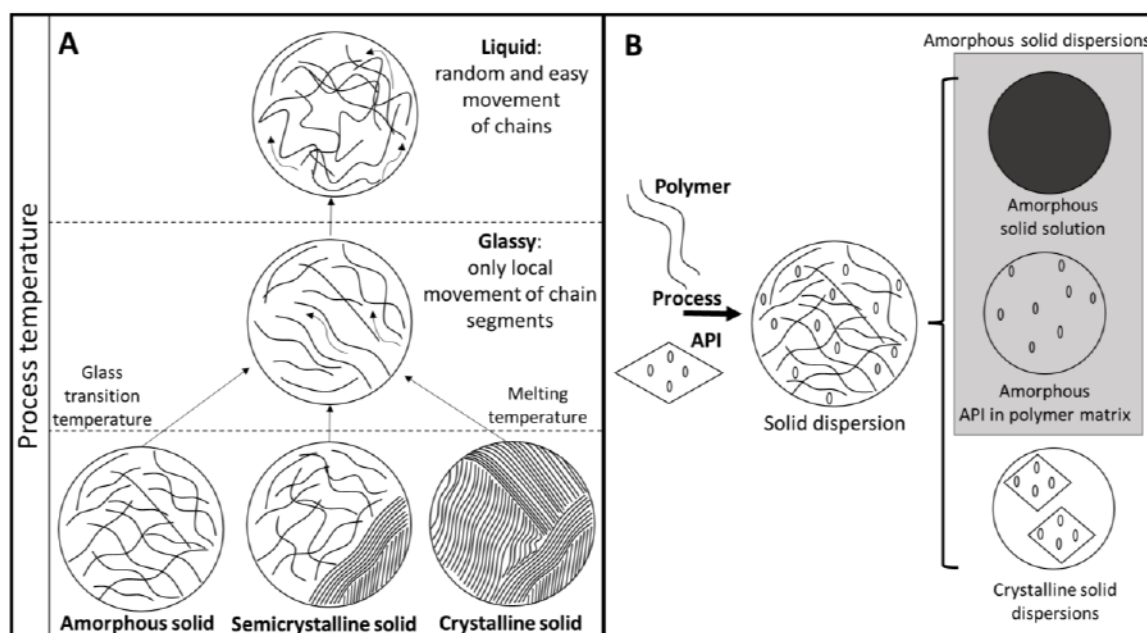


Fig 2. Solid state properties of the polymer (A) and the API within the polymer matrix (B) during processing (adapted from [27]).

If the t_m is exceeded, the API will lose its crystalline structure. If the temperature is again below t_m , the API stays amorphous or recrystallizes. During recrystallization, a different polymorph of the API might be formed.

Even if the process temperature is below t_m , it is possible that the API dissolves in the matrix without reaching the melting range [33]. Especially in case of Biopharmaceutics Classification System (BCS) class II and IV drug substances (see 1.1.3), it is important that the API is completely dissolved or amorphous dispersed in the polymer matrix [34]. The solid solution capacity is the maximum concentration of dissolved API in a matrix [1]. Lipophilicity, solubility parameter, hydrogen bonds and the interactions between functional groups of the polymer and the API determine the degree to which the API dissolves in the polymer [1, 35-37]. To verify the solid state of the API, DSC and X-ray crystallography can be applied to demonstrate solid state properties, considering the limits of quantification [38]. Since the amorphous state is thermodynamically unstable, (re)crystallization may occur [39]. Thereby, the original crystalline structure is not always formed, but another polymorph may be generated instead, unintentionally or intentionally. Targeted co-crystallization can occur if at least two APIs are processed which, under certain conditions, form a unique crystalline structure with their new properties [40]. The API tends to recrystallize if the water solubility is low not only in the polymer matrix, but also in gastric or intestinal fluids. The solubilization capacity of the carrier is essential to retain the dissolved state of the API in physiological environment [41].

1.1.1.2 Process parameters

The manufacturing process of a DDS by HME requires a high apparatus complexity where many process parameters can be adjusted [42]. However, some parameters cannot be considered separately from each other [1]. To set up an extrusion process, at least one screw is required in a closed barrel, where the end is limited by a die [43]. Openings of the barrel are only intended for feeding (liquid and solid), venting (degassing port or connection of a vacuum pump) and inline probes to prevent the melt from leaking out of the barrel [44]. The settings of the respective process components are explained below:

- **Screws**

The number of screws can vary between one and two. When operating a twin-screw extruder, the two screws are either co-rotating or counter-rotating [45]. In addition, the

length and the diameter of the screw(s) varies depending on extruder model. The length to diameter (L/D) ratio has been specified in order to simplify up- and down-scaling [46].

- **Screw configuration**

On a shaft, various screw elements are arranged in a certain manner, which can either be changed or are fixed in place. The screw configuration is essentially responsible for the quality of the product and effects many extrusion parameters. The mixing, the kneading, the dwell time of the material, the degree of barrel filling, the conveying of the material, the pressure in the barrel and especially at the die is among other factors influenced by the screw configuration [4,46].

- **Screw speed**

The screws are driven by a engine and the screw rotation speed can be set between 0-100%. Depending on the engine and the extruder, the screw speed varies, but is usually set between 0-300 rpm for HME. The throughput and the residence time of the material are influenced by the screw speed [47]. Furthermore, the shear stress is increased at high speed. At constant feeding rate, the barrel fill level is reduced by increased screw speed [48]. The screw speed is displayed in rpm.

- **Feed rate**

During extrusion, both solids and liquids are fed into the barrel by a predefined number of feeders at varying positions [49]. In a simple feeding process, a powder blend is fed from a hopper with the help of rotating screws into the extruder barrel. A distinguished difference is whether the powder falls into the barrel due to gravity, or whether the screws guide the powder directly to the screws in the barrel via fed force. The feeder can operate volumetrically (for blends with good flowability) or gravimetrically. Gravimetric feeders operate with transducers that measure loss in weight and generate, by adjusting the screw speed, constant flow rates [50]. The extrusion can be performed in flood-fed mode, where the screw beneath the feeder is filled. In starve-fed mode, the screw is not fully filled [51]. Typically, the unit of the feed rate is g/min or kg/h.

- **Hot-melt die**

Material is transported from the barrel through a die. The die is attached to the end of the barrel and represents the exit point of the melt. The die plate can be actively heated or

passively heated by the barrel. The die can vary in the number of exit holes, geometry, width, and length. Usually, probes are installed in the die to monitor the pressure and the temperature [52].

- **Venting**

To be able to remove gases that are produced during extrusion from material inside the barrel, a venting port can be installed in the barrel. To realize a more efficient degassing, for example of water vapor, a vacuum pump can be connected [44]. In most cases, the largest possible surface area of the melt is created by adjusting the screw configuration underneath the venting port with long pitch helices [49]. To prevent the melt from being vacuumed in the tubes to the pump, an adapter piece can be installed. Nevertheless, the pump needs to be started up slowly to prevent material from being drawn into the tubes of the vacuum pump, which can lead to clogging.

- **Shaping or cutting**

In the further processing of the melt, there are different ways of transforming the melt into the desired shape at different temperatures (Fig. 3) [53]. In the case of direct shaping, a distinction is made between continuous shaping with the help of calendering, where the melt is forced into cavities located in rolls after exiting the die and semicontinuous injection molding, where the melt is forced by forward moving of the screw (often single screw extrusion) through a gate into the cavity [54,55]. After shaping/molding, the finished drug products are cooled under defined conditions [56]. These techniques are applied to produce among other dosage forms implants and intravaginal inserts [57].

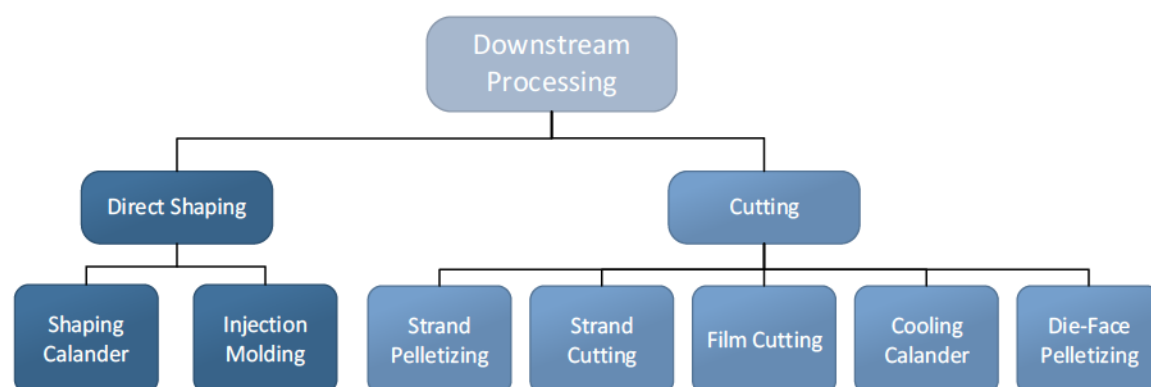


Fig 3. Downstream processing of melts and extrudates after exiting the barrel (adapted from [54]).

To cut the melt instead of shaping, cutting devices are chosen that either perform a hot cut (“face-cut” or “die-face”) directly at the die [58] or the cutting is carried out after the melt has cooled down [59]. For both hot and cold cutting, guillotine type knife, rotating knives or rollers with sharp ends are commonly applied [60-62].

- **Cooling of the melt**

The melt is cooled after it has left the die. Active cooling can take place by means of compressed air or, in the case of water-insoluble matrices, using a water bath. The melt can also be cooled by the ambient temperature [54].

- **Conveying**

For the further conveying of produced strands, a variety of downstream equipment can be used. Conveyor rolls that are lined up one above the other and/or one behind the other are often utilized [63]. In addition to conveyor rolls, conveyor belts are also used, which are varied in width and length. Here, it is important to ensure adhesion to the conveyor so that the speed-determining step is not determined by the ejection of the melt from the extruder, but by the conveying.

1.1.1.3 CPPs for the process-formulation interplay

- **Controllable CPPs**

Early development and late-stage optimization are both governed by the often complex process-formulation interplay. Changes in the formulation may change process parameters or lead to the fact that an adjustment of the process is possible or necessary, and inversely [1]. During extrusion, the screw speed can be adapted easily. The screw configuration is defined before the extrusion process starts and may not be changed during extrusion. The feeding type (pre-blend or multiple feeds; liquid or solid feeding) is selectable but might also not be changed during extrusion. The feed rate and pulsations in feeding rate are altered during extrusion. The formulation is selected before extrusion. Especially when using multiple feeds, the ratio might be varied. The barrel temperature can be adjusted during extrusion through heating or cooling.

- **Resulting CPPs**

The mass flow of the melt through the extruder is a resulting CPP. The barrel fill level and the residence time distribution of the material are influenced through the formulation, the screw set-up, the feeding set-up, and the temperature. These parameters also impact the temperature and the pressure at the die. The thermal and mechanical energy imparted into the formulation are also resulting CPPs. The homogeneity of the melt and the dissolution behavior of API in the matrix are resulting from complex process-formulation interplay.

- **Interplay of controllable and resulting CPPs**

Polymers with low melt viscosity and high thermal conductivity experience a more efficient melting process [64]. Changes in the screw configuration are necessary to improve the melting process of the excipients, homogeneity of the melt and mass flow of the melt through the extruder. Feed rate, feeding type (preblend or multiple feeds), and pulsations in feeding rate, influence the barrel fill level, which in turn affects the homogeneity, thermal and mechanical energy imparted into the formulation [65].

Through the addition of suitable plasticizer, the t_g of the polymer carrier might be lowered to decrease the melt viscosity [19]. The dissolved API can also act as a plasticizer in the polymer matrix with the benefit of a lower melt viscosity [30]. Modularity in screw configuration also affects mechanical shear of the material. Applying more shear to the polymer through the adaption of the screw configuration and the screw speed result in further reduction of the viscosity enhancing diffusivity and dissolution rate of the drug in the carrier. The barrel set temperature, screw speed and residence time distribution may affect dissolution behavior of API in the matrix, which is in favor if the API is poorly soluble [66].

The lower t_g of the carrier also has the effect that the barrel set temperature can be lowered if high process temperature is critical for the degradation of API [67]. In this case, not only the temperature shall be lowered, but also the duration of thermal stress shall be shortened. By adaption of the feed rate, the screw speed, and the screw configuration the average residence time can be shortened, and the conveying of the melt to the die can be optimized so that the total residence time is as short as possible [68]. The balance of energy input and heat history result in acceptable extrudate quality or with the extreme combination of these two variables, result in either degradation or inhomogeneous material [69].

To keep the experimental effort as low as possible, a simulation of the extrusion process is desirable. Ludovic® and XimeX®-TSE are simulation software to optimize the co-rotating twin screw extrusion process by proposing an in-dept analysis of the material. While Ludovic® shows global results (e.g., torque, power consumption), 1D/2D thermomechanical results of the distribution along the screw and the residence time distribution of the material, XimeX®-TSE shows all the above results and displays the thermomechanical results in 3d maps [70].

The aim of the experimental trials and the software simulation are necessary to characterize the direct and measurable impact of potential CPPs on product quality. In addition, it is necessary to perform a scale up from lab to commercial scale. Based on the material properties and processing considerations, one of the four scale-up strategies can be applied: volumetric, power, heat transfer or die scale-up. With all four methods, it is important that the product quality is maintained [68]. In its report “Pharmaceutical Quality for the 21st Century: A Risk-Based Approach”, the FDA urges pharmaceutical companies for quality by design concept to be built into the development of a product with an understanding of the product and the processes by which it is developed and manufactured, as well as an understanding of the risks associated with manufacturing the product and how those risks can best be mitigated [72]. This includes a risk assessment on input parameters as well as defining a design space of potential CPPs.

To define the important quality attributes of the product, to realize the scale-up procedure, and to identify the CPPs, supporting analytical methods are needed that can be applied during or after the manufacturing process.

1.1.2 Process and product analyzers

Process analytical technology (PAT) can measure critical process parameters with the aim to analyze, control, and design manufacturing processes. Regarding the set-up of PAT, there are four different ways in which the tool can be installed:

- **In-line**

Analysis is performed during the process without diversion of material.

- **On-line**

Analysis is performed during the process on a diverted material, which is afterwards reunited with the remaining product.

- **At-line**

Analysis is performed in proximity in time and space to the process after removal of material from the process.

- **Off-line**

Analysis is performed after removal of material from the process with no proximity (neither time nor space) to the process.

The positioning of PAT in the extrusion process for measuring CPPs during processing and after sampling is illustrated in Fig. 4.

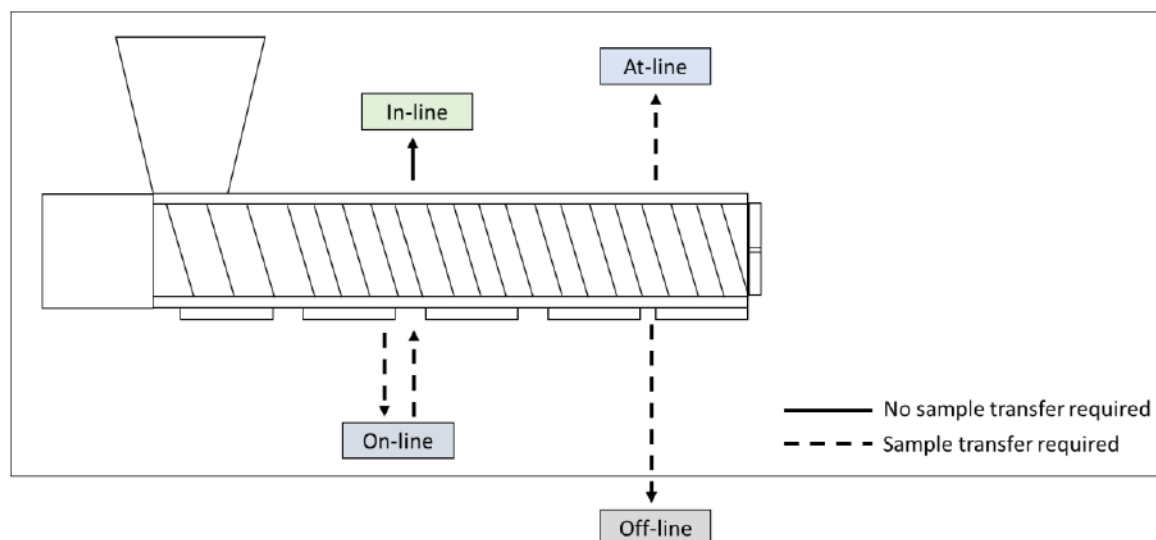


Fig 4. Positioning of PAT in the extrusion process for measuring critical process parameters during extrusion and after sampling (adapted from Hitzer et al.[72]).

Process analyzers can either be part of the machine itself, be integrated of a device connected to the machine, or detect signals with the help of a probe [73]. Off-line analytical methods are not suitable for rapid intervention or changes in the process. The results are only available after manufacturing and therefore prevent changes to the ongoing process [74]. Instead, in-line and on-line methods can be incorporated in a control strategy and are favored in a complex extrusion set up [75].

The melt can also be analyzed during the extrusion process with the help of probes. For this purpose, optical windows are installed in the barrel or probes are inserted into the barrel [76]. During implementation it is important to ensure that no material leaves the barrel or collects at an inlet, and that screw rotation is not impaired. Moreover, no material may accumulate at the probe so that the analysis is interfered. During analysis, the influence of the temperature on the result must always be considered [77].

After discharge, the intermediate/ drug product can be analyzed. Probes, cameras, and laser modules are applied at this stage. Often the intermediate/drug product is analyzed off-line after cooling [78].

1.1.3 Application in therapeutics

Since decades, HME has been used in pharmaceutical technology as an essential platform for drug delivery technology. In early development, the focus of processing APIs with HME is solubility and therefore bioavailability enhancement of new chemical entities (NCEs). Solubility enhancement minimizes the risk that APIs that are poorly soluble under physiological conditions do not reach the pharmacologically effective concentration. These APIs would not advance beyond the early stage of development. Poorly soluble APIs with high bioavailability in the dissolved state are categorized into class II of BCS and are referred to as BSC class II substances (Fig. 5). BCS class IV substances are the worst-case scenario for NCEs since they demonstrate both low solubility and low bioavailability.

When the highest dose strength of a drug is soluble in 250 mL aqueous medium (pH 1.0 to pH 7.5), the API is considered highly soluble [74]. All APIs used in this thesis are categorized as BSC class I or II substances [75-78]. In case of permeability, the API is considered highly permeable if 90% or more of the administered dose is absorbed [79].

In late-stage pharmaceutical product development, HME is used to keep already commercialized drug products sufficiently attractive for the market. Known as life cycle management (LCM), the process is particularly pursued for blockbuster drug substances, where more differentiated formulations can help distinguish one drug from other offerings in the same drug class or for the same disease [80].

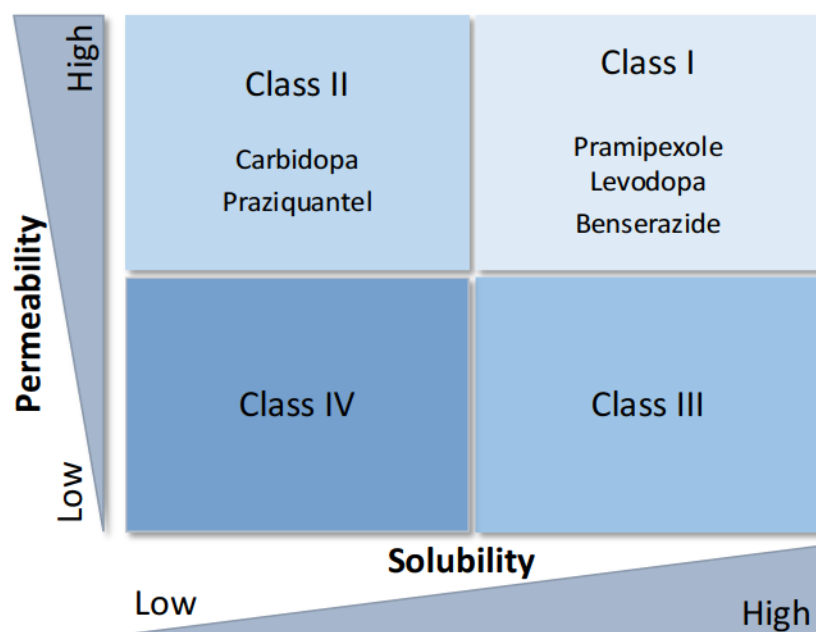


Fig 5. BCS modified with APIs used in this thesis according to Kawabata [73].

This process includes reformulation or formulation changes to improve the therapeutic benefit of the drug product and the compliance of patients [81]. LCM of an NCE can be employed to maintain competitive advantages after patent expiry. Therefore, patented line extensions though LCM can enable a brand to retain a higher share of the genericized market [80].

With the help of HME technology, a variety of dosage forms can be manufactured including pellets [82,83], granules [84,85], tablets compressed with melt-granules [86], three-dimensional (3d) printed DDS [87,88], oral fast dissolving systems with melt-granules [85], transdermal DDS [89,90], transmucosal DDS [91], vaginal DDS [92] and implants [93]. The production of all DDS involves that the API(s) and excipient(s) are processed by extrusion but differs in the choice of the die (geometry, diameter) and further processing downstream equipment [19]. Next to the potential effective improvement of the bioavailability through enhancement of the solubility of poorly soluble drugs, the DDSs profit from a potential improvement of stability due to formation of a solid dispersion or a solid solution [94], from modification of drug release [95], from taste masking of the API [96] and from abuse deterrent [97]. Since the manufacturing process is a continuous process, guarantees scale-up feasibility, operates solvent-free and offers the advantage of shaped delivery (e.g., strains, granules, films), the process is widely used in industry to manufacture drug products [98-101].

To produce filament geometries for the manufacturing of implants, vaginal rings, and intermediates, the generated melt is pressed through a die by conveying of screw(s) and the exiting strand is then cut into the desired length (in the hot stage or after cooling) [102].

1.1.4 Fused deposition modeling (FDM) three-dimensional (3d) printing and alternative manufacturing processes

The advantages of the extrusion process are used by 3d printing extrusion processes. With the help of FDM 3d printing, drug loaded polymer filaments are heated and conveyed through a nozzle resulting on deposited strands on a print bed forming a solid dosage form manufactured layer by layer [103].

Using digital computer-aided design software, the geometry (shape and size) is captured in an stereolithographic format. The layer and printing information is filed in a geometric code, which is digitally transferred to the selected 3d printer. The printing parameters are selected (e.g. resolution, temperature, printing time etc.), which are typically based on the printer type, drug characteristics and desired drug product [104].

There are minimum requirements of the material either for filament-direct drive extrusion, or filament-bowden extrusion such as mechanical resilience and heat stability. Furthermore, the melting behavior (e.g., melt viscosity) is essential for good printability [105].

Until today there is still no pharmaceutical market product, which is produced by FDM 3d printing. In research, filaments are used to print prototype DDS with different geometries, drug release profiles and different drug products (e.g., capsules, tablets, inserts). The advantages of using FDM 3d printing in the production of pharmaceuticals include design flexibility, cost-effectiveness, and high reproducibility [106]. HME technology and FDM 3d printing can also be combined into a single continuous process for higher process efficiency [107].

Currently, there are different 3d printing techniques for pharmaceuticals under investigation, which use different mechanism and raw materials. To date, FDM, selective laser sintering, stereolithography, binder jet printing, direct powder extrusion and semi-solid extrusion have all been explored to produce drug products [108]. Each technology comes with unique technical requirements and individual advantages and disadvantages. All 3d printing techniques have in common, that personalized drug products are produced

with a variety of characteristics compared to drug products produced with the help of conventional manufacturing techniques influencing the disintegration time, dissolution profiles, dosing intervals, swallowability, and texture [109-111].

Alternative manufacturing processes, which can address all parameters of additive manufacturing are not available. Fastly disintegrating tablets are usually manufactured by freeze-drying or rapidly dissolving excipients like mannitol resulting in orodispersible tablets [112]. Solid dispersions are often used in tablets in granulate form after being extruded or spray dried to enhance solubility of the drug and influence drug release [113]. Injection molding is used to produce individual geometries defined by the geometry of the mold, but other than 3d printed geometries the molds require a 100% infill [114].

The 3d printing technologies are not suitable to substitute conventional manufacturing mass production but may close the gap towards the on-demand production of small batches of highly flexible and personalized dosage forms.

1.2 Characterization and Quality Control of CQAs of Pharmaceutical Filaments

The characterization and the associated quality control strategy is depending on the intermediate/ drug product. A quality control strategy is a detailed inspection and control system that encompasses the production, evaluation, and distribution of drug products [115]. The production of medicine requires pharmaceutical quality, efficacy, safety, and provides assurance to the patient that the drug product will act consistently and satisfactory for the purpose for which it is recommended. For monitoring of CQAs, control charts are often used to detect systematic deviations of a quality characteristic from a target value and to write process reports [116]. In this work, the characterization is focused on extrudates, which are used as intermediate filament sticks for FDM 3d printing of oral dosage forms. Filament sticks are cylindric shaped rods with a defined diameter and length (Fig. 6).

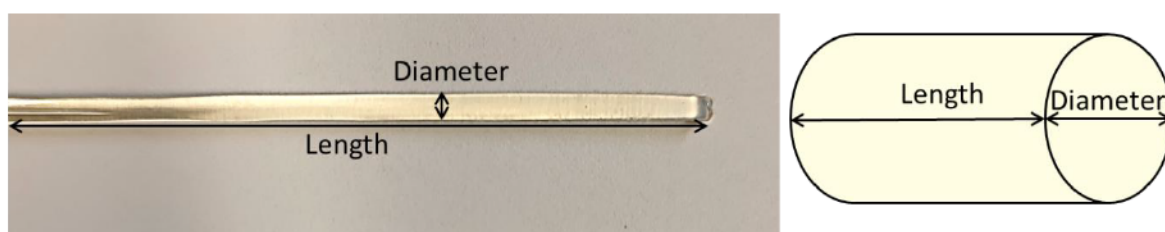


Fig 6. Diameter and length of extruded filament sticks (left: extruded filament; right: schematic drawing).

Intermediate CQAs of extrudate strands (filaments) are “blend” uniformity, solid state of the API and all excipients, diameter, diameter homogeneity, ovality, straightness, straightness of endings, residual moisture, density, tensile strength, and elasticity.

For filament storage in a filament reservoir of a FDM 3d printer, straightness, elasticity, and homogeneity of the diameter of the filament are crucial so that the filament can be stored in the reservoir and maintains its positioning.

For subsequent conveying from the reservoir to the printing nozzle, CQAs are the tensile strength and the elasticity of the filament [117]. Depending on the conveying mechanism (direct drive, bowden, piston) other specifications for mechanical properties are desired [4]. The tensile strength of the intermediate is also critical for the mechanical properties of the 3d printed tablet [118]. Depending on the printer, the minimum and maximum diameter of the used filament must be ensured [119]. The mass flow rate at the 3d printing nozzle is determined by the amount of melt exiting, in addition to other process parameters, so that

the diameter and density are important quality characteristics during 3d printing [120]. The homogeneity of the diameter and the ovality are essential prerequisites for uniform strand thickness and strand deposition during printing [121]. Residual moisture in the filament can lead to cavities in the strands after evaporation at high printing temperature. While processing multiple filament sticks into one drug product, curved ends may result in air entrapment/cavities causing inhomogeneous strand deposition.

Furthermore, content uniformity and drug release are CQA of pharmaceutical filaments. While the homogeneity of the API in the final drug product is tested based on the pharmacopeial acceptance value (AV) (Pharm. Eur. 2.9.40), the intermediate must not be characterized by the AV, but the API must be distributed within the filament homogeneously. The dissolution is affected by the solid-state properties of the API, which must not change during storage. Stability testing also involves the verification of the tensile strength and the elasticity, which may be influenced including residual moisture, change of solid-state properties, post-curing, and separation of plasticizer [122].

1.2.1 Diameter of filaments

Diameter and diameter homogeneity are CQA in the production of filaments. Diameter measurements can be performed during extrusion (implemented in the downstream equipment) or as an offline measurement.

- **Measurement method**

For the real-time diameter determination during extrusion, a laser is directed towards a high-resolution charge-coupled device (CCD) line that passes through the filament. A shadow image of the filament is generated on the line sensor. Intensity fluctuations occur at the transitions from dark to light, caused by the light diffraction at the surfaces of the measured material. Based on the theory of light diffraction, the tangents of the left and right geometric shadow boundaries are calculated from the information of the intensity fluctuations. Together with the tangents of the measuring plane offset by 90 degrees, this results in four tangents touching the measured material. The measurement of the third axis additionally allows the determination of ovality (eccentricity), which results from the difference of the two diameters [123].

- **Readout rate and measuring points**

The readout rate is determined by the device and is mainly depending on the exposure time and the acquisition time the CCD chip. The filament is transported through the device at a defined speed. During the extrusion process, the conveying is determined by the haul-off speed of the downstream equipment. As an offline measurement, the speed can be set as low or as fast as desired. The measuring points thus result from the concurrence of the laser, the readout rate, and the conveying of the filament through the diameter measuring module.

- **Acceptance range**

The target diameter is specified by the 3d printer nozzle and print head design. According to literature, the deviation from a diameter of 1.75 mm should not exceed ± 0.2 mm. However, there are no specifications or pharmacopeial guidelines available yet [105,124].

- **Contributing factors**

The mean diameter, the diameter variations, and the ovality are influenced by various process parameters and material properties. The haul-off speed, the throughput (determined by feed rate(s) and screw speed, as well as the die swelling influence the mean diameter of the filament [125]. Diameter fluctuations are also influenced by the throughput since a higher barrel fill level (based on the flood-feed method) leads to less fluctuations. Inhomogeneities of the melt and pressure fluctuations lead to variations in the diameter [126]. Often the screw configuration at the nozzle is configured with pressure building elements that have a large flight so that the melt is accumulated in front of the nozzle. To avoid air entrapment, which can lead to inhomogeneous diameter through unfolding, a vent port is installed in the barrel, or a vacuum pump is used. When using die with a round outlet, the ovality is mainly influenced by the properties of the melt, since too low viscosity leads to a collapse after exiting the die and the filament cross-section is oval instead of round. This can be influenced by changing the temperature or by the formulation itself.

1.2.2 Content uniformity in filaments

- **Regulatory aspects for content uniformity**

The test requirements for content uniformity of drug products are described in the pharmacopeias as the “Uniformity of Dose by Content Uniformity”. After determining the amount of API, the AV according to USP and Pharm. Eur. for stage 1 and stage 2 testing

is calculated. Samples must be taken at the beginning, middle and end of the respective manufacturing process.

Since the intermediate filament is not the drug product but rather a feedstock for 3d printing, this test is not applicable. The intermediate filament must be analyzed compared to a final blend or an intermediate granule and thus meet the blend uniformity criteria.

The USP criteria for blend uniformity is between 85-115% drug content, whereas the Pharm. Eur. sets the limits for blend uniformity between 90-110% [127]. At stage 1 testing, 10 samples (1 sample per location) must be analyzed, and all individual results must not deviate from the mean value by more than 10%. The relative standard deviation (RSD) of the 10 samples must be smaller or equal to 5.0%. At stage 2 testing, 20 additional samples need to be analyzed (n=30 in total, 3 samples per sample location), and again all individual results must not deviate from the mean value by more than 10%, but the RSD of the 30 samples must be smaller or equal to 6.0%. Samples must be taken after blending at different positions in the drum.

- **Drug content determination as an intermediate drug product**

For better process understanding, stratified sampling can be applied by selecting units from various locations within a batch from various phases or periods of a process. With these additional samples, a better product and process understanding might be generated. This type of sampling specifically targets locations or time points during the process where there is a higher risk of not meeting content uniformity results.

For blend uniformity improvement, the blending process including blender type, blending time and blender speed need to be optimized [128,129]. However, material properties such as cohesivity and differences in particle size of the API and the excipient(s) impact the homogeneity of a blend [130]. To define the highest attainable degree of interactive mixing, the Johnson-Egermann equation considers the particle size of the material (Equation 3):

$$CV = 100 \cdot \sqrt{\frac{\overline{m_x}}{G}} \quad (3)$$

where CV is the coefficient of variation (CV) of the drug content expressed as a percentage of the mean weight, $(\overline{m_x})$ is the mean mass of one API particle and G the mean drug content [131].

For a more accurate description of a binary mixture, a second equation considers not only the mean particle size of a particle of both components, but also the mass fractions of the two components. With the help of the Stange–Poole equation, the *CV* can be calculated according to Equation 4:

$$CV = \frac{100}{x} \cdot \sqrt{\frac{x \cdot y \cdot (\overline{m}_x \cdot y + \overline{m}_y \cdot x)}{M}} \quad (4)$$

where *x* is the relative mass fraction of API, *y* is the relative mass fraction of the polymer, (\overline{m}_x) is the mean mass of one API particle, (\overline{m}_y) is the mean mass of one polymer particle, and *M* is the mean mass of the filaments [132].

This formula was already used by Hermes et al. to illustrate that the RSD of the target concentration of minitablets highly depend on the sample size of powder blend [133]. In this work, the equation was used to demonstrate the limitation of the content uniformity of low-dosed API in filaments resulting from powder characteristics.

- **Drug content determination methods of intermediate filaments**

The drug load of a filament can be measured through destructive and non-destructive methods. Furthermore, the real time in-line analysis is preferred over off-line measurement since if the desired concentration is not reached, the process can be altered faster through adaption of the feed rate or other adaptable CPPs.

- **Off-line measurement for drug content determination**

For the analysis of drug products, samples are taken during production. These samples are analyzed in a different lab. Often destructive methods are applied, where the filament is dissolved in a suitable medium and then analyzed using a suitable analytical method. This is often done using high-performance liquid chromatography (HPLC). It is advantageous that several active ingredients can be analyzed during one method run, since the active ingredients are separated chromatographically.

- **In-line (real time) measurement for drug content determination**

To establish a non-destructive method, instrumental in-line methods are incorporated into the process. With the help of probes implemented into the barrel, the material can be examined during the process. Among the in-line methods, (near) infrared, Raman- and

fluorescence spectroscopy are used. These methods can serve as a check of the CQA or can be used as a release criterium [135].

1.2.3 Color of filaments

For pharmaceutical applications, colorimetry has already been tested as a quality control technique for various drug preparations as a non-destructive characterization method [136]. Color measurements were used for the correlation between the surface color and tensile strength of tablets, for evaluation of tablet coating effectiveness, and assessment of tablet stability [137-139]. Wickström et al. detected vitamin B containing layers conducted by inkjet-printing via colorimetric measurements, but they were limited to differentiating between the first 5 to 6 printed layers because the limits of the detection method have been reached [140]. The correlation between color change and heat stress during drying was analyzed by Lakio et al. for granules and pellets [141]. During extrusion, dyes or pigments are manually added into the barrel to determine the residence time distribution of the melt within the extruder barrel. Often this material is discarded afterwards [142]. For these measurements, the Commission Internationale de l'Eclairage $L^*a^*b^*$ (CIELAB) color space introduced in 1976 is applied, where colors are defined by three unique values: L^* for lightness, a^* for red and green color, and b^* for blue and yellow color. While L^* -values can vary between 0 (black) and 100 (white), both a^* and b^* values range from -128 (a^* : green, b^* : blue) to $+127$ (a^* : red, b^* : yellow), which leaves theoretically 6.5 million possibilities for describing different colors in this color space (Fig. 7) [141,143].

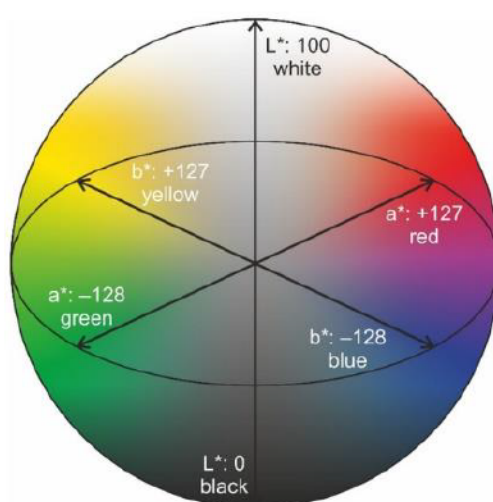


Fig 7. 3d illustration of the CIELAB color space introduced by the International Commission on Illumination in 1976 [144].

The solid-state properties and the physicochemical characteristics including degradation products determine the color of the extrudates. Extrudates are cylindric shaped with a curved surface, electromagnetic radiation and light scattering effects are caused not only by the color of the filament but also by the filament geometry. In the scope of this thesis, the aim was to investigate, whether the difference in concentration of an API is reflected in measurable color variation(s) of the filaments [144].

1.2.4 Intermediate filament sticks

- **Feedstock for new 3d printer**

Commercially available filaments are distributed wound on rolls and are exposed to environmental influences during the 3d printing process since the large coiled filaments are usually located outside the 3d printer. For pharmaceutical grade filaments, this type of feedstock storage is generally not suitable, as moisture uptake, light exposure and direct contact of the professionals with the material cannot be prevented. In addition, unwinding the coiled filament during 3d printing can cause the filament to become tangled and disrupt the continuous flow of material through the 3d printing nozzle. In the worst case, this leads to the need to stop the process, discard the 3d printed dosage form, and require intervention of professionals.

In addition, commercially available 3d printers work with filament-direct drive or filament-bowden principle for conveying, which is not suitable for all filaments. Particularly brittle, but also flexible filaments cannot be transported with this conveying mechanism, so that no continuous strand can be extruded from the printer nozzle [4,118].

Taking the disadvantages into account, the consortium of the Federal Ministry of Education and Research (BMBF) project “Polyprint” jointly developed a new 3d printer with a with an optimized feeding mechanism of the printhead that guarantees the transportation of filaments regardless of the formulation or texture. In addition, the feedstock is stored inside the printhead and has no contact with the environment or personnel.

To serve as adequate feedstock for the new 3d printer, the filaments should be cut into smaller filament sections resulting of the need of filament sticks. Since filament sticks are a novel type of feedstock material, it was necessary to meet the requirements for the new printhead in terms of straight cutting edges, straightness of the filament sticks and form stability during storage.

- **Filament cut**

Changing the feedstock from a “infinite” strand to filaments sticks, there is a change that multiple sticks are needed during the printing process. If the feedstock material of one stick is not sufficient to print one or more drug products, a second or more sticks are required, which must be fed subsequently so that the continuous material flow through the 3d printer nozzle is not interrupted.

This requires that the cross-sections of the filament sticks lie exactly on top of each other. The angle of the cutting edge is of importance, since sticks with an angled, fragile end run the risk of breaking off. Furthermore, when feeding the next filament stick from the reservoir, the stick must be rotated so that the edges of the previous and the new filament align perfectly, which is an additional complication of the feeding mechanism. Moreover from a manufacturing perspective, the angled cut is more complicated than a straight cut of the filament strand. As a result, a straight cut of the filament strand was preferred for this work.

1.3 The Potential of 3d Printing for the Pharmacotherapy of Parkinson Patients

1.3.1 Recent drug therapy of Morbus Parkinson

Parkinson's disease is a neurodegenerative disorder with the presence of bradykinesia combined with rest tremor and/or rigidity. The idiopathic Parkinson syndrome (IPS) is the most frequent Parkinson diagnosis with a predominance of approx. 75%, which is caused by neuronal loss in the basal ganglia structure "substantia nigra" [145]. The substantia nigra owes its name of black appearance in the computer-tomographic image of the stratum corneum in the nucleus subthalamicus to the presence of multiple nuclei, but their density accumulation steadily decreases in the progression [146]. The reasons for this include striatal dopamine (DA) deficiency, intracellular inclusions containing aggregates of α -synuclein, as well as the demise of numerous other cell types throughout the central and peripheral autonomic nervous system [147]. Until today, pharmacotherapy of IPS is exclusively based on a symptomatic treatment since no curative drug therapy, including all pharmacotherapy and gene therapy options, has been developed yet [148]. The main aim of the pharmacotherapy is to treat motor and nonmotor manifestations. Too low API concentrations do not lead to any improvement in cardinal and concomitant symptoms; too high API concentrations increase motor complications and promote undesirable adverse effects [149]. Thus, during therapy, it is necessary to always ensure that the therapeutic range defining the optimal drug concentrations in the blood is targeted, which narrows over time due to continuous neurodegeneration of dopaminergic neurons [150]. In the beginning of pharmacotherapy, the correct dose is titrated estimating the pharmacological effect. Usually, pharmacotherapy is limited to three doses per day. At late stage of IPS, the therapeutic range is narrowed, which requires the lowering of the individual dose and the increase the frequency of dosing (Fig. 8). Furthermore, the combination of APIs for Parkinson patients is often necessary to achieve the targeted pharmacological effect because each individual API represents a unique profile of clinical signs and symptoms [152]. The optimization of combined medications for patient's conditions is described in the S3-guideline, where medicine usage agrees with best evidence [153]. Especially in Parkinson's patients with motor disorders caused by tremor or swallowing difficulties, attention shall be laid on patient's individual need [150]. In 2016, the S3 guideline was revised and the changes in recommendations regarding pharmacotherapy were made to address patients' life circumstances, comorbidities, and increasing life expectancy [153]. Monoamine oxidase B (MAO-B) inhibitors, DA agonists, or levodopa should be used in

symptomatic therapy of early IPS. Levodopa should only be administered starting from 70 of age of the patient (late stage of IPS), as it leads to a rapid habituation process and an associated therapeutic limit. In case of nonresponse or deterioration, decarboxylase inhibitors and sustained released levodopa preparations are recommended.

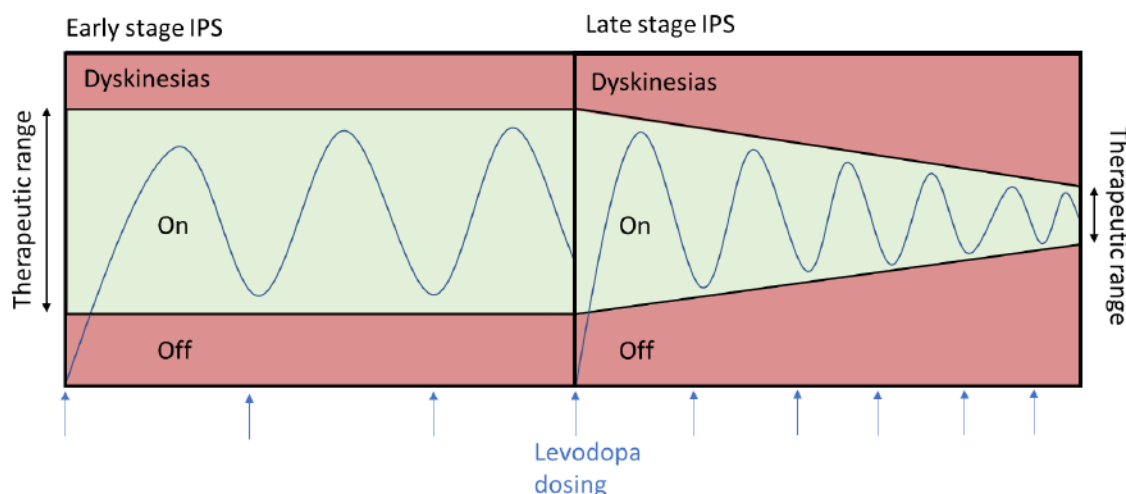


Fig 8. Dosing regimen of Levodopa for Parkinson patients of early and late stage IPS: Levodopa dosing in early stage IPS is usually conducted with high doses and a low frequency. At late stage of IPS, the therapeutic range is narrowed, which requires the lowering of the individual dose and the increase the frequency of dosing, adapted from [151].

For late stage IPS with motor complications, the additional administration of a catechol-O-methyltransferase (COMT) -inhibitor or a MAO-B-inhibitor or the combination of both is proposed. In addition, amantadine or apomorphine can be administered to reduce dyskinesia, with apomorphine additionally reducing the daily off-duration. The S3-guideline recommends consideration of deep brain stimulation therapy and continuous drug delivery pump therapies under defined conditions, with particular emphasis to age, comorbidities, and the patient's supportive environment to guide decisions about the eligibility of these elaborate therapies. To treat the symptoms of IPS in the best possible way, an optimized interaction of the drugs, the correct selection and application of the corresponding dosage forms and the effective plasma concentration of the API are indispensable [150-152]. The pharmacotherapy of Parkinson patients is complex and accompanied by the adjustment of medication over the entire duration of the therapy, which requires a personalized management of the pharmacotherapy throughout the disease.

1.3.2 Adaption of administration route, dosing, and dosing intervals

When treating IPS patients with dopaminergic pharmacotherapeutics, it is reasonable to assume that restoring the missing neurotransmitters will improve clinical deficits in a consistent and predictable manner [152]. Since the amount of DA in the dopaminergic neurons is difficult to determine, the blood plasma concentration is correlated with the clinical efficacy. To understand the physiological effects of DA, it is important to consider that DA has a stimulatory effect at dopamine 1 (D1) - receptors and an inhibitory effect at dopamine 2 (D2) - receptors. The D1-expressing “go”-pathway increases cortical activity and the D2-expressing “no-go” pathway reduces cortical activity and inhibits movement. DA increases the responsiveness of the “go”- pathway and decreases the influence of the “no-go”- pathway (Fig. 9a).

The reduction of the DA level benefits the inhibitory “no-go”- pathway (Fig 9b) and with long-term reduced DA, the experience-dependent cortical input to striatal neurons evolves resulting in long-term potentiation (LTP) and aberrant plasticity of the striatum (Fig 9c). If DA replacement or D1-receptor stimulation occurs through pharmacotherapy, the immediate effect the “go”- pathway is noticeable although LTP is not reversed in the “no-go”- pathway (Fig 9d). Only repeated and continuous long-term DA administration facilitates normal LTP of the “no-go”- pathway (Fig 9e).

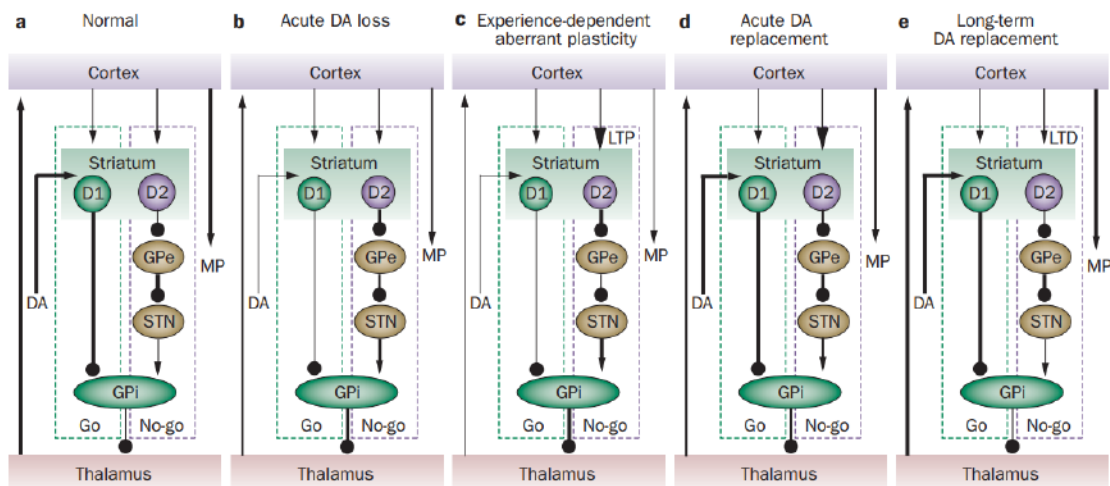


Fig. 9. Physiological effects of DA at D1- and D2- receptors under normal conditions (a), with acute DA loss (b), with experience-dependent aberrant plasticity (c), with acute DA replacement (d) and with long-term DA replacement (e) [154].

Thus, with single dose of levodopa the short-duration response is addressed, while at constant plasma-concentration level of levodopa over a long period of time the long-duration response (LDR) is guaranteed. Thus, continuous dopaminergic stimulation is associated with reduced incidence and severity of dyskinesia compared with pulsatile administration. However, as adverse levodopa tolerance occurs after time, the administration of levodopa is limited to daytime [154]. Several studies have shown that constant drug plasma levels lead to the best therapeutic results [155-157]. Optimal IPS therapy avoids drug concentration peaks and enables drug levels above the efficacy threshold. This range is called the therapeutic range [158]. Due to the poor solubility and instability of levodopa in aqueous solutions, continuous intravenous administration has not been pursued to date [159]. By using a duodenal pump of levodopa and carbidopa, the therapeutic range can be addressed by adjusting the dosing rate [160]. Since the pharmacotherapy through duodenal pumps is an invasive therapy that presents risks, is laborious to manage, and relies on assistance from others, compliance is often only established in the late stage of the disease [161].

As a consequence, medication is preferably administered perorally, with the intake of the tablets varying largely throughout the day. The aim of the dosing regime is to build up an LDR - this is done by giving multiple doses of levodopa throughout the day with the result that the motor response is high [154]. Since the blood plasma concentration of levodopa after oral administration resembles a Bateman function, the maximum concentration is reached after a certain time (stomach passage time) and the API concentration decreases afterwards due to constant elimination [162]. At this point, it is important to ensure that the next administration occurs so that the levodopa plasma concentration level is maintained within the therapeutic range. In regressing IPS, the width of the therapeutic range is reduced, which shortens the time that the levodopa plasma concentration is within the therapeutic range with an unchanged dosage regimen. Therefore, as the disease progresses, tablet intake is increased and the single dose is decreased to maximize the time in which the concentration is inside the therapeutic range, and the treatment regimen involves multiple tablet intake a day [163].

1.3.3 Combination drug products

A pharmacotherapy with multiple APIs requires the use of multiple medications, which is defined as polypharmacy [164]. If two or more APIs are combined in a single dosage form,

the drug product is referred to a combination drug product (FDA terminology [3]) or a fixed-dose combination (EMA terminology [165]).

The multidrug formulations are chosen because of synergistic effects (e.g., treatment of emesis, viruses, tension headache and migraine, attention deficit hyperactivity, narcolepsy, cardiovascular disease), prevention of metabolism (e.g., treatment of viruses, Parkinson's disease), or prevention of misuse of the API (e.g., treatment of emesis or pain) [166-170]. The formulation strategy also involves solubility enhancement by co-crystallization [171], drug targeting through nanoparticles [172], or manufactured to implants with targeted drug release [173].

Multidrug formulations include [174-176]:

- hard capsules containing pellets, (mini-) tablets, or microcapsules
- hard capsules containing encapsulated liquids
- soft capsules containing (mini-) tablets, granules, pellets, or hard capsules
- bilayer or multilayer tablets
- hot-melt (co) extruded delivery systems
- expandable drug delivery systems including hydrodynamically balanced systems (HBSs), raft-forming systems and expandable
- delivery systems produced by 2d and 3d printing technology (e.g., long-acting oral gastro-retentive DDS).

The efforts of multidrug formulations are particularly implemented for increased patient's compliance, and safety and efficacy of the individual API [177-179].

- **Combination drug product for Parkinson's disease**

The pharmacotherapy of Parkinson's disease combines two or more APIs in a way that, first, the metabolism of levodopa is delayed and, second, multiple pharmacological mechanisms can act synergistically. But the APIs described in chapter 1.3.1 differ in terms of half-life, effective dose, solubility, and bioavailability, which is why the APIs were mostly separately compounded in single dosage forms [180]. Hence, combination drug products are available for the treatment where levodopa and a decarboxylase inhibitor are

present within one tablet (tradenames: Madopar[®], Levocomp[®]) and a gel (tradename: Duodopa[®]) [181-184]. Madopar[®] HBS is a typical example of an HBS capsule containing a combination of levodopa and benserazide [185]. Accordion Pill[®] is an expandable placed in a hard capsule that contains carbidopa and levodopa as APIs and is currently being tested in clinical trials [186].

Levodopa and carbidopa are also combined with the COMT- inhibitor entacapone in combination drug products formulated to tablets (tradename: Stalevo[®]) and to a gel for abdominal application (tradename: Lecigon[®]) [187]. In this combination, the decarboxylase inhibitor prevents the metabolism of levodopa by the decarboxylase and the COMT- inhibitor prevents the metabolism of levodopa by the C-O-methyltransferase [188].

Other multidrug formulations are being investigated in research for Parkinson's disease such as multi-drug-loaded microcapsules [189], multidrug and dual drug loaded lipid-based nanoparticle suspension systems [190,191], long-acting oral gastro-retentive DDS [191], 3d printed intraparenchymal drug delivery devices [192] and 3d printed DDS [193,194].

The number of marketed products and multi-drug formulations indicates that this neurodegenerative disease is an important and interesting field for combination drug products including 3d printed DDS, which were produced and characterized within this research work.

1.3.4 Relevance of 3d printed medicine for large- and small-scale production for Parkinson's patients

- **3d printing in small-scale production**

Individual prescriptions are often prepared in the local pharmacy for the treatment of tropical diseases, but also for adjustment of the dose especially for dosage forms prescribed for children. Infusions or injection are prepared in a pharmacy including food for neonates, cytostatic drug preparations or preparation for application in the eye. Until now, there is no drug preparation produced in the pharmacy for Parkinson's patients, because only manufactured medicines are used for pharmacotherapy. However, counseling of the patients takes place especially at the start of therapy (e.g., explanation of the titration of DA agonists, awareness of adverse effects of levodopa) or when medical devices are handed out (e.g., duodenal pump, dosing equipment). The production of a patient tailored preparation would have many advantages to both the patient and the pharmacist [195,196].

Patient tailored medical products and devices are already finding wide application in dental application, surgery, bone/ tissue replacement and many more, which are manufactured in practices, clinics, or laboratories [197-199].

Areas, which are for professional hard to reach, are of interest to produce medicine via 3d printing for the treatment of Parkinson's disease. This includes remote villages, the marine, the space, war zones, hazard areas and other areas where the supply of medicine is problematic [193].

However, the manufacturing step involves testing according to pharmacopoeia of the starting materials and the manufactured preparation, which requires a yet unforeseeable amount of equipment. Only if the 3d printer and the required analyses can be reconciled with the operation site, it will be possible to implement the production at small-scale in a defined environment [200,201]. In the Netherlands, specialized compounding pharmacies have largely taken over compounding activities and show a great interest in 3d printing technologies [202].

Small scale-production is also of interest for preclinical studies. Here, smallest batch sizes are used to test drug products on small populations. Thus, in research of NCE for the treatment of Parkinson's disease, a small amount of drug products can be produced with 3d printing and will be available for faster testing.

- **3d printing in large-scale production**

3d printing has been investigated as an additive manufacturing process to manufacture drug preparations on large-scale production. Spritam® was the first (and until today still the only) 3d printed commercial drug preparation manufactured with the help of binder jet 3d printing [203]. This emergency antiepileptic medication is released as a generic drug product and is manufactured at large-scale production by 3d printing to generate a porous, fast disintegration oral dosage form to fasten the drug absorption during seizure [204].

To find further applications for 3d printing of medicine, a wide variety of 3d printing procedures are assessed, not only in research at universities or in small start-up companies but also major pharmaceutical companies are interested in the technology [205,206]. Eli Lilly has announced a partnership with the drug 3d printing company Triastek to develop 3d printed oral drug products [207]. Also, Merck and AMCM (Additive Manufacturing Customized Machines) started a collaboration in order to manufacture 3d printed tablets

[205,208]. Evonik recently invested in the US company Laxxon Medical, which is specialized on the production of 3d printed multi-layer structures and hopes for a controlled release of the API from its matrix when using its own polymers. Moreover, Evonik has been marketing its polymers for the (medical) 3d printing for implants [209]. GlaxoSmithKline is currently working on the implementation of 3d printed pharmaceuticals in its research and development environment to enhance productivity and deliver new benefits through innovative dosage forms [210]. The company is combining inkjet-based 3d printing with ultraviolet curing to build scaffolds and complex tablet geometries with extended-release profiles with Ropinirole for the treatment of Parkinson's disease. The pharmaceutical companies are not only interested in the production of drug products, but also in the testing of their drug products on human structures. For instance, Bayer is developing a drug testing platform using human heart tissues 3d printed in the laboratory for tissue engineering and regenerative medicine of the transfer company Ramot (Tel Aviv University's technology) [211]. Additionally, the manufacturing of transplantable lungs with the help of 3d printing is in clinical trials promising testing on living organs. Thus, in the early phase of the clinical study, NCE might be tested not only in vitro, but also in living cell and organ structures [212].

Before 3d drug technologies can find widespread use in the pharmaceutical manufacturing world, several regulatory challenges still need to be clarified. The FDA Guidance "Technical considerations for additive manufactured medical devices" is currently the only guidance for industry not to produce drug products but medical devices [213].

1.3.5 Market authorization status for 3d printed medicines and legal requirements of manufacturing steps

In 2015, the FDA approved the first and only 3d printed drug product Spritam® referring to the existing 505b (2) regulatory pathway of the Federal Food, Drug, and Cosmetic Act. The approval for tablets for the preparation of a suspension was declared as a new drug application and was approved for three dosage strengths: 500 mg, 750 mg, and 1000 mg [214-216]. However, the approval of Spritam® by the EMA is still pending.

Even though no other drug product has been approved since then, the FDA focuses on the establishment of a regulatory framework that can allow the manufacturing of 3d printed drug products under existing regulations. For submission, 3d printed drug products must meet the critical manufacturing and control standards described in 21 CFR 200s/ 300s and

must meet 505b(1) or 505b(2) legitimacy requirements. A subdivision of FDA, the Center for Drug Evaluation and Research, is working with FDA's Center for Devices and Radiological Health to develop risk maps for the respective printing technologies and the resulting new drug products [216]. Unlike known manufacturing processes, 3d printing presents new challenges for bulk pharmaceutical manufacturing, not only in terms of uncontrolled variables in the printing process, but also in terms of software malfunctions [217]. For the detection of variables during the printing process, the measurement frequency of quality systems must meet the criteria of 3d printing technology and process risk, which are present, for example, in complex drug product designs, combination of APIs, high potent API, and rapid throughput [218]. Risk analysis ensures that all product quality impacts are understood and appropriately managed in all operating conditions. Finally, as with any other routine commercial drug manufacturing operation, appropriate sampling, testing and quality control procedures and equipment mechanisms are required to detect and discard out-of-spec materials [216].

1.4 Aims of the Thesis/ Outline of the Thesis

Considering all recent advances and observations presented in the introduction, there are many areas where the manufacturing techniques HME and FDM 3d printing would be beneficial to the patient to realize personalized medication management, such as in the treatment of Parkinson's disease. To manufacture a combination drug product, both the intermediate filament and the 3d printed preparation have to meet all CQAs, which may require in addition novel analytical methods. A twin-screw extruder, a hot melt die, an air-cooling unit, two conveyor belts and a cutting unit were used for the manufacturing of filament sticks. Specific quality aspects apply to 3d printing of pharmaceutical filaments, including the development of the formulation, the printing process, and the printed dosage form. Therefore, technical approaches are necessary during HME and FDM 3d printing to assure pharmaceutical quality. For instance, the homogeneity of the filament diameter is not satisfactorily accessible to this day since there are many influencing factors from the formulation and the process parameters of the extrusion.

- The review identifies appropriate CQAs and provides a detailed outline of the individual requirements of the materials and the equipment, and describes procedures for detection. Furthermore, the impact of melt flow and the melt viscosity variation through temperature variation, and different screw configurations are elaborated in section 2.1 (Quality of FDM 3d Printed Medicines for Pediatrics: Considerations for Formulation Development, Filament Extrusion, Printing Process and Printer Design).

When using the new developed pharmaceutical FDM 3d printer of the BMBF consortium, the intermediate filaments are stored as filament sticks in a reservoir serving as the feedstock to produce 3d printed dosage forms. In continuous manufacturing of filaments, it is essential that the cutting process of the extruded filament strand is performed during extrusion. As a downstream equipment, the cutting device shall cut the variously thick filament strand in filaments sticks with a desired length.

- The patent application provides a cutting device that can be inserted into the downstream equipment of a continuous manufacturing extrusion process. The invention is described in detail in section 2.2 (patent application 2022 002 368.7).

In the production of a 3d printed dosage form containing high potent API, the dosage form may be printed with a high drug loaded filament in a very small size, or the dosage form may be large, but the drug load of the filament must be low. In the second case, the production of homogeneously distributed API within the filaments is challenging.

- A manufacturing process is demonstrated to produce filaments in which the API pramipexole is homogeneously distributed with a drug load of 0.1 w% (section 3.1: Precise Dosing of Pramipexole for Low-Dosed Filament Production by Hot Melt Extrusion Applying Various Feeding Methods).

The produced low-dosed filaments in section 3.1 were analyzed off-line using a destructive HPLC method, which required a high workload and was very time consuming. It is desirable to be able to detect the API content during production using a non-destructive method. Using an in-line method, the process and the process parameters can be monitored, and the method can be used to release the intermediate.

- In-line Raman spectroscopy to monitor the API content of very low-dosed filaments is presented in section 3.2 (Drug Content Determination of Low-Dosed Hot-Melt Extruded Filaments using Raman Spectroscopy).

When inserting the feed stock, there is until today no safety mechanism if false filaments are used (incorrect API(s), concentration(s), or matrix). Additionally, there is, to this day, no simple analytical method to analyze the filaments without major equipment and comprehensive analytical knowledge for example in a clinic environment, small laboratory, or pharmacy. Colorimetric measurements are proposed to serve as verification of the filaments.

- CIELAB- measurements were performed with the assistance of an in-house produced filament holder on various filaments with different APIs and excipients and are shown in section 3.3 (Introducing Fiber-Assisted Colorimetric Measurements as a Quality Control Tool of Hot Melt Extruded Filaments).

In the case of a targeted dose adjustment, a simultaneous change in the release of the APIs is undesirable. Based on approaches from literature, a correlation was to be developed between the dose variation and other CQA influencing the drug release profile.

- By maintaining a uniform surface area to volume SA/V ratio, the drug release was tried to keep invariant but change the dose. FDM 3d printing allowed both parameters the surface and the volume (thus also the dosage) to be varied easily by changing the geometry but keeping the ratio the same (Section 4.1: Dose-independent Drug Release from 3d Printed Oral Medicines for Patient-specific Dosing to Improve Therapy Safety).

Novel combination drug products require suitable analytical methods, especially if identification and quantification of different APIs in various concentration are involved. Being able to simultaneously detect low- and high-dosed APIs during drug release, the analytical method must cover different concentration ranges.

- By connecting a liquid-core waveguide to a conventional HPLC system, all three APIs that are to be processed in a combination drug product should be detected within one method. The high concentrations of levodopa and benserazide should be detected by an UV/Vis detector of the HPLC and the low concentrations of pramipexole should be analyzed by an in-house built sensitive liquid-core waveguide UV detector (section 4.2: Embedding a Sensitive Liquid-Core Waveguide UV Detector into an HPLC-UV System for Simultaneous Quantification of Differently Dosed APIs during Drug Release).

Finally, a combination drug product for Parkinson's disease treatment was realized. To produce an exemplary combination drug product with multiple APIs for the therapy of Parkinson's disease, the different release profiles due to differences in the absorption of the respective API were considered while designing. Not only the formulation, but also the geometry was varied for modifying the drug release for the APIs.

- To realize a combination drug product, levodopa and benserazide were prepared in a fixed-dose combination filament. A three-drug combination drug product was prepared by FDM-3d printing from the fixed-dose filament, and a second filament containing pramipexole. The release profiles were optimized by changing the geometry. In addition, swallowability was considered in the choice of geometry (section 4.2: 3d Printed Mini-Floating-Polypill for Parkinson's Disease: Combination of Levodopa, Benserazide, and Pramipexole in Various Dosing for Personalized Therapy)

1.5 References

- [1] Repka, M. A., Battu, S. K., Upadhye, S. B., Thumma, S., Crowley, M. M., Zhang, F., Martin, C., McGinity, J. W. (2007). Pharmaceutical applications of hot-melt extrusion: Part II. Drug Development and Industrial Pharmacy, 33(10), 1043-1057.
- [2] Patil, H., Tiwari, R. V., Repka, M. A. (2016). Hot-melt extrusion: from theory to application in pharmaceutical formulation. AAPS PharmSciTech, 17(1), 20-42.
- [3] Shah, S., Repka, M. (2013). Melt Extrusion in Drug Delivery: Three Decades of Progress. In: Repka, M., Langley, N., DiNunzio, J. (eds): Melt Extrusion. AAPS Advances in the Pharmaceutical Sciences Series, vol 9., pp. 3-46, Springer, NY, USA.
- [4] Repka, M. A., McGinity, J. W., Zhang, F., Koleng, J. J. (2002). Hot-melt extrusion technology. Encyclopedia of Pharmaceutical Technology, 1488-1491.
- [5] Elder, D. P., Kuentz, M., Holm, R. (2016). Pharmaceutical excipients—quality, regulatory and biopharmaceutical considerations. European J Pharm Sci, 87, 88-99.
- [6] Chavanpatil, M., Jain, P., Chaudhari, S., Shear, R., Vavia, P. (2005). Development of sustained release gastroretentive drug delivery system for ofloxacin: in vitro and in vivo evaluation. International Journal of Pharmaceutics, 304(1-2), 178-184.
- [7] Thakkar, R., Thakkar, R., Pillai, A., Ashour, E. A., Repka, M. A. (2020). Systematic screening of pharmaceutical polymers for hot melt extrusion processing: A comprehensive review. International Journal of Pharmaceutics, 576, 118989.
- [8] Pagar, R. R., Musale, S. R., Pawar, G., Kulkarni, D., Giram, P. S. (2022). Comprehensive Review on the Degradation Chemistry and Toxicity Studies of Functional Materials. ACS Biomaterials Science & Engineering, 8(6), 2161-2195.
- [9] Szymańska, E., Winnicka, K. (2015). Stability of chitosan—a challenge for pharmaceutical and biomedical applications. Marine Drugs, 13(4), 1819-1846.
- [10] Kachrimanis, K., Nikolakakis, I. (2015). Polymers as Formulation Excipients for Hot-Melt Extrusion Processing of Pharmaceuticals. In: Handbook of Polymers for Pharmaceutical Technologies; Thakur, V.K., Thakur, M.K. (eds), vol. 2, pp. 121–149, Scrivener Publishing LLC, MA, USA.
- [11] Kasaliwal, G. R., Gödel, A., Pötschke, P., Heinrich, G. (2011). Influences of polymer matrix melt viscosity and molecular weight on MWCNT agglomerate dispersion. Polymer, 52(4), 1027-1036.
- [12] Yan, D., Wang, W. J., Zhu, S. (1999). Effect of long chain branching on rheological properties of metallocene polyethylene. Polymer, 40(7), 1737-1744.
- [13] Hieber, C. A., Chiang, H. H. (1992). Shear-rate-dependence modeling of polymer melt viscosity. Polymer Engineering & Science, 32(14), 931-938.
- [14] Jani, R., & Patel, D. (2015). Hot melt extrusion: An industrially feasible approach for casting orodispersible film. Asian J Pharm Sci, 10(4), 292-305.
- [15] Domenech, T., Peuvrel-Disdier, E., Vergnes, B. (2013). The importance of specific mechanical energy during twin screw extrusion of organoclay based polypropylene nanocomposites. Composites Science and Technology, 75, 7-14.

References

- [16] Aho, J., Edinger, M., Botker, J., Baldursdottir, S., Rantanen, J. (2016). Oscillatory shear rheology in examining the drug-polymer interactions relevant in hot melt extrusion. *J Pharm Sci*, 105(1), 160-167.
- [17] Zheng, W., Lu, X., Wong, S. C. (2004). Electrical and mechanical properties of expanded graphite-reinforced high-density polyethylene. *Journal of Applied Polymer Science*, 91(5), 2781-2788.
- [18] Sprockel, O. L., Sen, M., Shivanand, P., Prapaitrakul, W. (1997). A melt-extrusion process for manufacturing matrix drug delivery systems. *International Journal of Pharmaceutics*, 155(2), 191-199.
- [19] Crowley, M. M., Zhang, F., Repka, M. A., Thumma, S., Upadhye, S. B., Kumar Battu, S., McGinity, J. W., Martin, C. (2007). Pharmaceutical applications of hot-melt extrusion: part I. Drug Development and Industrial Pharmacy, 33(9), 909-926.
- [20] Vieira, M. G. A., da Silva, M. A., dos Santos, L. O., Beppu, M. M. (2011). Natural-based plasticizers and biopolymer films: A review. *European Polymer Journal*, 47(3), 254-263.
- [21] Kolter, K. (2013). Properties and Applications of Polyvinylactam Polymers. In: Repka, M., Langley, N., DiNunzio, J. (eds) *Melt Extrusion. AAPS Advances in the Pharmaceutical Sciences Series*, vol 9. Springer, pp. 83-105, NY, USA.
- [22] Miller, J. C. (1963). Swelling behavior in extrusion. *Polymer Engineering & Science*, 3(2), 134-137.
- [23] Locati, G. (1976). A model for interpreting die swell of polymer melts. *Rheologica Acta*, 15(10), 525-532.
- [24] Jin, G., Jin, Y., Zhao, D., Dai, G., Zhang, Q. (2017). Cross-section design of multi-lumen extrusion dies: Study on the effects of die swell and gas flow rate of the lumen. *Microsystem Technologies*, 23(10), 5093-5104.
- [25] Park, S. J., Lee, J., Choi, J. W., Yang, J. H., Lee, J. H., Lee, J., Kim, S. H., Park, S. H. (2021). Additive manufacturing of the core template for the fabrication of an artificial blood vessel: the relationship between the extruded deposition diameter and the filament/nozzle transition ratio. *Materials Science and Engineering*, 118, 111406.
- [26] Kallakunta, V. R., Sarabu, S., Bandari, S., Tiwari, R., Patil, H., Repka, M. A. (2019). An update on the contribution of hot-melt extrusion technology to novel drug delivery in the twenty-first century: part I. *Expert Opinion on Drug Delivery*, 16(5), 539-550.
- [27] Desai, D., Sandhu, H., Shah, N., Malick, W., Zia, H., Phuapradit, W., Vaka, S. R. K. (2018). Selection of solid-state plasticizers as processing aids for hot-melt extrusion. *J Pharm Sci*, 107(1), 372-379.
- [28] Partheniadis, I., Toskas, M., Stavras, F. M., Menexes, G., Nikolakakis, I. (2020). Impact of hot-melt-extrusion on solid-state properties of pharmaceutical polymers and classification using hierarchical cluster analysis. *Processes*, 8(10), 1208.
- [29] Kallakunta, V. R., Sarabu, S., Bandari, S., Batra, A., Bi, V., Durig, T., Repka, M. A. (2020). Stable amorphous solid dispersions of fenofibrate using hot melt extrusion technology: Effect of formulation and process parameters for a low glass transition temperature drug. *Journal of Drug Delivery Science and Technology*, 58, 101395.
- [30] LaFountaine, J. S., McGinity, J. W., Williams, R. O. (2016). Challenges and strategies in thermal processing of amorphous solid dispersions: a review. *AAPS PharmSciTech*, 17(1), 43-55.

-
- [31] Yang, F., Su, Y., Zhang, J., DiNunzio, J., Leone, A., Huang, C., Brown, C. D. (2016). Rheology guided rational selection of processing temperature to prepare copovidone–nifedipine amorphous solid dispersions via hot melt extrusion (HME). *Molecular Pharmaceutics*, 13(10), 3494-3505.
 - [32] Kallakunta, V. R., Sarabu, S., Bandari, S., Batra, A., Bi, V., Durig, T., Repka, M. A. (2020). Stable amorphous solid dispersions of fenofibrate using hot melt extrusion technology: Effect of formulation and process parameters for a low glass transition temperature drug. *Journal of Drug Delivery Science and Technology*, 58, 101395.
 - [33] Ong, H. J., Pinal, R. (2018). Drug solubilization by means of a surface-modified edible biopolymer enabled by hot melt extrusion. *J Pharm Sci*, 107(1), 402-411.
 - [34] Pandi, P., Bulusu, R., Kommineni, N., Khan, W., Singh, M. (2020). Amorphous solid dispersions: An update for preparation, characterization, mechanism on bioavailability, stability, regulatory considerations and marketed products. *International Journal of Pharmaceutics*, 586, 119560.
 - [35] Breitzkreutz, J. (1998). Prediction of intestinal drug absorption properties by three-dimensional solubility parameters. *Pharmaceutical Research*, 15(9), 1370-1375.
 - [36] Just, S., Sievert, F., Thommes, M., Breitzkreutz, J. (2013). Improved group contribution parameter set for the application of solubility parameters to melt extrusion. *European Journal of Pharmaceutics and Biopharmaceutics*, 85(3), 1191-1199.
 - [37] Nagapudi, K., Jona, J. (2008). Amorphous active pharmaceutical ingredients in preclinical studies: preparation, characterization, and formulation. *Current Bioactive Compounds*, 4(4), 213-224.
 - [38] Kalivoda, A., Fischbach, M., Kleinebudde, P. (2012). Application of mixtures of polymeric carriers for dissolution enhancement of fenofibrate using hot-melt extrusion. *International Journal of Pharmaceutics*, 429(1-2), 58-68.
 - [39] Bhugra, C., Pikal, M. J. (2008). Role of thermodynamic, molecular, and kinetic factors in crystallization from the amorphous state. *J Pharm Sci*, 97(4), 1329-1349.
 - [40] Repka, M. A., Bandari, S., Kallakunta, V. R., Vo, A. Q., McFall, H., Pimparade, M. B., Bhagurkar, A. M. (2018). Melt extrusion with poorly soluble drugs—An integrated review. *International Journal of Pharmaceutics*, 535(1-2), 68-85.
 - [41] Patel, D., Sawant, K. K. (2009). Self micro-emulsifying drug delivery system: formulation development and biopharmaceutical evaluation of lipophilic drugs. *Current Drug Delivery*, 6(4), 419-424.
 - [42] Chokshi, R., Zia, H. (2004). Hot-melt extrusion technique: a review. *Iranian Journal of Pharmaceutical Research*, 3(1), 3-16.
 - [43] Martin, C. (2013). Twin Screw Extrusion for Pharmaceutical Processes. In: Repka, M., Langley, N., DiNunzio, J. (eds) *Melt Extrusion. AAPS Advances in the Pharmaceutical Sciences Series*, vol 9., pp. 47-79, Springer, NY, USA.
 - [44] Alshahrani, S. M., Morott, J. T., Alshetali, A. S., Tiwari, R. V., Majumdar, S., Repka, M. A. (2015). Influence of degassing on hot-melt extrusion process. *European J Pharm Sci*, 80, 43-52.
 - [45] Kohlgrüber, K. (2008) Historical development of the co-rotating twin screw. In: Kohlgrüber, K. (ed) *Co-rotating twin-screw extruders : Fundamentals, technology, and applications*. Carl Hanser Publishers, pp. 9-32, Munich, Germany.

- [46] Thiry, J., Krier, F., Evrard, B. (2015). A review of pharmaceutical extrusion: Critical process parameters and scaling-up. *International Journal of Pharmaceutics*, 479(1), 227-240.
- [47] Villmow, T., Kretschmar, B., Pötschke, P. (2010). Influence of screw configuration, residence time, and specific mechanical energy in twin-screw extrusion of polycaprolactone/multi-walled carbon nanotube composites. *Composites Science and Technology*, 70(14), 2045-2055.
- [48] Robinson, M., Cleary, P. W. (2019). Effect of geometry and fill level on the transport and mixing behaviour of a co-rotating twin screw extruder. *Computational Particle Mechanics*, 6(2), 227-247.
- [49] Thiele W. (2003) Twin-screw extrusion and screw design. In: Ghebre-Sellassie, I., Martin, C.E., Zhang, F., DiNunzio, J. (eds), *Pharmaceutical Extrusion Technology*, vol. 2, pp. 71-94, CRC Press, NY, USA.
- [50] Schenck, L., Lowinger, M., Troup, G. M., Li, L., McKelvey, C. (2019). Achieving a hot melt extrusion design space for the production of solid solutions. *Chemical Engineering in the Pharmaceutical Industry: Drug Product Design, Development, and Modeling*, 469-487.
- [51] Wilczyński, K., Lewandowski, A., Wilczyński, K. J. (2012). Experimental study for starve-fed single screw extrusion of thermoplastics. *Polymer Engineering & Science*, 52(6), 1258-1270.
- [52] Baronsky-Probst, J., Möltgen, C. V., Kessler, W., Kessler, R. W. (2016). Process design and control of a twin screw hot melt extrusion for continuous pharmaceutical tamper-resistant tablet production. *European J Pharm Sci*, 87, 14-21.
- [53] DiNunzio, J.C., Martin, C., Zhang F. (2010). Melt extrusion: shaping drug delivery in the 21st century. *Pharmaceutical Technology*, 1, 30–37.
- [54] Treffer, D., Wahl, P., Markl, D., Koscher, G., Roblegg, E., Khinast, J. G. (2013). Hot melt extrusion as a continuous pharmaceutical manufacturing process. In: Repka, M., Langley, N., DiNunzio, J. (eds) *Melt Extrusion. AAPS Advances in the Pharmaceutical Sciences Series*, vol 9. Springer, pp. 363-396, NY, USA.
- [55] Vynckier, A., Dierickx, L., Voorspoels, J., Gonnissen, Y., Remon, J. P., Vervaet, C. (2014). Hot-melt co-extrusion: requirements, challenges and opportunities for pharmaceutical applications. *Journal of Pharmacy and Pharmacology*, 66(2), 167–179.
- [56] Markl, D., Wahl, P. R., Menezes, J. C., Koller, D. M., Kavsek, B., Francois, K., Roblegg, E., Khinast, J. G. (2013). Supervisory control system for monitoring a pharmaceutical hot melt extrusion process. *AAPS PharmSciTech*, 14(3), 1034-1044.
- [57] Maniruzzaman, M., Nokhodchi, A. (2016). Advanced implantable drug delivery systems via continuous manufacturing. *Critical Reviews in Therapeutic Drug Carrier Systems*, 33(6).
- [58] Alshetaili, A. S., Almutairy, B. K., Alshahrani, S. M., Ashour, E. A., Tiwari, R. V., Alshehri, S. M., Xin Feng, Alsulays, B. B., Majumdar, S., Langley, N., Kolter, K., Gryczke, A, Martin, S. T., Repka, M. A. (2016). Optimization of hot melt extrusion parameters for sphericity and hardness of polymeric face-cut pellets. *Drug Development and Industrial pharmacy*, 42(11), 1833-1841.
- [59] Muhindo, D., Ashour, E. A., Almutairi, M., Repka, M. A. (2022). Development and evaluation of raloxifene hydrochloride-loaded subdermal implants using hot-melt extrusion technology. *International Journal of Pharmaceutics*, 121834.

- [60] Mishra, S. M., Richter, M., Mejia, L., Sauer, A. (2022). Downstream Processing of Itraconazole: HPMCAS Amorphous Solid Dispersion: From Hot-Melt Extrudate to Tablet Using a Quality by Design Approach. *Pharmaceutics*, 14(7), 1429.
- [61] Loxley, A. (2013). Devices and implants prepared using hot melt extrusion. In: Repka, M., Langley, N., DiNunzio, J. (eds) *Melt Extrusion. AAPS Advances in the Pharmaceutical Sciences Series*, vol 9. Springer, pp. 281-298, NY, USA.
- [62] Spoerk, M., Koutsamanis, I., Kottlan, A., Makert, C., Piller, M., Rajkovaca, M., Paudel, A., Khinast, J. (2022). Continuous processing of micropellets via hot-melt extrusion. *AAPS PharmSciTech* 23, 264.
- [63] Martin, C. (2008). Continuous mixing of solid dosage forms via hot-melt extrusion. *Pharmaceutical Technology*, 32(10).
- [64] Zhang, N., Gilchrist, M. D. (2012). Characterization of thermo-rheological behavior of polymer melts during the micro injection moulding process. *Polymer Testing*, 31(6), 748-758.
- [65] Thompson, S. A., Williams III, R. O. (2021). Specific mechanical energy—An essential parameter in the processing of amorphous solid dispersions. *Advanced Drug Delivery Reviews*, 173, 374-393.
- [66] Bochmann, E. S., Steffens, K. E., Gryczke, A., Wagner, K. G. (2018). Numerical simulation of hot-melt extrusion processes for amorphous solid dispersions using model-based melt viscosity. *European Journal of Pharmaceutics and Biopharmaceutics*, 124, 34-42.
- [67] Lu, J., Obara, S., Ioannidis, N., Suwardie, J., Gogos, C., Kikuchi, S. (2018). Understanding the Processing Window of Hypromellose Acetate Succinate for Hot-Melt Extrusion, Part I: Polymer Characterization and Hot-Melt Extrusion. *Advances in Polymer Technology*, 37(1), 154-166.
- [68] Tiwari, R. V., Patil, H., Repka, M. A. (2016). Contribution of hot-melt extrusion technology to advance drug delivery in the 21st century. *Expert Opinion on Drug Delivery*, 13(3), 451-464.
- [69] Schenck, L., Mann, A. K., Liu, Z., Milewski, M., Zhang, S., Ren, J., Dewitt, K., Hermans, A., Cote, A. (2019). Building a better particle: Leveraging physicochemical understanding of amorphous solid dispersions and a hierarchical particle approach for improved delivery at high drug loadings. *International Journal of Pharmaceutics*, 559, 147-155.
- [70] Durin, A., De Micheli, P., Nguyen, H. C., David, C., Valette, R., Vergnes, B. (2014). Comparison between 1D and 3D approaches for twin-screw extrusion simulation. *International Polymer Processing*, 29(5), 641-648.
- [71] Tetzlaff, R. F., Buckwalter, J. M. (2016). FDA's Risk-Based Approach to Inspections. *Pharmaceutical Pre-Approval Inspections*. CRC Press, 181, 27-58.
- [72] Hitzer, P., Bäuerle, T., Drieschner, T., Ostertag, E., Paulsen, K., van Lishaut, H., Lorenz, G., Rebner, K. (2017). Process analytical techniques for hot-melt extrusion and their application to amorphous solid dispersions. *Analytical and bioanalytical chemistry*, 409, 4321-4333.
- [73] Kawabata, Y., Wada, K., Nakatani, M., Yamada, S., Onoue, S. (2011). Formulation design for poorly water-soluble drugs based on biopharmaceutics classification system: basic approaches and practical applications. *International journal of pharmaceutics*, 420(1), 1-10.

References

- [74] Food and Drug Administration (2000). Guidance for industry: waiver of in vivo bioavailability and bioequivalence studies for immediate-release solid oral dosage forms based on a biopharmaceutics classification system. Food and Drug Administration, Rockville, MD.
- [75] Łaszcz, M., Trzcińska, K., Kubiszewski, M., Kosmacińska, B., & Glice, M. (2010). Stability studies and structural characterization of pramipexole. *Journal of Pharmaceutical and Biomedical analysis*, 53(4), 1033-1036.
- [76] Krisai, K., Charnvanich, D., Chongcharoen, W. (2020). Increasing the solubility of levodopa and carbidopa using ionization approach. *Thai J Pharm Sci*, 44(4).
- [77] Cabrera-Pérez, M. Á., Pham-The, H., Cervera, M. F., Hernández-Armengol, R., Miranda-Pérez de Alejo, C., Brito-Ferrer, Y. (2018). Integrating theoretical and experimental permeability estimations for provisional biopharmaceutical classification: Application to the WHO essential medicines. *Biopharmaceutics & Drug Disposition*, 39(7), 354-368.
- [78] Dinora, G. E., Julio, R., Nelly, C., Lilian, Y. M., Cook, H. J. (2005). In vitro characterization of some biopharmaceutical properties of praziquantel. *International Journal of Pharmaceutics*, 295(1-2), 93-99.
- [79] Chavda, H., Patel, C., & Anand, I. (2010). Biopharmaceutics classification system. *Systematic Reviews in Pharmacy*, 1(1), 62.
- [80] Ellery, T., Hansen, N. (2012). The life cycle of a pharmaceutical brand. In: *Pharmaceutical lifecycle management: making the most of each and every brand*. John Wiley & Sons, pp 38-54, NJ, USA
- [81] Repka, M. A., Shah, S., Lu, J., Maddineni, S., Morott, J., Patwardhan, K., Mohammed, N. N. (2012). Melt extrusion: process to product. *Expert Opinion on Drug Delivery*, 9(1), 105-125.
- [82] Bialleck, S., & Rein, H. (2011). Preparation of starch-based pellets by hot-melt extrusion. *European Journal of Pharmaceutics and Biopharmaceutics*, 79(2), 440-448.
- [83] Palem, C. R., Dudhipala, N., Battu, S. K., Goda, S., Repka, M. A., Yamsani, M. R. (2015). Combined dosage form of pioglitazone and felodipine as mucoadhesive pellets via hot melt extrusion for improved buccal delivery with application of quality by design approach. *Journal of Drug Delivery Science and Technology*, 30, 209-219.
- [84] Liu, Y., Thompson, M. R., O'donnell, K. P. (2018). Impact of non-binder ingredients and molecular weight of polymer binders on heat assisted twin screw dry granulation. *International Journal of Pharmaceutics*, 536(1), 336-344.
- [85] Gryczke, A., Schminke, S., Maniruzzaman, M., Beck, J., Douroumis, D. (2011). Development and evaluation of orally disintegrating tablets (ODTs) containing Ibuprofen granules prepared by hot melt extrusion. *Colloids and Surfaces B: Biointerfaces*, 86(2), 275-284.
- [86] Crowley, M. M., Schroeder, B., Fredersdorf, A., Obara, S., Talarico, M., Kucera, S., McGinity, J. W. (2004). Physicochemical properties and mechanism of drug release from ethyl cellulose matrix tablets prepared by direct compression and hot-melt extrusion. *International Journal of Pharmaceutics*, 269(2), 509-522.
- [87] Goyanes, A., Martinez, P. R., Buanz, A., Basit, A. W., Gaisford, S. (2015). Effect of geometry on drug release from 3D printed tablets. *International Journal of Pharmaceutics*, 494(2), 657-663.

-
- [88] Reddy Dumpa, N., Bandari, S., A. Repka, M. (2020). Novel gastroretentive floating pulsatile drug delivery system produced via hot-melt extrusion and fused deposition modeling 3D printing. *Pharmaceutics*, 12(1), 52.
 - [89] Repka, M. A., Gerding, T. G., Repka, S. L., McGinity, J. W. (1999). Influence of plasticizers and drugs on the physical-mechanical properties of hydroxypropylcellulose films prepared by hot melt extrusion. *Drug Development and Industrial Pharmacy*, 25(5), 625-633.
 - [90] Repka, M. A., McGinity, J. W. (2001). Bioadhesive properties of hydroxypropylcellulose topical films produced by hot-melt extrusion. *Journal of Controlled Release*, 70(3), 341-351.
 - [91] Palem, C. R., Kumar Battu, S., Maddineni, S., Gannu, R., Repka, M. A., Yamsani, M. R. (2013). Oral transmucosal delivery of domperidone from immediate release films produced via hot-melt extrusion technology. *Pharmaceutical Development and Technology*, 18(1), 186-195.
 - [92] Clark, M. R., Johnson, T. J., McCabe, R. T., Clark, J. T., Tuitupou, A., Elgendy, H., Friend, D. R., Kiser, P. F. (2012). A hot-melt extruded intravaginal ring for the sustained delivery of the antiretroviral microbicide UC781. *J Pharm Sci*, 101(2), 576-587.
 - [93] Koutsamanis, I., Spoerk, M., Arbeiter, F., Eder, S., Roblegg, E. (2020). Development of porous polyurethane implants manufactured via hot-melt extrusion. *Polymers*, 12(12), 2950.
 - [94] DeBoyace, K., Wildfong, P. L. (2018). The application of modeling and prediction to the formation and stability of amorphous solid dispersions. *J Pharm Sci*, 107(1), 57-74.
 - [95] Sethia, S., Squillante III, E. (2003). Solid dispersions: revival with greater possibilities and applications in oral drug delivery. *Critical Review in Therapeutic Drug Carrier Systems*, 20(2-3).
 - [96] Maniruzzaman, M., Boateng, J. S., Snowden, M. J., Douroumis, D. (2012). A review of hot-melt extrusion: process technology to pharmaceutical products. *International Scholarly Research Notices*.
 - [97] Butreddy, A., Sarabu, S., Dumpa, N., Bandari, S., Repka, M. A. (2020). Extended release pellets prepared by hot melt extrusion technique for abuse deterrent potential: Category-1 in-vitro evaluation. *International Journal of Pharmaceutics*, 587, 119624.
 - [98] Kapoor, K. G., Wagner, M. G., Wagner, A. L. (2015). The sustained-release dexamethasone implant: expanding indications in vitreoretinal disease. *Seminars in Ophthalmology*, 30(5-6), 475-481.
 - [99] Matic, J., Paudel, A., Bauer, H., Garcia, R. A. L., Biedrzycka, K., Khinast, J. G. (2020). Developing HME-based drug products using emerging science: a fast-track roadmap from concept to clinical batch. *AAPS PharmSciTech*, 21(5), 1-18.
 - [100] Li, J., Li, C., Zhang, H., Gao, X., Wang, T., Wang, Z., Zheng, A. (2022). Preparation of Azithromycin Amorphous Solid Dispersion by Hot-Melt Extrusion: An Advantageous Technology with Taste Masking and Solubilization Effects. *Polymers*, 14(3), 495.
 - [101] Kesisoglou, F., Wang, M., Galipeau, K., Harmon, P., Okoh, G., Xu, W. (2019). Effect of amorphous nanoparticle size on bioavailability of anacetrapib in dogs. *J Pharm Sci*, 108(9), 2917-2925.
 - [102] Auriemma, G., Tommasino, C., Falcone, G., Esposito, T., Sardo, C., Aquino, R. P. (2022). Additive Manufacturing Strategies for Personalized Drug Delivery Systems and Medical Devices: Fused Filament Fabrication and Semi Solid Extrusion. *Molecules*, 27(9), 2784.

- [103] Vo, A. Q., Zhang, J., Nyavanandi, D., Bandari, S., Repka, M. A. (2020). Hot melt extrusion paired fused deposition modeling 3D printing to develop hydroxypropyl cellulose based floating tablets of cinnarizine. *Carbohydrate Polymers*, 246, 116519.
- [104] Vithani, K., Goyanes, A., Jannin, V., Basit, A. W., Gaisford, S., Boyd, B. J. (2019). An overview of 3D printing technologies for soft materials and potential opportunities for lipid-based drug delivery systems. *Pharmaceutical Research*, 36, 1-20.
- [105] Quodbach, J., Bogdahn, M., Breitzkreutz, J., Chamberlain, R., Eggenreich, K., Elia, A. G., Gottschalk, N., Gunkel-Grabole, G., Hoffmann, L., Kapote, D., Kipping, T., Klinken, S., Loose, F., Marquetant, T., Windolf, H., Geißler, S., Spitz, T. (2022). Quality of FDM 3D printed medicines for pediatrics: Considerations for formulation development, filament extrusion, printing process and printer design. *Therapeutic Innovation & Regulatory Science*, 56, 910-928.
- [106] Tan, D. K., Maniruzzaman, M., Nokhodchi, A. (2018). Advanced pharmaceutical applications of hot-melt extrusion coupled with fused deposition modelling (FDM) 3D printing for personalised drug delivery. *Pharmaceutics*, 10(4), 203.
- [107] Melocchi, A., Parietti, F., Maroni, A., Foppoli, A., Gazzaniga, A., Zema, L. (2016). Hot-melt extruded filaments based on pharmaceutical grade polymers for 3D printing by fused deposition modeling. *International Journal of Pharmaceutics*, 509(1-2), 255-263.
- [108] Alhnan, M. A., Okwuosa, T. C., Sadia, M., Wan, K. W., Ahmed, W., Arafat, B. (2016). Emergence of 3D printed dosage forms: opportunities and challenges. *Pharmaceutical Research*, 33, 1817-1832.
- [109] Goyanes, A., Martinez, P. R., Buanz, A., Basit, A. W., Gaisford, S. (2015). Effect of geometry on drug release from 3D printed tablets. *International Journal of Pharmaceutics*, 494(2), 657-663.
- [110] Palekar, S., Nukala, P. K., Mishra, S. M., Kipping, T., Patel, K. (2019). Application of 3D printing technology and quality by design approach for development of age-appropriate pediatric formulation of baclofen. *International Journal of Pharmaceutics*, 556, 106-116.
- [111] Menditto, E., Orlando, V., De Rosa, G., Minghetti, P., Musazzi, U. M., Cahir, C., Kurczewska-Michalak, M., Kardas, P., Costa, E., Sousa Lobo, J. M., Almeida, I. F. (2020). Patient centric pharmaceutical drug product design—The impact on medication adherence. *Pharmaceutics*, 12(1), 44.
- [112] Pahwa, R., Piplani, M., Sharma, P. C., Kaushik, D., Nanda, S. (2010). Orally disintegrating tablets-Friendly to pediatrics and geriatrics. *Archives of Applied Science Research*, 2(2), 35-48.
- [113] Mendonsa, N., Almutairy, B., Kallakunta, V. R., Sarabu, S., Thipsay, P., Bandari, S., Repka, M. A. (2020). Manufacturing strategies to develop amorphous solid dispersions: An overview. *Journal of Drug Delivery Science and Technology*, 55, 101459.
- [114] Fuenmayor, E., O'Donnell, C., Gately, N., Doran, P., Devine, D. M., Lyons, J. G., McConville, C., Major, I. (2019). Mass-customization of oral tablets via the combination of 3D printing and injection molding. *International Journal of Pharmaceutics*, 569, 118611.
- [115] Yu, L. X. (2008). Pharmaceutical quality by design: product and process development, understanding, and control. *Pharmaceutical Research*, 25, 781-791.

- [116] Pramod, K., Tahir, M. A., Charoo, N. A., Ansari, S. H., Ali, J. (2016). Pharmaceutical product development: A quality by design approach. *International Journal of Pharmaceutical Investigation*, 6(3), 129.
- [117] Korte, C., Quodbach, J. (2018). Formulation development and process analysis of drug-loaded filaments manufactured via hot-melt extrusion for 3D-printing of medicines. *Pharmaceutical Development and Technology*, 23(10), 1117-1127.
- [118] Sola, A. (2022). Materials Requirements in Fused Filament Fabrication: A Framework for the Design of Next-Generation 3D Printable Thermoplastics and Composites. *Macromolecular Materials and Engineering*, 307(10), 2200197.
- [119] Sadhya, S., Goyal, K. K., Singh, G., Singh, J., Akula, V. (2023). Development of lab-scale extruder to produce feedstock filament for 3D printing using recycled thermoplastics. *Materials Today: Proceedings*, 80, 150-155.
- [120] Azad, M. A., Olawuni, D., Kimbell, G., Badruddoza, A. Z. M., Hossain, M. S., Sultana, T. (2020). Polymers for extrusion-based 3D printing of pharmaceuticals: A holistic materials–process perspective. *Pharmaceutics*, 12(2), 124.
- [121] Fischer, D., Eßbach, C., Schönherr, R., Dietrich, D., Nickel, D. (2022). Improving inner structure and properties of additive manufactured amorphous plastic parts: the effects of extrusion nozzle diameter and layer height. *Additive Manufacturing*, 51, 102596.
- [122] Keikhosravi, N., Mirdamadian, S. Z., Varshosaz, J., Taheri, A. (2020). Preparation and characterization of polypills containing aspirin and simvastatin using 3D printing technology for the prevention of cardiovascular diseases. *Drug Development and Industrial Pharmacy*, 46(10), 1665-1675.
- [123] Dubbeldam, G. C. (1986). Laser shadow method for measuring the diameter of a transparent filament. *Optics in Engineering Measurement*, 599, 370-373.
- [124] Gottschalk, N., Bogdahn, M., Harms, M., Quodbach, J. (2021). Brittle polymers in Fused Deposition Modeling: An improved feeding approach to enable the printing of highly drug loaded filament. *International Journal of Pharmaceutics*, 597, 120216.
- [125] Rauwendaal, C. J. (1981). Analysis and experimental evaluation of twin screw extruders. *Polymer Engineering & Science*, 21(16), 1092-1100.
- [126] Breitenbach, J. (2002). Melt extrusion: from process to drug delivery technology. *European Journal of Pharmaceutics and Biopharmaceutics*, 54(2), 107-117.
- [127] Boehm, G., Clark, J., Dietrick, J., Foust, L., Garcia, T., Gavini, M., Gelber, L., Geoffroy, J. M., Jimenez, P., Mergen, G., Muzzio, F., Planchard, J., Prescott, J., Timmermans, J., Takiar, N. (2003). The use of stratified sampling of blend and dosage units to demonstrate adequacy of mix for powder blends. *PDS J PharmSciTech*, 57, 59-74.
- [128] de Villiers, M.M., van der Watt, J.G. (1994). The Measurement of Mixture Homogeneity and Dissolution to Predict the Degree of Drug Agglomerate Breakdown Achieved Through Powder Mixing. *Pharmaceutical Research*, 11, 1557–1561.
- [129] Popo, M., Romero-Torres, S., Conde, C., Romañach, R. J. (2002). Blend uniformity analysis using stream sampling and near infrared spectroscopy. *AAPS PharmSciTech*, 3(3), 61-71.

- [130] M.C.R. Johnson. (1972). Particle size distribution of the API for solid dosage forms of low dosage. *Pharmaceutica Acta Helvetiae*, 47, 546–559.
- [131] Egermann, H. (1985). Extension of Johnson's equation of homogeneity of random mixtures. *Journal of Pharmacy and Pharmacology*, 37, 491–492.
- [132] Egermann, H.; Frank, P. (1992). Novel approach to estimate quality of binary random powder mixtures: Samples of constant volume. I: Derivation of equation. *J Pharm Sci*, 81, 551–555.
- [133] Hermes, M. (2012). Kindgerechte, Niedrigdosierte Zubereitungen Mit Enalaprilmaleat. (doctorial thesis), Heinrich Heine University Düsseldorf, Germany.
- [134] Saerens, L., Ghanam, D., Raemdonck, C., Francois, K., Manz, J., Krüger, R., Krüger, S., Vervaet, C., Remon, J.P., De Beer, T. (2014). In-line solid state prediction during pharmaceutical hot-melt extrusion in a 12 mm twin screw extruder using Raman spectroscopy. *European Journal of Pharmaceutics and Biopharmaceutics*, 87(3), 606-615.
- [135] Gryczke, A. (2013). Hot-melt extrusion process design using process analytical technology. *Melt Extrusion: Materials, Technology and Drug Product Design*, 397-431.
- [136] Chen, Q., Zhang, C., Zhao, J., Ouyang, Q. (2013). Recent advances in emerging imaging techniques for non-destructive detection of food quality and safety. *Trends in Analytical Chemistry*, 52, 261-274.
- [137] Siddiqui, A., Nazzal, S. (2007). Measurement of surface color as an expedient QC method for the detection of deviations in tablet hardness. *International Journal of Pharmaceutics*, 341(1-2), 173-180.
- [138] Bogdanský, F. M. (1975). Measurement of surface color and color difference of tablet colorants by tristimulus colorimetry. *J Pharm Sci*, 64(2), 323-328.
- [139] Barimani, S., Tomaževič, D., Meier, R., Kleinebudde, P. (2022). 100% visual inspection of tablets produced with continuous direct compression and coating. *International Journal of Pharmaceutics*, 614, 121465.
- [140] Wickström, H., Nyman, J. O., Indola, M., Sundelin, H., Kronberg, L., Preis, M., Rantanen, J., Sandler, N. (2017). Colorimetry as quality control tool for individual inkjet-printed pediatric formulations. *AAPS PharmSciTech*, 18, 293-302.
- [141] Lakio, S., Heinämäki, J., & Yliruusi, J. (2010). Colorful drying. *AAPS PharmSciTech*, 11, 46-53.
- [142] Van Renterghem, J., Van de Steene, S., Digkas, T., Richter, M., Vervaet, C., De Beer, T. (2019). Assessment of volumetric scale-up law for processing of a sustained release formulation on co-rotating hot-melt extruders. *International Journal of Pharmaceutics*, 569, 118587.
- [143] ISO 11664-4: 2008/CIE S 014-4 (2007): Colorimetry—Part 4: CIE 1976 L*a*b* uniform colour space. CIE Draft Standard: Vienna, Austria.
- [144] Chamberlain, R., Mangiorou, E., Fischer, B. (2022). Introducing Fiber-Assisted Colorimetric Measurements as a Quality Control Tool of Hot Melt Extruded Filaments. *Pharmaceutics*, 14(5), 1055.

- [145] Cadogan, C., Ryan, C., Gormley, G., Passmore, P., Francis, J., Kerse, N., Hughes, C. (2015). Dispensing appropriate polypharmacy to older people in primary care: a qualitative, theory-based study of community pharmacists' perceptions and experiences. *Int J Pharm Pract*, 23(32).
- [146] Poewe, W., Seppi, K., Tanner, C. M., Halliday, G. M., Brundin, P., Volkmann, J., Schrag, A. E., Lang, A. E. (2017). Parkinson disease. *Nature Reviews Disease Primers*, 3(1), 1-21.
- [147] Bloem, B. R., Okun, M. S., Klein, C. (2021). Parkinson's disease. *The Lancet*, 397(10291), 2284-2303.
- [148] Hauser, R. A. (2009). Levodopa: past, present, and future. *European Neurology* 62(1), 1-8.
- [149] Camargo, S. M., Vuille-dit-Bille, R. N., Mariotta, L., Ramadan, T., Huggel, K., Singer, D., Götze, O., Verrey, F. (2014). The molecular mechanism of intestinal levodopa absorption and its possible implications for the treatment of Parkinson's disease. *Journal of Pharmacology and Experimental Therapeutics*, 351(1), 114-123.
- [150] Bellucci, A., Mercuri, N. B., Venneri, A., Faustini, G., Longhena, F., Pizzi, M., Götze, O., Spano, P. (2016). Parkinson's disease: from synaptic loss to connectome dysfunction. *Neuropathology and Applied Neurobiology*, 42(1), 77-94.
- [151] Chamberlain, R., Windolf, H., Breitzkreutz, J. (2022). Arzneizubereitungen für die Therapie des idiopathischen Parkinson-Syndroms, *Pharmakon*, 10, 216–226.
- [152] Straka, I., Minár, M., Gažová, A., Valkovič, P., Kyselovič, J. (2018). Clinical aspects of adherence to pharmacotherapy in Parkinson disease: a PRISMA-compliant systematic review. *Medicine*, 97(23).
- [153] S3 Leitlinie für Diagnostik und Therapie in der Neurologie: Idiopathisches Parkinson-Syndrom Leitlinie https://dgn.org/wp-content/uploads/2013/01/030010_LL_kurzfassung_ips_2016.pdf, accessed on 10.01.2023.
- [154] Zhuang, X., Mazzoni, P., Kang, U. J. (2013). The role of neuroplasticity in dopaminergic therapy for Parkinson disease. *Nature Reviews Neurology*, 9(5), 248-256.
- [155] Senek, M., Nielsen, E. I., and Nyholm, D. (2017) Levodopa-entacapone-carbidopa intestinal gel in Parkinson's disease: A randomized crossover study." *Movement Disorders* 32.2, 283-286.
- [156] Olanow, C. W., Schapira, A. H. (2013). Therapeutic prospects for Parkinson disease. *Annals of Neurology*, 74(3), 337-347.
- [157] Poewe, W., Antonini, A., Zijlmans, J. C., Burkhard, P. R., Vingerhoets, F. (2010). Levodopa in the treatment of Parkinson's disease: an old drug still going strong. *Clinical Interventions In Aging*, 5, 229.
- [158] World Health Organization (2018). Technical report on the pharmacokinetics and pharmacodynamics (PK (No. WHO/CDS/TB/2018.6).
- [159] Fasinu, P., Pillay, V., Ndesendo, V. M., du Toit, L. C., Choonara, Y. E. (2011). Diverse approaches for the enhancement of oral drug bioavailability. *Biopharmaceutics & Drug Disposition*, 32(4), 185-209.

- [160] Abbruzzese, G., Barone, P., Bonuccelli, U., Lopiano, L., Antonini, A. (2012). Continuous intestinal infusion of levodopa/carbidopa in advanced Parkinson's disease: efficacy, safety and patient selection. *Functional Neurology*, 27(3), 147.
- [161] Nyholm, D., Aquilonius, S. M. (2004). Levodopa infusion therapy in Parkinson disease: state of the art in 2004. *Clinical Neuropharmacology*, 27(5), 245-256.
- [162] Weiss, M. (1996). A novel extravascular input function for the assessment of drug absorption in bioavailability studies. *Pharmaceutical Research*, 13(10), 1547-1553.
- [163] Pezzoli, G., Zini, M. (2010). Levodopa in Parkinson's disease: from the past to the future. *Expert Opinion on Pharmacotherapy*, 11(4), 627-635.
- [164] Hughes, C. M., Cadogan, C. A., Patton, D., Ryan, C. A. (2016). Pharmaceutical strategies towards optimising polypharmacy in older people. *International Journal of Pharmaceutics*, 512(2), 360-365.
- [165] Janczura, M., Sip, S., Cielecka-Piontek, J. (2022). The Development of Innovative Dosage Forms of the Fixed-Dose Combination of Active Pharmaceutical Ingredients. *Pharmaceutics*, 14(4), 834.
- [166] Aapro, M., Rugo, H., Rossi, G., Rizzi, G., Borroni, M. E., Bondarenko, I., Sarosiek, T., Oprean, C., Cardona-Huerta, S., Lorusso, V., Karthaus, M., Schwartzberg, L., Grunberg, S. (2014). A randomized phase III study evaluating the efficacy and safety of NEPA, a fixed-dose combination of netupitant and palonosetron, for prevention of chemotherapy-induced nausea and vomiting following moderately emetogenic chemotherapy. *Annals of Oncology*, 25(7), 1328-1333.
- [167] Lawitz, E., Poordad, F. F., Pang, P. S., Hyland, R. H., Ding, X., Mo, H., Symonds, W. T., McHutchison, J. G., Membreno, F. E. (2014). Sofosbuvir and ledipasvir fixed-dose combination with and without ribavirin in treatment-naïve and previously treated patients with genotype 1 hepatitis C virus infection (LONESTAR): an open-label, randomised, phase 2 trial. *The Lancet*, 383(9916), 515-523.
- [168] Orrell, C., Hagins, D. P., Belonosova, E., Porteiro, N., Walmsley, S., Falcó, V., Man, C. Y., Aylott, A., Buchanan, A. M., Wynne, B., Vavro, C., Aboud, M., Smith K. Y., Van Dam, C. N. (2017). Fixed-dose combination dolutegravir, abacavir, and lamivudine versus ritonavir-boosted atazanavir plus tenofovir disoproxil fumarate and emtricitabine in previously untreated women with HIV-1 infection (ARIA): week 48 results from a randomised, open-label, non-inferiority, phase 3b study. *The Lancet HIV*, 4(12), 536-546.
- [169] Salamon, A., Zádori, D., Szpisjak, L., Klivényi, P., Vécsei, L. (2020). Fixed-dose combination therapy for Parkinson's disease with a spotlight on entacapone in the past 20 years: a reduced pill burden and a simplified dosing regime. *Expert Opinion on Pharmacotherapy*, 21(18), 2265-2278.
- [170] Pergolizzi, J. V., Taylor, R., Raffa, R. B. (2015). The potential role of an extended-release, abuse-deterrent oxycodone/acetaminophen fixed-dose combination product for the treatment of acute pain. *Advances in Therapy*, 32(6), 485-495.
- [171] Wehland, M., Simonsen, U., Buus, N. H., Krueger, M., Grimm, D. (2020). An evaluation of the fixed-dose combination sacubitril/valsartan for the treatment of arterial hypertension. *Expert Opinion on Pharmacotherapy*, 21(10), 1133-1143.

- [172] Zewail, M. B., El-Gizawy, S. A., Osman, M. A., Haggag, Y. A. (2021). Preparation and In vitro characterization of a novel self-nano emulsifying drug delivery system for a fixed-dose combination of candesartan cilexetil and hydrochlorothiazide. *Journal of Drug Delivery Science and Technology*, 61, 102320.
- [173] Dierickx, L., Saerens, L., Almeida, A., De Beer, T., Remon, J. P., Vervaet, C. (2012). Co-extrusion as manufacturing technique for fixed-dose combination mini-matrices. *European Journal of Pharmaceutics and Biopharmaceutics*, 81(3), 683-689.
- [174] Janczura, M., Sip, S., Cielecka-Piontek, J. (2022). The Development of Innovative Dosage Forms of the Fixed-Dose Combination of Active Pharmaceutical Ingredients. *Pharmaceutics*, 14(4), 834.
- [175] Tiwari, R. V., Patil, H., Repka, M. A. (2016). Contribution of hot melt extrusion technology to advance drug delivery in the 21st century. *Expert Opinion on Drug Delivery*, 13(3), 451-464.
- [176] Awad, A., Trenfield, S. J., Gaisford, S., Basit, A. W. (2018). 3d printed medicines: A new branch of digital healthcare. *International Journal of Pharmaceutics*, 548(1), 586-596.
- [177] Webster, R., Castellano, J. M., Onuma, O. K. (2017). Putting polypills into practice: challenges and lessons learned. *The Lancet*, 389(10073), 1066-1074.
- [178] Breitzkreutz, J., Boos, J. (2007). Paediatric and geriatric drug delivery. *Expert Opinion on Drug Delivery*, 4(1), 37-45.
- [179] Mazarura, K. R., Kumar, P., Choonara, Y. E. (2022). Customized 3d printed multi-drug systems: an effective and efficient approach to polypharmacy. *Expert Opinion on Drug Delivery*, 19(9), 1149-1163.
- [180] Di Stefano, A., Sozio, P., Iannitelli, A., Cerasa, L. S. (2009). New drug delivery strategies for improved Parkinson's disease therapy. *Expert Opinion on Drug Delivery*, 6(4), 389-404.
- [181] Osafo, N., Obeng, S., Obiri, D.D., Yeboah, O.K., Essel, L.B. (2020). Pharmacological management of Parkinson's disease. In: Uddin, M. S., & Rashid, M. (eds.) *Advances in neuropharmacology: drugs and therapeutics*. CRC Press, FL, USA.
- [182] Gasser, U. E., Fischer, A., Timmermans, J. P., Arnet, I. (2013). Pharmaceutical quality of seven generic Levodopa/Benserazide products compared with original Madopar®/Prolopa®. *BMC Pharmacology and Toxicology*, 14(1), 1-6.
- [183] Modi, N. B. (2017). Application of pharmacokinetics and pharmacodynamics in product life cycle management. A case study with a carbidopa-levodopa extended-release formulation. *The AAPS Journal*, 19(3), 607-618.
- [184] Pålhagen, S. E., Sydow, O., Johansson, A., Nyholm, D., Holmberg, B., Widner, H., Dizdar, N., Linder, J., Linder, J., Jansson, R., Bergmann, L., Kjellander, S., Marshall, T. S. (2016). Levodopa-carbidopa intestinal gel (LCIG) treatment in routine care of patients with advanced Parkinson's disease: an open-label prospective observational study of effectiveness, tolerability and healthcare costs. *Parkinsonism & Related Disorders*, 29, 17-23.
- [185] Dupont, E., Andersen, A., Boas, J., Boisen, E., Borgmann, R., Helgetveit, A. C., Kjær, M. O., Kristensen, T. N., Mikkelsen, B., Pakkenberg, H., Presthus, J., Stien, R., Worm-Petersen, J., Buch, D. (1996). Sustained-release Madopar HBS® compared with standard Madopar® in the long-term treatment of de novo parkinsonian patients. *Acta Neurologica Scandinavica*, 93(1), 14-20.

References

- [186] Navon, N. (2019). The Accordion Pill®: unique oral delivery to enhance pharmacokinetics and therapeutic benefit of challenging drugs. *Therapeutic Delivery*, 10(7), 433-442.
- [187] Senek, M., Nielsen, E. I., & Nyholm, D. (2017). Levodopa-entacapone-carbidopa intestinal gel in Parkinson's disease: A randomized crossover study. *Movement Disorders*, 32(2), 283-286.
- [188] Gallagher, D.A., Schapira, A. (2010). Medical management of motor complications. In: Schapira, A. (ed.) *Parkinson's disease*. Oxford University Press, pp. 63-73, NY, USA.
- [189] Baek, J. S., Choo, C. C., Qian, C., Tan, N. S., Shen, Z., Loo, S. C. J. (2016). Multi-Drug-Loaded Microcapsules with Controlled Release for Management of Parkinson's Disease. *Small*, 12(27), 3712-3722.
- [190] Hanning, S. M., Muhamed, J., Orlu-Gul, M. (2015). Investigation into the dosage form attributes of currently UK licensed cardiovascular and Parkinson's disease drug products. *International Journal of Pharmaceutics*, 479(1), 159-162.
- [191] Leyva-Gomez, G., Cortes, H., Magana, J. J., Leyva-García, N., Quintanar-Guerrero, D., Florán, B. (2015). Nanoparticle technology for treatment of Parkinson's disease: the role of surface phenomena in reaching the brain. *Drug Discovery Today*, 20(7), 824-837.
- [192] Kutlehria, S., D'Souza, A., Bleier, B. S., Amiji, M. M. (2022). Role of 3d Printing in the Development of Biodegradable Implants for Central Nervous System Drug Delivery. *Molecular Pharmaceutics*, 19(12), 4411-4427.
- [193] Windolf, H., Chamberlain, R., Breitzkreutz, J., Quodbach, J. (2022). 3d Printed Mini-Floating-Polypill for Parkinson's Disease: Combination of Levodopa, Benserazide, and Pramipexole in Various Dosing for Personalized Therapy. *Pharmaceutics*, 14(5), 931.
- [194] Gültekin, H. E., Tort, S., Tuğcu-Demiröz, F., Acartürk, F. (2021). 3D printed extended release tablets for once daily use: an in vitro and in vivo evaluation study for a personalized solid dosage form. *International Journal of Pharmaceutics*, 596, 120222.
- [195] Rautamo, M., Kvarnström, K., Sivé, M., Airaksinen, M., Lahdenne, P., Sandler, N. (2020). Benefits and prerequisites associated with the adoption of oral 3d-printed medicines for pediatric patients: a focus group study among healthcare professionals. *Pharmaceutics*, 12(3), 229.
- [196] Schröder, S., Martus, P., Odin, P., Schaefer, M. (2012). Impact of community pharmaceutical care on patient health and quality of drug treatment in Parkinson's disease. *International Journal of Clinical Pharmacy*, 34(5), 746-756.
- [197] Tahayeri, A., Morgan, M., Fugolin, A. P., Bompolaki, D., Athirasala, A., Pfeifer, C. S., Ferracane, J. L. Bertassoni, L. E. (2018). 3d printed versus conventionally cured provisional crown and bridge dental materials. *Dental Materials*, 34(2), 192-200.
- [198] Di Prima, M., Coburn, J., Hwang, D., Kelly, J., Khairuzzaman, A., Ricles, L. (2016). Additively manufactured medical products—the FDA perspective. *3d Printing in Medicine*, 2(1), 1-6.
- [199] Everett, H. (2022). 3d printed Mybone maxillofacial graft approved for patient use in Europe, <https://3dprintingindustry.com/news/3d-printed-mybone-maxillofacial-graft-approved-for-patient-use-in-europe-211938/>, accessed on 03.05.2023.

- [200] Zema, L., Melocchi, A., Maroni, A., & Gazzaniga, A. (2017). Three-dimensional printing of medicinal products and the challenge of personalized therapy. *J Pharm Sci*, 106(7), 1697-1705.
- [201] Preis, M., Öblom, H. (2017). 3d-printed drugs for children—are we ready yet?. *AAPS PharmSciTech*, 18(2), 303-308.
- [202] Beer, N., Kaae, S., Genina, N., Sporrang, S. K., Alves, T. L., Hoeber, J., De Bruin, M. L., Hegger, I. (2023). Magistral Compounding with 3D Printing: A Promising Way to Achieve Personalized Medicine. *Therapeutic Innovation & Regulatory Science*, 57(1), 26-36.
- [203] Trenfield, S. J., Awad, A., Goyanes, A., Gaisford, S., Basit, A. W. (2018). 3D printing pharmaceuticals: drug development to frontline care. *Trends in Pharmacological Sciences*, 39(5), 440-451.
- [204] Souto, E. B., Campos, J. C., Filho, S. C., Teixeira, M. C., Martins-Gomes, C., Zielinska, A., Carbone, C., Silva, A. M. (2019). 3D printing in the design of pharmaceutical dosage forms. *Pharmaceutical Development and Technology*, 24(8), 1044-1053.
- [205] Wang, S., Chen, X., Han, X., Hong, X., Li, X., Zhang, H., Li, M., Wang, Z., Zheng, A. (2023). A Review of 3D Printing Technology in Pharmaceuticals: Technology and Applications, Now and Future. *Pharmaceutics*, 15(2), 416.
- [206] Mohammed, A. A., Algahtani, M. S., Ahmad, M. Z., Ahmad, J., Kotta, S. (2021). 3D printing in medicine: Technology overview and drug delivery applications. *Annals of 3D Printed Medicine*, 4, 100037.
- [207] Ragelle, H., Rahimian, S., Guzzi, E. A., Westenskow, P. D., Tibbitt, M. W., Schwach, G., Langer, R. (2021). Additive manufacturing in drug delivery: Innovative drug product design and opportunities for industrial application. *Advanced Drug Delivery Reviews*, 178, 113990.
- [208] Schrimpf, G. (2020). Merck and AMCM / EOS Cooperate in 3D Printing of Tablets. Press release. <https://www.merckgroup.com/en/news/3d-printing-of-tablets-27-02-2020.html>, accessed on 04.05.2023.
- [209] Evonik (2023). 3D-printed medications. Press release. https://elements.evonik.com/markets-and-regions/3d_printed_medication, accessed on 04.05.2023.
- [210] Petch, M. (2017). Scientists 3d print Parkinson's medicine for first time with UV inkjet 3d printing, <https://3dprintingindustry.com/news/scientists-3d-print-parkinsons-medicine-first-time-uv-inkjet-3d-printing-117695/>, accessed on 04.05.2023.
- [211] Henningsen, M., Stachwitz, P., Fahimi-Weber, S. (eds.), (2022). *Die digitale Arztpraxis: Technik, Tools und Tipps zur Umsetzung*. Medizinisch Wissenschaftliche Verlagsgesellschaft, Berlin.
- [212] Matai, I., Kaur, G., Seyedsalehi, A., McClinton, A., Laurencin, C. T. (2020). Progress in 3D bioprinting technology for tissue/organ regenerative engineering. *Biomaterials*, 226, 119536.
- [213] U.S. Food and Drug Administration (2017). FDA Guidance: Technical considerations for additive manufactured medical devices, Guidance for Industry and Food and Drug Administration Staff. <https://www.fda.gov/regulatory-information/search-fda-guidance-documents/technical-considerations-additive-manufactured-medical-devices>, accessed on 04.05.2023.

References

- [214] Aprelia Pharmaceuticals (2015). Aprelia online: FDA approves the first 3d printed drug product, <https://www.aprelia.com/news/fda-approves-the-first-3d-printed-drug-product>, accessed on 04.03.2023.
- [215] U.S. Food and Drug Administration (2019). FDA online: Abbreviated Approval Pathways for Drug Product: 505(b)(2) or ANDA? <https://www.fda.gov/drugs/cder-small-business-industry-assistance-sbia/abbreviated-approval-pathways-drug-product-505b2-or-anda>, accessed on 04.03.2023.
- [216] U.S. Food and Drug Administration (2017). FDA online: CDER Researchers Explore the Promise and Potential of 3D Printed Pharmaceuticals, <https://www.fda.gov/drugs/news-events-human-drugs/cder-researchers-explore-promise-and-potential-3d-printed-pharmaceuticals>, accessed on 04.03.2023.
- [217] Norman, J., Madurawe, R. D., Moore, C. M., Khan, M. A., Khairuzzaman, A. (2017). A new chapter in pharmaceutical manufacturing: 3d-printed drug products. *Advanced Drug Delivery Reviews*, 108, 39-50.
- [218] Lepowsky, E., Tasoglu, S. (2018). 3d printing for drug manufacturing: A perspective on the future of pharmaceuticals. *International Journal of Bioprinting*, 4(1).

2 Filament Intermediates for Pharmaceutical FDM 3d Printing

2.1 Quality of FDM 3d Printed Medicines for Pediatrics: Considerations for Formulation Development, Filament Extrusion, Printing Process and Printer Design

Evaluation of authorship:

author	idea [%]	study design [%]	experimental [%]	evaluation [%]	manuscript [%]
Julian Quodbach	12.5	5.9	0	5.9	15
Malte Bogdahn	5	5.9	0	5.9	5
Jörg Breitzkreutz	5	5.9	0	5.9	5
Rebecca Chamberlain	5	5.9	100	5.9	5
Karin Eggenreich	5	5.9	0	5.9	5
Alessandro-Guisepe Elia	5	5.9	0	5.9	5
Nadine Gottschalk	5	5.9	0	5.9	5
Gesine Gunkel-Grabole	5	5.9	0	5.9	5
Lena Hoffmann	5	5.9	0	5.9	5
Dnyaneshwar Kapote	5	5.9	0	5.9	5
Thomas Kipping	5	5.9	0	5.9	5
Stefan Klinken	5	5.9	0	5.9	5
Fabian Loose	5	5.9	0	5.9	5
Tristan Marquetant	5	5.9	0	5.9	5
Hellen Windolf	5	5.9	0	5.9	5
Simon Geißler	12.5	5.9	0	5.9	5
Tilman Spitz	5	5.9	0	5.9	10

Evaluation of Copyright permission:

This article is licensed under a Creative Commons Attribution 4.0 International License, which permits use, sharing, adaptation, distribution and reproduction in any medium or format, as long as you give appropriate credit to the original author(s) and the source, provide a link to the Creative Commons licence, and indicate if changes were made. The images or other third party material in this article are included in the article's Creative Commons licence, unless indicated otherwise in a

Quality of FDM 3d Printed Medicines for Pediatrics: Considerations for Formulation Development, Filament Extrusion, Printing Process and Printer Design

credit line to the material. If material is not included in the article's Creative Commons licence and your intended use is not permitted by statutory regulation or exceeds the permitted use, you will need to obtain permission directly from the copyright holder. To view a copy of this licence, visit <http://creativecommons.org/licenses/by/4.0/>.

Quality of FDM 3d Printed Medicines for Pediatrics: Considerations for Formulation Development, Filament Extrusion, Printing Process and Printer Design

Julian Quodbach¹, Malte Bogdahn², Jörg Breitzkreutz¹, Rebecca Chamberlain¹, Karin Eggenreich⁴, Alessandro Giuseppe Elia³, Nadine Gottschalk², Gesine Gunkel-Grabole³, Lena Hoffmann¹, Dnyaneshwar Kapote⁴, Thomas Kipping³, Stefan Klinken¹, Fabian Loose⁵, Tristan Marquetant³, Hellen Windolf¹, Simon Geißler², Tilmann Spitz⁵

¹*Institute of Pharmaceutics and Biopharmaceutics, Heinrich Heine University, Universitätsstrasse 1, 40225 Duesseldorf, Germany*

²*Merck Healthcare KGaA, Frankfurter Str. 250, Darmstadt, Germany*

³*Merck Life Science KGaA, Frankfurter Str. 250, Darmstadt, Germany*

⁴*Gen-Plus GmbH & Co. KG, Stafelseestr. 6, München, Germany*

⁵*Laboratory for Manufacturing Systems, University of Applied Sciences Cologne, Betzdorfer Str. 2, 50679 Cologne, Germany*

Therapeutic Innovation & Regulatory Science

<https://doi.org/10.1007/s43441-021-00354-0>



Quality of FDM 3D Printed Medicines for Pediatrics: Considerations for Formulation Development, Filament Extrusion, Printing Process and Printer Design

Julian Quodbach¹ · Malte Bogdahn² · Jörg Breitzkreutz¹ · Rebecca Chamberlain¹ · Karin Eggenreich⁴ · Alessandro Giuseppe Elia³ · Nadine Gottschalk² · Gesine Gunkel-Grabole³ · Lena Hoffmann¹ · Dnyaneshwar Kapote⁴ · Thomas Kipping³ · Stefan Klinken¹ · Fabian Loose⁵ · Tristan Marquetant³ · Hellen Windolf¹ · Simon Geißler² · Tilmann Spitz⁵

Received: 1 October 2021 / Accepted: 4 November 2021 / Published online: 26 November 2021
© The Author(s) 2021

Abstract

3d printing is capable of providing dose individualization for pediatric medicines and translating the precision medicine approach into practical application. In pediatrics, dose individualization and preparation of small dosage forms is a requirement for successful therapy, which is frequently not possible due to the lack of suitable dosage forms. For precision medicine, individual characteristics of patients are considered for the selection of the best possible API in the most suitable dose with the most effective release profile to improve therapeutic outcome. 3d printing is inherently suitable for manufacturing of individualized medicines with varying dosages, sizes, release profiles and drug combinations in small batch sizes, which cannot be manufactured with traditional technologies. However, understanding of critical quality attributes and process parameters still needs to be significantly improved for this new technology. To ensure health and safety of patients, cleaning and process validation needs to be established. Additionally, adequate analytical methods for the in-process control of intermediates, regarding their printability as well as control of the final 3d printed tablets considering any risk of this new technology will be required. The PolyPrint consortium is actively working on developing novel polymers for fused deposition modeling (FDM) 3d printing, filament formulation and manufacturing development as well as optimization of the printing process, and the design of a GMP-capable FDM 3d printer. In this manuscript, the consortium shares its views on quality aspects and measures for 3d printing from drug-loaded filaments, including formulation development, the printing process, and the printed dosage forms. Additionally, engineering approaches for quality assurance during the printing process and for the final dosage form will be presented together with considerations for a GMP-capable printer design.

Introduction

The general principle of pharmaceutical 3d printing, or additive manufacturing, renders this approach a promising candidate for the automated manufacturing of solid pediatric medicines [1]. Solid medicines have significant benefits over the use of liquids for the treatment of children. They provide a high microbial stability, good chemical and physical stability, enable controlled release properties and demonstrate high dosing accuracy [2]. With common manufacturing approaches, dosages can be varied only incrementally in certain ranges. 3d printing enables manufacturing of medicines with precise and fully variable dosing. Dosage forms are printed layer-by-layer in a shape predefined in a computer aided design (CAD) software. In theory, every imaginable size and shape can be printed. A

✉ Julian Quodbach
julian.quodbach@hhu.de

¹ Institute of Pharmaceutics and Biopharmaceutics, Heinrich Heine University Düsseldorf, Universitätsstr. 1, 40225 Düsseldorf, Germany

² Merck Healthcare KGaA, Frankfurter Str. 250, Darmstadt, Germany

³ Merck Life Science KGaA, Frankfurter Str. 250, Darmstadt, Germany

⁴ Gen-Plus GmbH & Co. KG, Staffelseestr. 6, München, Germany

⁵ Laboratory for Manufacturing Systems, University of Applied Sciences Cologne, Betzdorfer Str. 2, 50679 Cologne, Germany

direct consequence of this approach is the ability to modify the dosage simply and conveniently, a lack of which is widely recognized as a major hurdle in pediatric therapy [3]. Besides the inherently possible size adaption, which is key to improve acceptability [4], 3d printing techniques also allow the manufacturing of small batches down to a single individual dosage form for a given patient.

While several 3d printing techniques exist and are investigated for pharmaceutical use [5], *fused deposition modeling* (FDM) emerges as one of the most interesting technologies for the manufacturing of pediatric medicines. In FDM, filaments, drug-loaded polymer wires, are fed into the printhead of the 3d printer. In the printhead, the filament is heated and extruded through a nozzle on a temperature-controlled print bed. A kinematic system allows movement of the printhead in *x*-, *y*-, and *z*-direction respective to the printhead, enabling the layer-wise deposition of the polymer-drug matrix until the dosage form is printed. Filaments are manufactured in a hot-melt extrusion (HME) step, which has to be performed industrially due to the required equipment, environment, and process understanding. This results in two main advantages. Firstly, a properly developed formulation and hot-melt extrusion process result in a high-quality intermediate that undergoes proper quality testing. Secondly, the active pharmaceutical ingredient (API) is bound in a polymer matrix within the filament, significantly reducing the risk of drug exposure for the professional operating the printer. The combination of these advantages makes FDM the most promising candidate for manufacturing of (pediatric) medicines also in decentralized settings, e.g., hospitals, compounding centers and community pharmacies. Other technologies require either the manufacturing of aqueous intermediates that cannot be prepared easily industrially due to the risk of contamination during storage [6] or the handling of powders in the final printing step, e.g., binder jetting and selective laser sintering [5], which bears a high risk of operator exposure. If a semi-solid formulation is prepared in decentralized settings, proper quality control of the API distribution within the semi-solid and printed dosage forms requires significant analytical effort that cannot be performed for individual batches.

While many publications cover proof-of-concept studies of novel dosage form designs and approaches to formulation and process development [7, 8] quality consideration of excipients, formulations, processes, filaments and medicines are frequently mentioned but rarely formalized. This lack was recognized by the United States Pharmacopeia (USP) and the International Association for Pharmaceutical Technology (APV) who co-organized a 4-day workshop on quality and standards considerations of 3d printed medicines (Homepage workshop). Even though quality aspects are mentioned for dosage forms for adult drug therapy, no

publications about the quality of pediatric 3d printing are available until now.

This publication aims to remedy this issue. The authors are members of the PolyPrint project [9] a project funded by the German Federal Ministry of Education and Research (BMBF). The project consortium exists of the companies Merck KGaA and Gen-Plus, the Laboratory for Manufacturing Systems of the University of Applied Sciences Cologne and the Institute of Pharmaceutics and Biopharmaceutics at Heinrich Heine University Düsseldorf. In the project, novel polymers for pharmaceutical FDM 3d printing are developed and thoroughly tested and benchmarked. Additionally, a novel type of FDM printer is developed to enable high-quality and cGMP compliant 3d printing of medicines. Here, we reflect on the status of the complete manufacturing process of 3d printed pediatric medicines beginning with the raw materials and ending with the final dosage form. We highlight existing shortcomings and provide guidance based on the experience gathered in the PolyPrint project.

Key Attributes of Raw Materials

Quality Aspects of Pharmaceutical Excipients

Pediatric formulation developments are obliged to follow the guidance of the EMA ensuring the overarching goal: “The development of pediatric formulations and presentations is necessary to ensure that children of all ages and their caregivers have access to safe and accurate dosage forms of medicines.” [10]

More detailed information is provided in the “Guideline on pharmaceutical development of medicines for pediatric use” [11]. In general, solid oral dosage forms such as tablets and capsules can offer advantages of greater stability, accuracy of dosing and improved portability over liquid formulations. To assure suitable swallowability the size of tablets and capsules should be kept as small as possible [2].

The choice of excipients plays an important role in pediatric formulation development, both for safety and acceptability of the resulting dosage forms. The physiology of neonates and infants differs considerably from that of adults. They exhibit significantly different clearance and volume of distribution as well as differences in the metabolic profile [12]. Prominent excipient examples for the resulting challenges and issues are propylene glycol or sorbitol in infants. Also, polyethylene glycol (PEG)—a useful additive for filament plasticity and solubility enhancement—needs careful consideration regarding maximum intake. While studies confirm safe use of, e.g., PEG 3350–4000 as laxative, undesired laxative effects and potential gastrointestinal disorders limit the use of PEG to 10 mg/kg/d [13].

Looking at FDM based 3d printed formulations, usually the polymer makes up more than 50% of the formulation. Given the comparatively high intake of these excipients, the safety of polymers and additives (glidants, plasticizers) in pediatric formulations is a very important factor, especially if (partial) degradation of the polymer in the gastrointestinal tract (GIT) is to be expected. Therefore, not only polymer but also degradants and synthesis constituents of the polymer need to be carefully integrated into the safety assessment for pediatric medications. To date, several pharmaceutical polymers, such as methacrylates and ethylcellulose, are commercialized in pediatric products. Unfortunately, most polymers are used in comparatively low amounts as coating agents for taste masking and release modification [14]. Little information is available for polymers used as matrix agent and related high daily intake. Although observed adverse reactions from coated formulations might be used to prevent further incompatibilities, the maximum acceptable intake for children is critical and not easily derived from toxicological studies performed in adults. An important tool for assessing the safety of relevant excipients is the STEP database (Safety and Toxicity of Excipients for Pediatrics) [15].

In addition to safety, the taste sensation of excipients needs to be carefully considered. Polymers and additives should be taste- and odorless and ideally offer opportunities for obscuration of taste (see subsection on taste masking).

The important decision factors affecting the use of excipients are summarized by Yochana et al.: “Excipients for pediatric formulations should be carefully selected with reference to the age of the pediatric population, ADME developmental changes, and duration of treatment to ensure safety and efficacy of such formulations in pediatric population.” [16]

Polymer Requirements—Limitations in FDM

In recent years, the application of thermoplastic polymers in pharmaceutical development of 3d printed products via FDM has gained increasing interest. A multitude of different material requirements need to be fulfilled by the polymer for these applications, as illustrated in Fig. 1 (further details on these parameters can be found in the supplementary information in Table S1). Here, we summarized relevant properties and parameters, which influence the suitability of given polymers or APIs, respectively. For an overview of different polymer families and a selection of marketed products in the field of hot-melt extrusion, the reader is referred to Simoes et al. [17, 18]. 3d printing using the FDM technique requires further polymer prerequisites [19] in addition to the parameters important in HME development, which typically depend

on the product properties and the utilized API. During an FDM 3d printing process, the polymeric filament is subject to significant mechanical forces. A specific mechanical profile is required due to “pinching” of these filaments between two feeding gears in the printhead. Filaments carrying a high Young’s modulus ($> 300 \text{ N/mm}^2$, depending on printhead) can be conveyed without breakage or deformation [20, 21]. At the same time, the tensile strength and the brittleness of the extrudates are crucial parameters for successful printing [19, 21–28]. The latter of which may be assessed using the three-point bending test (breaking distance $> 1\text{--}1.5 \text{ mm}$ [21, 22] and breaking stress $> 2941\text{--}3126 \text{ g/mm}^2$ [22]). Nasereddin et al. evaluated a selection of the most commonly used polymers in FDM and developed a screening method to assess their brittleness including these parameters and thus evaluate printability [24].

Taste Masking

Taste is an important sensation to be considered in pharmaceutical development. Taste aversiveness might impact patients’ compliance and medication adherence. Sensory components of both the olfactory and the gustatory sensations have to be distinguished. Whereas substances which should develop the smell as an olfactory signal need to be volatile under the conditions of drug administration, the gustatory system is directly based on the tongue comprising different types of taste buds and papillae where the sensory receptors and ion channels for salty, sour, sweet, bitter, and umami taste are located. Depending on the properties of the poorly tasting components, various taste-masking techniques are available [14]. In pharmaceutical printing technologies, most of the proposed taste-masking approaches can be applied although scientific papers or patents are scarce:

- (a) One obvious approach is to mask the unpleasant taste of a printed object by the addition of differently tasting excipients, e.g., sweet carbohydrates (sucrose, fructose, glucose), sugar alcohols (mannitol, xylitol, sorbitol) or artificial sweeteners (saccharine, aspartame, cyclamate or acesulfame). An olfactory signal can be added to the printing formulation using volatile substances such as menthol or more complex organic or synthetic flavors [29]. However, it should be noted that one or more components of these mixtures will partly evaporate during the manufacturing and over storage time changing taste sensation as a key property to be controlled in stability studies.
- (b) Unpleasant tasting ingredients can be physically bound within inclusion complexes, e.g., by use of cyclo-

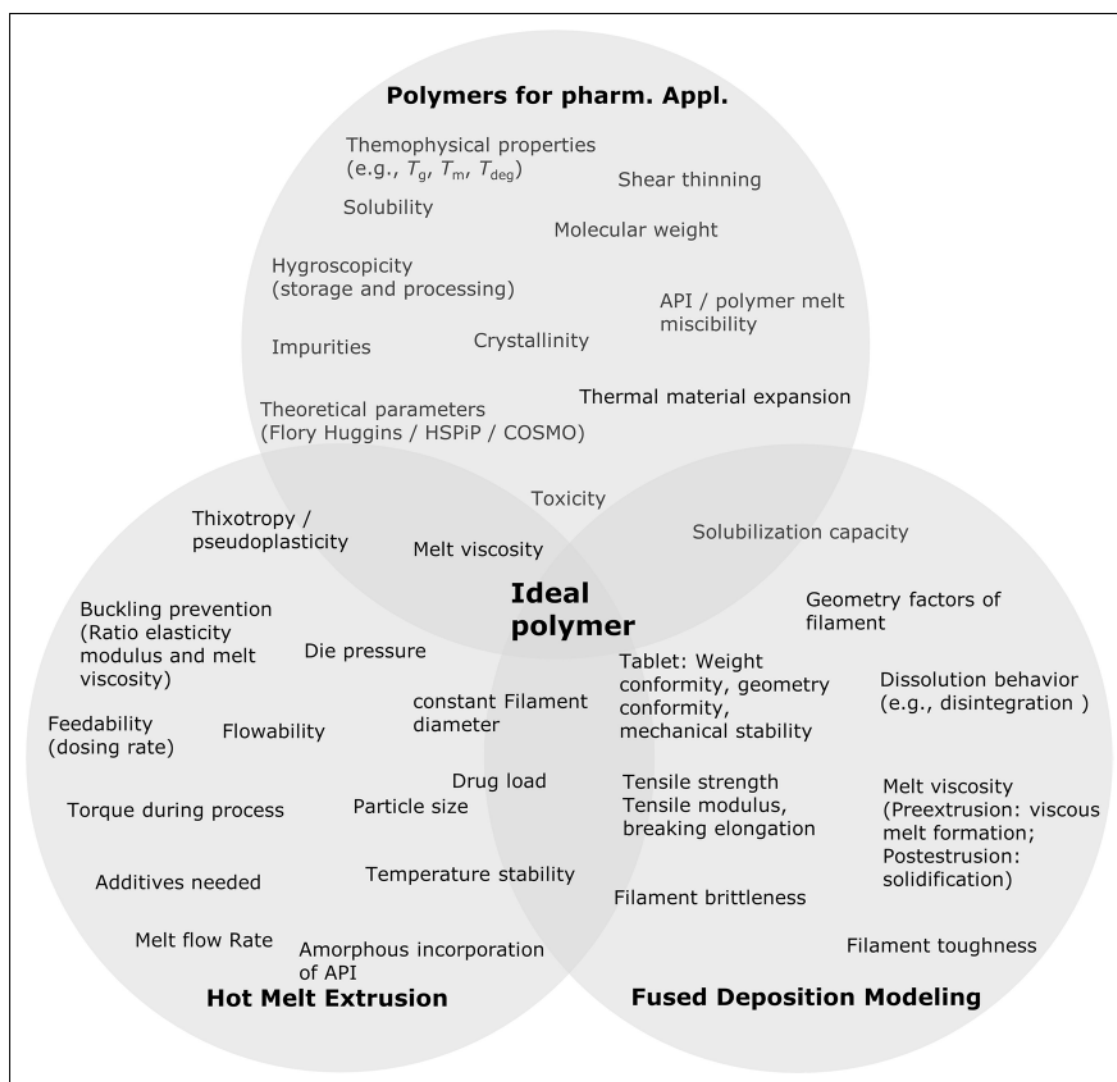


Figure 1 Selection of Parameters That are Relevant for Pharmaceutical Application of Polymers, Particularly in HME and FDM.

dextrins, or to polyelectrolytes (anionic or cationic polymers) which can also be part of the solid matrix. Entrapping by the printed polymers may be sufficient for taste masking of bitter compounds [30, 31].

- (c) High viscosity hydrophilic polymers may prevent fast hydration and dissolution of the dosage form, thereby reducing the migration to the taste receptors on the tongue and the resulting taste sensation.
- (d) Barriers inside or outside the printed dosage form may shield against quick dissolution and saliva contact.

The taste-masking effect of the applied pharmaceutical measures are usually demonstrated by using advanced dissolution setups [30] or electronic tongues in vitro [32], and human taste panels [31] or animal experiments like the BATA (brief-access taste aversion) model in vivo [33].

Hot-Melt Extrusion of Intermediates for Pediatric 3d Printing

Filament Extrusion—a Question of Homogeneity

The filament required for FDM 3d printing is generated as endless strand via twin-screw hot-melt extrusion. Filament extrusion comprises multiple individual unit operations and processes that must be considered to obtain an overview of relevant quality attributes. To meet quality attributes of products and establish robust processes, the Food and Drug Administration (FDA) recommends quality-by-design (QbD) approaches for formulation and process development [34]. This led to different implementations of QbD in pharmaceutical melt extrusion processes [34–36]. As mentioned in the section on polymer requirements, the mechanical properties

of filaments must allow proper feeding and extrusion from the printhead. Additionally, diameter homogeneity and API distribution are much more important compared to regular hot-melt extrusion processes. Usually, the obtained extrudate is milled or pelletized and a subsequent homogenization of the individual particles is performed. In FDM, the filament is commonly kept intact and printed as it exited the extrusion die. This means that diameter and API distribution inhomogeneities directly reflect in the printed amount of filament and API. This can be an issue for regularly sized dosage forms [37] and even more so for pediatric medicines of lower dose and mass. In this case, even small variations of diameter and API distribution can lead to non-compliance with monographs on the uniformity of dosage units and must be avoided. The API distribution is influenced primarily by the powder feeding process and hot-melt extrusion, the diameter homogeneity by the hot-melt extrusion process.

Powder Feeding

In twin-screw filament extrusion processes feeding of polymers, solid additives and APIs is a critical aspect. Unlike single-screw extruders, twin-screw extruders are run partially filled. Thus, the material flow inside the extruder depends on the flow rate of the feeder used. Process parameters like the specific feed load (SFL) and residence time distribution (RTD) are directly influenced by the feeding [38]. In Fig. 2 left, a typical residence time distribution curve of a filament extrusion process is shown. On the right, feeding fluctuations are shown in black and the resulting output fluctuations after extrusion are shown in red. The reduction in fluctuations demonstrates the mixing and homogenizing abilities of extruders. As the reduction is not absolute, feeding should be as homogeneous as possible, to reduce output variations.

Several types of dispensing devices are available for feeding bulk solids. Vibrating trays or screws are a widespread method of conveying the material [39]. Simple devices feed

in volumetric mode at a constant actuating variable. In contrast, loss-in-weight or gravimetric feeders are equipped with an integrated load cell that detects fluctuations in the feed rate. The actuating variable is adjusted via a control mechanism, leading to a compensation of fluctuations [40]. Material properties as well as the target feed rate must be considered in selection of the most suitable dosing device [41]. Low dosing rates and poor flow properties result in particularly high demands on equipment attributes [42]. Matarazzo et al. has provided a checklist to assist in the selection of proper feeder equipment [43].

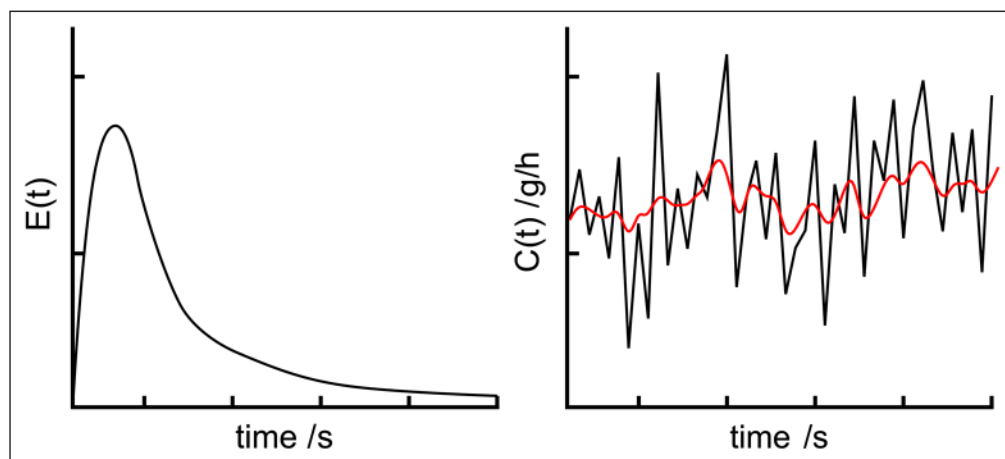
Bulk solid feed is evaluated in several studies usually by using an external scale where the fed material is collected. Data analysis of the dosing curve or its integral can be conducted using statistic parameters like measure of dispersion or target-actual-ratio of moving measures of central tendency [44, 45]. Another way is using discrete Fourier transform of dosing fluctuations, which provides information about the materials dosed [46].

Extruding Filaments as Intermediates

The efficiency of the melting process of polymers in HME depends on the properties of the excipients and the extruder design. In general, polymers with low melt viscosities and high thermal conductivities exhibit a more efficient melting process. Changes in the screw design are often necessary to improve the melting process of the powders and to improve mass flow of the melt through the extruder. Otherwise, solid material may block the screws transiently, which can result in increased torque if the melting process is incomplete.

Ponsar et al. highlighted the effect of the extruder barrel fill level on filament homogeneity. The higher the fill level, the lower are the fluctuation of the mean diameter (Fig. 3 left) [37]. Frequently, as diameter fluctuations are not necessarily normal distributed, the inter quartile range of the diameter is used to describe fluctuations. Besides having

Figure 2 Exemplary Drawing of: (left) a Typical Residence Time Distribution Function of a Hot-Melt Extrusion Process; (right) Fluctuations of the Feed Rate (Black) and Output Fluctuations After Extruder (Red).



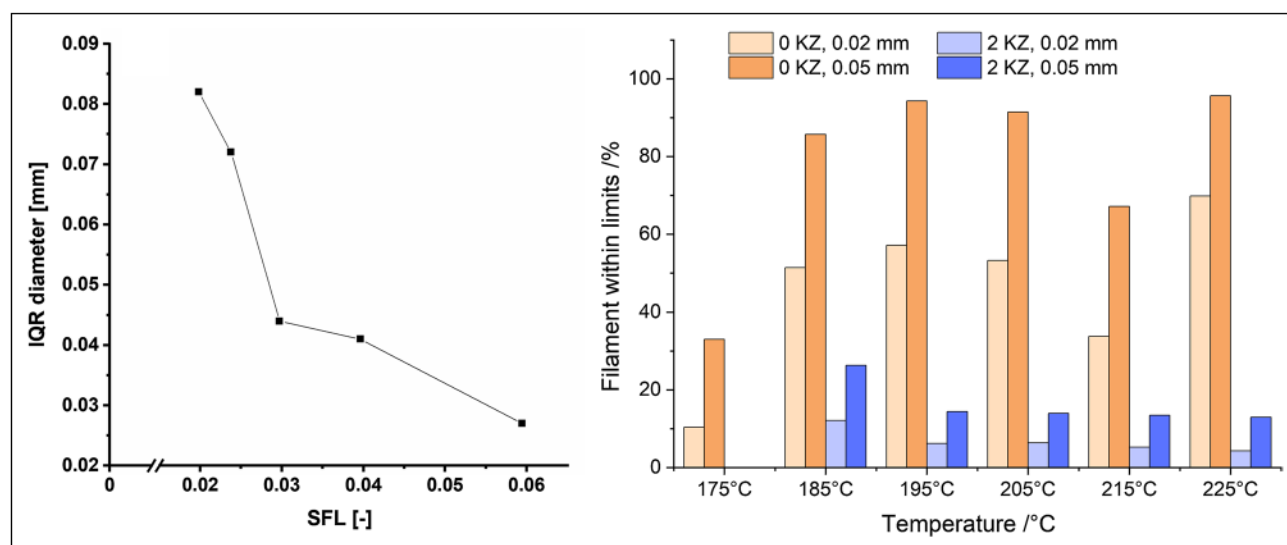


Figure 3 (Left) Interquartile Ranges of Diameter Measurements During Extrusion Correlated with SFL of the Extrusion Process [37], (Right) Amount of Filament Within ± 0.02 and 0.05 mm Specification

a measure for fluctuations, it is as important to set limitations for said variations. Usually, deviations of ± 0.02 mm or 0.05 mm from the set value are considered tolerable. By varying the temperature, the polymers, the process setting and the screw configuration in an extruder, the limits are met with varying degrees of success. In Fig. 3 right, the same formulation was extruded at different temperatures and with different screw designs (no kneading zones or two kneading zones). The best batch was extruded at a high temperature of 225°C with no kneading zone and the worst at the same temperature with two kneading zones. These data show the decrease of filament diameter within the ± 0.02 mm or 0.05 mm specification when adding two kneading zones. This observation indicates the importance of a continuous melt flow in the extruder, which is better provided by a screw configuration of only conveying elements. When adding kneading elements, the melt is retained before the kneading zones until enough pressure is build up by the following melt. To increase the homogeneity of the filament diameter further, a melt pump can be attached between the end of the extruder barrel and the die. The purpose of this attachment is to stabilize inevitable melt fluctuations that occur within the hot-melt extrusion process. The pump aligns those fluctuations by metering the melt flow to a very constant rate and therefore a very constant pressure level [47]. This leads to an increase of filament homogeneity since the fluctuations mentioned before are reduced drastically. This was shown by in-process monitoring of filament diameters [48].

After extrusion, it must be considered how to properly cool down the obtained filament. Commercial FDM filaments such as acrylonitrile butadiene styrene copolymer

With or Without Two Kneading Zones (KZ 1: $4 \times 90^{\circ}, 4 \times 60^{\circ}, 2 \times 30^{\circ}$, KZ 2: $8 \times 60^{\circ}$, Unpublished Data).

(ABS) or polyether ether ketone (PEEK) are not water soluble and can therefore be cooled down in a water bath. Polymers for pharmaceutical FDM applications are frequently at least partially water soluble and they contain one or more APIs. Consequently, cooling in a water bath cannot be performed, even though it is a highly effective and efficient cooling process. For pharmaceutical applications, proper cooling can be achieved by either passive cooling on a conveyor belt at atmospheric conditions or by using an air ring or air tunnel [49].

While polymer melt is being pushed out of the nozzle, a phenomenon can occur known in HME as “die swell”. Die swell is the expansion of molten polymer to a larger diameter than determined by the die itself, resulting in a filament thicker than desired. This effect is mainly related to the energy preserved by compression and force alignment of polymer chains being forced through the die, followed by the relaxation of those chains when exiting the die again [50]. The viscoelastic behavior of the melt as well as process parameters are major factors when die swell shall be reduced [37, 51]. A reduction of die swell can be achieved by increasing the temperature at the die. Even with thorough optimization, a larger mean diameter than desired will frequently result. To further adjust the mean diameter after extrusion, a pulling unit, e.g., a conveyor belt or the haul-off unit of a winder [37] can be implemented. The speed of haul-off units is variable and defines the final mean diameter of the filament, which can be wound or used as individual strands. Commercial filament diameters are typically 1.75 or 2.85 mm. For pharmaceutical purposes, a lower diameter is beneficial,

as potential inhomogeneities of diameter and content will have less of an impact relatively.

In Fig. 4, two prototype extrusion lines are shown. They consist of gravimetric powder feeders, twin-screw hot-melt extruders, cooling units (conveyor belt or cooling line with ring air-knives), laser-based diameter measurement system and optionally a filament winder.

Characterization of Filaments

To evaluate, optimize and monitor the process of filament production, different analytical tools can be used off-line and in-line.

Off-line Characterization

A simple and useful approach is the visual assessment of API-loaded filaments. This way, it is frequently possible to initially assess potential degradation via color changes and possible recrystallization of the active ingredient(s) especially for higher drug loadings and APIs that exhibit thermal sensitivity. As already discussed in the section on polymer requirements, the mechanical properties of filaments are an important factor for the feedability of the formulation that must be analyzed. The mechanical properties of filaments may change over time due to enthalpy relaxation [21] or because the included excipients are hygroscopic. Water

absorbed during processing or storage is a powerful plasticizer that lowers the glass transition temperature. It does not only affect the mechanical properties and appearance, but also drug stability, may induce degradation, and needs to be quantified for this reason [52, 53]. In vitro dissolution as per compendial monographs is used to determine the amount of drug dissolved over time and thereby to assess the performance of the formulation (filament/tablet) in regard to release behavior [54]. For the content determination and examination of homogeneous drug distribution as well as characterization of related substances within filaments and tablets, most frequently HPLC analysis is used [55].

In-line Characterization of Filaments via PAT

The physicochemical properties of filaments produced by HME are crucial for the 3d printing process. Quality and performance of the 3d printed tablet can be examined with PAT tools like spectroscopy, rheometry and optical coherence tomography (OCT) [56]. These tools enable capturing real-time information of process and filament properties during HME non-destructively. Some of the data can be easy to interpret, e.g., diameter and sphericity of filaments determined via multi-axes laser scanning modules (see Fig. 4). Some can be difficult to interpret and may require the preparation of multivariate, quantitative models, for example spectral information. Independent

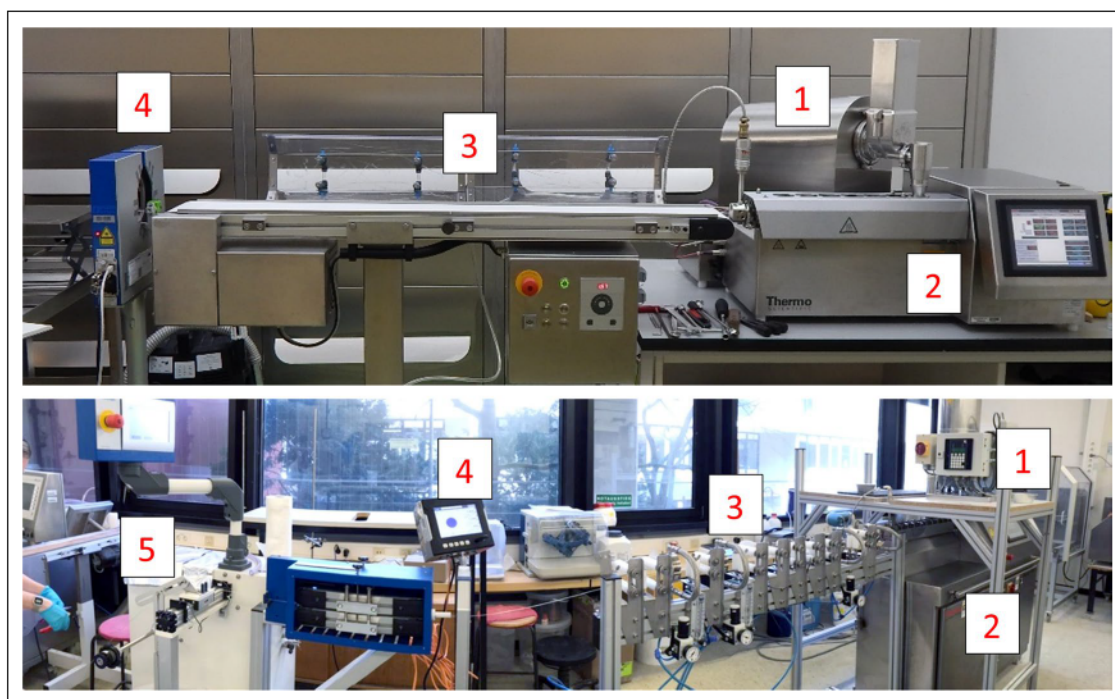


Figure 4 Two Filament Production Lines. (1) Gravimetric Feeders, (2) Twin-Screw Extruders, (3) Cooling via Conveyor Belt (Top) and Ring Air-Knives (Bottom), (4) Three-Axis Laser Micrometers, (5) Winding Unit.

of the data complexity, it can be utilized to monitor the process and initiate corrective actions to reach a desired state and potentially to allow real-time release [57]. In the following, relevant technologies are listed.

In-line Spectroscopy

UV–vis spectroscopy has been used and established as PAT tool in HME. Spoerk et al. used in-line UV–vis spectroscopy as an analytical tool for characterizing of active ingredients (Estradiol, Estriol, Ibuprofen) and polymer matrices (ethylene vinyl acetate, Eudragit RL-PO). The studies focused on the quantification of the drug for cleaning-in-place strategies [58]. Wesholowski et al. have investigated in-line UV–vis spectroscopy as a PAT tool for preparing solid dispersions of two APIs (carbamazepine and theophylline) with one polymer (copovidone) [59]. The obtained results revealed the suitability of the implemented tool to quantify the drug load in a typical range for pharmaceutical applications. The range of linearity differed with different formulation and was 5–30% for carbamazepine, whereas that for the theophylline formulations was 2.5–10%. They reported that the efforts to evaluate data was minimal due to univariate data analysis and in combination with a measurement frequency of 1 Hz, the system is sufficient for the real-time data acquisition. In-line near infrared (NIR) spectroscopy has also been used to investigate drug–polymer interactions and to validate a method for continuous API quantification during HME processing [60]. Vo et al. demonstrated the use of Fourier transform NIR spectroscopy in conjunction with multivariate analysis (MVA) for in-line API concentration monitoring during a HME process [61]. In this study, they used ketoprofen as model drug, Eudragit L100-55 as matrix polymer and stearic acid as processing aid. A principal component analysis (PCA) model was used to monitor the process state shift in response to disturbances of parameters, such as temperature and material feed rate. Thus, an NIR based quality monitoring methodology can be easily transferred from process development to manufacturing. Saerens et al. evaluated the suitability of Raman spectroscopy as PAT tool for the in-line determination of API concentration and the polymer-drug solid state during HME process [60]. They used different concentration of metoprolol tartrate (10%, 20%, 30%, and 40%) with Eudragit RL-PO mixtures, which were extruded and monitored in-line in the die using Raman spectroscopy. A PLS model was developed and validated, which allowed the real-time API concentration determination. They also investigated application of Raman spectroscopy in solid-state characterization and found that the mixtures containing solid

solution showed broadened Raman peak compared with the solid dispersion.

In-line Rheometry

In-line measurements of the rheological characteristics play an important role in real-time monitoring of torque, influence of drug load, and effect of formulation ingredients on the process. The real-time evaluation of rheology data in the extrusion process can be determined by pressure drop inside an extruder die connected to suitable instruments. In-line rheological characterization can enhance process control and understanding [62].

Optical Coherence Tomography (OCT)

OCT, a non-invasive method, is used as an off-line tool for semi-transparent and turbid media. It can be applied to measure parameters such as surface properties of filaments and layer thicknesses, e.g., of coating layers or filaments produced in hot-melt co-extrusion, and uniformity [63]. Koutsamanis and Eggenreich et al. reported the application of OCT to evaluate the integrity of the core/membrane interface and membrane thickness of vacuum compression molding formulations containing progesterone with ethylene vinyl acetate polymer [64].

Characterization of the Solid State

Even though some of the above-mentioned analytical tools can determine certain aspects of solid-state properties, other approaches are commonly used that provide a better understanding of materials. The solid state of an API incorporated in a polymer matrix can have a large impact on the performance of the final dosage form in terms of dissolution rate and bioavailability [65]. Poorly soluble APIs, which make up a large proportion of potential drug candidates [66], can be formulated as amorphous solid dispersions (ASD) where the crystalline structure of the API is broken up and the resulting molecular dispersions are stabilized by a polymer matrix. In contrast, an API can also be incorporated in filaments maintaining a crystalline structure [67, 68]. The presence or absence of crystalline structures strongly influences printability, such as mechanical [69] and rheological properties of filaments [70]. Consequently, the assessment of crystallinity in filaments is important in process development, quality control and stability studies. Even though this assessment can be supported by in-line measurements, traditional techniques are more widespread.

The formation and stability of the ASD is influenced by solubility and miscibility of the API and the polymer matrix [71]. Thermal and mechanical energy uptake during manufacturing facilitates the dispersion and reduces

the number and size of crystal nuclei, which may lead to premature precipitation of API in vivo or reduce physical stability during storage. To maintain the solid state during shipment and storage is important for the ASD itself, but for FDM the second heating cycle during printing needs to be considered, additionally. The thermal impact may not only impair the chemical stability of the formulation but can also lead to recrystallisation of API [28].

Several techniques can be applied to determine the solid state. Differential scanning calorimetry (DSC) as well as well as X-ray powder diffraction (XRPD) are well-established analytical methods to investigate the solid state of API dispersed in polymer matrices [72]. One caveat is the limit of detection of crystalline fractions in mostly amorphous systems [73]. The detection of small traces of crystalline fraction is possible by the use of polarized light microscopy [74]. However, this method lacks quantitative determination and selectivity.

In regard to the assessment of crystallinity in intermediate and final product the manufacturing process should be considered end to end for FDM printed solid dosage forms.

FDM Printing at Site of Care—Stricter Requirements for Dosing Precision and Quality Control

3d printing based on FDM has been state of the art for years and is used primarily in the consumer sector but also in industrial environments. Particularly in industry, a quality demand is placed on the products to be printed from the ground up. Unlike in pharmaceutical industry, however, the focus is primarily on geometric aspects.

Different consumer 3d printers are already being used in pharmaceutical research. One of several issues with off-the-shelf printers is that the amount of active ingredient processed cannot be verified. Thus, the quality of the pharmaceutical products is not verifiable. In contrast to classical manufacturing methods, 3d manufacturing is slow and only few dosage forms are printed [5]. Therefore, destructive quality control approaches are not profitable and in-line testing is unavoidable. Furthermore, there is hardly any system on the market that meets the cleaning requirements of pharmaceutical equipment [75].

In addition to the common requirements of mechanical engineering for the development and market placement of production machines, special requirements are part of the GMP guidelines [76]. For these reasons, it is imperative to rethink 3d printer design and adapt it to the needs of pharmaceutical manufacturing. The following sections highlight some of the most critical components.

Motion System and Overall Printer Design

The most common design in FDM 3d printing is the Cartesian printer, but other forms like the delta printer and the polar printer exist [77]. Cartesian printers operate by linear movement of the printhead in x-, y-, and z-direction respective to the print bed. In most cases, the axes, motors, and drives are designed for general industrial and mechanical engineering purposes and the requirements of the pharmaceutical industry are not considered. For example, many of the moving parts, which are usually lubricated, are not encapsulated and are, therefore, exposed to potential contaminants from filament and product. Since it is required for pharmaceutical production that all surfaces in contact with the product are cleanable, these elements do not meet the GMP standard [78].

During the development of new machines all requirements for the system need to be defined beforehand. In addition to the basic functions for a 3d printer almost all machines are designed to be as compact and as inexpensive as possible. To achieve this, many functions are implemented in a small space. When looking at existing printing systems under the prerequisites of the GMP guideline, several problems become apparent. In regular 3d printing systems, all subsystems such as material handling, material processing, build plate, and motions system are implemented openly in a very confined space. For a GMP-compliant implementation, however, it is recommended to separate all elements and to design individual and well controlled areas (Fig. 5).

For industrial and non-pharmaceutical applications, the print chamber usually does not have to be kept particle-free or sanitized. Axis systems for moving print head or print bed can be placed directly in the printing space. Since outgassing, particle detachment and other sources for (cross-) contamination must be contained or avoided during the print job, this arrangement is not applicable for GMP printers. The printing chamber should be as isolated as possible from all moving elements. In addition, surfaces should not have complex geometries or sharp angles to ensure cleanability.

In addition to the risk of contamination of the printer parts, attention must also be paid to the safety of the operator. During the processing of APIs, the user may be exposed to harmful chemicals. For example, in the case of outgassing, it must be ensured that substances cannot endanger the user. For this purpose, the printer should be equipped with appropriate protective devices such as air filters. In the pharmaceutical sector, little research has been done on the possible safety aspects of using 3d printing for the manufacture of pharmaceutical products [78].

Here, it is advisable to use approaches from industrial 3d printing as a starting point. Powder-based printing technologies in particular place great emphasis on user safety. The GMP guidelines stipulate that all surfaces in contact

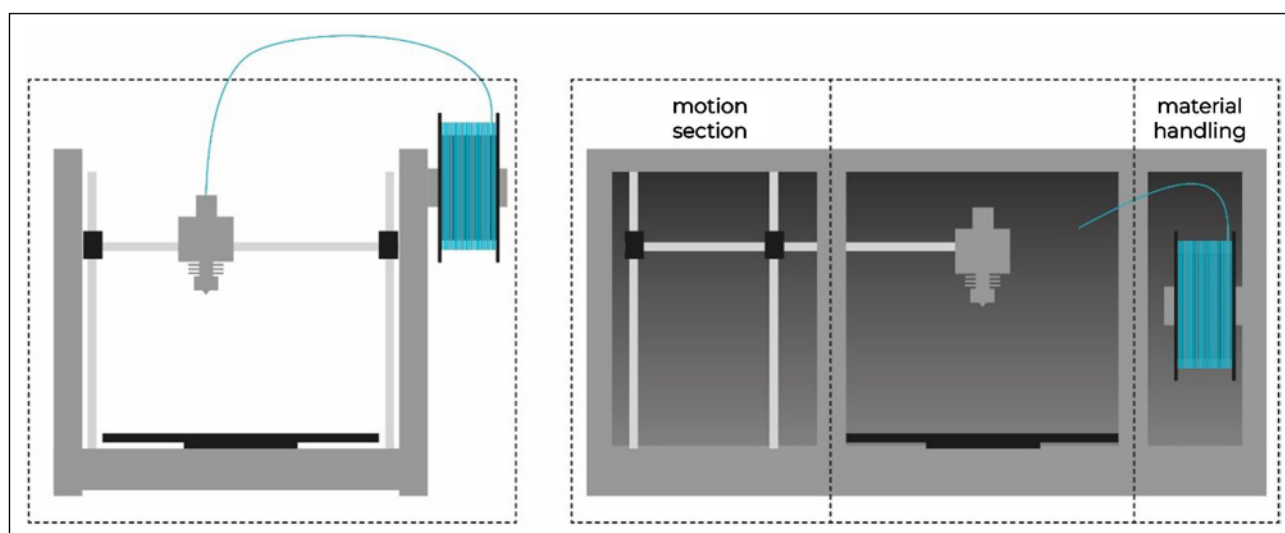


Figure 5 Schematic of an Off-the-Shelf 3D Printer (Left) and a 3D Printer with Separate Build, Motion, and Material Handling Section (Right).

with the product must be made of approved and cleaning-resistant materials, and that these must not have any edges, joints, undercuts or similar [79]. For this reason, all elements should be milled or machined from a single piece of material, if possible.

Feeding Mechanism, Filament, and Filament Storage

In commercially available printers, filament is conveyed in the extruder by two counter-rotating rollers. To increase the conveying force, at least one of the rollers is a gear wheel. This approach to filament transport is not suitable for pharmaceutical materials. The force exerted on the filament might become too high, resulting in slippage. Slippage, in turn, leads to small, usually statically charged filament grains that accumulate in the cavities of the feed roller and on other elements in the printhead. At high conveying resistances, i.e., high melt viscosities, this effect can even lead to breakage and creation of dislodged filament pieces. The consequence of this behavior is that the extruder must be cleaned extensively to avoid cross-contamination. In particular, the complex geometry of the gear wheel(s) with its many cavities prevents efficient cleaning. In addition, damage to the material leads to an undefined geometry of the filament and, thus, to an uncontrolled quantity of deposited material. Breakage of the filament will lead to printing process failure and manual intervention will be required to restart the process.

Traditional FDM 3d printing is based on a spool-based filament supply system. Technical polymers for classical FDM printing are designed and manufactured to display sufficient flexibility to be wound on a spool, but also enough

stiffness to be processed by a standard feeding mechanism. As described in the section on key attributes of excipients, pharmaceutical polymers often do not allow reliable feeding and printing easily due to their brittleness or undesirable deformation behavior. A filament provision and supply system must be developed that can handle a greater diversity of mechanical properties. To achieve this, both the bearing and the extruder technology must be completely revised.

Up to 450 m of filament can be wound onto a spool. When printing multiple large components this is an advantage. For the production of small dosage forms in lower quantities this is not necessary. If a lower amount of material is required, a smaller filament supply that is used up quicker reduces potential issues with the storage stability. Particularly in view of the API cost, smaller units of filaments are to be preferred. In addition, cross-contamination of filament must be avoided during handling so that encapsulation of the filament is necessary. For this reason, the currently selected filament geometry (“endless”) and the bearing units (coils) must be questioned.

The material storage, commonly designed as filament reel, should also be redesigned as part of a separate area. This is realized by some commercial printers that have cartridge systems, but large amounts of material are still wound on spools. We recommended to reduce the amount of material stored in or on the material accumulator. With reduced material amounts, coiled-up, long filaments strands that require feeding rollers or gears are not necessary, solving multiple issues with the current printer design. Omitting spools enables a new design of the storage system which can offer hermetic encapsulation of the filament. This would allow filament storage and transport under controlled conditions, similar to a tablet in a blister. Initial approaches can

already be found in printers from the company Stratasys [80]. Yet, these are not suitable for pharmaceutical manufacturing machines without significant modifications.

If filaments are not a continuous long strand anymore and new bearing units are designed, the conveying mechanism needs to be revised, too. Roller or gear-based feeding mechanisms should not be used for this purpose as they facilitate cross-contamination. Piston based mechanisms similar to those already used in certain bioprinters [81, 82] would be a superior approach, as slippage and breakage could be prevented.

Hotend and Coldend

One of the most central parts in a 3d printer is the hotend. With the help of electrical heating, the polymer is melted and extruded through a nozzle. Conventional hotends are optimized for high throughput and printing speeds. Technical polymers allow processing at temperatures well above the melting or glass transition temperature to reduce duration of melt formation. The result is a high temperature gradient from the core to the edge of the filament [83]. The use of additive manufacturing in the pharmaceutical environment, on the other hand, requires processing that is particularly gentle on the material, as many APIs are thermo-labile. Nevertheless, high printing speeds must still be achieved for a productive process. It is necessary to optimize the hotend in terms of uniform heat input to reduce the heat strain put on pharmaceutical filaments.

The other components of a common printhead are also not suitable for use in the pharmaceutical manufacturing. To compensate for the high temperatures, the upper parts of the printing core, the coldend, are cooled to prevent or reduce softening of the filament before the actual hotend. Commonly, active air cooling with cooling fins is used. Due to their complex and fine geometry these parts are particularly difficult to clean and increase the risk of cross-contamination. As the hotend is located directly above the product, evaporation of residual solvents, plasticisers and other volatile components is to be expected. They will be distributed in the printing chamber via the cooling air, further increasing the risk of cross-contamination and reducing cleanability. Pharmaceutical print heads must be completely cleanable. Purging with cleaning filaments, what is the common procedure in research, will not suffice to prevent cross-contamination. Since the material is fed through coldend and hotend, all elements that come into contact with the product must be cleaned without residues after each use and before each material change. To avoid changing the complete print head, a system design similar to the design of hot-melt extruders is recommended. Similar to the barrels, the printhead should be demountable and the material touching parts easily accessible [58]. The coldend of the printhead is placed in the

print chamber as well and its cooling fins cannot be cleaned properly. Switching to water cooling would solve this issue and provide a more accurate control of the temperature. This has been realized in some non-pharmaceutical systems such as the x500pro from German RepRap [84].

Sensors and Quality Control

A few years ago, 3d printing gained a detrimental reputation of being usable only for prototyping, due to frequent print failures, limited resolution, anisotropic mechanical properties, low production speeds and rough surface finish [85]. The reason for this is a lack of process and quality control. Even though the implementation of in-line quality is beginning in some 3d printing technologies, in FDM such methods are still at the experimental or research stage. The focus is mostly on thermal monitoring (melt pool analysis in selective laser sintering / melting) and layer monitoring [86]. Even though some of these approaches can also be used in a pharmaceutical context, they focus mostly on quality attributes for other manufacturing industries. Relevant pharmaceutical quality attributes cannot be captured with such systems. The use of the sensors applied for control issues only allows accurate control and regulation of the process. However, a quality statement regarding the solid state, API content or printed quantity is not possible. For 3d printers to be used for pharmaceutical manufacturing in the future, additional measures must be undertaken in addition to adapting the mechanical components. A major point is the quality control of the printed product.

Various types of defects in 3d printed parts are described in the literature [86, 87]. While structural integrity is key for technical applications of FDM, the doses of incorporated API in the final dosage form is the crucial parameter for medication manufactured by FDM. Especially medications to be used by children need to be manufactured in an accurate way, because the doses for children are typically lower and small deviations in the content of a dosage form result in higher relative over or underdosing potentially harming the patient.

To improve the quality of dosage forms, process control has to be improved as well. In general, three groups of parameters can be identified for in-process control.

1. Machine parameters derived from the control electronics. For example, motor and heater current, temperature of nozzle and cooling zone, vibrations etc.
2. Monitoring of the extruded volume or mass of the filament, either derived from measurements described in 1 or measured by dedicated sensors attached to the printer.
3. Non-destructive chemical analysis of the raw material and / or intermediate and final printed product.

The monitoring of machine parameters can be implemented in industrial control systems and do not necessarily rely on additional sensors which might lead to higher machine costs in the end. It has been described in literature to use the current of the feeding motor to detect a blocked nozzle [87, 88]. Chemical degradation and under-extrusion related to blocked nozzles is a major concern for the quality and accurate dosing of pharmaceutical dosage forms. In another example, Becker et al. [87, 89] used accelerometers to monitor the state of the printer and detect fluctuations in the flow of extruded raw material during the printing process. These substitute parameters can only be used if comparative data are available of the printing process for a specific raw material on a specific printer limiting the application to well understood processes. To circumvent these issues, dedicated sensors can be introduced into the printing system to directly measure the extruded volume or mass. Calculation of the printed dosage may act as a valuable in-process control, assuming that the active ingredient is homogeneously distributed in the raw material.

Optical systems were described to measure the distance between printed object and nozzle detecting under-extrusion [90, 91] providing error detection during a print process. It is also possible to monitor the movement and quality of filament by a camera [92]. Dosage forms with defects can then be discarded after the printing process and documented in a batch report for documentation. Of course, specialized sensors as well as integrated balances measuring the actual printed mass of filament could be an option to further improve the accuracy of 3d printed oral dosage forms, assuring the quality. For printing at the site of care, implementation of feedback loops based of the obtained data to automatically adjust the printing process of each individual dosage form will enable to meet the claimed dose and lead to an efficient manufacturing process with reduced waste and higher yields resulting in fast supply of high-quality medication to the patients.

Focusing more on the final product than the process itself, chemical analysis of the API incorporated in the printed dosage form could enable real-time release in a clinical printing setup. Different spectroscopic methods were described in the literature to analyze pharmaceutical dosage forms without destroying the samples. It was shown that NIR-chemical imaging of 3d printed objects can be used to measure the amount of printed API [93]. Transmission Raman measurements were reported in literature to investigate the amorphous and crystalline fraction of fenofibrate in solid oral dosage forms [94]. Such methods could be used in future pharmaceutical 3d printers to assure the quality of amorphous solid dispersions. Chemical analysis of printed objects can lead to full batch real-time release of medications printed at site of care ensuring that the quality of the final product was not negatively influenced by the printing

process. Downsides of non-destructive chemical imaging are high costs and large equipment, which might not be easily integrated in the printing platform.

Still, FDM as a digitally controlled manufacturing process opens the opportunity to integrate multiple sensors to not only monitor the quality of the printing process and product but furthermore adjusting critical process parameter on the fly to resemble a true rapid manufacturing process.

3d Printed Dosage Forms for Pediatric Use

General Consideration

Only few solid dosage forms have been investigated for their acceptability in children [95]. Of those, even less can be manufactured by 3d printing: minitabets, orodispersible films, (orodispersible) tablets, and capsules. A definite advantage of 3d printing is a freedom of design previously not possible. This is demonstrated by many novel dosage form designs [7, 96]. It is likely that such novel designs will also demonstrate high acceptability in children, e.g., because of more appealing coloring and dimensions. However, this has not been demonstrated in clinical trials and this section will focus mostly on the above-mentioned dosage forms. As the resolution of FDM printing is limited, small capsules suitable for pediatric treatment are not sensible to manufacturing via this route. Similarly, printing of orodispersible tablets and minitabets has not been established, yet.

Minitabets and Small Oblong Tablets

Tablets of < 4 mm diameter are usually considered to be minitabets [97]. As they have demonstrated acceptability in neonates, infants and children [2, 98] minitabets of 2 mm diameter are developed and manufactured more frequently than larger ones. Accurate printing of small objects is challenging in general. A typical nozzle diameter is 0.4 mm and tablets with a diameter of 2 mm are only five times larger than the nozzle diameter. These small geometries are on the lower limit of what is possible with the FDM process [99] and dimensional accuracy is difficult to achieve. Due to the small surface area of a single layer the cool down period of the material before the nozzle passes an area a second time is short, which may lead to insufficient mechanical stability of already printed layer. Several strategies are suitable to circumvent such issues. Reduction of print speed is generally associated with higher dimensional accuracy and improved surface quality. However, throughput and productivity will decrease with lower print speed. The manufacturing order of objects on one build plate can also be changed from sequential printing (complete all layers of one object, then

moving on to the next object) to layer-wise printing where the printing layer is changed after the specific layer of all objects is completed. While cooling time per object layer is associated with beneficial effects on dimensional accuracy, frequent changes between objects may introduce additional classes of printing errors like stringing and blobs [100]. Every additional travel movement comes with the risk of oozing filament and, therefore, inaccuracy of dose. The dosing of smaller tablets is even more challenging than with larger objects because the relative change of incorporated API due to printing defects is more significant. Krause et al. printed objects with a diameter of 4 mm, 3 mm, 2 mm and 1.5 mm with decreasing tablet mass and calculated the acceptance value according to Ph. Eur. 2.9.40. While the standard deviation of tablet mass was higher for the largest objects, their acceptance value was lower compared to smaller tablets. These results show that dosing accuracy is especially important for mini tablets and low dose drug forms [99].

Ayyoubi et al. printed spherical tablets with a diameter of 6 mm with channels to improve dissolution rate [101]. Small oblong tablets (9 mm × 5 mm × 4 mm (width × length × height)) were manufactured for children > 6 years old by Fanous et al. [102].

Another aspect besides the dimensionally accuracy is the geometric flexibility. Geometrical flexibility offers the opportunity to increase the compliance in pediatric patient as well as to reduce the resistance of taking medication in children. The reason lies in the possibility of 3d printing for personalized medicine to choose the color, shape and design of the tablet according to the child's wishes [103]. Scoutaris et al. imitated chewable STARMIX® sweets by printing objects in the shape of a heart, ring, bottle, bear and lion, which contained the model substance indomethacin, hypromellose acetate succinate (HPMCAS) and polyethylene glycol (PEG) as polymers. The aim for the development of this pediatric dosage forms with the STARMIX® design via hot-melt extrusion (HME) and FDM 3d printing was also to enhance the palatability [104].

Besides the flexibility in geometry FDM can also be used to manufacture layer-wise polypills [105]. Multiple APIs were printed into one solid oral dosage form. In case of the layer-based FDM process, chemical compatibility of these APIs is not as limiting as in traditional manufacturing processes since the compounds are separately printed into different compartments of the dosage form. The flexibility of a computer-controlled manufacturing process opens the possibilities to match the exact needs for pediatric patients, but deep understanding of the underlying processes and optimized print settings are necessary to ensure high quality of the final product.

Orodispersible Films

Orodispersible films are accepted by infants and children [95, 106, 107] and are dosage forms of choice for patient centric applications. The European Pharmacopoeia defines orodispersible films as solid oromucosal preparations intended for the administration in the mouth, where they disperse rapidly to deliver active substances (Ph. Eur. Monograph “Oromucosal preparations”). Dose adaption is possible by (1) modifying the API concentration in the formulation, (2) adapting the film thickness, and (3) by cutting films to the desired size, as both thickness and size defines the amount of incorporated API. However, the cutting approach can be accompanied by material waste and is prone to human errors.

Manufacturing routes of orodispersible films include solvent casting [108–110] and 2d and 3d printing technologies. In 2D printing [111, 112], the printing fluid consists of the drug dissolved in a suitable solvent or dispersed in a dispersant, which is printed onto a substrate which contains polymer(s) and additives (e.g., plasticizers, flavors) and is made in a separate manufacturing step. As for the solvent casting technique, the process parameters (drying temperature, humidity) need to be precisely controlled, as they significantly influence the final film properties [113, 114].

3d printing offers a waste-less route of precise manufacturing medicines for children. Jamróz and colleagues accurately printed orodispersible films containing aripiprazole [115], whereas Ethezazi et al. printed multi-layered films containing individual layers with paracetamol, ibuprofen and a taste-masking agent [29]. Cho et al. applied a variation of FDM printing to prepare an orodispersible film containing the poorly water soluble drug olanzapine [116]. They heated a polymer-API mixture until it melted and used pneumatic extrusion to drive the printing process, a approach similar to the one published by Musazzi et al. [108]. In another study, a bi-layer film was FDM printed with a mucoadhesive chitosan layer and drug containing layer and an ethyl cellulose backing layer that formed a permeation barrier, thus creating a unidirectional drug release [117].

Even though none of these studies directly investigated the suitability of FDM 3d printing to individualize the dose, they demonstrated sufficient mechanical properties to enable robust handling and acceptable accuracy that strongly hints at technological proficiency to produce pediatric orodispersible films. However, acceptability of orodispersible films was assessed with solvent-casted films and the different appearance of FDM printed films will have to be investigated separately in future studies.

Dosage Form Characterization

To ensure that printed dosage forms meet the requirements, physical properties need to be characterized, and the homogeneous distribution of the API has to be controlled to guarantee that patients receive the necessary therapeutic amount of API. For physical characterization, various tests are listed in the pharmacopeia: test for friability (Ph. Eur. 2.9.7), crushing strength (Ph. Eur. 2.9.8) and disintegration (Ph. Eur. 2.9.1). To check the homogeneity of the drug distribution, the content of the API in the tablets is determined via the uniformity of the mass or content (Ph. Eur. 2.9.5 / 2.9.6) or the uniformity of dosage units (Ph. Eur. 2.9.40). In addition, it is tested how the drug is released from the tablet over time (Ph. Eur. 2.9.3).

However, FDM printed tablets have different physical properties than compressed tablets, so further methods have been developed for physical characterization. Often, the printed tablets are less porous than the pressed ones, due to the individual layers fused together [118, 119]. Depending on the polymers used, the tablets cannot be crushed, do not disintegrate, or disintegrate very slowly, and do not exhibit abrasion [101, 120]. The porosity of the tablets can be easily controlled by the pattern and percentage of the infill of the design [120, 121]. To check the accuracy of the printing, as well as to determine the porosity of the printed tablets, μ CT measurements are often used [102, 122]. The visualization of the internal structure of dosage forms reveals the structural quality, how well the layers adhere to each other, and how well the geometry matches the desired design without destruction of the tablet [123, 124]. In a study by Alhijjaj et al., it was shown that the printing speed, printing temperature, build plate leveling and polymer viscosity (melt flow index) have a high influence on the precision of the print, weight of the object and print reproducibility [125]. The effects of these parameters can be registered in the μ CT and contribute to the improvement of the process.

As 3d printing is suitable for small, personalized batches, and produces a smaller throughput than industrial manufacturing machines, non-destructive methods are advantageous for this process. In addition, for the determination of the mass or content uniformity, the tablets must be dissolved, or the API must be extracted from the matrix. Therefore, there is also a growing interest in non-destructive content analysis, which is possible using NIR and Raman technology [102, 104]. This technique enables in-line and off-line implementation [126]. To verify the release of the API from the dosage form, in vitro studies must be performed. Here, the ingestion of the tablet, the residence time in the stomach and GIT are simulated. For children the dissolution studies were often adapted. For example, Starmix® candy-like dosage forms were dissolved in 2 ml saliva for 2 min, because children often are

expected to chew the tablets [104, 127]. In addition, volumes and dwell times can also be adjusted for the specific patient group. Accurate dosing is especially important for children, which can be realized with FDM printing. The individually produced batch can be adapted to the needs of the children. Not only the dose, but also the release behavior can be varied. This is possible with the choice of polymer, as well as with the SA/V ratio, which can be implemented with the choice of geometry [99, 128, 129]. Various approaches are also currently being pursued to predict release curves using ANNs so that non-destructive methods can be established here as well [130–132]. These predictions are based, among other things, on the infill pattern of the tablets and their influences on the release pattern. In the study of Obeid et al. the influence of the SA/V ratio was used to predict the resulting release profile of the printed tablet [131].

Outlook

This manuscript aims to provide an overview of pharmaceutical as well as engineering considerations for FDM printed medication for children. We reflected on current liabilities and intended to depict ways for further innovation in the engineering of unit operations to enhance suitability of equipment and dosage forms. As for 3d printing of solid dosage forms in general, formulation and print technology need to be considered in a holistic manner taking into account all aspects from raw materials to final dosage forms. We conclude that there is strong need to advance FDM printing technologies and excipients to accommodate for pharmaceutical needs—with even more elevated quality requirements for pediatric patients especially in the fields of excipient safety, acceptability, printing control and accuracy. Good news is that remedy is underway with commercial start-ups (e.g., Triastek) as well as public–private consortia such as PolyPrint actively working on the necessary technical innovation to meet pharma requirements. Also, the pediatric patient population will benefit from future capabilities of individualized therapy with precise dose adjustment and possibilities to enhance compliance via tablet morphology and size. First small clinical trials on medications for children applying other additive manufacturing techniques clearly demonstrated the future potential of the tech field [133] and we speculate that FDM—due to its technical maturity and accessibility—will be one of the key enabling technologies to advance and establish pharmaceutical 3d printing for individualized and decentralized production of dosage forms—for adults as well as children.

Author contributions

JQ: conceptualization, writing, editing; MB: conceptualization, writing, editing; JB: writing; RC: writing; KE: conceptualization, writing, editing; A-GE: writing; NG: writing; GG-G: writing; LH: writing; DK: writing, editing; TK: conceptualization, writing, editing; SK: writing; FL: writing; TM: writing; HW: writing; SG: conceptualization, writing, editing; TS: writing, editing.

Funding

Open Access funding enabled and organized by Projekt DEAL. The PolyPrint project is funded by the German Federal Ministry of Education and Research—project ‘ProMat Leben - Polymere’ ‘PolyPrint’ (Project No.: 13XP5064).

Declarations

Conflict of interest

The authors declare that they have no conflict of interest.

Open Access

This article is licensed under a Creative Commons Attribution 4.0 International License, which permits use, sharing, adaptation, distribution and reproduction in any medium or format, as long as you give appropriate credit to the original author(s) and the source, provide a link to the Creative Commons licence, and indicate if changes were made. The images or other third party material in this article are included in the article's Creative Commons licence, unless indicated otherwise in a credit line to the material. If material is not included in the article's Creative Commons licence and your intended use is not permitted by statutory regulation or exceeds the permitted use, you will need to obtain permission directly from the copyright holder. To view a copy of this licence, visit <http://creativecommons.org/licenses/by/4.0/>.

Supplementary Information

The online version contains supplementary material available at <https://doi.org/10.1007/s43441-021-00354-0>.

References

- Moreira M, Sarraguça M. How can oral paediatric formulations be improved? A challenge for the XXI century. *Int J Pharm*. 2020. <https://doi.org/10.1016/j.ijpharm.2020.119905>.
- Klingmann V, Spomer N, Lerch C. Favorable acceptance of mini-tablets compared with syrup: a randomized controlled trial in infants and preschool children. *J Pediatr*. 2013. <https://doi.org/10.1016/j.jpeds.2013.07.014>.
- Breitkreutz J, Boos J. Paediatric and geriatric drug delivery. *Expert Opin Drug Deliv*. 2007;4:37–45. <https://doi.org/10.1517/17425247.4.1.37>.
- Liu F, Ranmal S, Batchelor HK. Patient-centered pharmaceutical design to improve acceptability of medicines: similarities and differences in paediatric and geriatric populations. *Drugs*. 2014;74:1871–89. <https://doi.org/10.1007/S40265-014-0297-2>.
- el Aita I, Ponsar H, Quodbach J. A critical review on 3D-printed dosage forms. *Curr Pharm Des*. 2018;24:4957–78. <https://doi.org/10.2174/1381612825666181206124206>.
- el Aita I, Breitkreutz J, Quodbach J. Investigation of semi-solid formulations for 3D printing of drugs after prolonged storage to mimic real-life applications. *Eur J Pharm Sci*. 2020;146: 105266. <https://doi.org/10.1016/j.ejps.2020.105266>.
- Melocchi A, Ubaldi M, Cerea M. A graphical review on the escalation of fused deposition modeling (FDM) 3D printing in the pharmaceutical field. *J Pharm Sci*. 2020;109:2943–57. <https://doi.org/10.1016/j.xphs.2020.07.011>.
- Shaqour B, Samaro A, Verleij B. Production of drug delivery systems using fused filament fabrication: a systematic review. *Pharmaceutics*. 2020;12:517. <https://doi.org/10.3390/PHARMACEUTICS12060517>.
- PolyPrint | ProMatLeben—Polymere n.d. <https://promatleben.de/de/projekte/projekte-alphabetisch/polyprint/>. Accessed 2 Sep 2021.
- Paediatric formulations | European Medicines Agency n.d. <https://www.ema.europa.eu/en/human-regulatory/research-development/paediatric-medicines/paediatric-investigation-plans/paediatric-formulations>. Accessed 2 Sep 2021.
- Reflection paper: formulations choice paediatric population n.d. https://www.ema.europa.eu/en/documents/scientific-guide-line/reflection-paper-formulations-choice-paediatric-population_en.pdf. Accessed 2 Sep 2021.
- Thabet Y, Klingmann V, Breitkreutz J. Drug formulations: standards and novel strategies for drug administration in pediatrics. *J Clin Pharmacol*. 2018;58:S26–35. <https://doi.org/10.1002/JCPH.1138>.
- Rouaz K, Chiclana-Rodríguez B, Nardi-Ricart A. Excipients in the paediatric population: a review. *Pharmaceutics*. 2021. <https://doi.org/10.3390/PHARMACEUTICS13030387>.
- Walsh J, Cram A, Woertz K. Playing hide and seek with poorly tasting paediatric medicines: do not forget the excipients. *Adv Drug Deliv Rev*. 2014;73:14–33. <https://doi.org/10.1016/j.addr.2014.02.012>.
- STEP Database—EuPFI n.d. <http://www.eupfi.org/step-database-info/>. Accessed 2 Sep 2021.
- Yochana S, Yu M, Alvi M. Pharmaceutical excipients and pediatric formulations. *Chim Oggi*. 2012;30:56–61.
- Simões MF, Pinto RMA, Simões S. Hot-melt extrusion in the pharmaceutical industry: toward filing a new drug application. *Drug Discov Today*. 2019;24:1749–68. <https://doi.org/10.1016/j.drudis.2019.05.013>.
- Simões MF, Pinto RMA, Simões S. Hot-melt extrusion: a roadmap for product development. *AAPS PharmSciTech*. 2021. <https://doi.org/10.1208/S12249-021-02017-7>.
- Bandari S, Nyavanandi D, Dumpa N. Coupling hot melt extrusion and fused deposition modeling: critical properties for successful performance. *Adv Drug Deliv Rev*. 2021;172:52–63. <https://doi.org/10.1016/j.addr.2021.02.006>.
- Melocchi A, Parietti F, Maroni A. Hot-melt extruded filaments based on pharmaceutical grade polymers for 3D printing by fused deposition modeling. *Int J Pharm*. 2016;509:255–63. <https://doi.org/10.1016/j.ijpharm.2016.05.036>.
- Korte C, Quodbach J. Formulation development and process analysis of drug-loaded filaments manufactured via hot-melt extrusion for 3D-printing of medicines. *Pharm Dev Technol*. 2018;23:1117–27. <https://doi.org/10.1080/10837450.2018.1433208>.

22. Zhang J, Feng X, Patil H. Coupling 3D printing with hot-melt extrusion to produce controlled-release tablets. *Int J Pharm.* 2017;519:186–97. <https://doi.org/10.1016/j.ijpharm.2016.12.049>.
23. Fuenmayor E, Forde M, Healy AV. Material considerations for fused-filament fabrication of solid dosage forms. *Pharmaceutics.* 2018;10:44. <https://doi.org/10.3390/PHARMACEUTICS10020044>.
24. Nasereddin JM, Wellner N, Alhijaj M. Development of a simple mechanical screening method for predicting the feedability of a pharmaceutical FDM 3D printing filament. *Pharm Res.* 2018;35:1–13. <https://doi.org/10.1007/S11095-018-2432-3>.
25. Zhang J, Xu P, Vo A. Development and evaluation of pharmaceutical 3D printability for hot melt extruded cellulose-based filaments. *J Drug Deliv Sci Technol.* 2019;52:292. <https://doi.org/10.1016/J.JDDST.2019.04.043>.
26. Azad MA, Olawuni D, Kimbell G. Polymers for extrusion-based 3D printing of pharmaceuticals: a holistic materials-process perspective. *Pharmaceutics.* 2020;12:124. <https://doi.org/10.3390/PHARMACEUTICS12020124>.
27. Thakkar R, Thakkar R, Pillai A. Systematic screening of pharmaceutical polymers for hot melt extrusion processing: a comprehensive review. *Int J Pharm.* 2020;576: 118989. <https://doi.org/10.1016/J.IJPHARM.2019.118989>.
28. Gottschalk N, Bogdahn M, Harms M. Brittle polymers in fused deposition modeling: an improved feeding approach to enable the printing of highly drug loaded filament. *Int J Pharm.* 2021;597: 120216. <https://doi.org/10.1016/J.IJPHARM.2021.120216>.
29. Ehtezazi T, Algellay M, Islam Y. The application of 3D printing in the formulation of multilayered fast dissolving oral films. *J Pharm Sci.* 2018;107:1076–85. <https://doi.org/10.1016/J.XPHS.2017.11.019>.
30. Boniatti J, Januskaite P, da Fonseca LB. Direct powder extrusion 3D printing of praziquantel to overcome neglected disease formulation challenges in paediatric populations. *Pharmaceutics.* 2021. <https://doi.org/10.3390/PHARMACEUTICS13081114>.
31. Wang H, Dumpa N, Bandari S. Fabrication of taste-masked donut-shaped tablets via fused filament fabrication 3D printing paired with hot-melt extrusion techniques. *AAPS PharmSciTech.* 2020. <https://doi.org/10.1208/S12249-020-01783-0>.
32. Woertz K, Tissen C, Kleinebudde P. Taste sensing systems (electronic tongues) for pharmaceutical applications. *Int J Pharm.* 2011;417:256–71. <https://doi.org/10.1016/J.IJPHARM.2010.11.028>.
33. Soto J, Keeley A, Keating AV. Rats can predict aversiveness of active pharmaceutical ingredients. *Eur J Pharm Biopharm.* 2018;133:77–84. <https://doi.org/10.1016/J.EJPB.2018.09.027>.
34. Patwardhan K, Asgarzadeh F, Dassinger T. A quality by design approach to understand formulation and process variability in pharmaceutical melt extrusion processes. *J Pharm Pharmacol.* 2015;67:673–84. <https://doi.org/10.1111/JPHP.12370>.
35. Islam MT, Maniruzzaman M, Halsey SA. Development of sustained-release formulations processed by hot-melt extrusion by using a quality-by-design approach. *Drug Deliv Transl Res.* 2014;4:377–87. <https://doi.org/10.1007/S13346-014-0197-8>.
36. Agrawal A, Dudhedia M, Deng W. Development of tablet formulation of amorphous solid dispersions prepared by hot melt extrusion using quality by design approach. *AAPS PharmSciTech.* 2016;17:214–32. <https://doi.org/10.1208/S12249-015-0472-0>.
37. Ponsar H, Wiedey R, Quodbach J. Hot-melt extrusion process fluctuations and their impact on critical quality attributes of filaments and 3D-printed dosage forms. *Pharmaceutics.* 2020;12:511. <https://doi.org/10.3390/pharmaceutics12060511>.
38. Kohlgrüber K. *Co-rotating twin-screw extruders: fundamentals* | *Hanser-Fachbuch*. Munich: Hanser; 2008.
39. Coperion Download Center n.d. https://download.coperion.com/index_.html?download=111413. Accessed 2 Sep 2021.
40. Hopkins M. LOSS in weight feeder systems. *Meas Control.* 2006;39:237–40. <https://doi.org/10.1177/002029400603900801>.
41. Schulze D. *Powders and bulk solids—behavior, characterization, storage and flow* Dietmar Schulzel, vol. 22. New York: Springer; 2008.
42. Fahlenbock TD. Selecting a screw feed device for low-rate loss-in-weight feeding. *Powder Bulk Eng.* 2007;21(12):27–31.
43. Matarazzo P. Checklist for selecting a volumetric or gravimetric feeder. *Powder Bulk Eng.* 2010.
44. NAMUR. *Dosiergenauigkeit von kontinuierlichen Waagen.* 2006.
45. Meier R, Thommes M, Rasenack N. Granule size distributions after twin-screw granulation—do not forget the feeding systems. *Eur J Pharm Biopharm.* 2016;106:59–69. <https://doi.org/10.1016/J.EJPB.2016.05.011>.
46. Engisch WE, Muzzio FJ. Method for characterization of loss-in-weight feeder equipment. *Powder Technol.* 2012;228:395–403. <https://doi.org/10.1016/J.POWTEC.2012.05.058>.
47. Bruce C, Manning M. *Melt extruded thin strips containing coated pharmaceutical actives*, 2011.
48. Merck KGAA. *Shaping the future of formulation development with melt-based 3d printing technologies [White Paper]*. 2021. <https://www.pharmaexcipients.com/wp-content/uploads/2021/06/Shaping-the-Future-of-Formulation-Development-with-Melt-based-3D-Printing-Technologies.pdf>. Accessed Sept 21, 2021.
49. Vynckier A-K, Dierickx L, Voorspoels J. Hot-melt co-extrusion: requirements, challenges and opportunities for pharmaceutical applications. *J Pharm Pharmacol.* 2014;66:167–79. <https://doi.org/10.1111/JPHP.12091>.
50. Crowley MM, Zhang F, Repka MA. Pharmaceutical applications of hot-melt extrusion: part I. *Drug Dev Ind Pharm.* 2008;33:909–26. <https://doi.org/10.1080/03639040701498759>.
51. Liang JZ. Effects of extrusion conditions on die-swell behavior of polypropylene/diatomite composite melts. *Polym Test.* 2008;27:936–40. <https://doi.org/10.1016/J.POLYMERTES.2008.08.001>.
52. Öblom H, Zhang J, Pimparade M. 3D-printed isoniazid tablets for the treatment and prevention of tuberculosis—personalized dosing and drug release. *AAPS PharmSciTech.* 2019. <https://doi.org/10.1208/S12249-018-1233-7>.
53. Xie T, Taylor LS. Effect of temperature and moisture on the physical stability of binary and ternary amorphous solid dispersions of celecoxib. *J Pharm Sci.* 2017;106:100–10. <https://doi.org/10.1016/J.XPHS.2016.06.017>.
54. Awad A, Fina F, Trenfield SJ. 3D printed pellets (miniprintlets): a novel, multi-drug, controlled release platform technology. *Pharmaceutics.* 2019;11:148. <https://doi.org/10.3390/PHARMACEUTICS11040148>.
55. Eggenreich K, Windhab S, Schrank S. Injection molding as a one-step process for the direct production of pharmaceutical dosage forms from primary powders. *Int J Pharm.* 2016;505:341–51. <https://doi.org/10.1016/J.IJPHARM.2016.03.034>.
56. Repka M, Bandari S, Kallakunta V. Melt extrusion with poorly soluble drugs—an integrated review. *Int J Pharm.* 2018;535:68–85. <https://doi.org/10.1016/J.IJPHARM.2017.10.056>.
57. Sacerens L, Vervaeke C, Remon JP. Process monitoring and visualization solutions for hot-melt extrusion: a review. *J Pharm Pharmacol.* 2014;66:180–203. <https://doi.org/10.1111/JPHP.12123>.
58. Spoerk M, Koutsamanis I, Matic J. Novel cleaning-in-place strategies for pharmaceutical hot melt extrusion. *Pharmaceutics.* 2020;12:1–21. <https://doi.org/10.3390/PHARMACEUTICS12060588>.

59. Wesholowski J, Prill S, Berghaus A. Inline UV/Vis spectroscopy as PAT tool for hot-melt extrusion. *Drug Deliv Transl Res*. 2018;8:1595–603. <https://doi.org/10.1007/S13346-017-0465-5>.
60. Saerens L, Dierickx L, Lenain B. Raman spectroscopy for the in-line polymer–drug quantification and solid state characterization during a pharmaceutical hot-melt extrusion process. *Eur J Pharm Biopharm*. 2011;77:158–63. <https://doi.org/10.1016/J.EJPB.2010.09.015>.
61. Vo AQ, He H, Zhang J. Application of FT-NIR analysis for in-line and real-time monitoring of pharmaceutical hot melt extrusion: a technical note. *AAPS PharmSciTech*. 2018;19:3425. <https://doi.org/10.1208/S12249-018-1091-3>.
62. Kallakunta VR, Sarabu S, Bandari S. An update on the contribution of hot-melt extrusion technology to novel drug delivery in the twenty-first century: part I. *Expert Opin Drug Deliv*. 2019;16:539. <https://doi.org/10.1080/17425247.2019.1609448>.
63. Kim EJ, Kim JH, Kim M-S. Process analytical technology tools for monitoring pharmaceutical unit operations: a control strategy for continuous process verification. *Pharmaceutics*. 2021;13:919. <https://doi.org/10.3390/PHARMACEUTICS13060919>.
64. Koutsamanis I, Paudel A, Nickisch K. Controlled-release from high-loaded reservoir-type systems—a case study of ethylene-vinyl acetate and progesterone. *Pharmaceutics*. 2020. <https://doi.org/10.3390/PHARMACEUTICS12020103>.
65. Auch C, Harms M, Mäder K. How changes in molecular weight and PDI of a polymer in amorphous solid dispersions impact dissolution performance. *Int J Pharm*. 2019;556:372–82. <https://doi.org/10.1016/J.IJPHARM.2018.12.012>.
66. Ting J, William W, Porter I, Mecca JM. Advances in polymer design for enhancing oral drug solubility and delivery. *Bioconjug Chem*. 2018;29:939–52. <https://doi.org/10.1021/ACS.BIOCONJCHEM.7B00646>.
67. Đuranović M, Obeid S, Madžarević M, et al. Paracetamol extended release FDM 3D printlets: evaluation of formulation variables on printability and drug release. *Int J Pharm*. 2021. <https://doi.org/10.1016/J.IJPHARM.2020.120053>.
68. Gorkem Buyukgoz G, Soffer D, Defendre J. Exploring tablet design options for tailoring drug release and dose via fused deposition modeling (FDM) 3D printing. *Int J Pharm*. 2020. <https://doi.org/10.1016/J.IJPHARM.2020.119987>.
69. Prasad E, Islam MT, Goodwin DJ. Development of a hot-melt extrusion (HME) process to produce drug loaded Affinisol™ 15LV filaments for fused filament fabrication (FFF) 3D printing. *Addit Manuf*. 2019. <https://doi.org/10.1016/J.ADDMA.2019.06.027>.
70. Aho J, van Renterghem J, Arnfast L. The flow properties and presence of crystals in drug-polymer mixtures: rheological investigation combined with light microscopy. *Int J Pharm*. 2017;528:383–94. <https://doi.org/10.1016/J.IJPHARM.2017.06.012>.
71. Qian F, Huang J, Hussain M. Drug-polymer solubility and miscibility: stability consideration and practical challenges in amorphous solid dispersion development. *J Pharm Sci*. 2010;99:2941–7. <https://doi.org/10.1002/JPS.22074>.
72. Baird J, van Eerdenbrugh B, Taylor L. A classification system to assess the crystallization tendency of organic molecules from undercooled melts. *J Pharm Sci*. 2010;99:3787–806. <https://doi.org/10.1002/JPS.22197>.
73. Dedroog S, Pas T, Vergauwen B. Solid-state analysis of amorphous solid dispersions: why DSC and XRPD may not be regarded as stand-alone techniques. *J Pharm Biomed Anal*. 2020. <https://doi.org/10.1016/J.JPBA.2019.112937>.
74. Ma X, Williams RO III. Characterization of amorphous solid dispersions: an update. *J Drug Deliv Sci Technol*. 2019;50:113–24. <https://doi.org/10.1016/j.jddst.2019.01.017>.
75. Wadher K, Trivedi R, Wankhede N. 3D printing in pharmaceuticals: an emerging technology full of challenges. *Ann Pharm Fr*. 2021;79:107–18. <https://doi.org/10.1016/J.PHARMA.2020.08.007>.
76. Hauser G. *Hygienegerechte apparate und anlagen*, vol. 1. 1st ed. Weinheim: Wiley; 2008.
77. Kampker A, Triebs J, Kawollek S. Review on machine designs of material extrusion based additive manufacturing (AM) systems—status-Quo and potential analysis for future AM systems. *Procedia CIRP*. 2019;81:815–9. <https://doi.org/10.1016/J.PROCIR.2019.03.205>.
78. Melocchi A, Briatico-Vangosa F, Uboldi M. Quality considerations on the pharmaceutical applications of fused deposition modeling 3D printing. *Int J Pharm*. 2021. <https://doi.org/10.1016/J.IJPHARM.2020.119901>.
79. Leitlinien—EHEDG n.d. <https://ehedg.de/leitlinien/>. Accessed 2 Sep 2021.
80. Fortus 450mc | Stratasys™ Support Center n.d. <https://support.stratasys.com/en/printers/fdm/fortus-450mc>. Accessed 2 Sep 2021.
81. BIO X Syringe Pump Printhead—CELLINK n.d. <https://www.cellink.com/product/bio-x-syringe-pump-printhead/>. Accessed 2 Sep 2021.
82. SDS-5 3d printer Extruder | Hyrel3D n.d. <https://www.hyrel3d.com/portfolio/sds-5-extruder/>. Accessed 2 Sep 2021.
83. Serdeczny MP, Comminal R, Mollah MT. Numerical modeling of the polymer flow through the hot-end in filament-based material extrusion additive manufacturing. *Addit Manuf*. 2020. <https://doi.org/10.1016/J.ADDMA.2020.101454>.
84. x500pro | German RepRap GmbH n.d. <https://www.germanreprap.com/prINTER/x500pro.aspx>. Accessed 2 Sep 2021.
85. van Bracht R, Piller FT, Marquardt E. Das Potenzial der additiven Fertigung: digitale Technologien im Unternehmenskontext : Auswert 2019.
86. Kim H, Lin Y, Tseng TLB. A review on quality control in additive manufacturing. *Rapid Prototyping J*. 2018;24:645–69. <https://doi.org/10.1108/RPJ-03-2017-0048>.
87. Becker P, Gebert J, Roennau A et al. Online error detection in additive manufacturing: a review. In: *Proceedings of the 2021 IEEE 8th International Conference on Industrial Engineering and Applications, ICIEA 2021*, pp. 167–75. <https://doi.org/10.1109/ICIEA52957.2021.9436729>.
88. Tlegenov Y, Lu WF, Hong GS. A dynamic model for current-based nozzle condition monitoring in fused deposition modeling. *Progress Addit Manuf*. 2019;4:211–23. <https://doi.org/10.1007/S40964-019-00089-3>.
89. Rao P, Liu J, Mathew Roberson D, et al. Online real-time quality monitoring in additive manufacturing processes using heterogeneous sensors additive manufacturing view project fatigue life prediction from defect criticality for L-PBF parts view project online real-time quality monitoring in additive manufacturing processes using heterogeneous sensors. *J Manuf Sci Eng*. 2014. <https://doi.org/10.1115/1.4029823>.
90. Baumann F, Roller D. Vision based error detection for 3D printing processes. *MATEC Web Conf*. 2016;59:1–7. <https://doi.org/10.1051/conf/2016>.
91. Becker P, Spielbauer N, Roennau A. Real-time in-situ process error detection in additive manufacturing. In: *Proceedings of the 4th IEEE International Conference on Robotic Computing, IRC 2020*, 2020, pp 426–427. <https://doi.org/10.1109/IRC.2020.00077>.
92. Greeff GP, Schilling M. Closed loop control of slippage during filament transport in molten material extrusion. *Addit Manuf*. 2017;14:31–8. <https://doi.org/10.1016/j.addma.2016.12.005>.
93. Khorasani M, Edinger M, Rajjada D, et al. Near-infrared chemical imaging (NIR-CI) of 3D printed pharmaceuticals. *Int J*

- Pharm. 2016;515:324–30. <https://doi.org/10.1016/j.ijpharm.2016.09.075>.
94. Theil F, Milsman J, Anantharaman S, et al. Manufacturing amorphous solid dispersions with a tailored amount of crystallized API for biopharmaceutical testing. *Mol Pharm.* 2018;15:1870–7. <https://doi.org/10.1021/acs.molpharmaceut.8b00043>.
 95. Alessandrini E, Brako F, Scarpa M. Children's Preferences for Oral Dosage Forms and Their Involvement in Formulation Research via EPTRI (European Paediatric Translational Research Infrastructure). *Pharmaceutics.* 2021;13:730. <https://doi.org/10.3390/PHARMACEUTICS13050730>.
 96. Jamróz W, Szafraniec J, Kurek M. 3D printing in pharmaceutical and medical applications—recent achievements and challenges. *Pharm Res.* 2018. <https://doi.org/10.1007/S11095-018-2454-X>.
 97. Lennartz P, Mielck JB. Minitabletting: improving the compactability of paracetamol powder mixtures. *Int J Pharm.* 1998;173:75–85. [https://doi.org/10.1016/S0378-5173\(98\)00206-3](https://doi.org/10.1016/S0378-5173(98)00206-3).
 98. Klingmann V, Seitz A, Meissner T. Acceptability of uncoated mini-tablets in neonates—a randomized controlled trial. *J Pediatr.* 2015;167:893–896.e2. <https://doi.org/10.1016/J.JPEDS.2015.07.010>.
 99. Krause J, Müller L, Sarwinska D. 3D printing of mini tablets for pediatric use. *Pharmaceutics.* 2021;14:1–16. <https://doi.org/10.3390/PH14020143>.
 100. Parhi R. A review of three-dimensional printing for pharmaceutical applications: quality control, risk assessment and future perspectives. *J Drug Deliv Sci Technol.* 2021. <https://doi.org/10.1016/J.JDDST.2021.102571>.
 101. Ayyoubi S, Cerda JR, Fernández-García R. 3D printed spherical mini-tablets: geometry versus composition effects in controlling dissolution from personalised solid dosage forms. *Int J Pharm.* 2021. <https://doi.org/10.1016/J.IJPHARM.2021.120336>.
 102. Fanous M, Bitar M, Gold S. Development of immediate release 3D-printed dosage forms for a poorly water-soluble drug by fused deposition modeling: study of morphology, solid state and dissolution. *Int J Pharm.* 2021;599: 120417. <https://doi.org/10.1016/J.IJPHARM.2021.120417>.
 103. Vijayavenkataraman S, Fuh JYH, Lu WF. 3D printing and 3D bioprinting in pediatrics. *Bioengineering.* 2017. <https://doi.org/10.3390/BIOENGINEERING4030063>.
 104. Scoutaris N, Ross S, Douroumis D. 3D printed “Starmix” drug loaded dosage forms for paediatric applications. *Pharm Res.* 2018. <https://doi.org/10.1007/S11095-017-2284-2>.
 105. Pereira BC, Isreb A, Forbes RT. ‘Temporary Plasticiser’: a novel solution to fabricate 3D printed patient-centred cardiovascular ‘Polypill’ architectures. *Eur J Pharm Biopharm.* 2019;135:94–103. <https://doi.org/10.1016/J.EJPB.2018.12.009>.
 106. Klingmann V, Pohly CE, Meissner T. Acceptability of an orodispersible film compared to syrup in neonates and infants: a randomized controlled trial. *Eur J Pharm Biopharm.* 2020;151:239–45. <https://doi.org/10.1016/J.EJPB.2020.03.018>.
 107. Orlu M, Ranmal SR, Sheng Y. Acceptability of orodispersible films for delivery of medicines to infants and preschool children. *Drug Deliv.* 2017;24:1243–8. <https://doi.org/10.1080/10717544.2017.1370512>.
 108. Musazzi UM, Selmin F, Ortenzi MA. Personalized orodispersible films by hot melt ram extrusion 3D printing. *Int J Pharm.* 2018;551:52–9. <https://doi.org/10.1016/J.IJPHARM.2018.09.013>.
 109. Liu C, Chang D, Zhang X. Oral fast-dissolving films containing lutein nanocrystals for improved bioavailability: formulation development, in vitro and in vivo evaluation. *AAPS PharmSciTech.* 2017;18:2957–64. <https://doi.org/10.1208/S12249-017-0777-2>.
 110. Foo WC, Khong YM, Gokhale R. A novel unit-dose approach for the pharmaceutical compounding of an orodispersible film. *Int J Pharm.* 2018;539:165–74. <https://doi.org/10.1016/J.IJPHARM.2018.01.047>.
 111. Huanbutta K, Sriamornsak P, Singh I. Manufacture of 2D-printed precision drug-loaded orodispersible film prepared from tamarind seed gum substrate. *Appl Sci.* 2021;11:5852. <https://doi.org/10.3390/APP11135852>.
 112. Öblom H, Sjöholm E, Rautamo M. towards printed pediatric medicines in hospital pharmacies: comparison of 2D and 3D-printed orodispersible warfarin films with conventional oral powders in unit dose sachets. *Pharmaceutics.* 2019. <https://doi.org/10.3390/PHARMACEUTICS11070334>.
 113. Landová H, Vetchý D. Evaluation of the influence of formulation and process variables on mechanical properties of oral mucoadhesive films using multivariate data analysis. *BioMed Res Int.* 2014. <https://doi.org/10.1155/2014/179568>.
 114. Evans SE, Harrington T, Rodriguez Rivero MC, et al. 2D and 3D inkjet printing of biopharmaceuticals—a review of trends and future perspectives in research and manufacturing. *Int J Pharm.* 2021;599: 120443. <https://doi.org/10.1016/J.IJPHARM.2021.120443>.
 115. Jamróz W, Kurek M, Łyszczarz E, et al. 3D printed orodispersible films with Aripiprazole. *Int J Pharm.* 2017;533:413–20. <https://doi.org/10.1016/J.IJPHARM.2017.05.052>.
 116. Cho HW, Baek SH, Lee BJ, et al. Orodispersible polymer films with the poorly water-soluble drug, olanzapine: hot-melt pneumatic extrusion for single-process 3D printing. *Pharmaceutics.* 2020;12:1–16. <https://doi.org/10.3390/PHARMACEUTICS12080692>.
 117. Eleftheriadis GK, Ritzoulis C, Bouropoulos N, et al. Unidirectional drug release from 3D printed mucoadhesive buccal films using FDM technology: In vitro and ex vivo evaluation. *Eur J Pharm Biopharm.* 2019;144:180–92. <https://doi.org/10.1016/J.EJPB.2019.09.018>.
 118. Than YM, Titapiwatanakun V. Tailoring immediate release FDM 3D printed tablets using a quality by design (QbD) approach. *Int J Pharm.* 2021;599: 120402. <https://doi.org/10.1016/J.IJPHARM.2021.120402>.
 119. Nukala PK, Palekar S, Patki M, et al. Abuse deterrent immediate release egg-shaped tablet (Egglets) using 3D printing technology: quality by design to optimize drug release and extraction. *AAPS PharmSciTech.* 2019. <https://doi.org/10.1208/S12249-019-1298-Y>.
 120. Zhang J, Thakkar R, Zhang Y. Structure-function correlation and personalized 3D printed tablets using a quality by design (QbD) approach. *Int J Pharm.* 2020. <https://doi.org/10.1016/J.IJPHARM.2020.119945>.
 121. Palekar S, Nukala P, Mishra S. Application of 3D printing technology and quality by design approach for development of age-appropriate pediatric formulation of baclofen. *Int J Pharm.* 2019;556:106–16. <https://doi.org/10.1016/J.IJPHARM.2018.11.062>.
 122. Goyanes A, Fina F, Martorana A, et al. Development of modified release 3D printed tablets (printlets) with pharmaceutical excipients using additive manufacturing. *Int J Pharm.* 2017;527:21–30. <https://doi.org/10.1016/J.IJPHARM.2017.05.021>.
 123. Markl D, Zeitler JA, Rasch C. Analysis of 3D prints by X-ray computed microtomography and terahertz pulsed imaging. *Pharm Res.* 2016;34:1037–52. <https://doi.org/10.1007/S11095-016-2083-1>.
 124. Gioumouxouzis CI, Katsamenis OL, Fatouros DG. X-ray micro-focus computed tomography: a powerful tool for structural

- and functional characterisation of 3D printed dosage forms. *J Microsc.* 2019. <https://doi.org/10.1111/JMI.12798>.
125. Alhijaj M, Nasereddin J, Belton P. Impact of processing parameters on the quality of pharmaceutical solid dosage forms produced by fused deposition modeling (FDM). *Pharmaceutics.* 2019;11:633. <https://doi.org/10.3390/PHARMACEUTICS11120633>.
 126. Trenfield SJ, Goyanes A, Telford R, et al. 3D printed drug products: non-destructive dose verification using a rapid point-and-shoot approach. *Int J Pharm.* 2018;549:283–92. <https://doi.org/10.1016/J.IJPHARM.2018.08.002>.
 127. Rachid O, Rawas-Qalaji M, Estelle F. Dissolution testing of sublingual tablets: a novel in vitro method. *AAPS PharmSciTech.* 2011;2011(12):544–52. <https://doi.org/10.1208/s12249-011-9615-0>.
 128. Reynolds TD, Mitchell SA, Balwinski KM. Investigation of the effect of tablet surface area/volume on drug release from hydroxypropylmethylcellulose controlled-release matrix tablets. *Drug Dev Ind Pharm.* 2002. <https://doi.org/10.1081/DDC-120003007>.
 129. Goyanes A, Robles Martinez P, Buanz A, et al. Effect of geometry on drug release from 3D printed tablets. *Int J Pharm.* 2015. <https://doi.org/10.1016/j.ijpharm.2015.04.069>.
 130. Madzarevic M, Medarevic D, Vulovic A. Optimization and prediction of ibuprofen release from 3D DLP printlets using artificial neural networks. *Pharmaceutics.* 2019. <https://doi.org/10.3390/PHARMACEUTICS11100544>.
 131. Obeid S, Madžarević M, Krkobabić M, et al. Predicting drug release from diazepam FDM printed tablets using deep learning approach: Influence of process parameters and tablet surface/volume ratio. *Int J Pharm.* 2021;601: 120507. <https://doi.org/10.1016/J.IJPHARM.2021.120507>.
 132. Novák M, Boleslavská T, Grof Z, et al. Virtual prototyping and parametric design of 3D-printed tablets based on the solution of inverse problem. *AAPS PharmSciTech.* 2018;19:3414–24. <https://doi.org/10.1208/s12249-018-1176-z>.
 133. Goyanes A, Madla CM, Umerji A, et al. Automated therapy preparation of isoleucine formulations using 3D printing for the treatment of MSUD: First single-centre, prospective, crossover study in patients. *Int J Pharm.* 2019;567: 118497. <https://doi.org/10.1016/J.IJPHARM.2019.118497>.

2.2 Patent: Filament Cutting Device

Evaluation of authorship:

author	idea [%]
Rebecca Chamberlain	40
Stefan Stich	30
Jörg Breitzkreutz	25
Corell Spöringer	5

Schneidevorrichtung und Schneidverfahren für Schnittstücke von Extrudaten unterschiedlicher Länge

Rebecca Chamberlain ¹, Stefan Stich ¹, Jörg Breitzkreutz ¹, Corell Spöringer ²

¹Institute of Pharmaceutics and Biopharmaceutics, Heinrich Heine University, Universitaetsstrasse 1, 40225 Duesseldorf, Germany

²Feinmechanik Düsseldorf, Heinrich Heine University, Universitaetsstrasse 1, 40225 Duesseldorf, Germany

Patent DE102022002368A1

Summary

The invention relates to a cutting device for producing cut pieces of extrudates of different lengths using cutting disks which have at least one hole away from the axis of rotation, as well as a method for producing cut pieces of extrudates of different lengths using cutting disks which have at least one hole away from the axis of rotation and the use of such a cutting device, especially in the pharmaceutical industry and/or in additive manufacturing.



(10) **DE 10 2022 002 368 A1** 2024.01.04

(12) **Offenlegungsschrift**

(21) Aktenzeichen: **10 2022 002 368.7**

(22) Anmeldetag: **30.06.2022**

(43) Offenlegungstag: **04.01.2024**

(51) Int Cl.: **B26D 1/14 (2006.01)**

B29C 37/00 (2006.01)

B26D 3/16 (2006.01)

B26D 1/29 (2006.01)

B29B 9/00 (2006.01)

B29B 9/06 (2006.01)

B02C 18/18 (2006.01)

B01J 2/00 (2006.01)

A61J 3/00 (2006.01)

(71) Anmelder:
**Universität Düsseldorf. Körperschaft des
öffentlichen Rechts, 40225 Düsseldorf, DE**

(74) Vertreter:
**IPrime Bonnekamp Sparing
Patentanwalts-gesellschaft mbH, 40211
Düsseldorf, DE**

(72) Erfinder:
**Chamberlain, Rebecca, 47239 Duisburg, DE;
Breitkreutz, Jörg, 45721 Haltern am See, DE;
Stich, Stefan, 53179 Bonn, DE; Spöringer, Corell,
42781 Haan, DE**

(56) Ermittelter Stand der Technik:

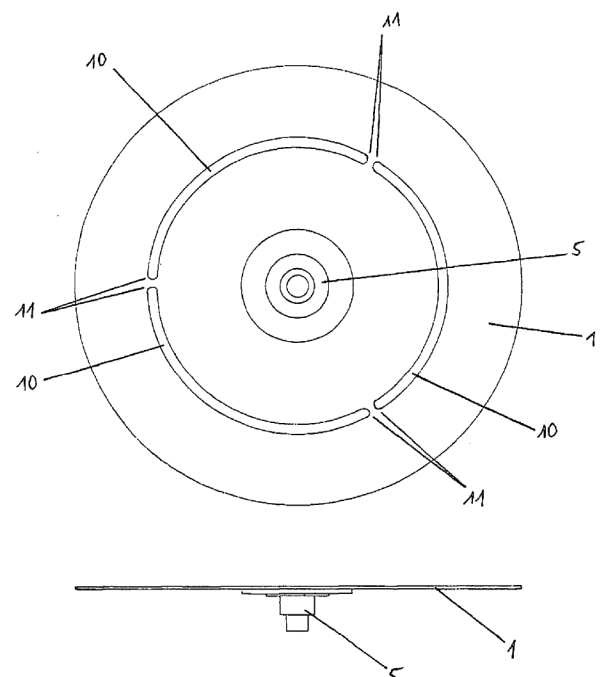
DE	10 2017 120 047	A1
DE	93 11 705	U1
DE	20 2008 013 118	U1
DE	693 32 246	T2
US	4 404 879	A
WO	96/ 34 728	A1

Rechercheantrag gemäß § 43 PatG ist gestellt.

Die folgenden Angaben sind den vom Anmelder eingereichten Unterlagen entnommen.

(54) Bezeichnung: **Schneidevorrichtung und Schneideverfahren für Schnittstücke von Extrudaten unterschiedlicher Länge**

(57) Zusammenfassung: Die Erfindung betrifft eine Schneidvorrichtung zur Herstellung von Schnittstücken von Extrudaten unterschiedlicher Länge mit Hilfe von Schneidscheiben, die mindestens ein Loch abseits der Rotationsachse aufweisen, sowie ein Verfahren zur Herstellung von Schnittstücken von Extrudaten unterschiedlicher Länge mit Hilfe von Schneidscheiben, die mindestens ein Loch abseits der Rotationsachse aufweisen und die Verwendung einer solchen Schneidvorrichtung, insbesondere in der pharmazeutischen Industrie und/oder in der additiven Herstellung.



Beschreibung

[0001] Die Erfindung betrifft eine Schneidvorrichtung zur Herstellung von Schnittstücken von Extrudaten unterschiedlicher Länge mit Hilfe von Schneidscheiben, die mindestens ein Loch abseits der Rotationsachse aufweisen, sowie ein Verfahren zur Herstellung von Schnittstücken von Extrudaten unterschiedlicher Länge mit Hilfe von Schneidscheiben, die mindestens ein Loch abseits der Rotationsachse aufweisen und die Verwendung einer solchen Schneidvorrichtung, insbesondere in der pharmazeutischen Industrie und/oder in der additiven Herstellung.

[0002] Die Extrusion ist ein häufig genutztes Mittel in der pharmazeutischen Herstellung, um feste Dispersionen oder Lösungen herzustellen. Ein großer Vorteil bietet hierbei das lösungsmittelfreie Arbeiten. Mit Hilfe von Polymeren, Wachsen, Lipiden und anderen Hilfsstoffen werden bevorzugt schlecht lösliche Arzneistoffe (BCS Klasse 2 und 4) zu festen Lösungen verarbeitet, um die Bioverfügbarkeit dieser Wirkstoffe zu erhöhen. Die Extrusion stellt ein kontinuierliches Verfahren da, bei dem die Weiterverarbeitung des extrudierten Materials, das sogenannte Downstreaming, ein weites Feld an Möglichkeiten bietet (Rundungsprozesse, Mahlprozesse, Schneidprozesse etc.).

[0003] Die technische Downstreaming Ausrüstung der pharmazeutischen Industrie beinhaltet bis heute keine Schneidevorrichtung, welche einen geraden Schnitt von Filamentstücken während der Herstellung garantiert. Für das Schneiden von Extrudaten in der pharmazeutischen Technologie sind rotierende Messer (Rotationscutter) bekannt, welche Extrudate (Schmelzextrudate oder Granulate) in kurze Extrudatstränge schneiden, allerdings keine geraden Schnitte garantieren.

[0004] Für die Herstellung von Pellets ist das ausreichend, allerdings ist dies inakzeptabel für die Herstellung von Filamentstücken für eine pharmazeutische, additive Herstellung. Diese additive Fertigung beinhaltet die Herstellung von pharmazeutischen Darreichungsformen mithilfe eines geeigneten 3D-Drucksystems. Hierfür sind 3D Drucker geeignet, welche mithilfe des Schmelzschichtverfahrens Geometrien fertigen, welche als Darreichungsformen verwendet werden können. Außerdem ist es wichtig, dass die Messer schnell betrieben werden, da diese ansonsten im Extrudat hängen bleiben und dadurch den Extrusionsprozess stoppen würden. Die Herstellung von längeren Stücken (> 3 mm) ist so nicht möglich. Es existieren weiterhin sogenannte Kopf-Abschneider (face cutter), die pharmazeutische Pellets durch einen Heißabschlag herstellen.

[0005] Da es allerdings insbesondere bei Polymeren bei unvollständiger Abkühlung zu einer Ausdehnung des Materials kommt, wird der Schnitt beim Abkühlen des Intermediats nachträglich negativ beeinflusst. Deswegen ist nach Abkühlung der Schmelzextrudate eine Abrundung an der Schnittkante zu erkennen, obwohl der Schnitt gerade vollzogen wurde.

[0006] In der Lebensmittel- und Kunststoffindustrie werden ebenfalls Methoden angewandt, welche Schnitte verschiedenster Kunststoffe oder Lebensmittel ermöglichen. Bei der Herstellung von Lebensmitteln werden meist Kopf-Abschneider eingesetzt oder die Schneidevorrichtungen werden beispielsweise mittels Ultraschall verstärkt, um eine Verbrennung der Ware zu vermeiden. Bei der Herstellung von Schläuchen werden Guillotinen, rotierende Klingen oder Sägen verwandt. Oft werden Schläuche über eine scharfe Klinge gedreht, um einen geraden Schnitt vollziehen zu können. Allerdings ist die Handhabung der Schneidevorrichtungen nicht auf die hohen pharmazeutischen Anforderungen an wirksstoffhaltige Extrudate zu übertragen. Außerdem sind aus dem Stand der Technik Schneidemethoden bekannt, die nicht während des Prozesses (inline), sondern erst nach dem Prozess (offline) erfolgen. Dies hat den Nachteil, dass Material verworfen werden muss. Daher ist das Ziel einen vollständig, kontinuierlich ablaufenden Prozess zu generieren, damit Zeit, Material und Kosten gespart werden können.

[0007] Aus der DE9311705U1 ist eine Schneidevorrichtung mit Förderkanal und einer diesem zugeordneten Fördereinrichtung für einen Kunststoffstrang bekannt, wobei der Förderkanal über eine Öffnung in eine Zerkleinerungseinrichtung mündet, die ein um eine Messerdrehachse rotierbares Messerelement mit wenigstens einem Schneidkante aufweisenden Messer hat, und wobei sich an die Zerkleinerungseinrichtung eine Transport- und eine Plastifiziereinrichtung zur Plastifizierung und für den Ausstoß des zerkleinerten Kunststoffmaterials anschließen. Der Nachteil dieser Vorrichtung ist, dass kein Strang mit beliebiger Länge geschnitten werden kann und der Schnitt nur von einer Seite mit geradem Messer erfolgt.

[0008] Die WO 9634728 A1 beschreibt eine Granuliertorrichtung für Strangmaterialien mit einer Einzugsvorrichtung zur Erfassung des Strangmaterials und dessen Förderung zu einem Gegenmesser, wobei das Gegenmesser mit einer mit dem Gegenmesser zusammenarbeitenden Messerwalze zum Zerschneiden des Strangmaterials zu Granulat eingesetzt wird. Diese Vorrichtung dient jedoch nur zum Zerkleinern, Pelletieren oder Granulieren. Es werden nur kurze Stücke erhalten.

[0009] Die DE 69332246 T2 beschreibt eine Strangschneidevorrichtung zum Schneiden von wenigstens einem linear ausgebildeten Strang mit einem Rotationsklingen Aufbau. An einer Drehwelle sind eine Vielzahl von Rotationsklingen angeordnet, die an und um die Drehwelle herum radial befestigt sind. Die Vorrichtung ermöglicht den Schnitt des Stranggutes nur von einer Seite und es werden nur kurze Stücke erzeugt, da eine Filamentweiterführung nicht vorgesehen ist.

[0010] Die US 4404879 A zeigt eine rotierende Schneidevorrichtung, die eine Schere, eine angetriebene Vorschubwalze und eine angetriebene Gegenwalze umfassen, die sich um parallele Achsen auf Wellen in entgegengesetzte Richtungen zueinander drehen. Auch bei dieser Vorrichtung erfolgt ein Schnitt nur von einer Seite und es kann kein Strang mit einer vorbestimmten Länge geschnitten werden.

[0011] Die DE 102017120047 A1 offenbart ein Verfahren zum Zerkleinern von pastösen Stoffen. Die pastösen Stoffe werden mittels einer Düse aus dem Extruder herausgedrückt und mit dem Austritts-Strömungsquerschnitt einem rotierenden Schneidwerkzeug zugeführt, wobei der Schnitt quer zur Austrittsrichtung erfolgt. Der Schnitt erfolgt vorliegend nur einseitig durch ein rotierendes Messer.

[0012] Aufgabe der Erfindung ist es eine Schneidevorrichtung für pharmazeutische Wirkstoffe enthaltende extrudierte, thermoplastische Fasern bereitzustellen, die ein verformungsfreies Schneiden der Filamente und ein nahtloses Zusammenführen insbesondere der Filamente in ein Fördersystem für die additive Fertigung mittels Schmelzschichtung von Medikamenten ermöglichen.

[0013] Die Aufgabe wird durch die Merkmale der unabhängigen Ansprüche 1, 5 und 9 gelöst.

[0014] Die Erfindung betrifft eine Schneidvorrichtung zum Schneiden von Extrudaten aus Extrusionsprozessen, ein Verfahren und eine Verwendung diesbezüglich, um pharmazeutische Extrudate in beliebig große Stücke schneiden zu können.

[0015] Unter Extrudat oder Extrudaten werden vorliegend plastisch verformbare bis dickflüssige Massen verstanden, die unter Druck kontinuierlich aus einer formgebenden Öffnung herausgepresst werden. Als Filament werden Fadenwerke bezeichnet, die allgemein eine einzelne Faser beliebiger Länge umfassen und als Bezeichnung auch für eine Mehrzahl an Fasern mit praktisch unbegrenzter Länge verwendet werden können. Filamente als Extrusionsstoff bzw. Extrudat können in vielerlei Form Verwendung finden, so als PLA (Polymilchsäure), ABS (Acrylonitril-Butadien-Styrol-Copolymer), PETG (PET, PETT) (Polyethylenterephthalat + Glykol),

Nylon (Polyamid) oder als TPE (Flexibel) (Thermoplastisches Elastomer). In der pharmazeutischen Industrie werden pharmazeutisch relevante Wirk- und Hilfsstoffe für die Herstellung von Extrudaten bzw. Filamenten für die jeweilige Anwendung verwendet.

[0016] Erfindungsgemäß ist vorgesehen, dass zur Erzeugung von Extrudatstücken oder Schnittstücken eine Vorrichtung bereitgestellt wird, die mindestens zwei Schneidscheiben mit jeweils mindestens einem Loch mit Schneidkante aufweist. Die Schneidscheiben werden über ein Lager koaxial geführt und rotieren gegenläufig. Die Schneidscheiben können aus Metall oder aus kunstharzgebundenen Verbindungen mit Korund oder Siliziumkarbid bestehen oder auch Nitridverbindungen oder Diamantstrukturen aufweisen. In jeder der Schneidscheiben ist mindestens ein Loch oder Durchbruch vorhanden, das abseits der Rotationsachse lokalisiert ist und über die ein Extrudat-bzw. Filamentstrang durch die Löcher gelangt und an einer Schneidkante der Löcher in Stücke geschnitten wird.

[0017] Durch das gegenläufige Rotieren der Schneidscheiben erfolgt der Schnitt nicht einseitig, was bedeutet, dass die Schnittfläche nicht in Rotationsrichtung gebogen, sondern plan ist und keine Extrudathaken an den Schnittstücken in Rotationsrichtung aufweist. Dies steht im Gegensatz zu geschnittenen Extrudaten bei Vorhandensein nur einer Schneidscheibe oder Rotation der Schneidscheiben in nur eine Richtung.

[0018] In den Schneidscheiben ist pro Schneidscheibe mindestens ein Loch ausgebildet, das radial an der Innenseite des Lochs eine Schneidkante aufweist. Es muss mindestens ein Loch pro Schneidscheibe vorhanden sein. Es können jedoch auch mehr als ein Loch, beispielsweise zwei, drei, vier oder mehr Löcher pro Schneidscheibe vorhanden sein, wobei auch eine konzentrierte Anordnung von Schneidscheiben, d.h. eine Anordnung von Schneidscheiben, bei der eine Scheibe mindestens ein Loch weniger aufweist als die andere, möglich ist. Die Schneidkante der Langlöcher ist entsprechend der Querschnittsfläche der Schnittware ausgestaltet und kann bei runder Querschnittsfläche bogenförmig ausgebildet werden.

[0019] Weiterhin kann eine Schneidkante nur einen Teilbereich eines Lochs umfassen, aber das Loch auch vollumfänglich mit einer Schneidkante ausgebildet sein. Durch die Größe und/oder Form des Lochs in den Schneidscheiben können unterschiedliche Extrudatschnitte und Extrudatschnittformen bzw. Filamentschnitte generiert werden.

[0020] Die Extrusionsmasse bzw. das Extrudat wird aus einem Extruder direkt über Führungseinsätze

am Gehäuse der Schneidvorrichtung an die Schneidscheiben geleitet und dort in die gewünschte Länge geschnitten. Die Führungseinsätze sind mit Dichtungen am Gehäuse versehen, um einen gleichmäßigen und geradlinigen Fluss der Extrusionsmasse bzw. des Extrudats zu gewährleisten. Dies ist insbesondere deswegen erforderlich, um einen glatten planen Schnitt gewährleisten zu können.

[0021] Besonders bei der Verwendung von Extrudat- oder Filamentstücken, welche in der Regel für die additive Fertigung von Darreichungsformen eine Länge von über 10 cm aufweisen sollen, ist es wichtig, dass bei Nachladung des Materials in den 3D-Drucker der Materialfluss kontinuierlich erfolgen kann, um eine genaue Dosierung zu ermöglichen. Dies kann nur garantiert werden, wenn die Extrudate oder Filamente gerade und plan geschnitten werden und diese kolbenförmig, ohne Störstellen im Druckkopf des 3D-Druckers zur Düse gelangen.

[0022] In einer besonderen Ausgestaltung sind die Löcher in den Schneidscheiben als Langlöcher ausgestaltet. Ein Langloch ist erfindungsgemäß eine längliche Bohrung oder Nut in den Schneidscheiben. Die schmalen Seiten der Langlöcher werden durch Halbkreise gebildet, deren Durchmesser der Breite des Langlochs entsprechen, wobei die Längsseiten des Langloches parallel zueinander verlaufen. Entlang der Längsseiten und/oder der Halbkreise der Langlöcher ist radial an der Innenseite eine Schneidkante ausgebildet mittels dieser die Extrudate oder Filamente geschnitten werden. Durch die Länge der Langlöcher wird das zeitliche Auftreffen auf die Schnittware festgelegt. Es können mehrere Langlöcher auf der Schneidscheibe vorhanden sein. Die Schneidkante kann sich somit über die gesamte Länge der Längsseiten der Langlöcher erstrecken oder auch nur einen radialen Endbereich der Halbkreise der Langlöcher umfassen. Die Schneidkanten können analog zu der runden Querschnittsfläche der Extrudate oder Filamente bogenförmig ausgestaltet sein. Die bogenförmige Ausgestaltung der Schneidkante hat den Vorteil, dass ein bogenförmiger Schnitt der Extrudate oder Filamente entlang der Rotationsrichtung der Schneidscheiben erfolgt. Die Ausgestaltung der Löcher als Langlöcher hat gegenüber kreisrunden Löchern den Vorteil, dass der kontinuierliche Herstellungsprozess nicht unterbrochen wird, da das Extrudat oder Filament bei Rotation der Schneidscheiben durch die Langlöcher weiter gefördert wird ohne geschnitten zu werden. Es ist insbesondere von Vorteil, dass der gesamte Prozess der Herstellung von Extrudatschnittstücken durch die Schneidvorrichtung kontinuierlich erfolgt. Dadurch kann das Extrudat während des Extrusionsprozesses kontinuierlich weiter gefördert und in die gewünschte Länge geschnitten werden. Der Extrusionsprozess muss nicht unterbrochen werden oder erst nachträglich ein Zerkleinern der bereits erzeugten und abge-

kühlten Extrudatstränge vorgenommen werden. Daher kann der gesamte Herstellungsprozess schneller und kostengünstiger erfolgen.

[0023] Erfindungsgemäß ist ferner ein Verfahren zur Herstellung von Schnittstücken unterschiedlicher Länge mit Hilfe von Schneidscheiben vorgesehen, wobei die Extrudate aus einem Extruder über Führungseinsätze mit Dichtungen an einem Gehäuse zu mindestens einem Loch pro Schneidscheibe geführt und durch mindestens zwei Schneidscheiben geschnitten werden, wobei die Schneidscheiben gegenläufig und coaxial rotieren und pro Loch eine Schneidkante abseits der Rotationsachse aufweisen. Durch das Verfahren wird gewährleistet, dass der Schnitt nicht einseitig erfolgt. Die Schnittfläche der Schnittstücke der Extrudate ist daher nicht in Rotationsrichtung gebogen, sondern plan und weist keine Extrudathaken in Rotationsrichtung auf.

[0024] In einer vorteilhaften Ausgestaltung werden die zu schneidenden Extrudate durch mindestens ein Langloch geführt, welches jeweils eine Schneidkante aufweist. Die Ausgestaltung der Löcher als Langlöcher hat gegenüber kreisrunden Löchern den Vorteil, dass der Ausgleich von Toleranzen bei der Führung der Extrudate oder Filamente in die Löcher der Schneidscheibe vereinfacht ist. Die Löcher sind dabei mit den Schneidkanten in der Regel horizontal ausgestaltet und verlaufen bogenförmig.

[0025] Es ist ferner festzustellen, dass die gewünschte Länge der Schnittstücke mittels der erfindungsgemäßen Schneidvorrichtung gesteuert und/oder des erfindungsgemäßen Verfahrens eingestellt werden kann. So wird die gewünschte Länge der Schnittstücke insbesondere durch die Transportgeschwindigkeit der Extrudate bei gleichbleibender Rotationsgeschwindigkeit der Schneidscheiben und durch die Länge des Loches und durch das Auftreffen auf die Schneidkante auf das Extrudat bestimmt.

[0026] Die erfindungsgemäße Schneidvorrichtung kann zur Herstellung von Schnittstücken unterschiedlicher Länge, insbesondere für die pharmazeutischen Industrie und/oder für eine additive Herstellung verwenden werden.

[0027] Die Erfindung wird anhand der nachfolgenden Figuren nochmals eingehend erläutert:

Fig. 1 zeigt eine vertikale Schnittzeichnung einer Schneidvorrichtung mit zwei Schneidscheiben 1, 2, die über zwei Aufnahmen 3 umseitig gelagert sind. Die Schneidscheiben 1, 2 werden über eine Aufnahme 5 geführt und über die Antriebsräder 6 angetrieben, wobei die Schneidscheiben gegenläufig rotieren. Über Führungseinsätze 4 werden Extrudate in die Löcher 10 (nicht dargestellt) geleitet.

In **Fig. 2** ist eine Explosionszeichnung der erfindungsgemäßen Schneidvorrichtung dargestellt. Die Schneidscheiben 1, 2 sind innerhalb eines Gehäuses 7 angeordnet und über umseitige Lagerungen 3 mit dem Gehäuse 7 verbunden. Mittels Aufnahmen 5a werden die gegenläufigen Schneidscheiben 1, 2 am Gehäuse 7 arretiert und über Aufnahmen 5b mit einem Antriebsrad verbunden. Weiterhin ist zu erkennen, dass Führungseinsätze 4a mit Dichtungen 4b am Gehäuse angeordnet sind, die die Extrudate in die vorliegend nicht dargestellten Löcher (10) mit den Schneidkanten (11) leiten.

a	Aufnahme verbunden mit Schneidscheibe
b	Aufnahme zur Befestigung des Antriebsrads
6	Antriebsrad
7	Gehäuse
8	Befestigung des Gehäuses
9	Befestigungsschrauben
10	Loch
11	Langlochende/ Schneidkante

In **Fig. 3** ist eine Auf- und Seitenansicht der erfindungsgemäßen Schneidvorrichtung mit dem Gehäuse 7 dargestellt. Man erkennt auf der linken Seite der Abbildung eine Schneidscheibe 1, 2, die über eine Aufnahme 5 im Gehäuse 7 angeordnet ist. Die Gehäusehälften 7 werden über Schrauben 8, 9 aneinander befestigt, innerhalb dessen sich die Schneidscheiben 1, 2 befinden. Ferner sind die Antriebsräder 6 der gegenläufigen und coaxial gelagerten Schneidscheiben 1, 2 dargestellt.

Fig. 4 zeigt eine Aufsicht und eine horizontale Schnittansicht der erfindungsgemäßen Schneidvorrichtung. Man erkennt die Befestigungen 8, 9 der Gehäusehälften des Gehäuses 7. Über die umseitige Lagerung 3 werden die Schneidscheiben 1, 2 geführt, die über die Aufnahme 5 coaxial und gegenläufig zueinander rotieren. Mittels der Führungseinsätze 4 werden die Extrudate bzw. Filamente in die Löcher 10 mit den Schneidkanten 11 geführt (nicht dargestellt).

Aus **Fig. 5** erkennt man eine Schneidscheibe 1 in einer Aufsicht und horizontalen Ansicht, bei der umlaufend drei Löcher 10 in Form eines Langlochs vorhanden sind, die bogenförmig ausgebildet sind. An den radialen Endbereichen der Langlöcher 10 sind Schneidkanten 11 lokalisiert, die ein Extrudat oder Filament, das über Führungseinsätze in die Langlöcher 10 geleitet wird, schneiden können. Die Schneidscheibe 1 wird über eine Aufnahme 5 geführt, die die Rotationsachse der Schneidscheibe 1 bildet.

Bezugszeichenliste:

1	Schneidscheibe 1
2	Schneidscheibe 2 (gegenläufig)
3	Lagerung der Schneidscheibe
4	Führungseinsatz für Extrudate/Filamente
a	Führungseinsatz
b	Abdichtung des Führungseinsatzes
5	Aufnahme der Schneidscheibe

ZITATE ENTHALTEN IN DER BESCHREIBUNG

Diese Liste der vom Anmelder aufgeführten Dokumente wurde automatisiert erzeugt und ist ausschließlich zur besseren Information des Lesers aufgenommen. Die Liste ist nicht Bestandteil der deutschen Patent- bzw. Gebrauchsmusteranmeldung. Das DPMA übernimmt keinerlei Haftung für etwaige Fehler oder Auslassungen.

Zitierte Patentliteratur

- DE 9311705 U1 [0007]
- WO 9634728 A1 [0008]
- US 4404879 A [0010]
- DE 102017120047 A1 [0011]

Patentansprüche

1. Schneidvorrichtung zur Herstellung von Schnittstücken von Extrudaten unterschiedlicher Länge mit Hilfe von Schneidscheiben (1, 2), die über ein Antriebsrad angetrieben und über ein Lager (3) geführt sind, wobei die Schneidscheiben (1, 2) über Aufnahmen (5a, 5b) gehalten und die Schnittware durch Einsätze geführt werden, **dadurch gekennzeichnet**, dass die Schneidvorrichtung mindestens zwei Schneidscheiben (1, 2) aufweist, die gegenläufig und koaxial rotieren und eine Schneidkante (11) in jeweils einem Loch (10) der Schneidscheiben (1,2) abseits der Rotationsachse vorhanden ist.

2. Schneidvorrichtung nach Anspruch 1, **dadurch gekennzeichnet**, dass das Loch (10) als Langloch entlang der Schneidscheibe (1, 2) ausgestaltet ist.

3. Schneidvorrichtung nach Anspruch 1 oder 2, **dadurch gekennzeichnet**, dass das Loch (10) bogenförmig ausgestaltet ist.

4. Schneidvorrichtung nach einem der Ansprüche 1 bis 3, **dadurch gekennzeichnet**, dass der Transport der Schnittware durch die Schneidvorrichtung kontinuierlich erfolgt.

5. Verfahren zur Herstellung von Schnittstücken von Extrudaten unterschiedlicher Länge mit Hilfe von Schneidscheiben (1, 2), die mindestens ein Loch (10) abseits der Rotationsachse aufweisen, **dadurch gekennzeichnet**, dass die Schnittstücke über zu mindestens einem Loch (10) pro Schneidscheibe (1, 2) geführt und durch mindestens zwei Schneidscheiben (1, 2) geschnitten werden, wobei die Schneidscheiben (11, 2) gegenläufig und koaxial rotieren und pro Loch (11) eine Schneidkante (11) abseits der Rotationsachse aufweisen.

6. Verfahren zur Herstellung von Schnittstücken nach Anspruch 5, **dadurch gekennzeichnet**, dass die Schnittware durch mindestens ein Langloch geführt wird, welches jeweils eine Schneidkante (11) aufweist.

7. Verfahren zur Herstellung von Schnittstücken nach Anspruch 5 oder 6, **dadurch gekennzeichnet**, dass die Anzahl und die Länge der Langlöcher in der Schneidscheibe entsprechend der Länge der Schnittware gewählt werden kann.

8. Verfahren zur Herstellung von Schnittstücken nach einem der Ansprüche 5 bis 7, **dadurch gekennzeichnet**, dass die Schneidkanten entsprechend der Geometrie der Schnittware und somit in den Ausführungsformen gerade, gekrümmt oder bogenförmig ausgestaltet sind.

9. Verfahren zur Herstellung von Schnittstücken nach einem der Ansprüche 5 bis 8, **dadurch gekennzeichnet**, dass die Länge der Schnittstücke durch die Transportgeschwindigkeit bei gleichbleibender Rotationsgeschwindigkeit der Schneidscheiben (1, 2) durch die Länge des Loches (10) und durch das Auftreffen der Schneidkante auf die Schnittware bestimmt wird.

10. Verwendung einer Schneidvorrichtung zur Herstellung von Schnittstücken unterschiedlicher Länge mit Hilfe von Schneidscheiben (1, 2), die abseits der Rotationsachse mindestens ein Loch (10) aufweisen, wobei die Schneidvorrichtung mindestens zwei Schneidscheiben (1, 2) mit jeweils einer Schneidkante (11) aufweist, die gegenläufig und koaxial rotieren und jeweils eine Schneidkante (11) in jeweils einem Loch (10) abseits der Rotationsachse angeordnet ist, in der pharmazeutischen Industrie und/oder für eine additive Herstellung.

Es folgen 5 Seiten Zeichnungen

Anhängende Zeichnungen

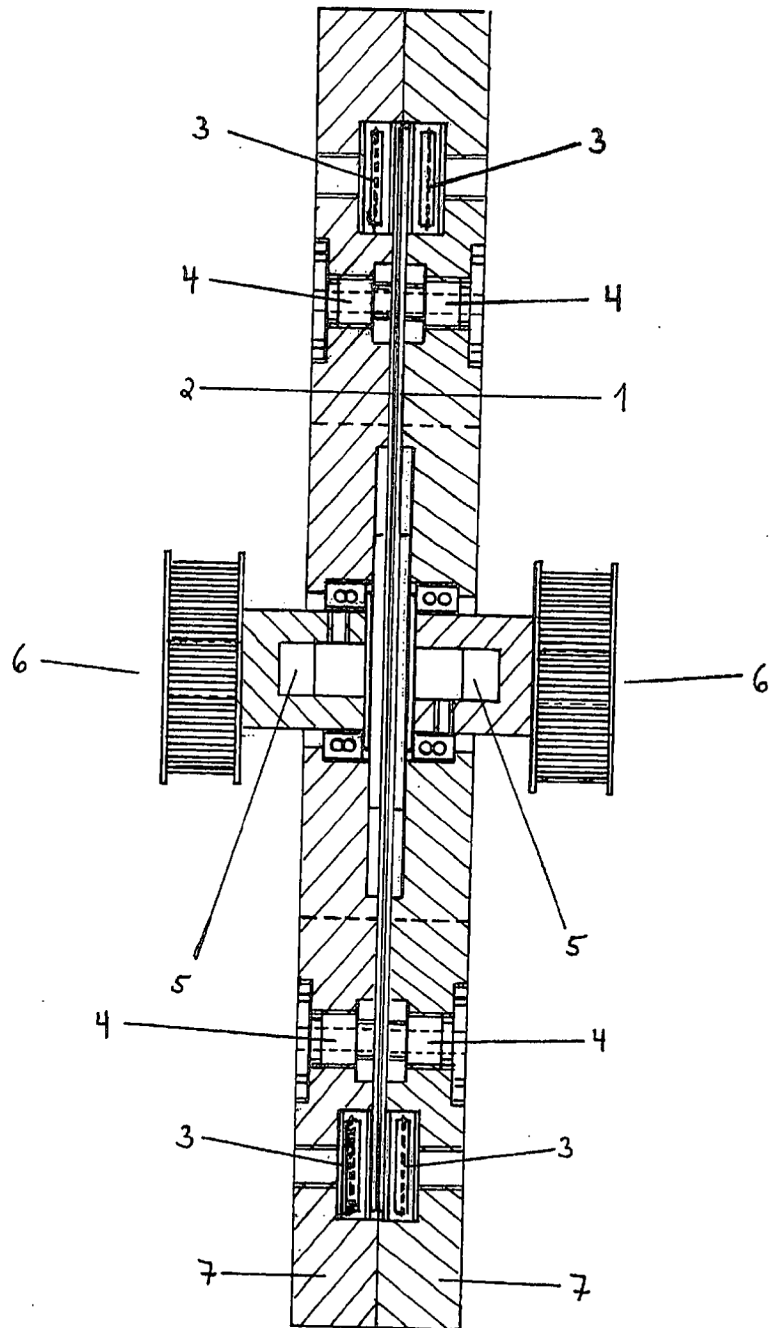


Fig.1

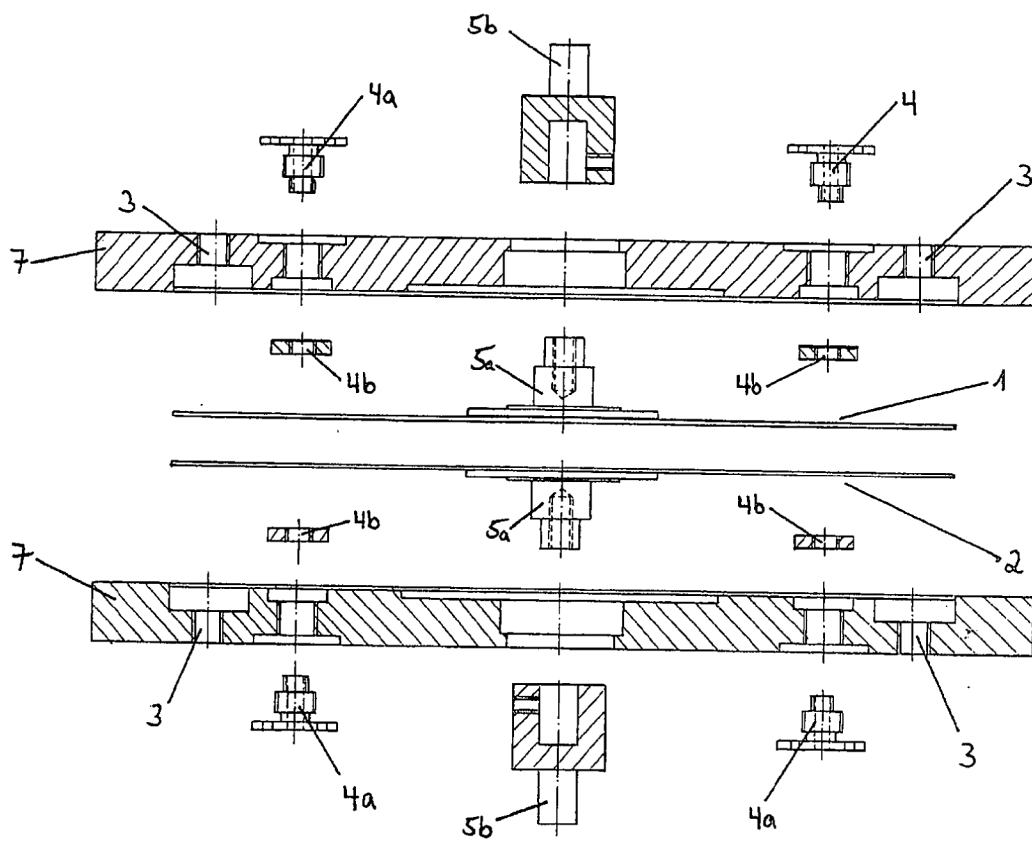


Fig.2

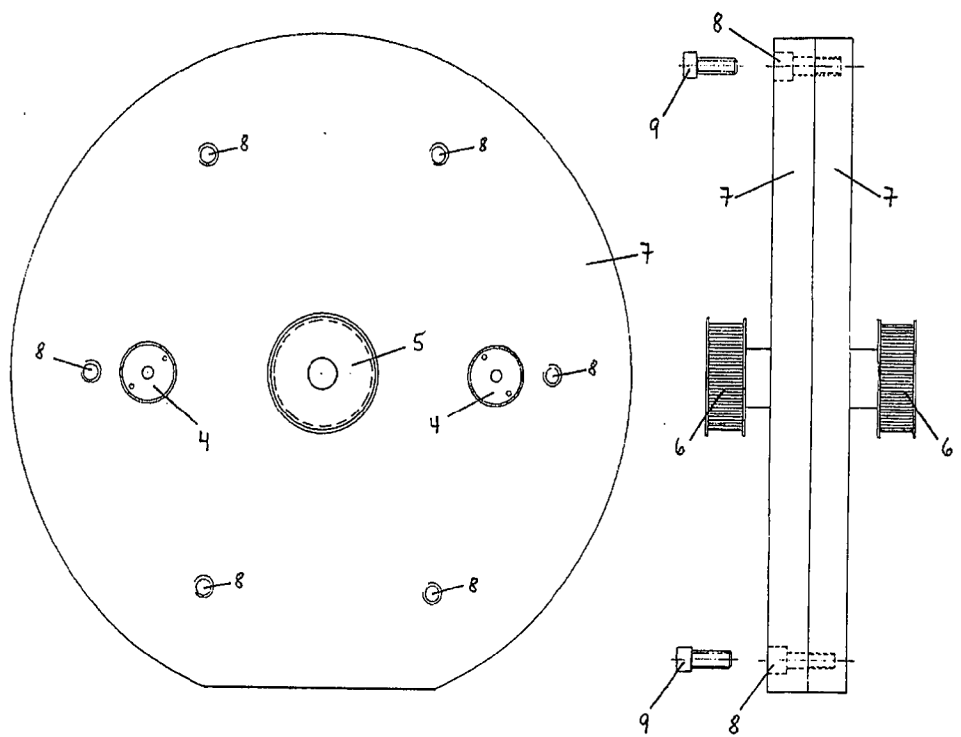


Fig.3

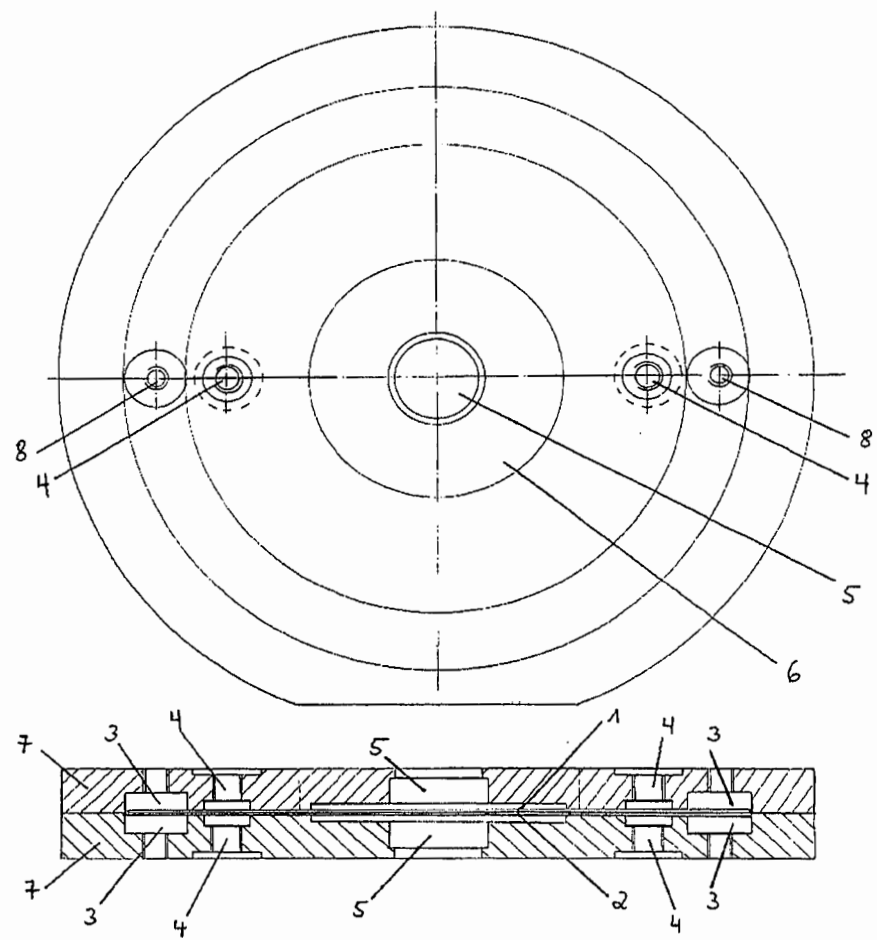


Fig.4

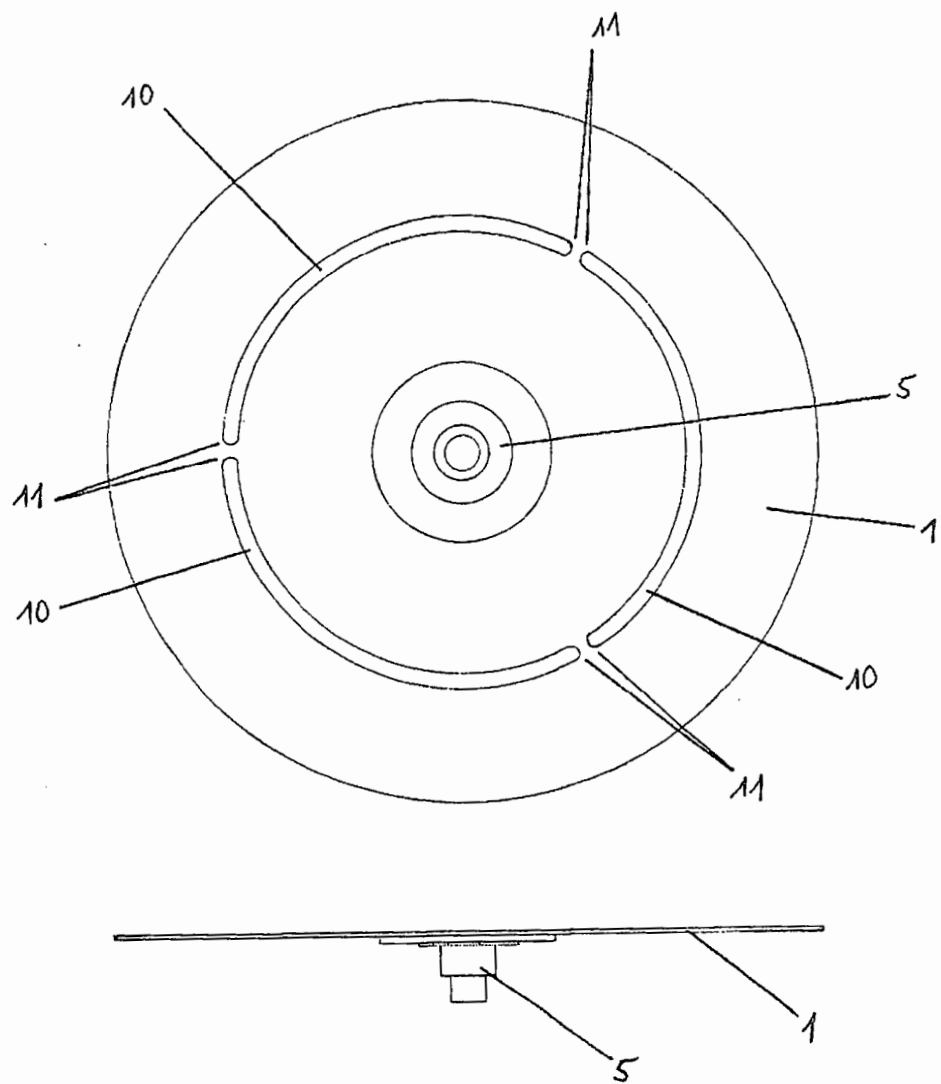


Fig.5

3 Characterization and Quality Control of Drug-loaded Filaments

3.1 Precise Dosing of Pramipexole for Low-Dosed Filament Production by Hot Melt Extrusion Applying Various Feeding Methods

Evaluation of authorship:

author	idea [%]	study design [%]	experimental [%]	evaluation [%]	manuscript [%]
Rebecca Chamberlain	60	80	80	100	80
Hellen Windolf	20	10	20	-	15
Simon Geissler	5	-	-	-	-
Julian Quodbach	5	10	-	-	5
Jörg Breitzkreutz	10	-	-	-	-

Evaluation of Copyright permission:

© 2022 by the authors. Licensee MDPI, Basel, Switzerland. This article is an open access article distributed under the terms and conditions of the Creative Commons Attribution (CC BY) license (<https://creativecommons.org/licenses/by/4.0/>).

Precise Dosing of Low-Dosed Filament Production by Hot Melt Extrusion Applying Various Feeding Methods

Rebecca Chamberlain ¹, Hellen Windolf ¹, Simon Geissler ², Julian Quodbach ^{1,*} and Jörg Breitzkreutz ¹

¹ *Institute of Pharmaceutics and Biopharmaceutics, Heinrich Heine University, Universitätsstraße 1, 40225 Düsseldorf, Germany;*

² *Merck KGaA, Frankfurter Straße 250, 64293 Darmstadt, Germany; simon.geissler@merckgroup.com*

Pharmaceutics

<https://doi.org/10.3390/pharmaceutics14010216>



Article

Precise Dosing of Pramipexole for Low-Dosed Filament Production by Hot Melt Extrusion Applying Various Feeding Methods

Rebecca Chamberlain ¹, Hellen Windolf ¹, Simon Geissler ², Julian Quodbach ^{1,*} and Jörg Breitzkreutz ¹

¹ Institute of Pharmaceutics and Biopharmaceutics, Heinrich Heine University, Universitätsstraße 1, 40225 Düsseldorf, Germany; rebecca.chamberlain@hhu.de (R.C.); hellen.windolf@hhu.de (H.W.); joerg.breitzkreutz@hhu.de (J.B.)

² Merck KGaA, Frankfurter Straße 250, 64293 Darmstadt, Germany; simon.geissler@merckgroup.com

* Correspondence: julian.quodbach@hhu.de; Tel.: +49-211-81-10076

Abstract: The aim of this research was the production of low-dosed filaments via hot-melt extrusion (HME) with the model drug pramipexole for the treatment of Parkinson's disease. The active pharmaceutical ingredient (API) and one of the polymers polyvinyl alcohol (PVA) or basic butylated methacrylate copolymer (bPMMA) were fed by various dosing techniques with the aim of achieving the smallest deviation (RSD) from the target concentration of 0.1% (*w/w*) pramipexole. It was found that deviation from target pramipexole concentration occurred due to degradation products in bPMMA formulations. Additionally, material temperature above 120 °C led to the formation of the anhydrous form of pramipexole within the extruded filaments and need to be considered in the calculation of the recovered API. This study clearly shows that even if equilibrium state of the extrusion parameters was reached, equilibrium condition for drug content was reached relatively late in the process. In addition, the RSD calculated by the Stange–Poole equation was proposed by us to predict the final content uniformity considering the sample size of the analyzed filament. The calculated RSD, depending on sample size and drug load, can serve as upper and lower limits of variation from target concentration and can be used to evaluate the deviations of drug content in equilibrium conditions of the HME process. The lowest deviations from target concentration in equilibrium condition for drug content were obtained in filaments extruded from previously prepared granule mixtures (RSD = 6.00%, acceptance value = 12.2). These promising results can be transferred to other API–excipient combinations to produce low-dosed filaments, which can be used for, e.g., fused filament 3D printing. The introduced calculation of the RSD by Stange–Poole equation can be used for precise determination of the homogeneity of an extruded batch.

Keywords: hot melt extrusion; low-dosed filament production; analytics of extruded filaments; fused filament 3D printing; oral dosage form; various dosing techniques; content uniformity; personalized medicine



Citation: Chamberlain, R.; Windolf, H.; Geissler, S.; Quodbach, J.; Breitzkreutz, J. Precise Dosing of Pramipexole for Low-Dosed Filament Production by Hot Melt Extrusion Applying Various Feeding Methods. *Pharmaceutics* **2022**, *14*, 216. <https://doi.org/10.3390/pharmaceutics14010216>

Academic Editors: Ionela Andreea Neacsu and Bogdan Stefan Vasile

Received: 15 December 2021

Accepted: 13 January 2022

Published: 17 January 2022

Publisher's Note: MDPI stays neutral with regard to jurisdictional claims in published maps and institutional affiliations.



Copyright: © 2022 by the authors. Licensee MDPI, Basel, Switzerland. This article is an open access article distributed under the terms and conditions of the Creative Commons Attribution (CC BY) license (<https://creativecommons.org/licenses/by/4.0/>).

1. Introduction

High-potent active ingredients have the desired pharmacological effect even at very low concentrations. In this study, the non-ergoline dopamine agonist pramipexole was chosen as a model substance because it is used at low dose strengths (lowest dose < 100 µg) in the treatment of Parkinson's disease and is water soluble (BCS class I) [1,2]. It is difficult to manufacture low-dosed drug products, wherein the API represents less than 1% (*w/w*) of the total mixture regardless of the number of excipients [3]. Especially for high-potency drugs, which often have a narrow therapeutic window, the API shall be as uniformly distributed within the matrix as possible in order to enable an accurate dosing. The European Pharmacopeia regulates the homogeneity of a batch with the help of the acceptance value for the drug product, which leaves a large margin and is highly dependent on the

mass [4]. Therefore, it is recommended that the blend, or in this study, the intermediate filament, be analyzed. Homogeneous mixing of particles with different sizes and shapes is particularly difficult and must be considered in the evaluation of the deviation from target drug content [5,6]. In hot melt extrusion (HME), either blending of powder particles occur before extrusion or mixing takes place alongside extrusion using kneading and conveying elements in the screw configuration. It is also possible that mixing involves both processes, but it must also be remembered that demixing can occur while feeding and/or extruding [7]. Once HME process parameters for producing low-dosed filaments are found, scale-up of HME is much easier to achieve than the scale-up of batch processes, since increasing the batch size requires for this continuous process only a longer run [8]. Since potential drawbacks such as heat stress and shear force on API, which could prevent the production of low-dosed filaments, have been overcome by choosing suitable excipients and self-emulsifying preparations, the focus of hot melt extrusion has increased for the preparation of many drug-loaded extrudates [9–11]. After cooling, it is possible that the produced solid dispersion or solid solution shows segregation and re-crystallization, and therefore the maintenance of content uniformity must be tested in a stability study [12]. In previous studies, the API was fed as an anti-solvent suspension into the barrel or even as a physical mixture to form a content uniform batch [13,14]. Sacher et al. developed a novel micro-feeder that was integrated into a continuous manufacturing line with the advantage of a separate feeding of the API [15]. Nevertheless, the properties of the API are indispensable for all described dosing methods in the literature, since in the case of an anti-solvent, the API must not be soluble in the solvent (e.g., water; otherwise, work must be carried out under explosion protection). In the case of a very low concentration of the API in a physical mixture and feeding by a self-made hopper, the solid properties, e.g., flowability, particle size distribution, and adhesion to surfaces, play an important role [16]. In addition, the sample size was not considered in the determination of the drug content, which, however, influences the standard deviation and therefore the validity of the information about content uniformity. The focus of this work was to produce low-dosed filaments for fused filament 3D printing, wherein the active ingredient was homogeneously distributed in a solid solution with the help of pharmaceutical-grade polymers. In order for these filaments to be obtained, PVA and bPMMA were chosen to form the polymer matrices. After PVA has been identified as the suitable matrix former, different dosing methods of the API were performed and the findings on the distribution of the low-dosed drug as well as the deviation of the target content (0.1% (*w/w*)) were described. Not only were difficulties of the individual dosing steps examined, but also the influence of the process parameters on the starting materials and the API was investigated.

2. Materials and Methods

The materials, which have been used for extrusion, are listed in Table 1. As HME is a heat-intensive process, the model substance was chosen regarding thermal resistance. The melting range of PDM, which also represents the temperature of decomposition, is 296–305 °C [1]. PVA was chosen as a polymer, representing an erodible and swelling polymer that predefines prolonged release of the API due to formation of a hydrocolloid matrix [17]. bPMMA was used as a second polymer, depicting an erodible matrix without swelling behavior [18]. For the formulation of printable filaments with bPMMA, mannitol (10% (*w/w*)) and sorbitol (5% (*w/w*)) were used serving as additives with plasticizing effect. Fumed silica (1% (*w/w*)) was used as a glidant for a better flowability of the powder during feeding in the course of dry granulation.

Table 2. Cont.

Temperature Profile in Zone 2–10/°C										
Zone	2	3	4	5	6	7	8	9	10	
PVA-P ("3 kneading zones")	die-10 CE 1 L/D-KZ 1: $4 \times 90^{\circ}$ - $3 \times 60^{\circ}$ - $3 \times 30^{\circ}$ -5 CE 1 L/D-KZ 2: $4 \times 90^{\circ}$ - $3 \times 60^{\circ}$ - $3 \times 30^{\circ}$ -5 CE 1 L/D-KZ 3: $10 \times 60^{\circ}$ -8 CE 1 L/D-1 CE $\frac{1}{2}$ L/D-2 CE 3/2 L/D-1 L/D adapter-gear									
PVA-P ("split feeding")	die-8 CE 1 L/D-KZ 1: $4 \times 90^{\circ}$ - $4 \times 60^{\circ}$ - $4 \times 30^{\circ}$ -5 CE 1 L/D-KZ 2: $5 \times 90^{\circ}$ - $4 \times 60^{\circ}$ - $3 \times 30^{\circ}$ -6 CE 1 L/D-3 DE L/D-3 CE 1 L/D-4 CE 3/2 L/D-1 L/D adapter-gear									
PVA-P ("granule feeding")	die-10 CE 1 L/D-KZ 1: $6 \times 60^{\circ}$ -5 CE 1 L/D-KZ 2: $6 \times 60^{\circ}$ -6 CE 1 L/D-KZ 3: $4 \times 90^{\circ}$ - $2 \times 60^{\circ}$ - $2 \times 30^{\circ}$ -10 CE 1 L/D-2 CE 3/2 L/D-1 L/D adapter-gear									
PVA-P ("liquid feeding")	die-10 CE 1 L/D-KZ 1: $5 \times 60^{\circ}$ -2 CE 1 L/D-2 CE LP 1 L/D-KZ 2: $5 \times 60^{\circ}$ -7 CE 1 L/D-KZ 3: $4 \times 90^{\circ}$ - $3 \times 60^{\circ}$ - $3 \times 30^{\circ}$ -10 CE 1 L/D-2 CE 3/2 L/D-1 L/D adapter-gear									

* CE = conveying element, KZ = kneading zone, DE = distributive element, LP = long pitch.

2.1.1. Split Feeding Setup

A second gravimetric feeder (PFW S 20 kg, Three-Tec, Seon, Switzerland) was installed on a table next to the extruder so that the same opening of the barrel could be used for feeders 1 and 2. The feed stock of feeder 1 was only polymer (feed rate: 5 g/min) and a mixture with 15.5% (*w/w*) API and 1% (*w/w*) anhydrous silica, and polymer was fed with a feed rate of 50 rpm with the help of feeder 2. Two kneading zones were used to guarantee the mixture of polymer and API. The temperature profile was selected the same as for the physical mixture of polyvinyl alcohol and pramipexole (PVA-P).

2.1.2. Liquid Feeding Setup

The feed stock consisting of polymer was fed with the powder feed rate of 2 g/min. A pramipexole solution in demineralized water with a concentration of 40 mg PDM/mL was prepared and was dosed from a 50 mL glass syringe with the help of a syringe pump (Legato 100, KD Scientific, Holliston, MA, USA) with the dosing rate of 50 µL/min through an inhouse-produced barrel element to zone 4. Therefore, the temperature of zones 2–4 was kept low to prevent blockages and guarantee conveyance of the material within the barrel. A vacuum pump was installed to zone 7 to eliminate water and water vapor. To increase the residence time of the melt under the pump so that sufficient degassing would occur, we set the screw speed to 20 rpm [20]. The maximum temperature was reduced to 205 °C.

2.1.3. Granule Feeding Setup

To produce dry granules, we performed two different runs (Table 3) on a roll compactor (BRC 25, L.B. Bohle, Ennigerloh, Germany). Since PVA stucked to the rolls and the ribbons showed lamination, anhydrous silica was added to formulation 2, which was blended for 20 min in a Turbula mixer.

Table 3. Composition of formulations used for roll compaction.

	PVA	Pramipexole Dichloride	Fumed Silica
Formulation 1	100%	-	-
Formulation 2	98%	1%	1%

The roll compactor was equipped with a hybrid sealing system, knurled roles, and a 360° rotating conical 1.5 mm rasp sieve (BTS100, L.B. Bohle, Ennigerloh, Germany). The gap width was set to 2 mm, the roll speed to 1 rpm, and the specific compaction force to 2 kN/cm. The fine (<500 µm) was reused for a second compaction to avoid wasting

material. Granules were sieved, and the fraction between 500 and 800 μm was used for the extrusion run. The physical mixture of granules with 1% (*w/w*) API and PVA granules was feed by feeder 1. The temperature in zone 2 was increased to 120 °C since the torque was too high due to the high granule strength of the material. The screw speed was changed to 20 rpm. The screw configuration included three kneading zones.

2.2. Sample Preparation and HPLC Measurements

For sample preparation, filaments were dissolved in flasks ($n = 1$), which were filled with either 0.1 N HCl (bPMMA matrix) or demineralized water (PVA matrix) up to the 100 mL mark. The content of drug loaded filaments was determined by high-performance liquid chromatography (HPLC) analysis. The HPLC system (Dionex, Sunnyvale, CA, USA) was equipped with a quaternary pump (P 580 A, Dionex, Sunnyvale, CA, USA) and an autosampler (ASI-100, Dionex, Sunnyvale, CA, USA). For the HPLC method, a C18-column (Eurospher II 100-5, Knauer, Berlin, Germany) with integrated precolumn was used. The eluent consisted of methanol (mobile phase B) and ammonium acetate buffer (0.05 M, pH 4). The flow rate was set to 1 mL/min, the oven temperature for tempering the column was set to 40 °C, and the injection volume was 50 μL . The gradient was as follows: mobile phase B was increased from 5 to 95% (*v/v*) within the first 10 min, it was held for 5 min at 95% (*v/v*), and it decreased to 5% (*v/v*) again until 20 min after the sample injection. An equilibration time of 3 min per run was allowed to pass before the next sample was injected. Detection was achieved by measuring the UV absorption of the sample at 264 nm.

2.3. Production of Melts

The accurate heating of the differential scanning calorimetry device (Mettler Toledo, Giessen, Germany) was used to melt bPMMA and PVA mixtures with different amounts of PDM in aluminum pans ($n = 1$). Therefore, powder mixtures were heated from 20 to 130 °C and were hold for 15, 22.5, and 30 min. Samples were dissolved in 0.1 N HCl and characterized by the HPLC method described in Section 2.2.

2.4. Differential Scanning Calorimetry of Pramipexole

Differential scanning calorimetry (DSC, Mettler Toledo, Giessen, Germany) was used to analyze pramipexole dihydrochloride monohydrate. Here, the powder was heated from 20 to 170 °C, cooled down to 20 °C, and heated up again to 320 °C with a heating rate of 10 K/min. The difference of the heat flow between the sample and the standard was detected according to the applied temperature.

2.5. Mercury Porosimetry

Mercury porosimetry measurements were performed using mercury porosimetry (Pascal-Quecksilberporosimeter, Thermo Scientific, Waltham, MA, USA). The relationship between intruded volume of mercury and the intrusion pressure was analyzed with the software SOLID version 1.6.6 (Applied Biosystems, Waltham, MA, USA). At the beginning of every determination, the penetrometer was evacuated up to a pressure of 0.013147 MPa. Then, it was filled with mercury under increasing pressure to 0.41 MPa. Penetration pressures were applied in 48 steps in the high-pressure stage. The pore sizes corresponding to the intrusion pressures were calculated by assuming cylindrical pores, a contact angle of 140 °C, and a surface tension for mercury of 485 mN/m. An equilibration time of 10 s was kept for every step between the measurements. The cumulative pore volume was converted into percent for representing a pore size distribution. Porosimeter tests were carried out in duplicate in order to see if the measurement showed any differences.

2.6. Laser Diffraction

The particle size distribution of the extruded powders (API and polymer) was determined by laser diffraction using the Mastersizer 3000 (Malvern Panalytical, Malvern, UK). Samples were split using a rotational sample divider (PT100, Retsch, Haan, Germany).

They were measured at 0.8-bar dispersion pressure. All off-line samples were measured in threefold.

2.7. High-Resolution Mass Spectrometry

The degradation product was separated by UPLC and was analyzed by mass spectrometry (Bruker maXis, Bruker, Billerica, MA, USA) using electrospray ionization (ESI) for fragmentation and measuring in positive mode. For the UPLC method, a C18-column (Waters Atlantis T3 3.0 × 100 mm, 3 µm, Waters, Milford, MA, USA) was used. The eluent consisted of methanol (mobile phase B) and ammonium acetate buffer (0.05 M, pH 4). The flow rate was set to 0.6 mL/min, and the oven temperature for tempering the column was set to 40 °C. The gradient was as follows: mobile phase B was increased from 0 to 20% (v/v) within the first 4 min, it was held for 3 min at 20% (v/v), and it decreased to 0% (v/v) again until 11 min after the sample injection (µL).

2.8. Thermogravimetry

Thermal analysis ($n = 2$) was conducted using a thermal analyzer (TG 209 F3 Tarsus®, Netzsch, Selb, Germany). The experimental TG sample carrier type S was equipped with a supporting PtRh10-Pt thermocouple to display thermal events during heating in nitrogen atmosphere. The temperature range was set from 30 °C to 300 °C, and the heat rate was 10 K/min.

2.9. Theoretical Background of the Deviation from Target Concentration

When the deviation from target concentration of the analyzed concentration of API in hot-melt extruded filaments are assessed, various error sources must be considered. For the analysis of filaments produced by a physical mixture of API and polymer, where only one feeder was used, the deviation from target concentration, expressed as the variance (σ^2_{total}), can be described with the following Equation [21]:

$$\sigma^2_{\text{total}} = \sigma^2_{\text{sampling}} + \sigma^2_{\text{analytical}} + \sigma^2_{\text{demix}} + \sigma^2_{\text{perfect mix}} \quad (1)$$

The calculation and consideration for each variance can be reconstructed on the basis of the literature sources [21–23]. For filaments produced by two feeders, the feeding error resulting from both feeders must be taken into account. Therefore, Equation (1) must be extended by another variance caused by the feeding process, which results in Equation (2):

$$\sigma^2_{\text{total}} = \sigma^2_{\text{sampling}} + \sigma^2_{\text{analytical}} + \sigma^2_{\text{demix}} + \sigma^2_{\text{perfect mix}} + \sigma^2_{\text{feeding}} \quad (2)$$

For liquid feeding, the variation of demixing must not be considered if the feeding of an ideal solution is assumed. By adding a second feeder, the error of the gravimetric loss of weight feeding system becomes important for the calculation of the overall deviation from target concentration [24]. Since the analytical error was similar to all extrusion setups, the impact of the remaining errors was analyzed. To find out the lowest deviation of the target concentration, which results from the (solid) properties of the raw materials and at the same time to consider the sample size, we calculated the relative standard deviation (RSD) with the help of a modification of the Stange–Poole equation (Equation (3))

$$\text{RSD} = \frac{100}{x} = \sqrt{\frac{x \times y \times (\overline{m}_x \times y + \overline{m}_y \times x)}{M}} \quad (3)$$

where x is the relative mass fraction of pramipexole, y is the relative mass fraction of the polymer, \overline{m}_x is the mean mass of one pramipexole particle, \overline{m}_y is the mean mass of one polymer particle, and M is the mean mass of the filaments [25]. The masses of the powder particles were calculated from the apparent density and of the mean particle size (D_{x50}). This formula was used by Hermes et al. to illustrate that the relative standard deviation of the target concentration of minitables highly depend on the sample size of powder

blends [26]. In this study, the calculation was chosen to assign the deviation from the target concentration to a defined filament weight, which was analyzed for the determination of the content uniformity of the extruded batch. This formula cannot be used in the extrusion setup “liquid feeding” because the API is not particulate but dissolved in water. For the calculation of deviation of the extruded batches, the standard deviation (SD) and the relative standard deviation (RSD) were determined.

3. Results

3.1. Pramipexole Degradation within the Hot Melt Extrusion Process

The target drug load of 100% API (drug concentration within the filament: 0.1% (*w/w*)) could not be achieved for the physical mixtures of PVA-P and bPMMA-P. One reason for this was the fact that the first extruded API-free polymer amount led to dilution of the afterwards extruded drug-loaded powder mixture in the barrel due to the retention of a dead volume in the barrel, which could not be compensated during the set extrusion time of approximately 60 min. Therefore, after finding suitable extrusion parameters with placebo mixture, we first cleaned the extruder and prepared it again accordingly so that the API was dosed from the beginning and the dilution effect, which would negatively affect the content uniformity, was avoided. Another reason for the low recovery rate of PDM in bPMMA filaments was that degradation products were found in HPLC analysis of filaments containing 5% (*w/w*) PDM (Figure 1), which could not be detected in the low-dosed filaments (0.1% (*w/w*)) due to the limit of detection of the degradation product. This was further analyzed by preparing melts with 1, 2.5, and 5% (*w/w*) PDM according to 2.3 to represent the thermal stress of the extruder but neglecting the shear stress of the HME process. Figure 1 shows that there is a concentration-dependent increase of the degradation product, which is accelerated by thermal stress.

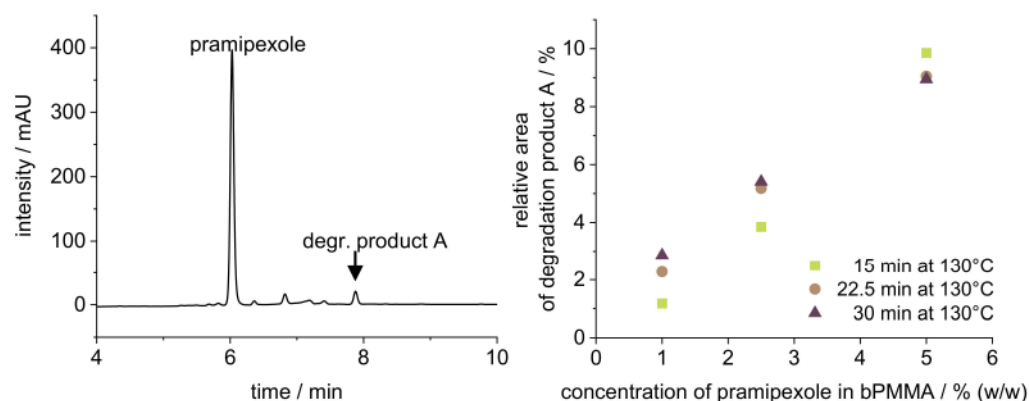


Figure 1. HPLC chromatogram (left) of 5% (*w/w*) pramipexole filament and evaluation of the relative area degradation product A of the pramipexole peak (right) of three different pramipexole concentrations (1, 2.5, and 5% (*w/w*)) exposed to 130 °C in DSC for 15, 22.5, and 30 min.

High-resolution MS was able to identify the degradation product as a pramipexole derivative, an adduct of pramipexole and formaldehyde. Not only 6-propylamino-4,5,6,7-tetrahydrobenzothiazol-2-yl-amine was found, but also 2-methyleneamino-N-propyl-4,5,6,7-tetrahydrobenzothiazol-6-amine. Thus, it was decided that further dosing studies would be conducted with PVA and PDM only, as the degradation product only occurs in combination with bPMMA. Although no degradation product of PDM was found in the PVA filaments in the HPLC chromatograms, a recovery rate of 100% API could not be achieved. Thus, this can be explained by the formation of an anhydrate of PDM due to high temperature used for the extrusion with PVA (up to 220 °C barrel temperature). To confirm this hypothesis, we analyzed the compound by DSC (Figure 2). During initial heating, care was taken to ensure that the degradation temperature, which is also the melting temperature, was not

reached. An exothermic event could be detected, which reached its maximum at 140 °C. During second heating, this peak can no longer be detected. It was assumed that during the first heating phase, the crystal structure of PDM decomposed because the water of crystallization was removed, and PDM remained in its anhydrate form. To support this result, we performed an additional thermogravimetric study. Both the starting substance (PDM) and the prepared filaments (PVA filament and filament with 5% (*w/w*) PDM in PVA matrix) were examined (Figure 3). It was found that the pure substance of PDM exhibited a weight loss of 5.82% between 100 and 150 °C. This mass difference represents the mass of the hydrate because PDM has a molecular weight of 302 g/mol and the (hydrate) water 18 g/mol, which is about 6% of the salt. The DTG represents the rate of mass loss at given temperature (dm/dT in mg/min unit). Here, the DTG curve indicates a thermal event within the temperature range between 120° and 150 °C with two maxima at 128 °C and 151 °C. While in the TG curve of PVA filament, a decrease in mass of 2.1% could be detected between 100 °C and 240 °C, the mass of 5% PVA-P filaments decreased by 3.44% between 100 °C and 200 °C. For the filaments with PDM, there was a continuous decrease in weight with a small bend in the curve at 170 °C, but no abrupt change in weight between 130 °C and 150 °C, suggesting that the anhydride was present in the filament. Further studies are needed to show why the mass of PVA changed even though the degradation temperature in the literature was above 250 °C. For this study, these results are necessary to calculate the recovery rate. The amount of API was calculated, considering that the anhydrous form rather than the monohydrate was present, which corresponded to a target concentration of 0.094% (*w/w*), not 0.1% (*w/w*). Therefore, the target drug loading was calculated for pramipexole dichloride (PD) and not for pramipexole dihydrochloride monohydrate (PDM). This represents a difference of 6% in the recovery rate and led to the fact that the total amount of API could be found in the equilibrium state for drug content. However, it should be noted that the pharmacopoeia lists only pramipexole dihydrochloride monohydrate [27]. Since a different form of pramipexole is now present due to the extrusion process, it is mandatory that a monography for pramipexole dihydrochloride will be available in the future, as PD is seen as a new active ingredient in clinical studies. This will also occur with other active ingredients, which undergo a similar chemical change due to the hot-melt extrusion process. Therefore, API–polymer combinations must be tested in advance if any degradation product might be formed. Moreover, all active ingredients, which contain hydrate water and are hot-melt extruded at higher temperatures, should be investigated for the presence of the hydrate form.

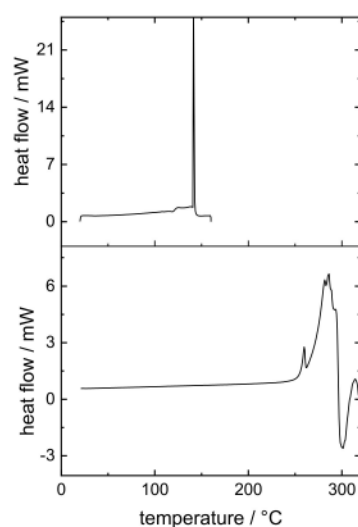


Figure 2. Thermograms of the first and second heating of PDM.

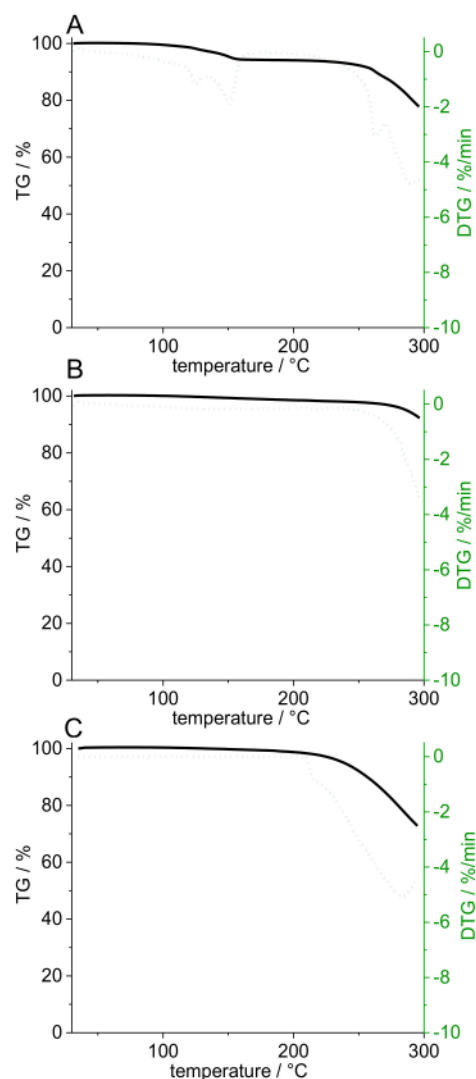


Figure 3. Gravimetric loss (%) and thermal events (%/min) during heating of PDM powder (A), PVA placebo filament (B), and pramipexole-PVA (5% (*w/w*) PDM) filament (C).

3.2. Equilibrated Conditions for Extrusion

During extrusion, the adjusted process parameters must be kept constant so that a state of equilibrium can occur. The process parameters are responsible for the resulting torque and the pressure at the die [19]. The barrel filling level results not only from the screw speed but also from the dosing rate. Since the barrel filling volume does not have to be the same over the barrel if, for example, kneading elements are installed or the residence time within the barrel varies due to the screw configuration, a true equilibrium is not always achieved. Figure 4 shows the logged process parameters of the extruder for PVA-P “3 kneading zones” for the power consumption and the pressure at the die. For this extrusion run, 25 min passed before both parameters achieved the equilibrium stage. For the other extrusions, the time until equilibrium conditions did not vary much from the shown data (25 ± 5 min). Extrusion run setup with “3 kneading zones” shows a periodically recurring picture of the maxima of the power consumption and the pressure at the die (highlighted by arrows).

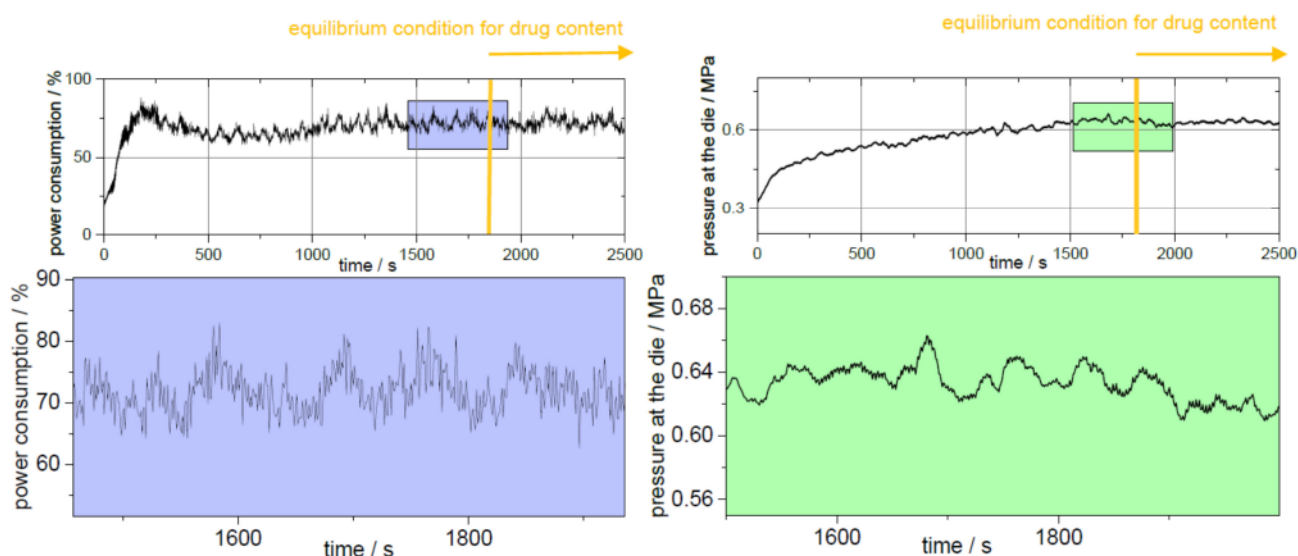


Figure 4. Steady-state conditions of process parameters of extrusion setup “physical mixture” of PVA-P (left: power consumption; right: pressure at the die) with the time-delayed starting of the equilibrium condition for drug content.

The installation of the third kneading zone in the screw configuration resulted in the melt presumably being held up at kneading zone 1 closed to the die, and only when sufficient material accumulated at the 90° kneading elements of the kneading block was the polymer-API melt conveyed further to the nozzle. These periodic fluctuations of the process parameters were reflected in the periodic diameter variations of the filaments (Figure 5, Table 4). Here, every 3 min a maximum diameter was detected, which indicated that the melt was not homogeneously transported over the entire time period through the nozzle since the melt accumulated at the additionally introduced kneading zone. The RSD of the target concentration could be improved from 10.76% to 8.28% (AV values of 21.6 and 16.4) by the optimization of the additional kneading capacity (Table 5). The maximum allowed acceptance value for manufactured batches of solid dosage forms (e.g., by fused filament 3D printing) would be exceeded in both cases solely by the inaccuracy of the manufacturing process of the filaments without taking into account the inaccuracy of the printing process. In both cases, demixing (σ^2_{demix}) might cause the high deviation from the mean concentration (Equation (2)). Therefore, the focus was shifted from the settings of the extruder to the type of dosing and the feeding material, respectively. The extrusion setup “physical mixture” resulted in the highest diameter fluctuation expressed as the interquartile range between 1% and 99% (IQR₁₋₉₉ of 0.152, 0.155, and 0.151 mm), while filaments extruded in extrusion run “liquid feeding” showed the lowest diameter fluctuations with IQR₁₋₉₉ of 0.105, 0.188, and 0.096 mm (Table 4). The filaments extruded with the help of extrusion setting PVA-P “3 kneading zones” achieved the lowest value of 0.017 mm for filament ovality. The highest value for ovality was 0.043 mm, which was obtained by extrusion with granules.

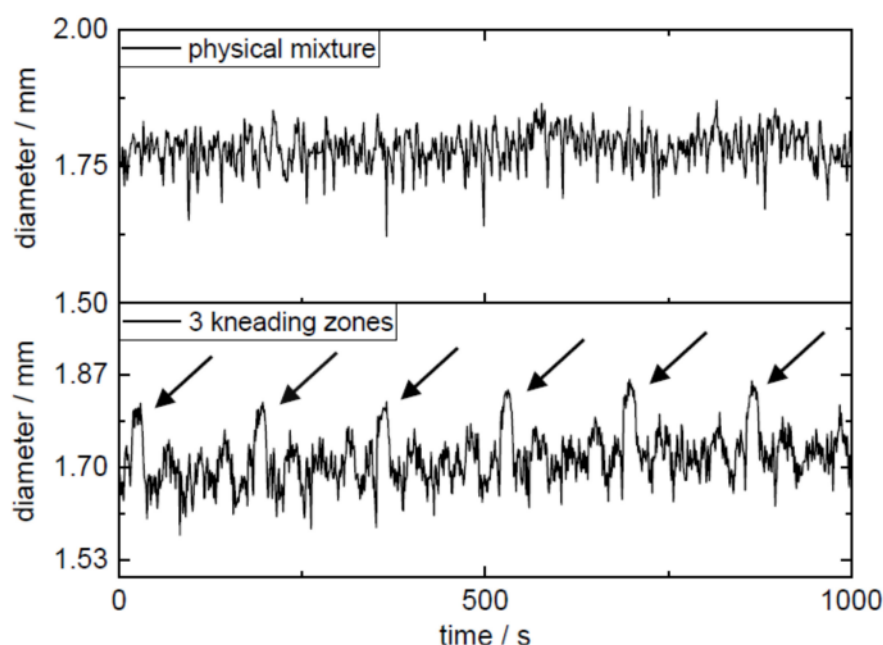


Figure 5. Diameter fluctuation of extrusion setups “physical mixture” and “3 kneading zones”.

Table 4. Diameter and ovality measurements as inline measurements during extrusion runs expressed as the interquartile range (IQR) between 1 and 99% and the coefficient of variation (CV) in millimeters.

Extrusion Setup	Diameter		Diameter (x)		Diameter (y)		Ovality (dx–dy)	
	IQR _{1–99}	CV	IQR _{1–99}	CV	IQR _{1–99}	CV	IQR _{1–99}	CV
bPMMA-P (“physical mixture”)	0.152	1.82	0.155	1.80	0.151	1.85	0.034	6.69
PVA-P (“physical mixture”)	0.582	8.72	0.582	1.57	0.582	8.72	0.022	21.23
PVA-P (“3 kneading zones”)	0.252	2.76	0.256	2.78	0.251	2.75	0.017	14.42
PVA-P (“split feeding”)	0.253	1.77	0.255	1.79	0.253	2.81	0.03	26.72
PVA-P (“granules”)	0.167	2.03	0.179	1.81	0.159	1.99	0.043	23.87
PVA-P (“liquid feeding”)	0.105	1.23	0.118	1.38	0.096	1.24	0.037	15.89

Table 5. Content uniformity of the extruded batches: determination of the mean content of pramipexole dihydrochloride, and the standard deviation (SD) from target concentration of 0.1% (*w/w*) of pramipexole in PVA filaments and calculation of the relative standard deviation (RSD). The acceptance value was calculated according to Eur. Pharm. 2.9.40 with the acceptability constant of 2.0 at level 2 (*n* = 30).

	Mean Content/%	SD/%	Content Uniformity (RSD)/%	Acceptance Value
PVA-P (“physical mixture”)	0.098	0.011	10.76	21.6
PVA-P (“3 kneading zones”)	0.099	0.008	8.28	16.4
PVA-P (“split feeding”)	0.091	0.010	11.21	27.9
PVA-P (“granules”)	0.101	0.006	6.00	12.2
PVA-P (“liquid feeding”)	0.096	0.006	6.35	14.7

The standard deviation of the target concentration was not improved by dosing the API with a second feeder. Thus, the relative standard deviation RSD of target concentration of API within the filaments of this extrusion run was 11.21% ($AV > 27$) (Table 5). The installation of a syringe pump, which fed the API solution, led to the RSD of this extrusion run being low (6.35%), but some outliers could be observed, and still the resulting AV value of 14.7 exceeded the maximum limit of L1 ($AV = 14$). Since the installation of a second feeder or a syringe pump causes the dosing error to originate from both the first and the second dosing system, the dosing error had an additive effect, as Wahl et al. have already demonstrated in their work [28]. This can also be explained by the additional factor in the calculation of the variance ($\sigma^2_{\text{feeding}}$) (Equation (3)). The smallest deviations from the target concentration were achieved in extrusion with granules with an RSD of 6.00% and a resulting AV value of 12.2, even though the ovality of the filaments was not satisfactory. For further processing of the filaments into a dosage form by fused-filament 3D printing, round shaped filaments are desirable and diameter fluctuations are undesirable, as they can lead to problems during feeding and variation of the mean diameter can lead to weight fluctuations if the volume flow is kept constant during printing. Diameter fluctuations can be minimized by other methods, e.g., the implementation of a melt pump between barrel and extruder [29], but were not further optimized in this work, since the homogeneity of the drug loading was in focus. By dividing the extrudates into sections during extrusion process, we were able to accurately assign each filament to the extrusion time. Subsequently, the time was examined when the target concentration was reached.

3.3. Equilibrium Condition for Drug Content

As already mentioned, hot-melt extrusion was carried out with API from the beginning since it was found that when starting only with polymer, there was an unwanted dilution effect. Even if API was incorporated within the mixture or granule mixture or fed by the second feeder or the syringe pump from the beginning of the extrusion, it can be recognized from the results in Figure 4 that it took a longer period of time to reach the target concentration in the filaments even if a state of equilibrium was established. For “granule feeding” setup, it took 45 min to reach the target concentration of 0.1% (w/w) PD. Only 30 min passed, when pramipexole was fed in solution (“liquid feeding”), to reach the calculated drug content of 100%. Thus, it is indispensable to use the filaments for further processing only after the time of this adjustment phase. In order for this phase to be detected in the most efficient way, a process analytical technology, which can detect the equilibrium state while extrusion, is desirable. However, the distinction of small quantities ($<0.1\%$ (w/w)) is problematic, and thus the question whether the selected method can analyze the differences must be answered. Wesholowski et al. could not differ between less than 3.51% for carbamazepine and 1.93% for theophylline by using UV–VIS spectroscopy as PAT for concentrations larger than 5% (w/w) (carbamazepine) and 2.5% (w/w) (theophylline) [30]. After it was found that an equilibrium state for content uniformity of low-dosed filaments must be set in addition to the extrusion process equilibrium (Figure 4), criteria were needed, which would evaluate the deviations from the target drug content.

3.4. Limitation for Deviations of Drug Content

Since no guideline exists for assessing content uniformity of manufacturing intermediates such as drug-loaded filaments, a methodology was developed to define the required sample size depending on variations for the RSD of the content of API [26]. Filaments do not represent dosage forms but serve as intermediates for fused-filament 3D printing [31,32], and therefore the acceptance value will not be used to evaluate the content uniformity of the filaments. Instead, the Stange–Poole equation was used in order to identify the sample size depending relative standard deviation (RSD) from the target drug load. The density of PDM and PVA as well as their particle sizes are shown in Table 6.

Table 6. Mercury density ($n = 2$) and particle sizes of raw materials ($n = 3$).

	PDM	PVA
Density (at 0.4 MPa)	1.2343 g/cm ³	1.2321 g/cm ³
Particle size	D _{x10} 6.0 µm	D _{x10} 11.8 µm
	D _{x50} 22.2 µm	D _{x50} 42.7 µm
	D _{x90} 68.1 µm	D _{x90} 96.7 µm

The calculation of the RSD was performed according to Equation (3) for sample sizes between 5 and 100 mg filament in 0.01% steps for pramipexole content from 0.01 to 10% (w/w) and is graphical illustrated in a contour plot for sample sizes between 0 and 60 mg (Figure 6). To verify the applicability of the contour plot, we examined higher loaded filaments with respect to the deviation of the content in different sample sizes. As Figure 6 indicates, the RSD decreased with increasing sample size. This was true for both 1 and 5% (w/w) pramipexole-loaded filaments, which were selected to verify the feasibility of this method (Table 7). The contour plots showed that the standard deviation for the respective sample size was the same for both filaments, although the loading with API varied. For all tested sample sizes, the RSD was within the calculated limits of the Stange–Poole equation or even lower. Thus, for 0.1% (w/w) loaded filaments, a similarly small RSD had to be maintained. For the determination of content uniformity, the sample size was depicted to be 50 mg, which means that with a drug load of 0.1% (w/w), the RSD must not exceed 6%. To test whether the limit of $\pm 6\%$ calculated by the modified Stange–Poole equation could be met, we selected the extrusion “granule feeding” to show in equilibrium state for content uniformity whether the deviations were within the allowed range. Since the physical mixture of granules was fed with the help of only one dosing unit, the limits could be complied in equilibrium conditions after filament segment 15 (Figure 7). In equilibrium condition for drug content, 100% of the measured filament fragments were within the set limits (after segment 15).

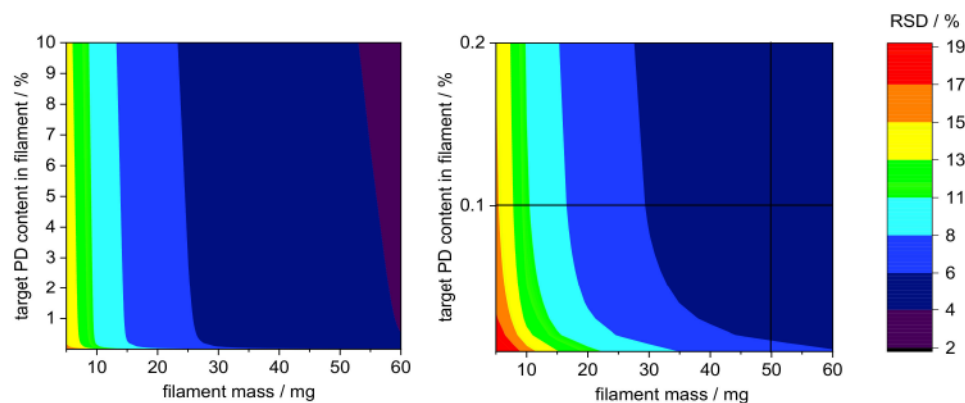


Figure 6. Contour plots for limitations of deviations calculated by Stange–Poole equation: (left) colored RSD of PD target concentration depending on target PD content in filament (from 0–10%) and filament mass (0–60 mg); (right) RSD from selected filament mass (50 mg) with predetermined PD concentration in filament (0.1% (w/w)).

Table 7. Determination of the relative standard deviation (RSD) of PVA-P “physical mixture” filaments loaded with 1 and 5% (*w/w*) PDM analyzing four different sample sizes (10, 20, 30, and 50 mg filaments) and comparison with results from Stange–Poole equation.

	Filament Mass	RSD	Calculated RSD by Stange–Poole Equation
5% (<i>w/w</i>) filament	10 mg	8.95%	8–11%
	20 mg	8.00%	6–8%
	30 mg	3.57%	4–6%
	50 mg	4.35%	4–6%
1% (<i>w/w</i>) filament	10 mg	9.45%	8–11%
	20 mg	5.05%	6–8%
	30 mg	3.19%	4–6%
	50 mg	3.55%	4–6%

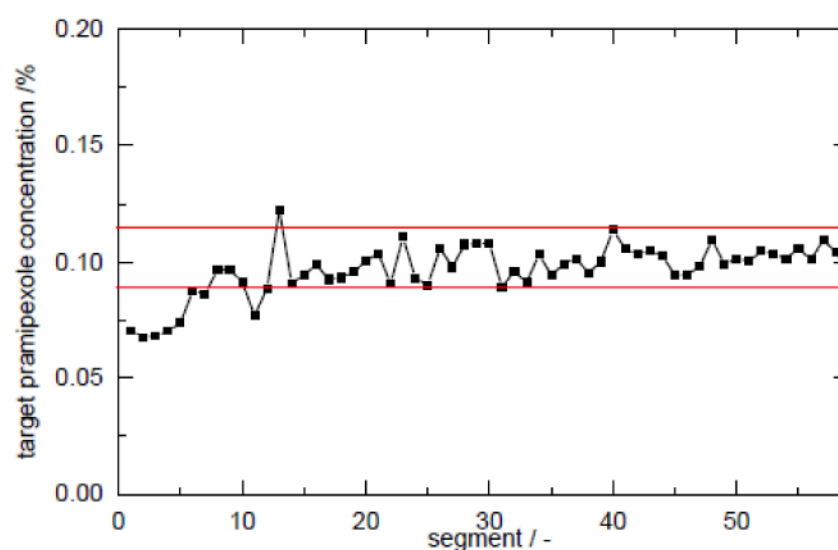


Figure 7. Control chart of extrusion setup “granule feeding” with upper and lower limits calculated from Stange–Poole equation (target content of PDM: 0.1%, filament mass 50 mg).

This pretreatment, namely, the granulation step and the mixing of polymer granules and API-loaded granules before extrusion, is the most promising solution for producing low-dosed filaments with a homogeneous distribution of the API. Even if this extrusion run with pretreatment of the powders seems very complex, it is necessary to go through all these processes, namely, the mixing of powders, the granulation of placebo formulation and API–polymer mixture, the following mixing of the two granules, and the hot melt extrusion process. This setup guaranteed the production of homogeneous low-dosed filaments.

4. Discussion

A suitable feeding method was found to obtain the target concentration of 0.1% (*w/w*) pramipexole in a pharmaceutical filament that can be used for fused filament 3D printing. With the help of a previously applied dry granulation process, homogeneous pramipexole granules with a drug load of 1% (*w/w*) can be produced, which were mixed with granules (1:10 ratio) of the same excipient before extrusion and are fed by the same gravimetric feeder. Due to the change in the feedstock from powder to granules, however, care must be taken to adjust the extrusion process, especially the temperature and the screw configuration. The largest variations from target drug loading were found for the extrusion runs, wherein the physical mixture was fed by one feeder and where the API was fed with the help of a second gravimetric feeder (extrusion run “split feeding”) due to demixing processes and the additive variation from the second feeder. In addition, the importance of the consideration of the analyzed sample size was clarified since for the evaluation of

the homogeneity of a batch, the sample size should be considered. Accurate calculation of the expected relative standard deviation from target drug load can be made using the Stange–Poole equation. This equation was used to specify a range of how accurately an active ingredient can be dosed at a desired concentration in regard of the sample size. In this study, it was shown that filaments of a mass of 50 mg could be prepared homogeneously and would meet the criteria of content uniformity of the European Pharmacopoeia. Thereby it was important to wait for the accumulation of the active ingredient in the melt in the beginning of the extrusion runs and to take samples in the identified equilibrium condition for drug content. However, this accumulation phase varied, requiring samples to be taken from the beginning to identify the beginning of the equilibrium state. Additionally, it should be tested in future studies as to whether the pre-run of the extrusion might be reduced in time to increase the economic efficiency of the process.

5. Conclusions

In this study, we were able to extrude homogenous low-dosed filaments containing PVA and pramipexole, which can be used for fused filament 3D printing to produce solid dosage forms. Since low API concentration causes problems for analytics because the limit of detection for many analytical methods is not reached, it is recommended that higher concentrated filaments be produced first, which are more likely to determine degradation products and changes in solid state properties. Our study showed that with the extrusion with pramipexole and bPMA, an unwanted degradation product occurred. As well as this, at material temperatures higher than 120 °C, the anhydrous form of PDM was present, and this needed to be considered in the calculation of the drug load. The extrusion of granules with PVA and pramipexole resulted in homogenous filaments after reaching a plateau phase for drug content. Other feeding methods showed higher deviations from target drug content. The results of this study clearly showed that both the dosing error due to segregation during extrusion and the additive error due to an additional feeder had an impact on the homogeneity of the filament. To find limitations for variation of API content, we used the Stange–Poole equation to calculate the allowed RSD. In the plateau phase, the limitations for variation of the drug content could be achieved for most of the samples, which were analyzed by HPLC analysis. In order for the API distribution within the filament to be improved, detailed evaluation of process parameters and adjustment may therefore be required. To evaluate fluctuation in equilibrium state for drug content, one should have inline, non-invasive PAT that can determine quantities of the API, even in very small steps and with less effort than the descriptive HPLC method. In future studies, other low-dosed API–excipient combination will be extruded, and the attempt will be made to reduce the pre-run of the extrusion in time by, e.g., starting with slightly higher concentrations of API. In addition, it will also be investigated as to whether the precision of a pharmaceutical fused filament 3D printer is able to deposit the layers precisely so that higher dosed filaments can be 3D printed to form dosage forms that achieve accurate dosing without the need for the extensive production of low-dosed filaments.

Author Contributions: Conceptualization, R.C., J.B. and J.Q.; formal analysis, R.C.; funding acquisition, J.B.; investigation, R.C.; methodology, R.C., H.W., and S.G.; supervision, J.B.; validation, R.C.; visualization, R.C.; writing—original draft, R.C.; writing—review and editing, H.W., S.G., J.Q. and J.B. All authors have read and agreed to the published version of the manuscript.

Funding: This research was funded by Bundesministerium für Bildung und Forschung—project ProMat Leben—Polymere ‘PolyPrint’, project no.: 13XP5064B.

Institutional Review Board Statement: Not applicable.

Informed Consent Statement: Not applicable.

Data Availability Statement: The data presented in this study are available upon request from the corresponding author.

Acknowledgments: The authors want to thank Evonik and Merck for supplying polymers. They are also grateful for Andrea Michel's and Annika Wilms' help during measurements. This work is associated with the German Federal Ministry of Education and Research—project 'ProMat Leben-Polymere-PolyPrint' (project no.: 13XP5064B).

Conflicts of Interest: The authors declare no conflict of interest. Evonik and Merck KGaA had no role in the design of the study; in the collection, analyses, or interpretation of data; in the writing of the manuscript, and in the decision to publish the results.

Abbreviations

API	active pharmaceutical ingredient(s)
AV	acceptance value
bPMMA	basic butylated methacrylate copolymer
CV	coefficient of variation
DSC	differential scanning calorimetry
DTG	derivative thermogravimetry
HME	hot melt extrusion
IQR	interquartile range
MS	mass spectrometry
P	pramipexole
PD	pramipexole dichloride
PDM	pramipexole dichloride monohydrate
PVA	polyvinyl alcohol
RSD	relative standard deviation
SD	standard deviation

References

- Dooley, M.; Markham, A. Pramipexole. *Drugs Aging* **1998**, *12*, 495–514. [\[CrossRef\]](#)
- Gültekin, H.E.; Serdar, T.; Füsün, A. An effective technology for the development of immediate release solid dosage forms containing low-dose drug: Fused deposition modeling 3D printing. *Pharm. Res.* **2019**, *36*, 1–13. [\[CrossRef\]](#)
- Zheng, J. (Ed.) *Formulation and Analytical Development for Low-Dose Oral Drug Products*; John Wiley & Sons: Hoboken, NJ, USA, 2009; p. 10.
- European Pharmacopoeia Commission. 2.9.40. Uniformity of dosage units. In *European Pharmacopoeia*; European Directorate for the Quality of Medicines (EDQM): Strasbourg, France, 2020; p. 3118.
- Ganderton, D.; Hunter, B.M. A comparison of granules prepared by pan granulation and by massing and screening. *J. Pharm. Pharmacol.* **1971**, *23*, 1S–10S. [\[CrossRef\]](#) [\[PubMed\]](#)
- Hersey, J.A. Ordered mixing: A new concept in powder mixing practice. *Powder Technol.* **1975**, *11*, 41–44. [\[CrossRef\]](#)
- Tian, Y.; Jones, D.S.; Donnelly, C.; Brannigan, T.; Li, S.; Andrews, G.P. A new method of constructing a drug–polymer temperature–composition phase diagram using hot-melt extrusion. *Mol. Pharm.* **2017**, *15*, 1379–1391. [\[CrossRef\]](#)
- Patil, H.; Tiwari, R.V.; Repka, M.A. Hot-melt extrusion: From theory to application in pharmaceutical formulation. *AAPS PharmSciTech* **2016**, *17*, 20–42. [\[CrossRef\]](#) [\[PubMed\]](#)
- Breitenbach, J. Melt extrusion: From process to drug delivery technology. *Eur. J. Pharm. Biopharm.* **2002**, *54*, 107–117. [\[CrossRef\]](#)
- Loreti, G.; Maroni, A.; Dorly del Curto, M.; Melocchi, A.; Gazzaniga, A.; Zema, L. Evaluation of hot-melt extrusion technique in the preparation of HPC matrices for prolonged release. *J. Pharm. Sci.* **2014**, *52*, 77–85. [\[CrossRef\]](#)
- Lagan, C.; Huckle, J.E.; Katz, J.M.; Khorsand, B.; Daurio, D.; Andrews, G.P.; Chung, J.; Alvarez-Nunez, F. Hot Melt Extrusion of a Thermally Labile, High Melting Point Compound. *AAPS PharmSciTech* **2021**, *22*, 235. [\[CrossRef\]](#) [\[PubMed\]](#)
- Wegiel, L.A.; Mauer, L.J.; Edgar, K.J.; Taylor, L.S. Crystallization of amorphous solid dispersions of resveratrol during preparation and storage—Impact of different polymers. *J. Pharm. Sci.* **2013**, *102*, 171–184. [\[CrossRef\]](#)
- Llusa, M.; Mohr, S.; Baumgartner, R.; Paudel, A.; Koscher, G.; Khinast, J.G. Continuous low-dose feeding of highly active pharmaceutical ingredients in hot-melt extrusion. *Drug Dev. Ind. Phar.* **2016**, *42*, 1360–1364. [\[CrossRef\]](#) [\[PubMed\]](#)
- Park, J.B.; Kang, C.Y.; Kang, W.S.; Choi, H.G.; Han, H.K.; Lee, B.J. New investigation of distribution imaging and content uniformity of very low dose drugs using hot-melt extrusion method. *Int. J. Pharm.* **2013**, *458*, 245–253. [\[CrossRef\]](#) [\[PubMed\]](#)
- Sacher, S.; Heindl, N.; Urlich, J.A.A.; Kruisz, J.; Khinast, J.G. A solution for low-dose feeding in continuous pharmaceutical processes. *Int. J. Pharm.* **2020**, *591*, 119969. [\[CrossRef\]](#)
- Repka, M.A.; Gerding, T.G.; Repka, S.L.; McGinity, J.W. Influence of plasticizers and drugs on the physical-mechanical properties of hydroxypropylcellulose films prepared by hot melt extrusion. *Drug Dev. Ind. Phar.* **1999**, *25*, 625–633. [\[CrossRef\]](#)
- Skowrya, J.; Pietrzak, K.; Alhnan, M.A. Fabrication of extended-release patient-tailored prednisolone tablets via fused deposition modelling (FDM) 3D printing. *Eur. J. Pharm. Sci.* **2015**, *68*, 11–17. [\[CrossRef\]](#)

18. Wang, H.; Dumpa, N.; Bandari, S.; Durig, T.; Repka, M.A. Fabrication of Taste-Masked Donut-Shaped Tablets Via Fused Filament Fabrication 3D Printing Paired with Hot-Melt Extrusion Techniques. *AAPS PharmSciTech* **2020**, *21*, 1–11. [[CrossRef](#)]
19. Martin, C. Twin screw extrusion for pharmaceutical processes. In *Melt Extrusion*; Springer: New York, NY, USA, 2013; pp. 47–79.
20. Alshahrani, S.M.; Morott, J.T.; Alshetali, A.S.; Tiwari, R.V.; Majumdar, S.; Repka, M.A. Influence of degassing on hot-melt extrusion process. *Eur. J. Pharm. Sci.* **2015**, *80*, 43–52. [[CrossRef](#)]
21. Gentzler, M.; Michaels, J.N.; Tardos, G.I. Quantification of segregation potential for polydisperse, cohesive, multi-component powders and prediction of tablet die-filling performance—A methodology for practical testing, re-formulation and process design. *Powder Technol.* **2015**, *285*, 96–102. [[CrossRef](#)]
22. Ellison, S.L.R.; Williams, A. *Quantifying Uncertainty in Analytical Measurement*; Eurachem/Citac: Teddington, UK, 2012.
23. Anglov, T.; Byrialsen, K.; Carstensen, J.K.; Christensen, F.; Christensen, S.; Madsen, B.S.; Sørensen, E.; Sørensen, J.N.; Toftegård, K.; Winther, H.; et al. Uncertainty budget for final assay of a pharmaceutical product based on RP-HPLC. *Accredit. Qual. Assur.* **2003**, *8*, 225–230. [[CrossRef](#)]
24. Hanson, J. Control of a system of loss-in-weight feeders for drug product continuous manufacturing. *Powder Technol.* **2018**, *331*, 236–243. [[CrossRef](#)]
25. Eggermann, H.; Frank, P. Novel approach to estimate quality of binary random powder mixtures: Samples of constant volume. I: Derivation of equation. *J. Pharm. Sci.* **1992**, *81*, 551–555. [[CrossRef](#)]
26. Hermes, M. Kindgerechte, Niedrigdosierte Zubereitungen Mit Enalaprilmaleat. Ph.D. Thesis, HHU Düsseldorf, Göttingen, Germany, 2012.
27. European Pharmacopeia. 8.0, Pramipexole Dihydrochloride Monohydrate. In *European Pharmacopoeia*; European Directorate for the Quality of Medicines (EDQM): Strasbourg, France, 2014.
28. Wahl, P.R.; Treffer, D.; Mohr, S.; Roblegg, E.; Koscher, G.; Khinast, J.G. Inline monitoring and a PAT strategy for pharmaceutical hot melt extrusion. *Int. J. Pharm.* **2013**, *455*, 159–168. [[CrossRef](#)]
29. Peng, F.; Zhao, Z.; Xia, X.; Cakmak, M.; Vogt, B.D. Enhanced impact resistance of three-dimensional-printed parts with structured filaments. *ACS Appl. Mater. Interfaces* **2018**, *10*, 16087–16094. [[CrossRef](#)] [[PubMed](#)]
30. Wesholowski, J.; Prill, S.; Berghaus, A.; Thommes, M. Inline UV/Vis spectroscopy as PAT tool for hot-melt extrusion. *Drug Deliv. Transl. Res.* **2018**, *8*, 1595–1603. [[CrossRef](#)] [[PubMed](#)]
31. Goyanes, A.; Buanz, A.B.; Basit, A.W.; Gaisford, S. Fused-filament 3D printing (3DP) for fabrication of tablets. *Int. J. Pharm.* **2014**, *476*, 88–92. [[CrossRef](#)] [[PubMed](#)]
32. Windolf, H.; Chamberlain, R.; Quodbach, J. Predicting Drug Release from 3D Printed Oral Medicines Based on the Surface Area to Volume Ratio of Tablet Geometry. *Pharmaceutics* **2021**, *13*, 1453. [[CrossRef](#)]

3.2 Drug Content Determination of Low-dosed Hot-melt Extruded Filaments using Raman Spectroscopy

Evaluation of authorship

author	idea [%]	study design [%]	experimental [%]	evaluation [%]	manuscript [%]
Rebecca Chamberlain	80	80	80	80	80
Björn Fischer	10	20	20	10	10
Jörg Breitzkreutz	10	-	-	10	10

Evaluation of Copyright permission:

© 2024 by Taylor & Francis Group. This article is not an open access article. This article is accessible via: <https://www.tandfonline.com/doi/full/10.1080/10837450.2024.2323622>.

Drug Content Determination of Low-Dosed Hot-Melt Extruded Filaments using Raman Spectroscopy

Rebecca Chamberlain, Jörg Breitzkreutz, Björn Fischer

Institute of Pharmaceutics and Biopharmaceutics, Heinrich Heine University, Universitätsstrasse 1, 40225 Düsseldorf, Germany

Pharmaceutical Development and Technology

<https://doi.org/10.1080/10837450.2024.2323622>

Abstract

The aim of this study was to evaluate the suitability of a non-disruptive Raman spectroscopic method to quantify drug concentrations below 5 w% within a polymer matrix produced by hot-melt extrusion (HME). For calibration, praziquantel (PZQ) - polyvinylpyrrolidone-vinylacetat-copolymer (PVP-VA) mixtures were extruded. By focusing the laser light of the Raman probe to a diameter of 1 mm and implementing a self-constructed filament holder, the signal-to-noise (S/N) ratio could be reduced considerably. The obtained Raman spectra show quite high fluorescence, which is likely to be caused by dissolved pharmaceutical active ingredient (API) in the polymer matrix. For content

determination, HPLC analysis was conducted as a reference method using the same filament segments. A partial least squares (PLS) model, regressing the PZQ concentrations from HPLC method analysis versus the off-line collected Raman spectra, was developed. The linear correlation for a suitable extrusion run for the production of low-dosed filaments (extrusion 1, two kneading zones) is acceptable ($R^2 = 0.9915$) while the correlation for a extrusion set-up with low miscibility (extrusion 2; without kneading zone) is unacceptable ($R^2 = 0.5349$). The predictive performance of the calibration model from extrusion 1 is rated by the root mean square error of estimation (RMSEE), which was 0.08%. This calibration can now be used to validate the content of low-dosed filaments during HME.

Keywords

Hot-melt extrusion; low-dosed; Raman spectroscopy; drug content determination; non-destructive measurement; in-line analytics

Acknowledgements

The team responsible for the work presented here would like to acknowledge Peter Kleinebudde for his scientific input and support for continuous in-line Raman measurements.

Disclosure statement

The authors report there are no competing interests to declare.

Data availability statement

The data that support the findings of this study are available from the corresponding authors, [RC, BF], upon reasonable request.

Additional information - Funding

This research was funded by Bundesministerium für Bildung und Forschung – Project ‘ProMat Leben–Polymere’ ‘PolyPrint’, project number.: 13XP5064B.

3.3 Introducing Fiber-Assisted Colorimetric Measurements as a Quality Control Tool of Hot Melt Extruded Filaments

Evaluation of authorship

author	idea [%]	study design [%]	experimental [%]	evaluation [%]	manuscript [%]
Rebecca Chamberlain	80	80	50	100	90
Eirini Mangiorou	10	10	40	-	5
Björn Fischer	10	10	10	-	5

Evaluation of Copyright permission:

© 2022 by the authors. Licensee MDPI, Basel, Switzerland. This article is an open access article distributed under the terms and conditions of the Creative Commons Attribution (CC BY) license (<https://creativecommons.org/licenses/by/4.0/>).

Introducing Fiber-Assisted Colorimetric Measurements as a Quality Control Tool of Hot Melt Extruded Filaments

Rebecca Chamberlain, Eirini Mangiorou and Björn Fischer



Institute of Pharmaceutics and Biopharmaceutics, Heinrich Heine University, Universitaetsstrasse 1, 40225 Duesseldorf, Germany

Pharmaceutics

<https://doi.org/10.3390/pharmaceutics14051055>

Article

Introducing Fiber-Assisted Colorimetric Measurements as a Quality Control Tool of Hot Melt Extruded Filaments

Rebecca Chamberlain , Eirini Mangiorou and Björn Fischer 

Institute of Pharmaceutics and Biopharmaceutics, Heinrich Heine University, Universitätsstraße 1, 40225 Düsseldorf, Germany; up1055165@upnet.gr (E.M.); bjoern.fischer@hhu.de (B.F.)

* Correspondence: rebecca.chamberlain@hhu.de; Tel.: +49-211-81-10076

Abstract: Pharmaceutical and medicinal printing technologies allow personalization and on-demand manufacturing of drug and medicinal products. Being able to manufacture patient tailored dosage forms or medical devices in a pharmacy, medical office, dental laboratory, or hospital at the point of care raises new demands on quality control procedures. For Fused Deposition Modeling, for example, it must be ensured that the starting materials, the (drug-loaded) filaments, are not accidentally exchanged by the operator. This study investigated the potential of colorimetric measurements for direct and indirect determination of the identity of extruded filaments consisting of polymer matrix, different API and/or coloring agents. Since reflection measurements were affected by surface properties of the filaments, a self-constructed filament holder was utilized with an optical fiber positioned in a 180° angle to a white light LED to perform transmission measurements. It was possible to distinguish filaments with different API concentrations by their color values, taking into account that transmission partially decreased by increased API concentration. Therefore, the intensity of the light source had to be adjusted depending on the transparency of the filament. It was shown that colorimetry can be used as a quality control tool to detect differences in drug-loading and is able to distinguish various extruded batches. Additionally, if differences in API/polymer concentrations do not lead to significant changes in L*a*b values, coloring agents were used as additives in low concentrations to color code filaments. In future studies, the setup must be supplemented with a standardized light source and obscuring filters for light intensity adjustments.

Keywords: CIELAB measurements; colorimetry; pharmaceutical filaments; color-coded filaments; hot melt extrusion; analytics of extruded filaments; personalized medicine; fixed-dose combinations; FDM printing; quality control



Citation: Chamberlain, R.; Mangiorou, E.; Fischer, B. Introducing Fiber-Assisted Colorimetric Measurements as a Quality Control Tool of Hot Melt Extruded Filaments. *Pharmaceutics* **2022**, *14*, 1055. <https://doi.org/10.3390/pharmaceutics14051055>

Academic Editor: Pedro Dorado

Received: 14 April 2022

Accepted: 11 May 2022

Published: 14 May 2022

Publisher's Note: MDPI stays neutral with regard to jurisdictional claims in published maps and institutional affiliations.



Copyright: © 2022 by the authors. Licensee MDPI, Basel, Switzerland. This article is an open access article distributed under the terms and conditions of the Creative Commons Attribution (CC BY) license (<https://creativecommons.org/licenses/by/4.0/>).

1. Introduction

The application of 3D printing for patient-specific therapy is gaining more and more interest, as medical and pharmaceutical 3D printers as well as medical grade printing materials are already commercially available. The “one-size-fits-all” approach is being replaced more and more by targeted and personalized medicine [1]. With the help of medical Fused Deposition Modeling (FDM) 3D printing, patient-specific medical devices, such as implants, prostheses, and surgical guides are printed using biocompatible materials (e.g., PCL, PLA, PVA). Additionally, non-biocompatible materials (e.g., ABS, TPU) are used for printing medical models for perioperative surgical planning and simulations [2]. In pharmaceutical FDM 3D printing, various thermoplastic polymers are processed by hot melt extrusion (HME) with active substances [3]. The intermediate filament is then used to produce solid dosage forms such as tablets, capsules, inserts, implants, and films [4]. The ongoing research may lead to a future where solid dosage forms will be printed at the point of care (PoC) allowing personalization of drug content, drug release, and the supply of medicines containing more than one drug for the treated patient [5]. To avoid incorrect application when using a wide variety of pharmaceutical grade filaments, for

example in hospitals or local pharmacies, the fact that the matrix, the active ingredient, and/or other additives are responsible for the coloration of the filaments might be used for colorimetric measurements. In this context, the CIE $L^*a^*b^*$ (CIELAB) color space introduced by the International Commission on Illumination in 1976 was utilized, where colors are defined by three unique values: L^* for lightness, a^* for red and green color, and b^* for blue and yellow color [6]. While L^* -values can vary between 0 (black) and 100 (white), both a^* and b^* values range from -128 (a^* : green, b^* : blue) to $+127$ (a^* : red, b^* : yellow), which leaves theoretically 6.5 million possibilities for describing different colors [7]. These $L^*a^*b^*$ values are distributed in the three-dimensional space in such a way that a sphere results (Figure 1). For pharmaceutical applications, colorimetry has already been tested as a quality control (QC) tool for various drug preparations since it represents a non-destructive characterization method [8]. For tablet analysis, Siddiqui et al. could determine a correlation between the surface color and tensile strength of tablets and were also able to detect deviations in tablet hardness through differences in color measurements [9]. Differences in surface color of coated tablets were studied by Bogdansky [10]. Berberich et al. were able to determine the period of time uncoated tablets remained white during storage by color measurement [11]. Gren and Nyström used colorimetry for an estimation of the surface coverage of particles with colored and uncolored stearic acid [12]. Barimani et al. used CIELAB measurements for visual inspection of tablet coating produced with continuous direct compression to ensure a defect-free coating of each measured tablet [13]. CIELAB measurements were also performed by Lakio et al., who analyzed granules and pellets as color indicators for potential heat stress during drying processes [7]. Wickström et al. detected vitamin B containing layers conducted by Inkjet-Printing via differences in CIELAB values but were limited to differentiating between the first 5–6 printed layers since the b^* value reached color saturation [14]. The findings of the listed studies were taken as an example to use the distinguished extruded pharmaceutical filaments. For this purpose, a filament holder was designed, where the filament could be inserted and both reflection and transmission measurements could be performed. An optical multi-core fiber was used, which can both transmit light from a white light LED towards the sample and collect light after reflection. The same fiber was used collecting light from a second LED after being transmitted through or partly directed around the filament. The fade of the applied electromagnetic radiation and light scattering effects caused by the filament geometry and composition are not analyzed in depth in this study. In this study, the aim was to investigate, whether the difference in concentration of an active pharmaceutical ingredient (API) is reflected in measurable color difference of the filaments. Pramipexol (P), levodopa (LD), benserazide (BZ), and praziquantel (PZQ) served as model APIs. Since the active ingredients led to a change in transparency, it was important to ensure that the light intensity was appropriate to visualize differences between the active ingredients or active ingredient concentrations. If a dose increase and associated change in polymer-API concentration did not result in a desired color change, a pharmaceutical coloring agent was added to the formulation [15–18]. Here, it was necessary to conduct preliminary tests without an active ingredient to determine which differences in concentrations of the additive led to significantly different color values in the CIELAB color space. The added color agents were either dissolved or dispersed in the polymer melt. The bright yellow, crystalline powder riboflavin (RF), also known as vitamin B2, and indigo carmine (IC), a blue coloring agent, were chosen to serve as additives. Thus, when both coloring agents were used (yellow and blue) the extruded filaments appeared green. Thereby, only slight differences in the concentration of the coloring agent were chosen to analyze whether these were also reflected in different color values. The dosing accuracy during extrusion was examined in content uniformity studies conducted via high-performance liquid chromatography (HPLC) analysis. These experiments were performed to develop new analytical techniques for dosage investigation, batches of filaments consisting of different concentrations of API, and indirect determination using a coloring agent on the polymer-API composition using CIELAB measurements.

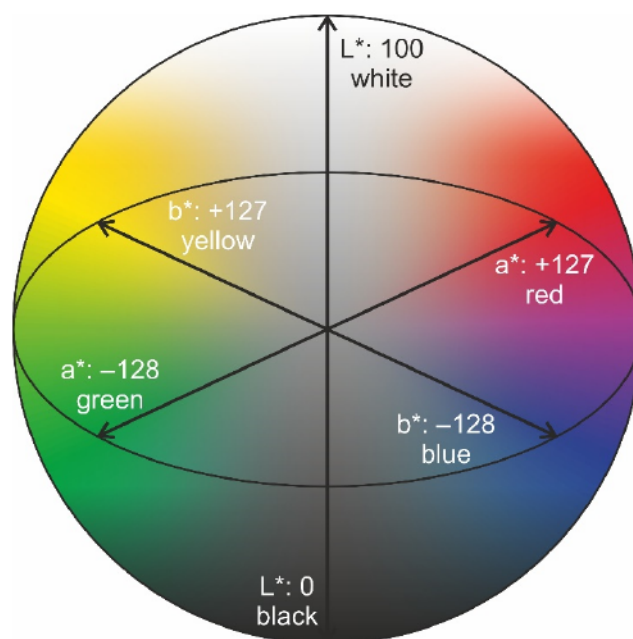


Figure 1. $L^*a^*b^*$ three-dimensional color space.

2. Materials and Methods

The polymers including ethylene-vinyl acetate copolymer (EVA, 82:18, Escorene[®], FL 01418, TER Chemicals, Hamburg, Germany) and vinylpyrrolidone-vinyl acetate copolymer (VA, 6:4, Kollidon[®] VA 64, BASF, Ludwigshafen am Rhein, Germany) served as polymer matrices. Four thermal stable model substances, praziquantel (PZQ, Bayer AG, Leverkusen, Germany), levodopa (LD, Zhejiang Wild Wind Pharmaceutical Co. Ltd., Dongyang, China), benserazide hydrochloride (BZ, s.p. Quimica, Tarragona, Spain), and pramipexole dihydrochloride monohydrate (P, Chr. Olesen, Copenhagen, Denmark) were tested in this study. For coloring agents, riboflavin (RF, Caesar & Loretz GmbH, Hilden, Germany) and sodium 3,3'-dioxo-[2,2'-biindolylidene]-5,5'-disulfonate (indigo carmine, IC, bld pharmatech GmbH, Kaiserslautern, Germany) were used.

2.1. Hot Melt Extrusion

All filaments were prepared by HME using a co-rotating twin-screw extruder with a hot-melt extrusion die (Pharmalab HME 16, Thermo Fisher Scientific, Waltham, MA, USA). A gravimetric feeder (K-SFS-24/6, Coperion, Stuttgart, Germany) was used for all experiments. An in-house manufactured die with a diameter of 1.85 mm was used. The desired filament diameter was achieved using a belt hauled-off unit of a winder (Brabender, Duisburg, Germany) with a belt speed of 1.5–1.9 m/min and the filament was pulled through a roll-system with four 360° air flow ring nozzles (Super Air Wipe, Exair, Cincinnati, OH, USA) for active cooling of the filament. With a laser-based diameter measurement module (Laser 2025 T, Sikora, Bremen, Germany) the filament diameter was controlled [19]. The screw speed was set to 30 rpm and powder feed rate to 5 g/min. The screw configuration included two kneading zones and a degassing port was installed [20]. All temperatures of the heating zones were set for each extrusion according to Table 1 depending on the polymer matrix of the filament [21,22]. The powder mixtures were blended for 20 min in a Turbula[®] mixer. Filament samples were only collected when extrusion runs reached equilibrium condition for drug content [20].

Table 1. Temperature profile of zones 2–10 for extrusion runs with selected polymers.

Polymer	Temperature Profile in Zone 2–10/°C								
	2	3	4	5	6	7	8	9	10
EVA	20	20	50	85	85	85	85	85	85
VA	20	30	75	165	180	180	180	180	180

2.2. Colorimetry Measurements of Filaments

The hot melt extruded filaments were cut into filament sticks of 4 cm and were placed in an in-house produced stainless steel sample holder with an inner diameter of 1.9 mm. Dual output channels of the power supply (Rigol DP832, Meilhaus Electronic GmbH, Alling, Germany) were utilized for the regulation of two light-emitting diodes (LED, 333-2UTC/S400-A6, Everlight, Hsinchu, Taiwan). For the assembly of the individual components for colorimetric measurements, a system bar, sliders, a mounting cube, a tower, and a height adjustable table were obtained from OWIS® (OWIS GmbH, Staufen im Breisgau, Germany).

For reflection measurements, a dual fiber optical probe with SMA connectors (SMA905, Ø600 µm, 300–1200 nm, BFY600HS02, Thorlabs, Newton, NJ, USA) was attached to the sample holder and was guided from the LED to the sample and backwards to the camera (WIFI Digital Microscope 8595776342, AHSNOPTIC, Beijing, China). In a second setup (Setup 2, Figure 2), the dual fiber bundle was exchanged to a multi-core fiber probe (RP21, Ø200 µm, 400–2400 nm, FG200LEA, Thorlabs, Newton, NJ, USA), whereby a single fiber leg was directed to the first LED for reflection measurements. The probe leg “6-around-1” fiber configuration was guided to the sample and the 6-fiber leg was directed to the camera. For transmission measurements, a second LED was installed in an 180° angle to the above-mentioned fiber probes using the same orientation of the fiber legs and the same camera (Figure 2). The fibers were directly attached to the filament holder or fixed on adjustable sliders (OWIS GmbH, Staufen im Breisgau, Deutschland) in front of the LED or the camera with SMA connectors. Through an integrated metal platform tensioned by two springs within the holder, the filament was always in contact with the curvature facing the fiber optic probe to ensure accurate positioning.

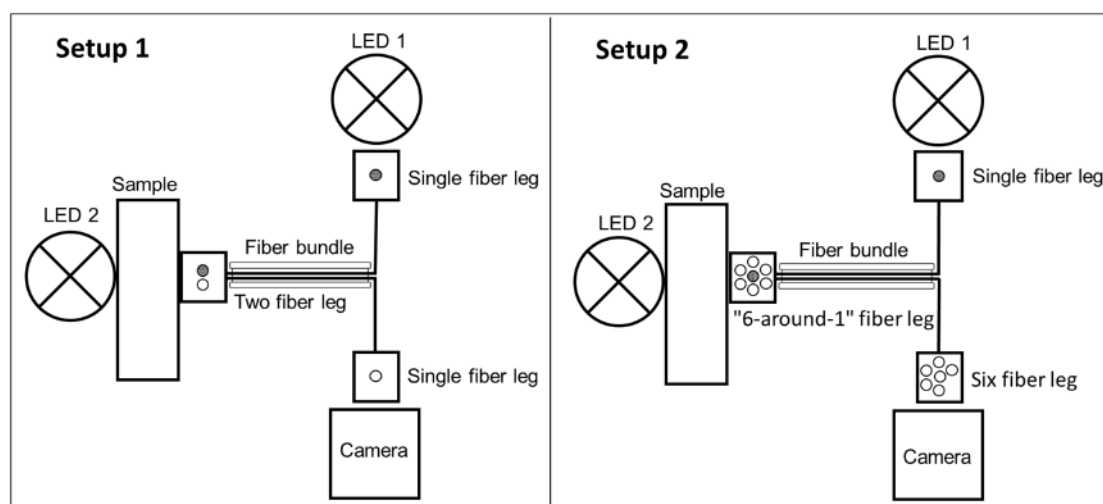


Figure 2. Assembly of the components for reflection and transmission measurements for Setup 1 and 2: light is applied from LED 1 and enters and exits at the same fiber bundle or light from LED 2 passes through the filament and transmitted light is collected into the fiber bundles. A picture of the fiber leg (single- or six-fiber leg) was taken by a camera.

2.3. Data Evaluation of Colorimetry Measurements

The mean L^* , a^* , b^* values of the pictures illustrating the respective fiber leg were obtained by analyzing a defined area via Corel® PHOTO-PAINT X7 (17.6.0.1021). Mimicking the circular surface of the fiber, a circular area was selected as the to be analyzed area, but edge areas were left out (Figure 3). Only one L^* , a^* , and b^* value per filament was measured in the first set up, since a single fiber leg was analyzed. For the second set up, six circular areas were evaluated separately or a mean value of all six fiber bundles with standard deviation was calculated for each filament.

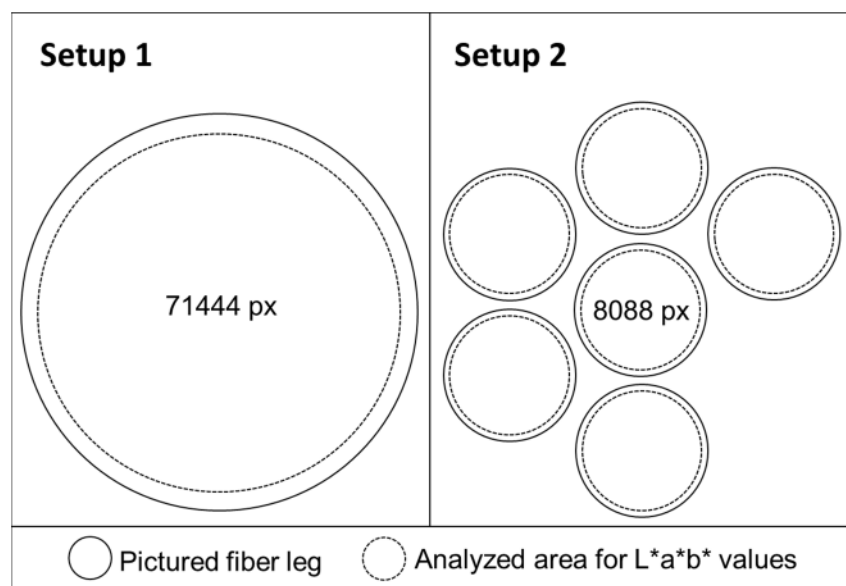


Figure 3. Schematic visualization of the pictured fiber leg for Setup 1 and 2 with the selected area to be analyzed (for Setup 1: 71444 Pixel; and for Setup 2: six fiber legs with each 8088 Pixel) for one filament in Corel PHOTO-PAINT.

2.4. Reference Method for Determination of Drug Content (HPLC-UV)

For sample preparation, filaments were dissolved in flasks ($n = 10$), which were filled with demineralized water up to 50 or 100 mL. All the agents that were used except EVA are water soluble. The content of drug-loaded filaments was determined by high performance liquid chromatography (HPLC) analysis. The HPLC system (Dionex, Sunnyvale, CA, USA) was equipped with a quaternary pump (P 580 A, Dionex, Sunnyvale, CA, USA) and an autosampler (ASI-100, Dionex, Sunnyvale, CA, USA). A 250×4.6 mm column (Eurospher II 100-5 C18A, Knauer, Berlin, Germany) with an integrated precolumn was used. Three different HPLC methods were used for the analysis of the active and color ingredients. For the first method, ammonium acetate buffer and methanol (mobile phase B) served as eluents. The gradient was set as follows: mobile phase B was increased from 1 to 5% (v/v), within the first minute, held at 5% (v/v) for 4 min, increased from 5 to 10% (v/v) within 1 min, held at 10% (v/v) for 4 min, increased again from 10 to 20% (v/v) within 1 min, held for 4 min at 20% (v/v), increased again from 20 to 99% (v/v) within 5 min, held for 2 min at 99% (v/v) and decreased to 1% (v/v) within 0.5 min, again until 22.5 min after sample injection [23]. An equilibration time of 3.5 min per run was maintained before the next sample was injected. An injection volume of 200 μ L was chosen to analyze benserazide (280 nm), levodopa (280 nm), pramipexole (264 nm), and indigo carmine (280 nm). The second HPLC method was used to quantify praziquantel at the wavelength of 280 nm. Phosphate buffer and acetonitrile (mobile phase B) served as eluents and the flow rate was 1.5 mL/min. The gradient was set as follows: mobile phase B was increased from 30 to 95% (v/v), within the first 8 min, held at 95% (v/v) for 3 min, decreased to 30% (v/v) within 1 min, again until 12 min after sample injection. An equilibration time of 2 min per run was kept before the next sample was injected. The third HPLC method was necessary to

evaluate the concentration of riboflavin (280 nm). Phosphate buffer and acetonitrile (mobile phase B) served as eluents and the flow rate was 1.0 mL/min. The gradient was set as follows: mobile phase B was stable at 10% (v/v) the first 5 min, increased to 20% (v/v), the next 15 min, held at 20% (v/v) for 5 min, increased again to 50% (v/v) within 10 min, held at 50% (v/v) for another 10 min, and decreased to 10% (v/v) within 2 min, again until 47 min after sample injection [24].

3. Results

3.1. Transmission and Reflection Measurements of Filaments

When comparing reflection and transmission measurements, it is noticeable that the resulting $L^*a^*b^*$ values of the two measurement techniques using Setup 1 (Figure 2) give very different results when analyzing the same filament batch. For example, the L^* value obtained by a transmission measurement of filaments consisting of vinylpyrrolidone-vinyl acetate copolymer and 5% (w/w) pramipexole (VA-5% P) is 18.4, and reflection measurement for the same batch the median L^* value is 82.6 (Table 2). All b^* values obtained by transmission measurements differ from the results of the reflection measurements of both the three batches with pramipexole and the three batches with praziquantel. While the median b^* value obtained by the transmission measurement of VA-1% P is 7.4, of VA-5% P is 8.5, and of VA-10% is 9.1, the median b^* values obtained by reflection measurements for all three batches are -0.2 ± 0.3 . b^* values of -3.0 ± 0.3 were measured for all three batches of vinylpyrrolidone-vinyl acetate copolymer-praziquantel filaments with a drug load of 5, 10, and 15% (w/w) (VA-5% PZQ, VA-10% PZQ, VA-15% PZQ) using the transmission assembly of Setup 1. Reflection measurements of these praziquantel filaments obtained median b^* values of 16.7 ± 1.1 . Similar values for transmission and reflection measurements were found for the L^* values of VA-1% P filaments (transmission: $\bar{x} = 60.4$, reflection: $\bar{x} = 66.7$) and for the a^* values of this batch (transmission: $\bar{x} = -7.9$, reflection: $\bar{x} = -8.3$). Nevertheless, it can be concluded that when specifying the $L^*a^*b^*$ values, it should always be mentioned at which angle the emitted light is collected by the fiber and, therefore, specify if the filament was analyzed in reflection or transmission. The reflectance measurements show higher deviations of $L^*a^*b^*$ values compared to the transmission measurements (Figure 4). The determination of the filament content does not reflect the large deviations of the reflection measurements, so it was concluded that this was due to the measurement method. The high variations might be caused by the varying positioning of the filaments to the two-fiber leg due to the cylindrical geometry of the sample, by composition of the matrix (e.g., suspended particles) and by surface irregularities resulting in complex scattered light effects. Thus, it was decided that only transmission measurements would be performed for further measurements. However, it is noticeable that the $L^*a^*b^*$ values of the transmission measurements for all three batches of VA-PZQ filaments show very similar values. For VA-P filaments, on the other hand, a different L^* value occurs for the filament batch of VA-1% P compared to the other two filament batches with pramipexole.

This can be explained since pramipexole is suspended in the VA matrix and filaments with 1% pramipexole are transparent and both the 5% and the 10% pramipexole filaments are not translucent. Consequently, the VA-1% P filament batch can be clearly distinguished from the VA-5% P and VA-10% P batches by the L^* value, although the b^* value is very similar compared to the other two pramipexole batches and the a^* value shows a very high deviation and does not show a significant difference. To further optimize the transmission measurements and reduce the potential uncertainty of differences in reflection of the incident light caused by the curvature of the filaments, a new fiber bundle with a 6-fiber end was used (Setup 2, Figure 2).

Table 2. $L^*a^*b^*$ values of transmission and reflection measurement of the filaments obtained with Setup 1 ($n = 10$; mean, Q1–Q3) despite the analyzed content uniformity determined by HPLC analysis ($n = 10$; mean, SD).

Batch VA-	Transmission						Reflection						Drug Content/%	
	L^* Value		a^* Value		b^* Value		L^* Value		a^* Value		b^* Value		\bar{x}	SD
	\bar{x}	Q1–Q3	\bar{x}	Q1–Q3	\bar{x}	Q1–Q3	\bar{x}	Q1–Q3	\bar{x}	Q1–Q3	\bar{x}	Q1–Q3	\bar{x}	SD
1% P	60.3	4.5	−7.9	1.9	7.4	0.6	66.7	19.9	−8.3	1.5	−0.5	2.3	0.98	0.15
5% P	18.4	1.3	−5.9	0.1	8.5	0.8	82.6	11.4	−9.0	0.5	0.1	0.3	5.01	0.13
10% P	13.4	1.2	−5.6	0.3	9.1	0.3	88.3	7.5	−10.6	1.0	0.1	0.2	10.02	0.09
5% PZQ	32.7	6.6	−4.0	0.4	−3.0	0.7	60.1	17.3	−9.6	1.5	17.0	6.3	4.98	0.11
10% PZQ	33.8	8.0	−4.1	0.3	−2.7	0.7	57.0	20.5	−10.5	2.3	17.8	3.5	10.00	0.12
15% PZQ	39.1	3.1	−4.5	0.7	−3.2	0.7	76.6	8.5	−11.1	0.9	15.6	4.3	15.01	0.09

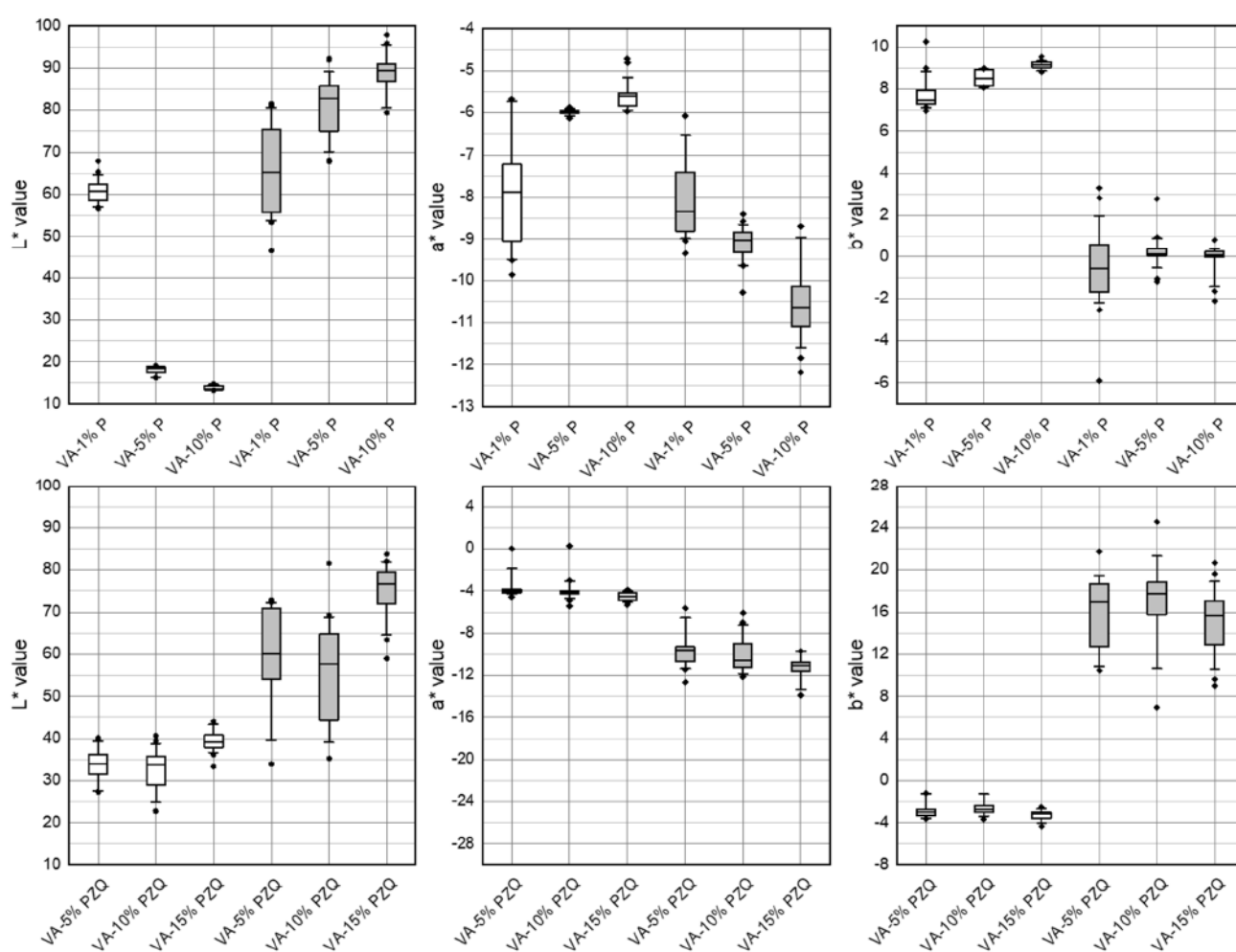

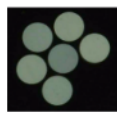

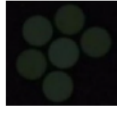


Figure 4. Box-whisker plots of $L^*a^*b^*$ values of transmission (white) and reflection (grey) measurement of VA-1,5,10% P and VA-5,10,15% PZQ filaments obtained with Setup 1 ($n = 10$, Q1/Q3 \pm 1.5 IQR, outliers).

3.2. Optimization of Transmission Measurements with Setup 2 and Voltage Adaption





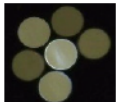
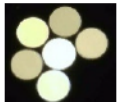




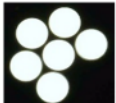







Compared to Setup 1, the emitted light was not collected by only one fiber, but by six circular arranged fibers ("6 around 1" fiber leg) so that light was captured from six different angles. In the 6-fiber leg, the fibers are arranged in such a way that one fiber is centered, which can lead to irritations since the fiber was circularly arranged at the sample side. It is noticeable that the captured images of the 6-fiber leg show different $L^*a^*b^*$ values for the six individual fibers (Table 3).

Table 3. $L^*a^*b^*$ values determined for fibers 1–6 using Setup 2 of VA-1% P, VA-5% P, and VA-10% P filaments at 2.50 V.

Setup 2	Filament	Fibers	L*, a*, b* Values of Fibers 1–6						
	VA-1% P		L*	1	2	3	4	5	6
			L*	58.9	57.6	53.6	56.6	55.1	49.8
			a*	−8.6	−8.7	−9.0	−9.1	−10.2	−8.1
	VA-5% P		b*	9.0	8.6	6.1	8.3	7.4	4.0
			L*	19.7	19.3	20.6	19.4	20.4	21.3
			a*	−7.0	−6.8	−6.7	−6.9	−6.8	−5.9
	VA-10% P		b*	3.7	4.2	4.2	4.1	4.2	3.9
			L*	13.3	13.2	16.0	13.2	15.0	16.9
			a*	−6.0	−5.7	−7.0	−7.7	−7.1	−7.0
b*	3.7	4.2	4.2	4.2	4.2	3.9			

A regularity could not be found with respect to which fiber was consistently darker or lighter (L^* value), or whether the a^* and b^* values showed systematic tendencies. The L^* value shows the greatest fluctuations for the VA-1% P filament and varies between 49.8 (fiber 1) and 58.9 (fiber 6). Here, the b^* values also differ by 5.0 (9.0 and 4.0), but the a^* values are nearly the same (−8.6 and −8.1). For the other measured values, the fluctuations of the $L^*a^*b^*$ values are in the range of 0.5–1.8. However, the obtained data lead to the assumption that there was a variability in $L^*a^*b^*$ values due to the geometry of the filaments. Additionally, the influence of the brightness of the imaged fiber on the a^* and b^* values was investigated by varying the light intensity of the LED. The different $L^*a^*b^*$ values of the six fibers of EC- 20% LD/5% BZ, VA-5% P, and VA-10% PZQ filaments by varying the voltage of the LED from 2.30 to 3.20 V are listed in Table 4.

Table 4. Color observation of transmitted light on selected drug loaded filaments.

Batch	Pictures of Filaments	Voltage of LED with Corresponding Image of the 6-Fiber Leg				
		2.30	2.40	2.50	2.80	3.20
EC-20% LD/5% BZ						
						
VA-10% PZQ						

By setting low volt values, the fibers appear black, and at high volt values, they appear white. In both cases, color differences can no longer be observed between the six fibers. If the filaments were not transparent and/or colored (EC- 20% LD/ 5% BZ filaments) a higher voltage of the LED had to be set so that color values of the respective fibers could be determined. For EC- 20% LD/ 5% BZ filaments 2.80 V were applied to ensure that the brown color of the filaments could be determined from the fibers. For VA-5% P filaments, voltages below 2.40 led to black fibers and voltages above 2.80 V resulted in white fibers.

Similarly, for VA-10% PZQ filaments voltages above 2.80 V led to white fibers. Since the filaments were transparent, 2.50 V still caused fibers to appear white, but at 2.40 V the fibers were already very dark. To understand the light intensity dependent influence on a^* and b^* values, the voltages were systematically changed and the $L^*a^*b^*$ values were determined (Figures 5–7). There was a noticeable difference between the a^* and b^* values: the brighter or darker the imaged fiber was, the closer the two values approached to zero. This can be explained by the fact that the $L^*a^*b^*$ color space is represented three-dimensionally as a sphere (Figure 1). White has the $L^*a^*b^*$ value of $L^* 100$ $a^* 0$ and $b^* 0$ and black has the $L^*a^*b^*$ value of $L^* 0$ $a^* 0$ and $b^* 0$ and consequently the color value of a very bright fiber approaches the $L^*a^*b^*$ values of white and dark fibers approach the $L^*a^*b^*$ values of black [25]. We also observed that the $L^*a^*b^*$ values for the filaments changed as a function of the brightness of the LED, respectively, the voltage setting. For EC- 20% LD/ 5% BZ filaments, throughout the range of L^* , the a^* values only slightly decrease. However, the b^* value indicates a maximum value of 22.0 ± 7.3 at 2.77 V, when the L^* value is 43.4 ± 11.8 (Figure 5). This is consistent with the observations in Table 4, where the setting of 2.80 V shows fibers that appear yellow/brown, which affects the b^* value.

For the three filament batches with different pramipexole concentrations, the a^* and b^* values differ regarding the voltage of the LED (Figure 6). For VA-1% P filaments, the highest b^* value of 6.06 is at 2.47 V, for VA-5% P filaments the highest b^* value is at 2.63 V and corresponds to 9.61, and for VA-10% P filaments the highest b^* value of 8.84 was measured at 2.52 V. The range for VA-1% P filaments, in which the measured a^* and b^* values differ from -4 ± 6 , is from 2.40 to 2.57 V.

For the other two pramipexole batches, the range is between 2.44 and 2.67 V (VA-5% P filaments) and between 2.44 and 2.72 V (VA-10% P filaments). For the comparative measurements of the pramipexole batches, 2.50 V was selected, which was in the mentioned detection ranges and at the same time resulted in differences in $L^*a^*b^*$ values of the three batches. The same measurements were performed with all three praziquantel filament batches (Figure 7). The a^* and b^* values of all three batches varied from -8 to 1 despite one outlier at -17 (b^* value of VA-10% PZQ batch), which indicates the difficulties in seeing significant differences between the three batches with different API contents. For VA-5% PZQ filaments, the minimum b^* value of -5.69 is at 2.42 V, for VA-5% PZQ filaments the lowest b^* value is at 2.43 V and corresponds to -5.66 , and for VA-10% PZQ filaments the lowest b^* value of -5.89 was measured at 2.44 V. The range for VA-5% PZQ filaments, in which a^* and b^* values differ from 0 ± 1 , is from 2.39 to 2.48 V. For the other two praziquantel batches, the range is between 2.41 and 2.45 V (VA-10% PZQ filaments) and between 2.36 and 2.47 V (VA-15% PZQ filaments). Again, 2.50 V was selected for the comparative measurements of the three praziquantel batches. Distinct clusters are noticeable in the 2D graphs of the pramipexole batches (Figure 8A). Thus, the VA-1% P filaments are characterized by the highest L^* values and the lowest a^* values. The b^* values are similar to the b^* values of the other two batches. The clusters of VA-5% P filaments and VA-10% P filaments are closer to each other. However, the L^* values of VA-5% P filaments are higher and both the a^* and b^* values are lower in comparison to the a^* and b^* values of VA-10% P filaments. Clusters can also be identified for the praziquantel-containing filaments (Figure 8B). However, it is not possible to see significant differences between the batches since the standard deviations are very high and overlap for all three values. A trend can be recognized that with increasing concentration of praziquantel the L^* and a^* decrease, and the b^* value increases. As the three different praziquantel batches could not be significantly distinguished by colorimetric measurements, two coloring agents, which are commonly used in pharmaceutical coating processes [26,27], were added in different concentrations to create variability in $L^*a^*b^*$ values due to additives.

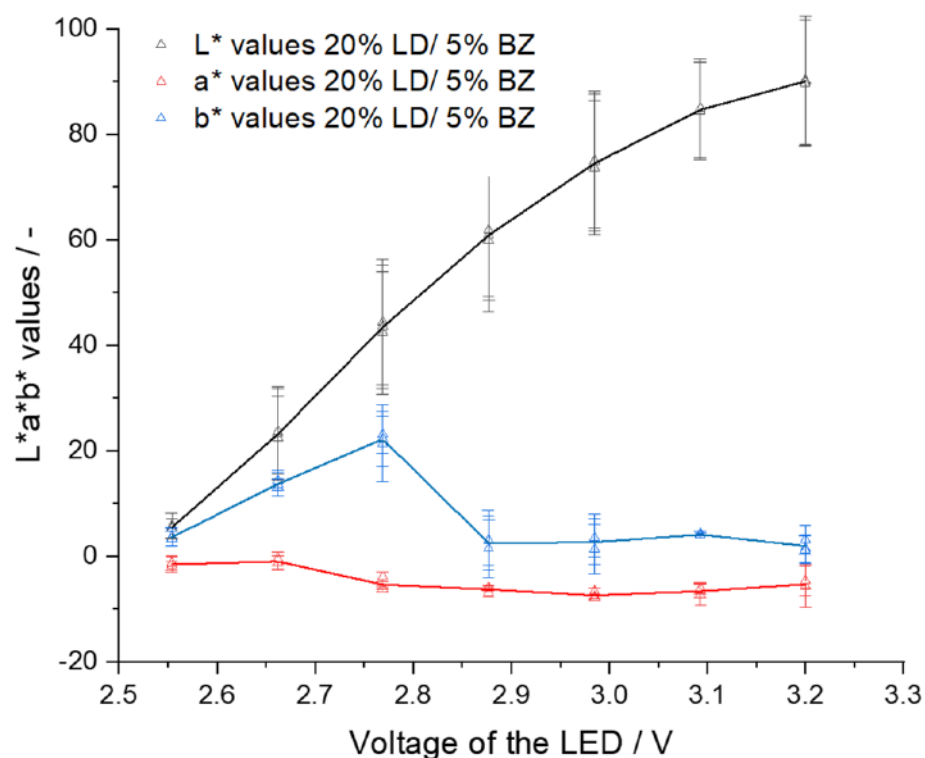


Figure 5. $L^*a^*b^*$ values depending on LED voltage for EC- 20% LD/ 5% BZ filaments (mean \pm SD, three filaments, $n = 6$).

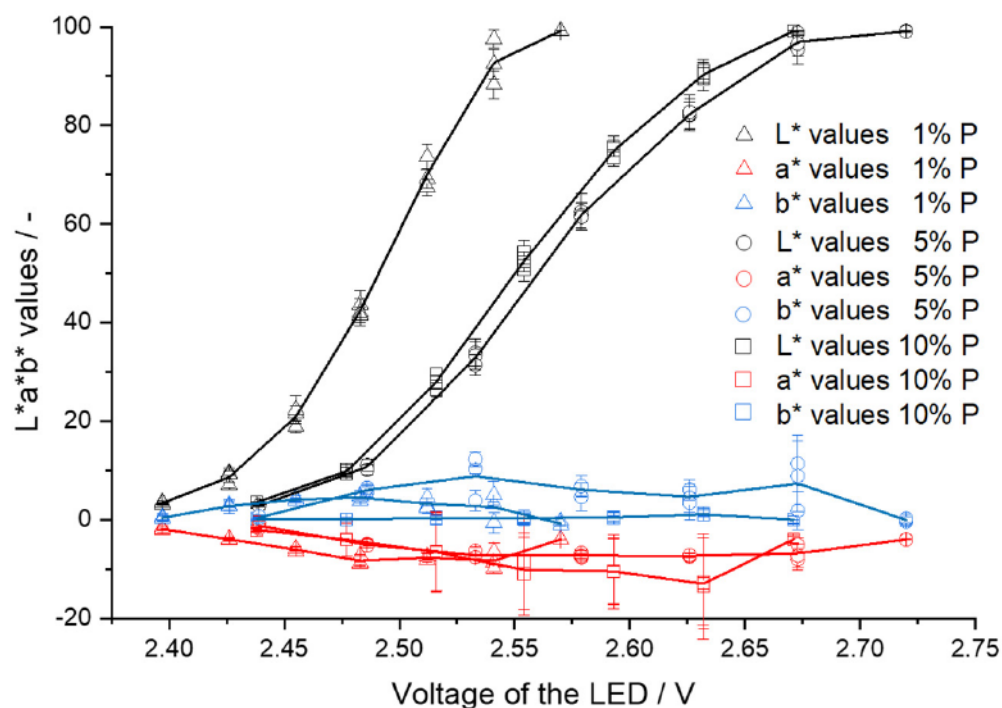


Figure 6. $L^*a^*b^*$ values depending on LED voltage for VA-1% P, VA-5% P, and VA-10% P filaments (mean \pm SD, each of the three filaments, $n = 6$).

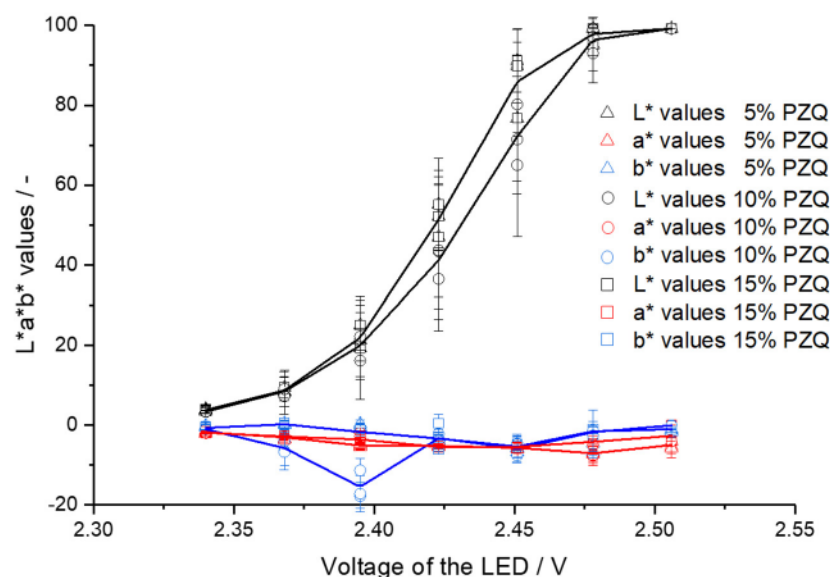


Figure 7. $L^*a^*b^*$ values depending on LED voltage for VA-5% PZQ, VA-10% PZQ, and VA-15% PZQ filaments (mean \pm SD, each of the three filaments, $n = 6$).

3.3. Color-Coded Filaments

To be able to distinguish filament batches by colorimetry, as the polymer-API filament compositions do not lead to a desired difference, coloring agents commonly used in pharmaceutical production were added to the powder mixture and were incorporated together with VA and praziquantel by HME. The excipients riboflavin (yellow) and indigo carmine (blue) caused the filaments to appear green. By maintaining the riboflavin (RF) concentration and only increasing the indigo carmine (IC) concentration, the ratio of additives changed from 1:1 (0.1% (*w/w*) RF, 0.1% (*w/w*) IC) for VA-5% PZQ filaments to 1:3 (0.1% (*w/w*) RF, 0.3% (*w/w*) IC) for VA-10% PZQ filaments, and to 1:5 (0.1% (*w/w*) RF, 0.5% (*w/w*) IC) for VA-15% PZQ filaments. The concentrations of the three ingredients (API and coloring agents) were analyzed by HPLC analysis and are shown in Table 5.

Table 5. Content of coloring agents determined by HPLC analysis.

Batch VA-	PZQ Content/%		RF Content/%		IC Content/%	
	\bar{x}	SD	\bar{x}	SD	\bar{x}	SD
5% PZQ-0.1% RF-0.1% IC	4.99	0.10	0.099	0.012	0.102	0.012
10% PZQ-0.1% RF-0.3% IC	10.02	0.09	0.098	0.011	0.299	0.009
15% PZQ-0.1% RF-0.5% IC	15.02	0.12	0.099	0.011	0.500	0.009

Again, seven different voltages were tested, and 2.50 V was selected for the comparative measurements of the three green praziquantel batches (Figure 9). According to the expectations, a significant difference in the L^*b^* 2D graph was found due to the addition of excipients that affect the b^* value significantly. Why the b^* values of VA-15% PZQ-0.1% RF-0.5% IC filaments are lower than those of A-10% PZQ-0.1% RF-0.3% IC cannot be explained by the higher amount of indigo carmine, but suspended particles must have an influence here. HPLC analysis showed that the concentration of IC increases with increasing concentration of praziquantel (Table 5). It was not investigated whether IC was dissolved or suspended in the polymer matrix and the saturation concentration of IC in VA was not determined. But blue particles were visible within the filament indicating suspended IC particles. However, by the addition of the two coloring agents to the formulation, the individual produced batches differ significantly from each other in the L^*b^* 2D graph (Figure 10).

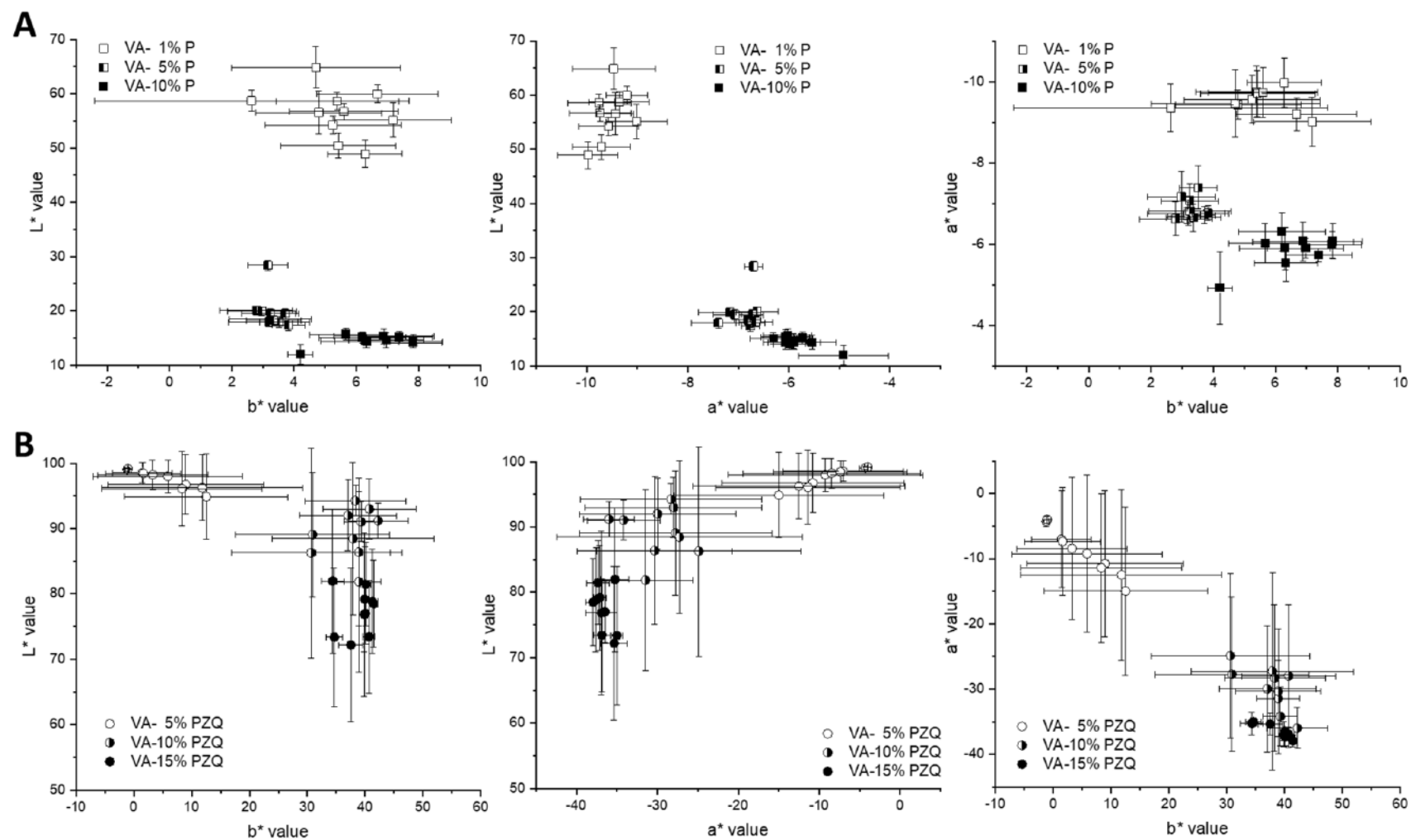


Figure 8. The 2D graphs of L*a*, L*b*, and a*b* values at 2.50 V for (A) pramipexole filaments (1, 5, 10% (w/w)) and (B) praziquantel filaments (5, 10, 15% (w/w)).

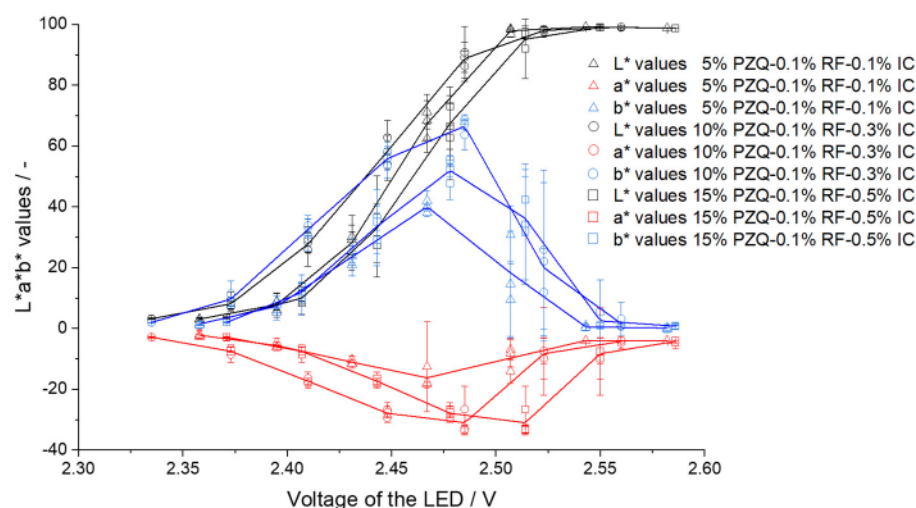


Figure 9. a^* and b^* values depending on LED voltage for the filaments of PZQ with different concentrations of RF and IC (VA-5% PZQ-0.1% RF-0.1% IC, VA-10% PZQ-0.1% RF-0.3% IC and VA-15% PZQ-0.1% RF-0.5% IC).

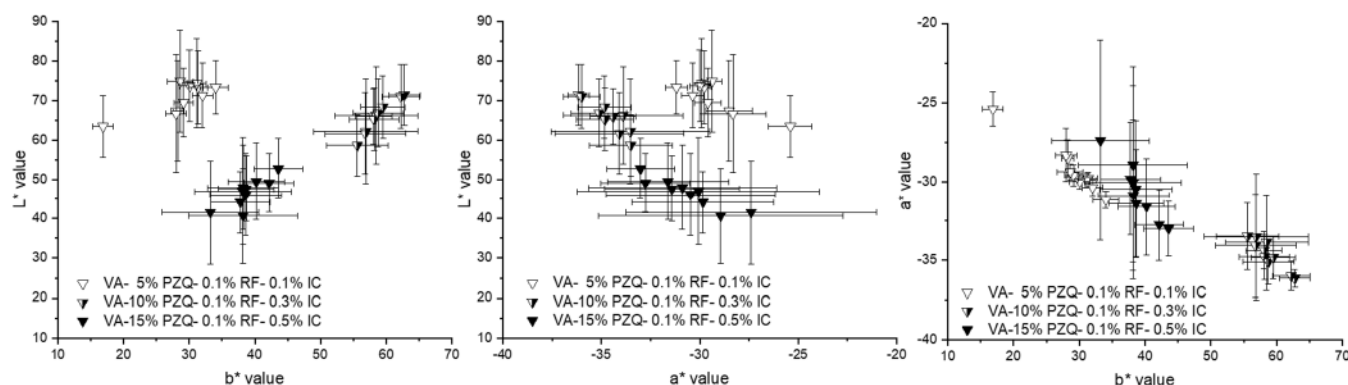


Figure 10. The 2D graphs of L^*a^* , L^*b^* , and a^*b^* values at 2.50 V for color-coded praziquantel filaments (VA-5% PZQ-0.1% RF-0.1% IC, VA-10% PZQ-0.1% RF-0.3% IC and VA-15% PZQ-0.1% RF-0.5% IC).

4. Conclusions

When performing colorimetric measurements with pharmaceutical filaments, this method can be used for distinguishing extruded filament batches with different API concentrations. Using a setup optimized for pharmaceutical filaments, extruded batches could be distinguished despite color differences generated by the amount of API or after using colored additives. The filaments were analyzed by a six-fiber bundle to depict light scattering effects caused by the filament geometry with the consequence that the fibers show high deviations. Despite the high deviations, clusters can be found in 2D graphs of L^*a^* , L^*b^* , and/or a^*b^* values which indicate a significant difference in the individual batches. If the matrix and the desired API concentration does not lead to differences in color changes despite other filaments, adding other excipients is a reasonable approach to achieve clustering of L^*a^* , L^*b^* , and/or a^*b^* values. Ensuring that the filaments were optimally illuminated, the power supply of the LED was regulated so that the a^* and b^* values of the analyzed filaments were not zero (black or white) because the fibers were either too dark or too bright. To further optimize the setup, measurements should be performed with a standardized light source at the same voltage and darkening needs be realized by additional optical filters. By implementing a filament holder, colorimetric measurements might also be performed during the HME process. Since the HME process is also used to manufacture granules and amorphous solid dispersions, this tool could be adapted to these

(intermediate) drug products. The fiber-assisted colorimetric analysis with the small-sized components can be easily installed after a few modifications in the downstream equipment of the HME process.

Author Contributions: Conceptualization, R.C., B.F.; data curation, R.C.; formal analysis, R.C., E.M.; investigation, R.C.; methodology, R.C.; visualization, R.C., B.F.; writing—original draft, R.C.; writing—review and editing, R.C., E.M., B.F. All authors have read and agreed to the published version of the manuscript.

Funding: Eirini Mangiorou’s stay at HHU was financially supported by the ERASMUS program (no. 1179/2020).

Institutional Review Board Statement: Not applicable.

Informed Consent Statement: Not applicable.

Data Availability Statement: The data presented in this study are available upon request from the corresponding author.

Acknowledgments: The authors want to thank BASF for supplying raw material.

Conflicts of Interest: The authors declare no conflict of interest. BASF had no role in the design of the study; in the collection, analyses, or interpretation of data; in the writing of the manuscript, and in the decision to publish the results.

Abbreviations

3D	three dimensional
ABS	acrylonitrile butadiene styrene
API	active pharmaceutical ingredient
CIELAB	commission internationale de l’éclairage L*a*b*
BZ	benserazide hydrochlorid
EC	ethylcellulose
EVA	ethylene-vinyl acetate copolymer
FDM	fused deposition modeling
HME	hot melt extrusion
HPLC	high-performance liquid chromatography
IC	indigo carmine
LD	levodopa
P	pramipexole dihydrochloride monohydrate
PCL	polycaprolactone
PCL-PVAc-PEG	polyvinyl caprolactam-polyvinyl acetate-polyethylene glycol graft copolymer
PLA	polylactic acid
PoC	point of care
PVA	polyvinyl alcohol
PZQ	praziquantel
QC	quality control
RF	riboflavin
SMA	subminiature version A
T _g	glass transition temperature
TPU	thermoplastic polyurethane
VA	vinylpyrrolidone-vinyl acetate copolymer

References

1. Tutton, R. Personalizing medicine: Futures present and past. *Soc. Sci. Med.* **2012**, *75*, 1721–1728. [[CrossRef](#)] [[PubMed](#)]
2. Tappa, K.; Jammalamadaka, U. Novel biomaterials used in medical 3D printing techniques. *J. Funct. Biomater.* **2018**, *9*, 17. [[CrossRef](#)] [[PubMed](#)]
3. Tan, D.K.; Maniruzzaman, M.; Nokhodchi, A. Advanced pharmaceutical applications of hot-melt extrusion coupled with fused deposition modelling (FDM) 3D printing for personalised drug delivery. *Pharmaceutics* **2018**, *10*, 203. [[CrossRef](#)] [[PubMed](#)]

4. Melocchi, A.; Ubaldi, M.; Cerea, M.; Foppoli, A.; Maroni, A.; Moutaharrik, S.; Palugan, L.; Zema, L.; Gazzaniga, A. A graphical review on the escalation of fused deposition modeling (FDM) 3D printing in the pharmaceutical field. *J. Pharm. Sci.* **2020**, *109*, 2943–2957. [\[CrossRef\]](#) [\[PubMed\]](#)
5. Pravin, S.; Sudhir, A. Integration of 3D printing with dosage forms: A new perspective for modern healthcare. *Biomed. Pharmacother.* **2018**, *107*, 146–154. [\[CrossRef\]](#) [\[PubMed\]](#)
6. ISO 11664-4: 2008/CIE S 014-4: 2007; Colorimetry—Part 4: CIE 1976 L*a*b* uniform colour space. CIE Draft Standard: Vienna, Austria, 2007.
7. Lakio, S.; Heinämäki, J.; Yliruusi, J. Colorful Drying. *AAPS Pharm. Sci. Tech.* **2010**, *11*, 46–53. [\[CrossRef\]](#) [\[PubMed\]](#)
8. Chen, Q.; Zhang, C.; Zhao, J.; Ouyang, Q. Recent advances in emerging imaging techniques for non-destructive detection of food quality and safety. *Trends Anal. Chem.* **2013**, *52*, 261–274. [\[CrossRef\]](#)
9. Siddiqui, A.; Nazzal, S. Measurement of surface color as an expedient QC method for the detection of deviations in tablet hardness. *Int. J. Pharm.* **2007**, *341*, 173–180. [\[CrossRef\]](#)
10. Bogdanský, F.M. Measurement of surface color and color difference of tablet colorants by tristimulus colorimetry. *J. Pharm. Sci.* **1975**, *64*, 323–328. [\[CrossRef\]](#)
11. Berberich, J.; Dee, K.-H.; Hayauchi, Y.; Pörtner, C. A new method to determine discoloration kinetics of uncoated white tablets occurring during stability testing—An application of instrumental color measurement in the development pharmaceuticals. *Int. J. Pharm.* **2002**, *234*, 55–66. [\[CrossRef\]](#)
12. Gren, T.; Nyström, C. Characterization of surface coverage of coarse particles coated with stearic acid. *Int. J. Pharm.* **1991**, *74*, 49–58. [\[CrossRef\]](#)
13. Barimani, S.; Tomažević, D.; Meier, R.; Kleinebudde, P. 100% visual inspection of tablets produced with continuous direct compression and coating. *Int. J. Pharm.* **2022**, 121465. [\[CrossRef\]](#) [\[PubMed\]](#)
14. Wickström, H.; Nyman, J.O.; Indola, M.; Kronberg, L.; Preis, M.; Rantanen, J.; Sandler, N. Colorimetry as Quality Control Tool for Individual Inkjet-Printed Pediatric Formulations. *AAPS Pharm. Sci. Tech.* **2017**, *18*, 293–302. [\[CrossRef\]](#) [\[PubMed\]](#)
15. Frimpong, G.; Adotey, J.; Ofori-Kwakye, K.; Kipo, S.L.; Dwomo-Fokuo, Y. Potential of aqueous extract of *Hibiscus sabdariffa* calyces as coloring agent in three pediatric oral pharmaceutical formulations. *J. Appl. Pharm. Sci.* **2014**, *4*, 1–7. [\[CrossRef\]](#)
16. Kanekar, H.; Khale, A. Coloring Agents: Current Regulatory Perspective for Coloring Agents Intended for Pharmaceutical & Cosmetic Use. *Int. J. Pharm. Phytopharmacol. Res.* **2014**, *2*, 1–20.
17. Deshpande, A.A.; Shah, N.H.; Rhodes, C.T.; Malick, W. Development of a novel controlled-release system for gastric retention. *Pharm. Res.* **1997**, *14*, 815–819. [\[CrossRef\]](#) [\[PubMed\]](#)
18. Roggo, Y.; Jent, N.; Edmond, A.; Chalus, P.; Ulmschneider, M. Characterizing process effects on pharmaceutical solid forms using near-infrared spectroscopy and infrared imaging. *Eur. J. Pharm. Biopharm.* **2005**, *61*, 100–110. [\[CrossRef\]](#)
19. Quodbach, J.; Bogdahn, M.; Breitzkreutz, J.; Chamberlain, R.; Eggenreich, K.; Elia, A.G.; Gottschalk, N.; Gunkel-Grabole, G.; Hoffmann, L.; Kapote, D.; et al. Quality of FDM 3D Printed Medicines for Pediatrics: Considerations for Formulation Development, Filament Extrusion, Printing Process and Printer Design. *Ther. Innov. Regul. Sci.* **2021**. [\[CrossRef\]](#)
20. Chamberlain, R.; Windolf, H.; Geissler, S.; Quodbach, J.; Breitzkreutz, J. Precise Dosing of Pramipexole for Low-Dosed Filament Production by Hot Melt Extrusion Applying Various Feeding Methods. *Pharmaceutics* **2022**, *14*, 216. [\[CrossRef\]](#)
21. Schneider, C.; Langer, R.; Loveday, D.; Hair, D. Applications of ethylene vinyl acetate copolymers (EVA) in drug delivery systems. *J. Control Release* **2017**, *262*, 284–295. [\[CrossRef\]](#)
22. Basf. Kollidon VA 64, Technical Information. 2019. Available online: <https://pharma.basf.com/technicalinformation/30499398/kollidon-va-64> (accessed on 10 April 2022).
23. Chamberlain, R.; Windolf, H.; Burckhardt, B.B.; Breitzkreutz, J.; Fischer, B. Embedding a Sensitive Liquid-Core Waveguide UV Detector into an HPLC-UV System for Simultaneous Quantification of Differently Dosed Active Ingredients during Drug Release. *Pharmaceutics* **2022**, *14*, 639. [\[CrossRef\]](#) [\[PubMed\]](#)
24. European Pharmacopoeia Commission. 10.0/0292 Riboflavinum. In *European Pharmacopoeia*; European Pharmacopoeia Commission: Strasbourg, France, 2020; p. 5529.
25. Del Mar Pérez, M.; Ghinea, R.; Rivas, M.J.; Yebra, A.; Ionescu, A.M.; Paravina, R.D.; Herrera, L.J. Development of a customized whiteness index for dentistry based on CIELAB color space. *Dent. Mater.* **2016**, *32*, 461–467. [\[CrossRef\]](#) [\[PubMed\]](#)
26. Gill, H.S.; Prausnitz, M.R. Coating formulations for microneedles. *Pharm. Res.* **2007**, *24*, 1369–1380. [\[CrossRef\]](#) [\[PubMed\]](#)
27. Vidal, D.T.R.; Augelli, M.A.; Do Lago, C.L. Determination of sildenafil and vardenafil by capillary zone electrophoresis using capacitively coupled contactless conductivity detection. *Anal. Methods* **2013**, *5*, 2041–2045. [\[CrossRef\]](#)

4. Development and Characterization of Combination Drug Product

4.1 Dose-independent drug release from 3d printed oral medicines for patient-specific dosing to improve therapy safety

Evaluation of authorship

author	idea [%]	study design [%]	experimental [%]	evaluation [%]	manuscript [%]
Hellen Windolf	70	70	70	80	70
Rebecca Chamberlain	20	10	20	20	20
Julian Quodbach	10	20	10	0	10

Evaluation of Copyright permission:

0378-5173/© 2022 Elsevier B.V. All rights reserved.

Article available at: <https://doi.org/10.1016/j.ijpharm.2022.121555>.

Dose-independent drug release from 3d printed oral medicines for patient-specific dosing to improve therapy safety

Hellen Windolf, Rebecca Chamberlain, Julian Quodbach

*Institute of Pharmaceutics and Biopharmaceutics, Heinrich Heine University, Universitaetsstrasse 1, 40225
Duesseldorf, Germany*

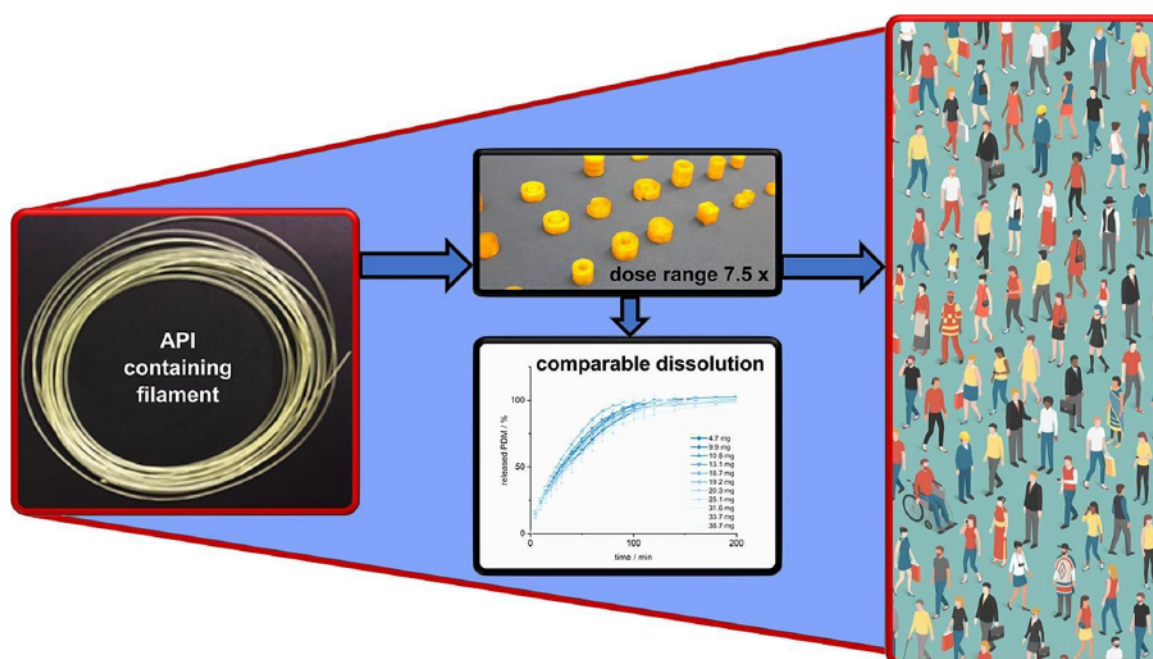
International Journal of Pharmaceutics

<https://doi.org/10.1016/j.ijpharm.2022.121555>

Abstract

Fused deposition modelling (FDM) 3D printing provides the ability to address individual patients' therapeutic needs without having to change the formulation every time. This is particularly interesting for dosing and release modelling. In this study, a geometry model was developed that can represent variable dosages while keeping the surface area to volume (SA/V) ratio alike, so the drug release profiles remain similar. The model was tested on three different formulations. Two BCS I active pharmaceutical ingredients (API), pramipexole and levodopa, and one BCS II API, praziquantel, were used. Polyvinyl alcohol (PVA, water soluble) and a combination of vinylpyrrolidone-vinyl acetate copolymer (PVP-VA, water soluble) and ethylene-vinyl acetate (EVA, water insoluble) were used as the polymer matrix. The curves were compared using the similarity factor (f_2 value) and mean dissolution time (MDT). Using a hollow cylinder-based (HCb) geometry model, a dose-independent drug release could be realized. For the PVA formulations, an 8-fold dose change could be obtained and for the EVA-PVP-VA formulation a factor of 5.5 could be achieved, with $f_2 > 50$. Due to the layer structure of the printed objects, very fine dose variation of 0.13 mg per layer is possible within these models. This allows variable dosing in small steps with only one basis formulation.

Graphical abstract



Introduction

Currently, there are over 7.92 billion people living on this planet and no one is alike. Each person does not only look different, but also the physiological processes in the body work individually for each person (Erdmann et al., 2021, Yu et al., 2021). If a person suffers from a certain disease, this process is just as individual as the adoption of treatment options. Precision medicine deals with the individual patient's requirements for their pharmacotherapy (Ashley, 2016, Balevic and Sagcal-Gironella, 2022, Bono et al., 2022, Hodson, 2016, MacEachern and Forkert, 2021, Oh et al., 2022). Metabolism, age, gender, and all existing diseases are considered for therapeutical treatment and therefore, individualized medicine displaces the common one-size-fits-all therapy (Collins and Varmus, 2015, Doble et al., 2016, Hamburg and Collins, 2010, McCarthy and Birney, 2021, Wening and Breitzkreutz, 2011). Since the focus of precision medicine lays on the individual patient, personalized medicine often cannot rely solely on market preparations produced in large quantities by industry, since only defined dosages, tablet shapes and drug release profiles are produced in high amounts. A dosage customized for an individual patient can be used to ensure that the minimum dose level is achieved for necessary efficacy, but does not exceed the toxic plasma level limit, thus reducing side effects and hazards of drug therapy. Additionally, this could result in an increase of patient medication adherence and thus the success of the therapy is guaranteed. To meet patients' individual requirements for drug therapy, 3D printing is currently being researched intensively, since this process allows small batches to be produced cheaply on demand (Aquino et al., 2018, Attaran, 2017, Bhuskute et al., 2022, Goyanes et al., 2017a, Goyanes et al., 2014, Norman et al., 2017, Quodbach et al., 2021, Rahman and Quodbach, 2021, Than and Titapiwatanakun, 2021, Zamboulis et al., 2022, Zhang et al., 2018). Possible manufacturing places could be local community pharmacies, compounding centres or hospital pharmacies. A wide variety of 3D printing techniques are currently being evaluated producing patient-specific therapies (Aquino et al., 2018, Attaran, 2017, Bhuskute et al., 2022, el Aita et al., 2020, Fina et al., 2017, Infanger et al., 2019, Kyobula et al., 2017, Norman et al., 2017, Zamboulis et al., 2022, Zhang et al., 2018). Fused deposition modelling (FDM) 3D printing is used to produce small individual batches. The shape, dose, and color of the produced medicine, as well as the dissolution time of the active pharmaceutical ingredient (API) can be specifically adjusted (Cailleaux et al., 2021, Gottschalk et al., 2021, Goyanes et al., 2017a, Kempin et al., 2017, Melocchi et al., 2016, Sadia et al., 2018, Windolf et al., 2021). A

disadvantage of the FDM process is the high thermal stress for the excipients (Kollamaram et al., 2018). For FDM 3D printing, which is also known as fused filament fabrication, a filament must first be produced via hot-melt extrusion (HME). In this process, a powder mixture is prepared beforehand, the polymers melted or softened, kneaded, conveyed through a nozzle, cooled and hauled-off to generate a homogeneous filament (Chamberlain et al., 2022, Korte, 2018, Ponsar et al., 2020). Afterwards, this intermediate is re-melted in the print head of the 3D printer, whereby the mass can be transported through the nozzle of usually 0.4 mm diameter and printed into the desired geometry. To withstand these processes without degradation, the API used must be heat resistant, or polymers with a low glass transition temperature, low melting point or low processing temperature must be used. If neither the API nor the polymers show degradation, it is possible to realize individual 3D printed geometries in patient-attractive forms, which vary in dosage and drug release time (Ayyoubi et al., 2021, Goyanes et al., 2017b, Sandler and Preis, 2016, Scoutaris et al., 2018). With the help of semi-solid 3D printing, el Aita et al. were able to adjust the dose over individual layers (el Aita et al., 2020). In another approach, the dose was changed by increasing the size of the FDM 3D printed tablet (Pietrzak et al., 2015, Skowrya et al., 2015). Korte et al. changed the dose of a FDM printed oral dosage form by changing the percentage of infill (Korte and Quodbach, 2018). The infill of a 3D printed tablet can be varied in patterns (e.g., honeycomb, grid), and percentage (0% = hollow, 100% = completely solid), and thus influence the dose, porosity, and printing time of a geometry. However, these dose adjustments lead to different surface area to volume (SA/V) ratio, which in turn affects the drug release (Barber et al., 2021, Goyanes et al., 2015, Reynolds et al., 2002, Sadia et al., 2018, Windolf et al., 2021, Zhang et al., 2021). The variable API release times result in different dosing intervals, which make these approaches unsuitable, for example for clinical application. Significant time constraints are already an issue in patient care and individual dosing intervals would interfere with the tight work schedule of care takers. They would require improvisations by clinical staff for each patient and very likely result in reduced therapeutic safety. Patients might receive a new dose at the wrong time, which could affect the blood plasma level of the API and put the patient at risk (Holford and Sheiner, 2012, Pelham et al., 2014, Tsiga et al., 2013). Of course, the same geometry can also be printed with different dose-loaded filaments to keep the dissolution profile similar. However, a specially produced filament must then be available for each batch.

To act economically and ecologically, it is desirable to print different geometries from one filament to generate medicine with various dosages. Gorkem Buyukgoz et al. tested five different approaches to achieve dose-independent release. They enlarged the tablet with increasing dose, used filaments with different API content but the same 3D geometry, and added placebo layers to the tablet to keep the SA/V ratio the same. In their study, dose-independent release was achieved by objects printed from filaments containing diverse content of API and from combinations of API-loaded and API-free filaments (Gorkem Buyukgoz et al., 2020). Yu et al. investigated in 2009 donut-shaped multi-layered drug delivery devices and found that it is possible to maintain the drug release profile also by varying the printed form (Yu et al., 2009).

This approach was used by our research group to determine which geometries could represent the widest possible dose range, which could be assumed to have the same release curve. The goal of this study was to enable dose changes in smallest steps to ensure patient-specific therapy. This should be realized with a single formulation to provide care to a wide range of patients with as little effort as possible. A so-called hollow cylinder-based (HCb)-Geometry Model was designed, in which the SA/V ratio remains almost unchanged, despite different sizes and volumes of the geometries. The models allow a margin for volume changes, resulting in maximum dose changes that should not affect the release behaviour of the drug. This model was tested for three different formulations with APIs of BCS classes I and II, and a water-soluble and water-insoluble polymer.

Section snippets

Materials

For the development of the dose-independent model, various formulations were used (Table 1). These were systematically developed for a robust extrusion process, high filament homogeneity and best printability (Windolf et al., 2021).

As HME and FDM 3D printing are heat intensive processes, the APIs were chosen, among other criteria, regarding thermal stability. The melting and decomposition point of pramipexole 2 HCl*H₂O (PDM) is 296–305 °C (Gültekin et al., 2019, Łaszcz et al., 2010, Panditrao...

Evaluation of printing precision based on tablet dimensions

The printed geometries correspond in their dimensions to the desired sizes with a deviation of ± 0.05 mm on average. The weight of the geometries within the printed batches is subject to minor variations, which is reflected in the low deviations in the content of the tablets. When designing the geometry with CAD, it was possible to calculate the volume and thus determine the desired dose of the geometry using the density of the formulation. The geometries were printed in a batch size of $n \geq 6$...

Conclusion

In these experiments, a model was developed that allows dose variations of an oral dosage form but does not affect the release profile of the API. With the HCb-Geometry Model and the combination of BCS I API and water-soluble polymer, it was possible to vary the dose 8-fold without changing the dissolution curves ($f_2 > 50$). If the water-soluble polymer is combined with a BCS II API, a 7.5-fold dose variation is possible. Due to the lower solubility of the API, the tolerance in pore and SA/V...

Declaration of Competing Interest

The authors declare that they have no known competing financial interests or personal relationships that could have appeared to influence the work reported in this paper...

Acknowledgement

The author wants to thank TER Chemicals for providing various EVA samples and Merck for supplying a large quantity of PVA. Further, the author would like to thank Andrea Michel for conducting the DSC measurements and Dr. Guido Kreiner and Daniel Komisarek for the XRD measurements. In addition, Sebastian Bollmann is acknowledged for his support during the μ CT measurements. This work is associated and funded by the Bundesministerium für Bildung und Forschung - Projekt 'ProMat Leben-Polymere'...

Funding

This work was funded by the Bundesministerium für Bildung und Forschung - Projekt 'ProMat Leben-Polymere' 'PolyPrint' (Project no.: 13XP5064B)...

4.2 Embedding a Sensitive Liquid-Core Waveguide UV Detector into an HPLC-UV System for Simultaneous Quantification of Differently Dosed APIs during Drug Release

Evaluation of authorship

author	idea [%]	study design [%]	experimental [%]	evaluation [%]	manuscript [%]
Rebecca Chamberlain	60	60	60	45	45
Hellen Windolf	30	40	40	35	35
Björn B. Burckhardt	-	-	-	5	5
Jörg Breitzkreutz	-	-	-	5	5
Björn Fischer	10	-	-	10	10

Evaluation of Copyright permission:

The research paper was published under a Creative Commons license (Open Access) and is free to share and adapt (MDPI | Open Access Information; accessed on 20.05.2023).

Embedding a Sensitive Liquid-Core Waveguide UV Detector into an HPLC-UV System for Simultaneous Quantification of Differently Dosed APIs during Drug Release

Rebecca Chamberlain¹, Hellen Windolf¹, Björn B. Burckhardt², Jörg Breitzkreutz¹, Björn Fischer¹

¹Institute of Pharmaceutics and Biopharmaceutics, Heinrich Heine University, Universitätsstrasse 1, 40225 Duesseldorf, Germany



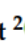
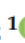
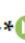
² Institute of Clinical Pharmacy and Pharmacotherapy, Heinrich Heine University, Universitätsstrasse 1, 40225 Düsseldorf, Germany

Pharmaceutics

<https://doi.org/10.3390/pharmaceutics14030639>

Article

Embedding a Sensitive Liquid-Core Waveguide UV Detector into an HPLC-UV System for Simultaneous Quantification of Differently Dosed Active Ingredients during Drug Release

Rebecca Chamberlain ¹, Hellen Windolf ¹, Bjoern B. Burckhardt ², Jörg Breitzkreutz ¹ and Björn Fischer ^{1,*}

¹ Institute of Pharmaceutics and Biopharmaceutics, Heinrich Heine University, Universitätsstraße 1, 40225 Düsseldorf, Germany; rebecca.chamberlain@hhu.de (R.C.); hellen.windolf@hhu.de (H.W.); joerg.breitzkreutz@hhu.de (J.B.)

² Institute of Clinical Pharmacy and Pharmacotherapy, Heinrich Heine University, Universitätsstraße 1, 40225 Düsseldorf, Germany; bjoern.burckhardt@hhu.de

* Correspondence: bjoern.fischer@hhu.de; Tel.: +49-211-81-10076

Abstract: Individual dosing of pharmaceuticals and personalized medicine have become important with regard to therapeutic safety. Dose adjustments, biorelevant drug release and combination of multiple active substances in one dosage form for the reduction in polymedication are essential aspects that increase the safety and acceptance of the patient's pharmacotherapy. Therefore, not only innovative drug products but also new analytical methods are needed during the drug development phase and for quality control that can simultaneously determine different active ingredients and cover wide concentration ranges. We investigated a liquid-core waveguide UV absorbance flow cell detector coupled to an existing HPLC-UV system. A Teflon AF 2400 capillary tubing of 20 cm length was connected in series to the HPLC flow line and enabled a lower limit of quantification of 1 ng/mL pramipexole (increase in sensitivity by 20 compared to common 0.9 cm flow cells). This allowed the low-concentration of pramipexole and the higher concentrations of levodopa and benserazide occurring during drug release to be determined in a single chromatographic run within 22.5 min.

Keywords: liquid-core waveguide; hot melt extrusion; low-dosed dosage forms; analytics of extruded filaments; fused filament 3D printing; oral dosage form; personalized medicine



Citation: Chamberlain, R.; Windolf, H.; Burckhardt, B.B.; Breitzkreutz, J.; Fischer, B. Embedding a Sensitive Liquid-Core Waveguide UV Detector into an HPLC-UV System for Simultaneous Quantification of Differently Dosed Active Ingredients during Drug Release. *Pharmaceutics* **2022**, *14*, 639. <https://doi.org/10.3390/pharmaceutics14030639>

Academic Editor: Igor Tsesis

Received: 15 February 2022

Accepted: 11 March 2022

Published: 14 March 2022

Publisher's Note: MDPI stays neutral with regard to jurisdictional claims in published maps and institutional affiliations.



Copyright: © 2022 by the authors. Licensee MDPI, Basel, Switzerland. This article is an open access article distributed under the terms and conditions of the Creative Commons Attribution (CC BY) license (<https://creativecommons.org/licenses/by/4.0/>).

1. Introduction

Current therapy guidelines for the treatment of non-communicable diseases (e.g., ESC guideline on hypertension) have recently changed their recommendations based on the latest scientific data towards a dual combination at the initiation of therapy [1]. A rational extension of this approach is to offer such dual or multiple combinations directly in one dosage form to increase patient adherence by reducing the number of drug products to be taken [2]. According to the FDA, a combination product is defined as a dosage form containing two or more drugs in a single pill [3]. Not only is the combination of drugs of interest, but personalized medicine also focuses on individual dosing for each patient in terms of age, weight and comorbidities. The “one-size-fits-all” approach of APIs that have a narrow therapeutic window and therefore risk side effects with small differences in dosage is in the process of being replaced by new approaches, e.g., 3D printing of medicines [4]. With 3D printing it is possible to fabricate complex geometries that incorporate multiple APIs with diverse release kinetics [5–8]. This potentially allows various active ingredients to be combined in a single 3D printed tablet. In previous studies, we found that even if the dose is varied, the release profile remains the same if the surface area to volume ratio is kept constant [9]. In analyzing release kinetics of all incorporated APIs especially during the development phase, analytical methods that can quantify all incorporated APIs simultaneously are useful. To ensure the detection of

a low concentration of a high-potent drug during drug release from its dosage form, a sensitive analytical method must be selected, the dissolution apparatus can be adjusted, or the volume of the medium in the dissolution vessel can be reduced [10–14]. Wang et al. found that dissolution studies conducted in mini vessel led to the same results as in a vessel prescribed by European Pharmacopeia, but the paddle speed had to be increased [15]. Mini paddle apparatus is recommended by Klein et al. to be used for powders, multiparticulate dosage forms and small tablets or capsules [16]. However, it is important that the dissolution study proceeds under sink conditions to avoid influencing the drug release behavior of the corresponding API, which would no longer be the case with high-concentrated APIs in a combination product [17]. The combination of high-performance liquid chromatography UV detection with mass spectrometry (MS) detection and high dynamic range diode array detection (high dynamic range DAD) is capable of covering a wide concentration range [18,19]. For a cost-effective and easy-to-integrate detection system, liquid-core waveguide detection systems are used and described in literature by several research groups. Li et al. have developed a portable setup with extended light path that can be used to detect very low concentrations [20]. A modified detection system compared to the detection system used in this work with a charged-coupled device including optical fibers and a liquid-core waveguide was utilized by Kottke et al. to detect low concentrations of desmopressin during permeation studies. However, they used fluorescence measurements to be able to detect 9.5 ng/mL of desmopressin, a method that was tenfold more sensitive in comparison with reference HPLC detection systems [21]. In this study, drug preparations of three different APIs were analyzed with substantially different dosage ranges. Levodopa (LD), the precursor to the neurotransmitter dopamine, is used in the clinical treatment of Parkinson's disease in a single dose with oral administration of 25–200 mg [22]. The decarboxylase inhibitor benserazide (BZ) is routinely administered orally in combination with levodopa in a ratio of 1:4 (BZ/LD) to prevent peripheral degradation of levodopa [23]. This results in a dosage range between 12.5 and 50 mg for benserazide. The dopamine agonist, pramipexole, is administered at a lower drug amount. Here, only 0.088–3.15° mg is required for pharmacologically efficient drug concentrations after oral administration [24]. The combination of these three APIs should reduce the number of tablets for Parkinson's patients and guarantee individualized dosing. The fluorescence detection cannot be applied as pramipexole does not show fluorescence in aqueous medium, which leads to an exclusion of the detector selection option. Consequently, UV measurement of pramipexole was favored, and the suitability of detection by a liquid-core waveguide ultraviolet absorbance detection system (LCW-UV) was investigated, which is frequently used in literature [25–32]. The extended detection path of the LCW should result in the detection range of UV measurement being extended into the low concentration range (minimum of 1 ng/mL pramipexole) while at the same time also allowing APIs to be detected in the higher concentration range (maximum of 2 µg/mL levodopa) by the UV detector of the HPLC covering a difference in concentration by a factor of 2000.

2. Materials and Methods

2.1. Experimental Procedure of Hot Melt Extrusion Runs

Poly-(ethylene-vinyl acetate)-copolymer (82:18) (EVA; Escorene® FL01418, TER Chemicals, Hamburg, Germany) and polyvinyl alcohol (PVA; Parteck MXP®, Merck, Darmstadt, Germany) were used as polymer matrices. Pramipexole (P, Chr. Olesen, Denmark), levodopa (Zhejiang Wild Wind Pharmaceutical, Dongyang, China) and benserazide (s.p. quimica, s.a., Barcelona, Spain) were used as model drugs. PVA was chosen as a matrix for pramipexole, and EVA was used for the matrix of the fixed combination of levodopa and benserazide within one filament. Poly-(vinylpyrrolidone-vinyl acetate)-copolymer (60:40) (VA; Kollidon VA 64®, BASF, Ludwigshafen, Germany) was incorporated into formulation 2 to act as a pore-forming agent. The composition of the two formulations is listed in Table 1.

Table 1. Composition of filaments.

APIs and Excipients	Concentration in % (w/w)	Function
Formulation 1 (PVA-P): Pramipexole 2 HCl·H ₂ O (P) Polyvinyl alcohol (PVA)	0.5 99.5	API matrix
Formulation 2 (EVA-LD-BZ): Levodopa (LD) Benserazide HCl (BZ) Poly (ethylene-vinyl acetate)-copolymer (82:18) (EVA) Poly (vinylpyrrolidone-vinyl acetate)-copolymer (60:40) (VA)	40 10 35 15	API API matrix pore former

All filaments were prepared by hot melt extrusion (HME) with a co-rotating twin-screw extruder with a hot-melt extrusion die (Pharmalab HME 16, Thermo Fisher Scientific, Rockford, IL, USA). A gravimetric feeder (K-SFS-24/6, Coperion K-Tron, Niederlenz, Switzerland) was used for all experiments. A vent port was set between kneading zones 1 and 2 for all extrusions. An in-house manufactured die with a diameter of 1.85 mm was used. The desired filament diameter was achieved using a belt hauled-off unit of a winder (Brabender, Duisburg, Germany) with a belt speed of 0.8 m/min, and the filament was pulled through a roll-system with four 360° air flow ring nozzles (Super Air Wipe, Exair, Cincinnati, OH, USA) for active cooling of the melt. With a laser-based diameter measurement module (Laser 2025 T, Sikora, Bremen, Germany), we continuously measured and logged the filament diameter during the process with a readout rate of 1 Hz to ensure diameter homogeneity [33] of PVA-P and EVA-LD-BZ filaments. The screw speed was set to 20 rpm and powder feed rate was set to 2 g/min. The screw configuration and the temperatures of the heating zones were set according to the physical properties of the polymers for both formulations and are summarized in Table 2.

Table 2. Adjusted temperatures and screw configuration of performed extrusions.

Temperature Profile in Zones 2–10/°C									
Zone	2	3	4	5	6	7	8	9	10
PVA-P formulation	30	100	180	180	180	180	180	195	195
EVA-LD-BZ formulation	30	180	190	200	220	220	220	220	220
Screw Configuration (Die–Gear)									
PVA-P/ EVA-LD-BZ formulation	die–10 CE 1 L/D–KZ 1: 5 × 60°–3 × 30°–5 CE 1 L/D–KZ 2: 4 × 90°–5 × 60°–3 × 30°–16 CE 1 L/D–2 CE 3/2 L/D–1 L/D adapter–gear								

CE = conveying element, KZ = kneading zone.

2.2. Dissolution Testing

According to European Pharmacopoeia monographs 2.9.3 and 5.17.1, release studies were performed with the basket method (method 1) in a dissolution tester (DT 700, Erweka, Langen, Germany) [13,34]. The baskets were 3D printed from water insoluble polylactide acid. They had to be adapted for extruded filaments, since the mesh size of the regular Ph. Eur. baskets is small, and the baskets were clogged by the swollen polymer of the PVA formulation [35]. This affected the hydrodynamic medium flow around the filament. Vessels contained 1000 mL of degassed 0.1 N hydrochloric acid at pH 1.2 at a temperature of 37 ± 0.5 °C, and the baskets were stirred at 50 rpm. Dissolution tests were performed under sink conditions of pramipexole ($c_s = 200$ mg/mL [36]; maximum concentration 0.1 µg/mL). For the comparison of released pramipexole from PVA matrix by MS vs. LCW–UV detection, 5 mL samples were taken from the dissolution medium after 5, 10, 15, 30, 45, 60, 90 and 120 min by a syringe. One 2.5 mL aliquot was used to fill HPLC vials for UV measurement, and another 2.5 mL was poured into a 96-well plate for mass spectrometric

analysis and mixed with 50 μL of internal standard (Figure 1, left side). No replenishment was conducted, but the amount of removed liquid volume by sampling was calculated for the corresponding subsequent sampling time point. The same dissolution testing setup was used for the simultaneous analysis of the PVA-P filament and EVA-LD-BZ filament, but samples were obtained by an autosampler (Vision[®] AutoFill[™] + AutoPlus[™], Teledyne Hanson Research, Chatsworth, CA, USA). The content of P, LD and BZ was analyzed by UV and LCW-UV detection (Figure 1, right side). To avoid oxidation processes of BZ, the whole dissolution tester was wrapped in aluminum foil for light protection, whenever filaments were released containing BZ [37].

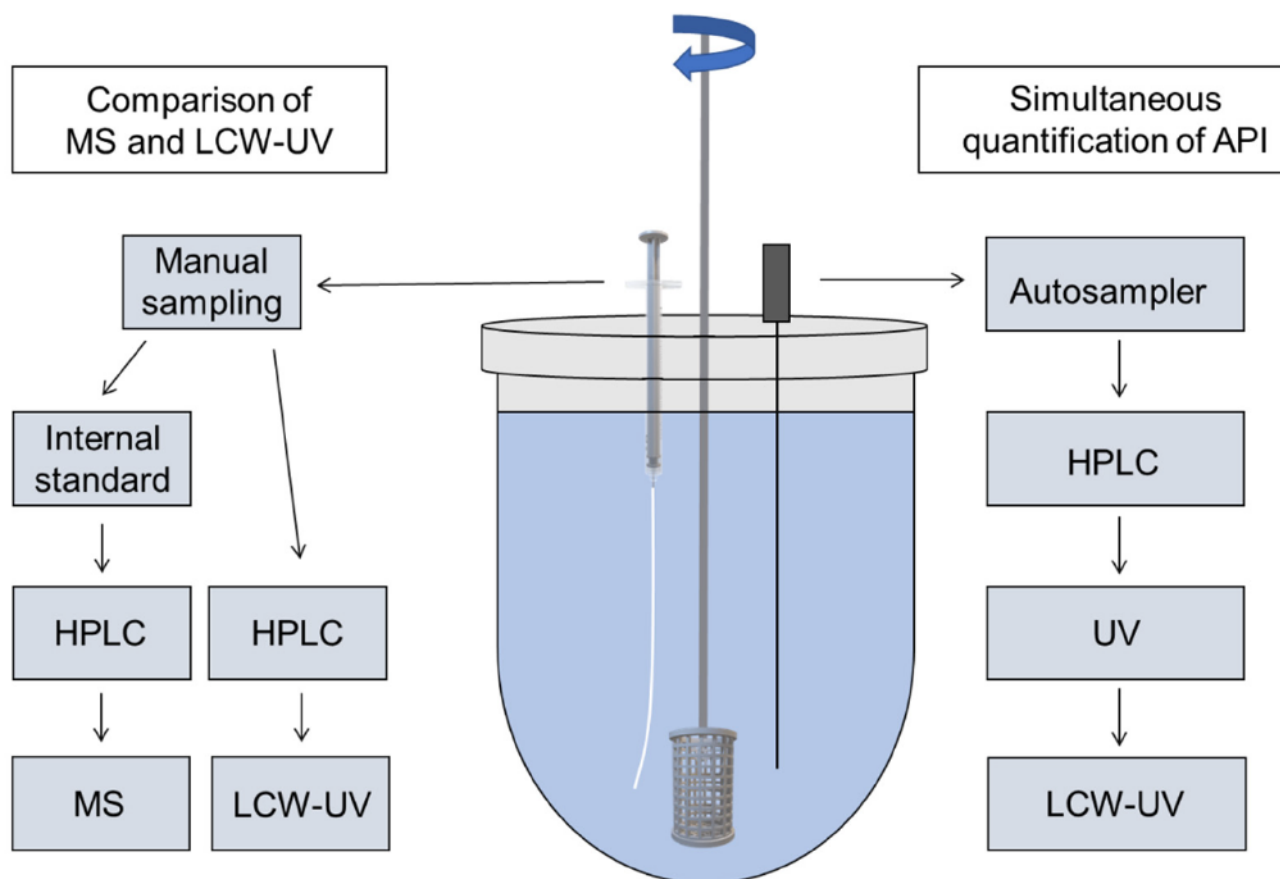


Figure 1. Modified dissolution testing with 3D printed basket based on Ph. Eur. monographs 2.9.3 and 5.17.1 with manual sampling (left side) for MS and LCW measurement of single pramipexole filaments and automatic sampling (right side) for the simultaneous content determination of three APIs (pramipexole, benserazide and levodopa) during dissolution by HPLC-UV and LCW-UV.

The dissolution tests were also performed under sink conditions of levodopa ($c_s = 12 \text{ mg/mL}$ [38]; maximum concentration 0.1 mg/mL) and benserazide ($c_s = 33.5 \text{ mg/mL}$; maximum concentration 0.025 mg/mL). Samples (1.5 mL) were taken by the autosampler and were filled in HPLC vials every 5 min for the first 30 min , then every 10 min for the next 30 min , followed by sampling at time point 90 and 120 min . After a release time of 120 min , samples were taken every 120 min until 10 h had passed. At every time point, 1.5 mL of 0.1 N hydrochloric acid was returned to the dissolution medium, and the amount of API removed by sampling was calculated for the corresponding subsequent sampling time point.

2.3. LC-MS/MS Quantification of Pramipexole during Dissolution

The mass spectrometric quantification of pramipexole was carried out on an Agilent 1200 Serie HPLC system (Agilent, Ratingen, Germany) coupled to a triple-quadrupole

tandem mass spectrometer API 4000 (SCIEX, Vaughan, ON, Canada) with an electrospray ionization (ESI) interface. Samples were injected by a CTC HTC PAL autosampler (CTC Analytics AG, Zwingen, Switzerland) equipped with a 20 μ L sample loop. Chromatographic separation was achieved on a Phenomenex Synergi Hydro RP (150.0 \times 2.0 mm; 4 μ m) column using isocratic condition with acetonitrile and 10 mM ammonium acetate in water as mobile phase (70/30 (v/v)). The compound specific parameters were as follows: declustering potential of 66 V/81 V, entrance potential of 8 V, cell entrance potential of 21 V/19 V and cell exit potential of 30 V/6 V. CAD gas was set to 7 psi, while gas 1 and gas 2 were adjusted to 32 and 45 psi, respectively. Curtain gas was 37 psi. Ion spray voltage was set to 5.5 kV with 600 $^{\circ}$ C ion source temperature. Time between injections was 2 min with retention times of 0.95 min for pramipexole and 1.1 min for talipexole. The mass-to-charge ratio of 212.2 to 153.1 m/z for pramipexole and 304.1 to 260.0 m/z for the internal standard talipexole was monitored utilizing multiple reaction monitoring and positive ionization mode. The method was characterized by a linear range from 0.19 to 100 ng/mL ($1/x^2$ weighing). The intra-run accuracy varied from -4.5 to 13.2% ($n = 3$ per quality control level). The collected data were analyzed using Analyst 1.6.2 (Applied Biosystems/MDS SCIEX, Concord, ON, Canada) with IntelliQuan[®] as the integration algorithm without smoothing.

2.4. Chromatographic Conditions for UV and LCW-UV Measurements

For dissolution analysis, dissolution medium of pramipexole filaments was analyzed by UV measurements. The HPLC system (Dionex, Sunnyvale, CA, USA) was equipped with a quaternary pump (P 580 A, Dionex, Sunnyvale, CA, USA) and an autosampler (ASI-100, Dionex, Sunnyvale, CA, USA). For the first HPLC method (method 1) analyzing only pramipexole, a 150 \times 4.6 mm column (Eurospher II 100-5 C18A, Knauer, Berlin, Germany) with an integrated precolumn was used. The mobile phase consisted of methanol (mobile phase B) and ammonium acetate buffer (0.05 M, pH 4). The flow rate was set to 1 mL/min, the oven temperature was set to 40 $^{\circ}$ C and the injection volume was 200 μ L. The gradient was as follows: mobile phase B was increased from 5 to 95% (v/v) within the first 10 min, held for 5 min at 95% (v/v) and decreased to 5% (v/v) again until 20 min after the sample injection. The column was equilibrated for 3 min before the next sample was injected. Detection was achieved by measuring the UV absorbance of the sample at 264 nm. This UV detector is described as the reference UV detector (UV). Since the release of 88 μ g pramipexole from a drug preparation is described (1% of released drug is 0.88 ng/mL), and thus the calibration curve must be extended, a liquid-core waveguide ultraviolet detection system (LCW-UV) was incorporated into the HPLC flow, which is described in Section 2.5. For the second HPLC method (method 2) encompassing all three APIs, a 250 \times 4.6 mm column (Eurospher II 100-5 C18A, Knauer, Berlin, Germany) with an integrated precolumn was utilized (Figure 2). The same mobile phase, flow rate and column temperature were used. The gradient was as follows: Mobile phase B was increased from 1 to 5% (v/v), within the first min, held at 5% (v/v) for 4 min, increased from 5 to 10% (v/v) within 1 min, held at 10% (v/v) for 4 min, increased again from 10 to 20% (v/v) within 1 min, held for 4 min at 20% (v/v), increased again from 20 to 99% (v/v) within 5 min, held for 2 min at 99% (v/v) and decreased to 1% (v/v) within 0.5 min and again until 22.5 min after sample injection. An equilibration time of 3.5 min per run was allowed to pass before the next sample was injected. An injection volume of 200 μ L was chosen to analyze the APIs during drug dissolution. Again, the second detector system (Section 2.5) was incorporated into the HPLC flow for the quantification of low pramipexole concentrations. Detection was achieved by measuring the absorbance of the sample at 264 nm using the UV detector (BZ, LD) and the LCW-UV detector (P) (Figure 2).

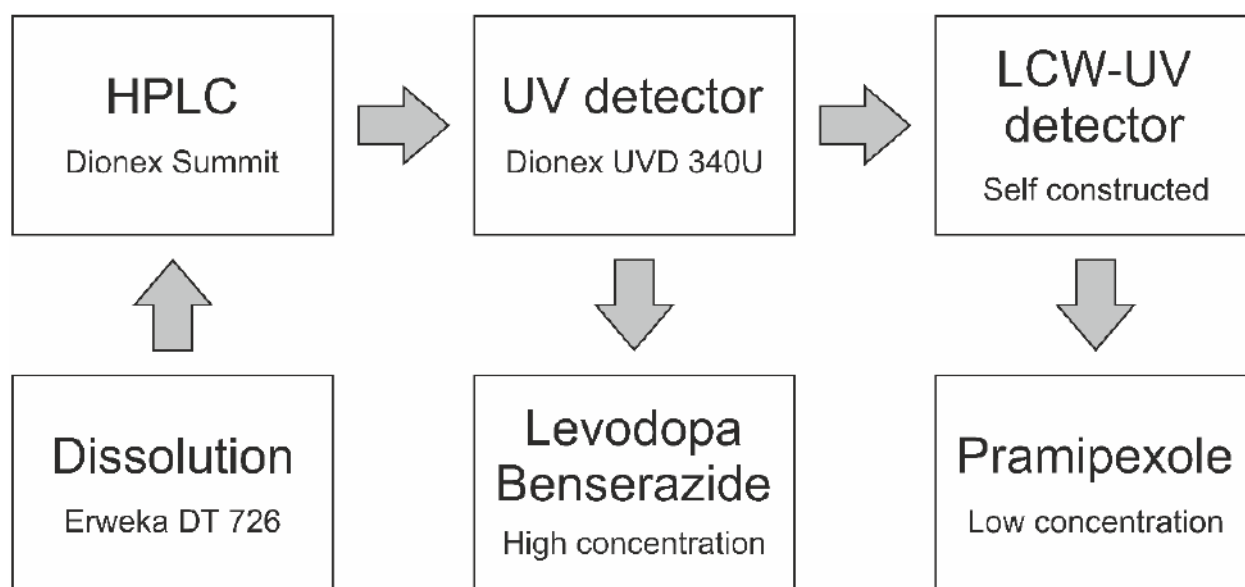


Figure 2. Inline coupling of a UV detector and LCW-UV detector for the simultaneous analysis of pramipexole, levodopa and benserazide.

2.5. Liquid-Core Waveguide Ultraviolet Detection System (LCW-UV)

Figure 3 shows the schematic composition of the LCW-UV detection system. Two stainless steel tees (U-428, 508 μm through hole, IDEX Health & Science, Oak Harbor, WA, USA) were applied to pass the eluent from the HPLC through a 20 cm liquid-core waveguide (LCW, Teflon AF 2400, RI = 1.29, $d_{\text{inner}} = 200 \mu\text{m}$, $d_{\text{outer}} = 813 \mu\text{m}$, Biogeneral, CA, USA). A UV-LED (LED33UV270-6060-100, LG Innotek, Seoul, Korea) was chosen as the light source providing a measured emission maximum at 275 nm. The light was guided into tee 1 at the pigtail end of an optical fiber ($d_{\text{inner}} = 600 \mu\text{m}$, FDP600660710, Laser Components GmbH, Olching, Germany). To avoid breakage of the fiber, the cladding of the fiber was not removed and the front side was optically polished together with the cladding. At the same time, the polymer cladding ensured sufficient tightness of the flow cell. Fluoropolymer sleeves (NanoTight Sleeve Green, $d_{\text{inner}} = 838 \mu\text{m}$, $d_{\text{outer}} = 1588 \mu\text{m}$, IDEX Health & Science, Oak Harbor, WA, USA) were used to match the dimensions between the LCW, the optical fibers and the tees.

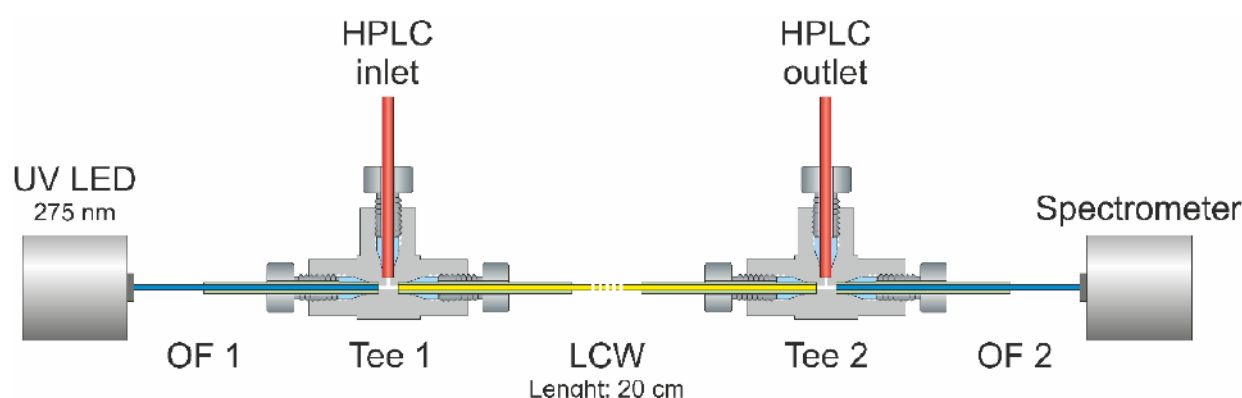


Figure 3. Assembly of the implemented liquid-core waveguide ultraviolet detection system consisting of a UV LED (absorption maximum: 275 nm), two optical fibers (OFs 1 and 2), a 20 cm liquid-core waveguide (LCW), two tee pieces and a charge-coupled device detector.

For detection, the light was collected by a second optical fiber connected to tee 2 and guided into a spectrometer (Kymera 328i B2 equipped with Newport diffraction grating).

600 L/mm, blaze 300 nm, Oxford Instruments, Abingdon, UK), assembled with a charge-coupled device detector (CCD, iDus DV420A BU2, Oxford Instruments, Abingdon, UK). For spectra acquisition, the exposure time was set to 0.03 s, and the number of accumulations for each spectrum was set to 16, resulting in an acquisition rate of 2.08 Hz. The readout mode was adjusted to full vertical binning, the vertical pixel shift was 16.25 μ s and the readout rate was 100 kHz.

2.6. Mathematical Description

The definition of absorbance is:

$$A = \log\left(\frac{I_0}{I}\right) = \varepsilon \times b \times c \quad (1)$$

A is the absorbance, I_0 is the incident intensity, I transmitted intensity, ε is the molar absorptivity, b is the path length and c is the molar concentration [39]. By increasing the light path b using a liquid-core waveguide, the absorbance A of pramipexole was increased, which was particularly important to be able to detect the low concentrations during dissolution testing.

Thus, in the first step, the LCW-UV setup was compared with an established method (mass spectrometry) for drug release of low-dosed filaments. To evaluate the similarity of the release curves measured by two different analytical methods, the mean dissolution time (MDT) and the similarity factor (f_2 -value) were calculated [40,41].

$$\text{MDT} = \frac{ABC}{c_\infty} = \frac{\sum_{i=0}^{\infty} \left[(c_{i+1} - c_i) \times \frac{t_i + t_{i+1}}{2} \right]}{c_\infty} \quad (2)$$

ABC stands for the area between the curves and is calculated via the trapezoidal equation with c as the concentration of the API released over time t and c_∞ as the initial drug load of the filament.

$$f_2 = 50 \times \log \left\{ \left[1 + \frac{1}{n} \sum_{t=1}^n (R_t - T_t)^2 \right] \times 100 \right\} \quad (3)$$

In this equation, R_t and T_t stand for the mean released amounts of the API in % at time point t of the reference (MS result) and the test method (LCW-UV result) and n for the number of time points. A f_2 -value around 100 is desired, which indicates that the curves are identical. A value of 50 or more is accepted, which indicates that the values differ by a maximum of 10%. Values below 50 indicate that the curves can no longer be considered similar [34].

3. Results and Discussion

3.1. Spectroscopic Evaluation of LCW-UV Measurements

A small range of the rising slope of the UV LED was used for the absorbance measurement. The grating of the spectrometer was adjusted so that the CCD detector was in saturation from 268.5 nm upwards. The evaluation was performed between 262 and 268 nm. With these settings, the lowest LLOQ could be achieved. The raw spectrum of the blank (pure mobile phase) is displayed in Figure 4, where the detector depicts the highest signal, since the eluent shows hardly any absorbance at the evaluated wavelength range. As the concentration of pramipexole increases, the signal intensity decreases because the API is absorbing light originating from the UV-LED. The corresponding signals in the peak maximum of a concentration series of 5–100 ng are also shown Figure 4. To obtain a chromatogram from raw data of the measured intensity, spectra were integrated between 262 and 268 nm and evaluated with respect to the measurement time. The obtained peaks of pramipexole can be identified in the chromatogram obtained by LCW-UV measurement after 8.9 (method 1) and 19.3 min (method 2). These settings were consequently used for

spectroscopic evaluation of LCW-UV detection systems for calibration curves and for the quantification of pramipexole during drug release.

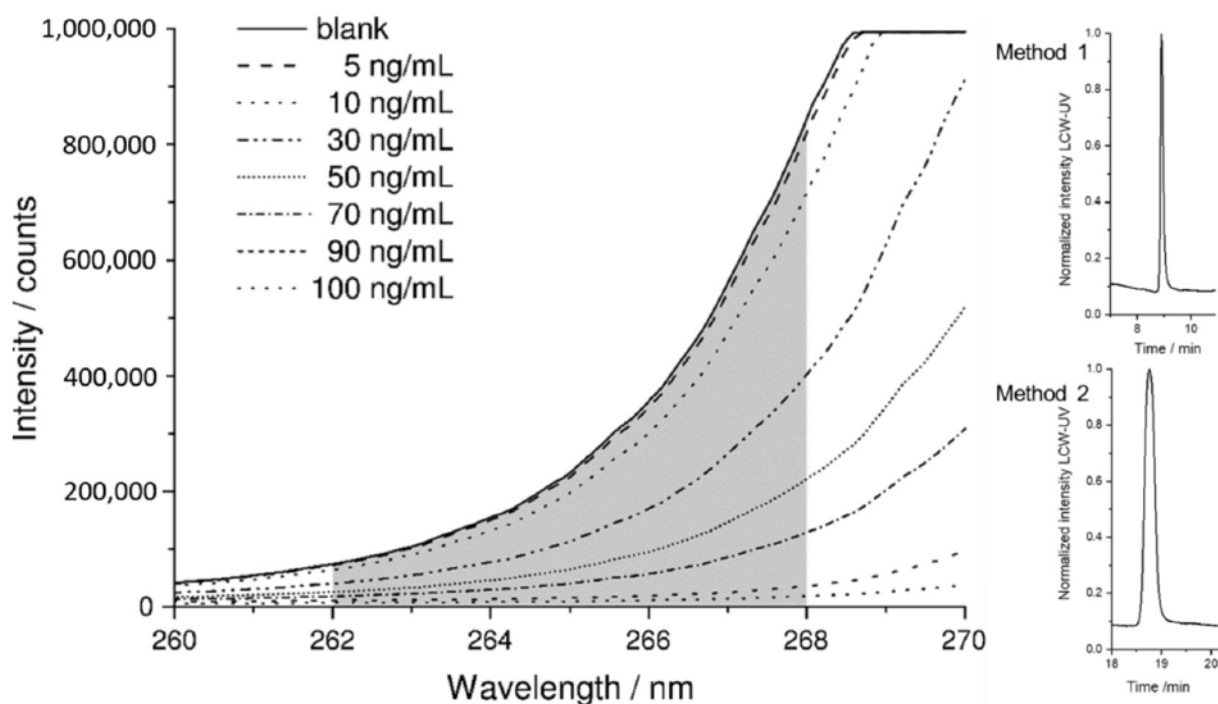


Figure 4. Measured intensity of a blank sample and of the peaks of various concentrations of pramipexole (5–100 ng/mL) with highlighted integration range between 262 and 268 nm (grey). Resulting pramipexole peaks (100 ng/mL) after integration for methods 1 and 2.

3.2. MS and LCW-UV Measurement in Comparison

For mass spectrometric measurements of pramipexole, an internal standard with a known concentration was used, which served to give a ratio of the signal intensity. Thus, the ratio of the areas of pramipexole and talipexole (area ratio P/T) was used for the calibration curve obtained by MS measurements. A linear range from 0.19 to 100 ng/mL (Figure 5B) was found; however, concentrations below 1 ng/mL were not relevant for the release study, since a higher concentration of pramipexole is already reached in the vessel after the first sample draw after 5 min. UV detection was able to quantify a concentration of 0.05 µg/mL (lower limit of quantification (LLOQ): 50 ng/mL with an S/N = 11) pramipexole, which for samples containing 88 µg pramipexole in 1000 mL release volume means that the release curve could only be described after a drug release of more than 56% (method 1). Thus, by using the LCW-UV detection system, the linear range of the UV investigation was extended, and a concentration of 2.5 ng/mL could be quantified (LLOQ: 2.5 ng/mL with S/N = 10). Applying the LCW-UV measurement, the detection limit was improved by a factor of 20, resulting in the ability to describe the drug release curve of low-dosed pramipexole preparations after a drug release of 2.5 ng/mL (2.8% API release). This enhancement of the detection limit only results from the extended light path evoked from the LCW, which is described by the Beer–Lambert law Equation (1). However, the measurements showed that the LCW has an upper limit of quantification at 100 ng/mL. Therefore, concentrations of pramipexole during drug release between 2.5 and 100 ng/mL (Figure 5A) can be determined by LCW-UV measurements, and concentrations above 100 ng/mL would need to be quantified by UV measurements. Since both methods have an overlapping linear range between 50 and 100 ng/mL, the evaluation of these concentrations of pramipexole could be depicted by both detection methods. After the calibration curve ranges of both methods were established, a drug release study was performed as described in Section 2.2. The dissolution profile of 0.5% (*w/w*) pramipexole filaments, which were

manufactured by HME (Section 2.1) and were collected in equilibrium condition for drug content [42], resulting from dissolution testing in 1000 mL of 0.1 N HCl, are shown in Figure 6.

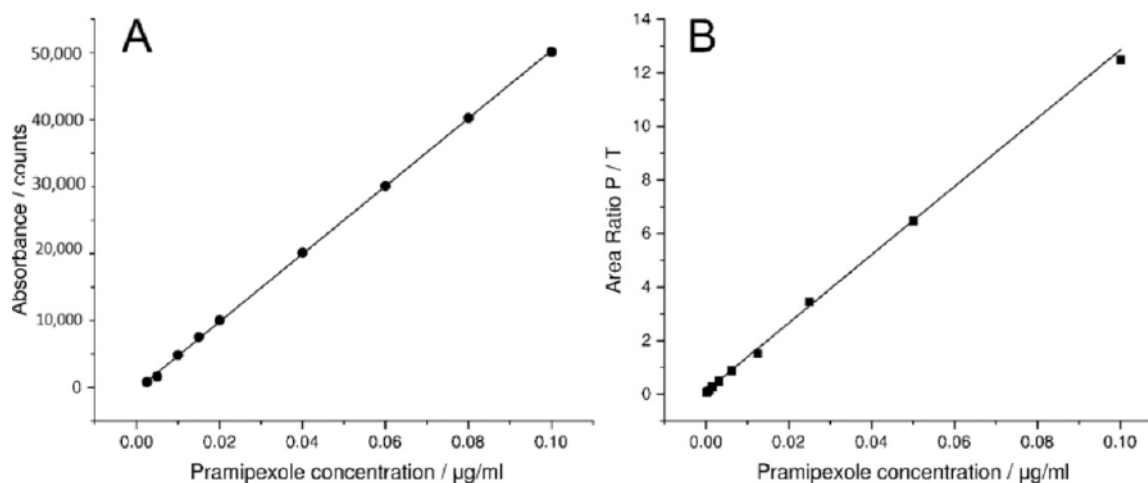


Figure 5. Calibration curve of LCW-UV detection system (A) of pramipexole (2.5–100 ng/mL) and calibration curve of MS analysis (B), where the ratio of the areas of pramipexole and talipexole (area ratio P/T) were plotted against the concentration of pramipexole (0.19–100 ng/mL).

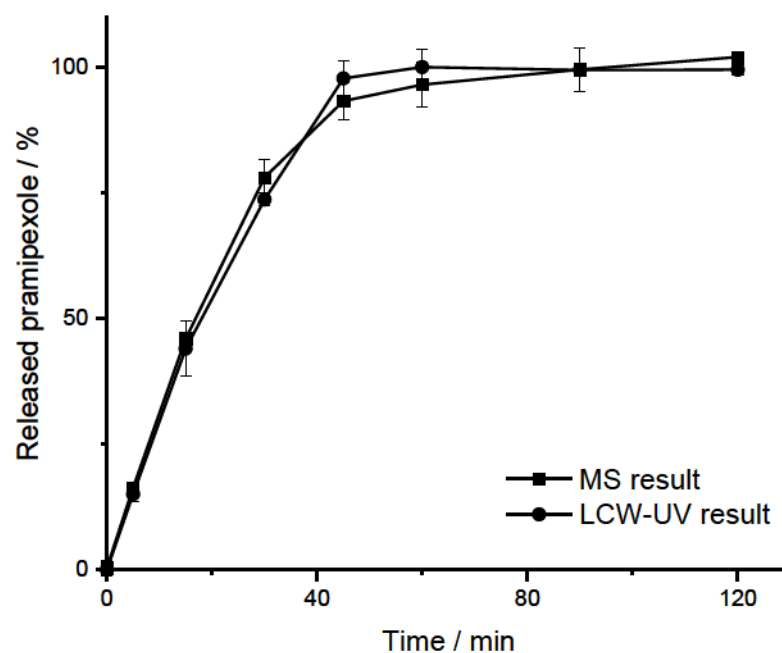


Figure 6. Release curve of 0.5% (w/w) pramipexole filaments ($\bar{m} = 17.61$ mg) determined by MS and LCW-UV measurement ($n = 3$, $\bar{x} \pm \text{SD}$).

The curves indicated that the results for MS and the LCW-UV result in a comparable dissolution profile. For MS results, the MDT is 20.38 min, and the MDT of the dissolution curve obtained by LCW-UV results is 19.73 min (Equation (2)). This results in a minimal discrepancy of the MDT in 33 s, which appears negligible. Since the calculated f_2 -value corresponds to 92, it was assumed that the analysis with LCW-UV would show similar results to the investigation with an established method for low concentrations of pramipexole during release. With these results, it was shown that the drug release of pramipexole from the PVA matrix can be appropriately described by the LCW-UV. In the next step, a method was developed that can detect both the low pramipexole concentrations and

the higher concentrated APIs during drug release that would all be incorporated in a polymedication in an ongoing study. Following the approach of Wollmer and Klein, who quantified levodopa and benserazide with two other API, a new chromatographic method was developed [43].

3.3. Simultaneous Quantification of Levodopa, Benserazide and Pramipexole in Dissolution Testing

For the quantitative evaluation of the amounts of LD, BZ and P in dissolution studies, a new HPLC method was developed that enabled separation and quantification of all three APIs (method 2, described in Section 2.4). Levodopa eluted first at a retention time (R_t) of 7.1 min with a peak width of 0.5 min, followed by benserazide (R_t : 10.9 min) with a peak width of 1.5 min and pramipexole (R_t : 19.3 min) with a peak width of 0.4 min (Figure 7A).

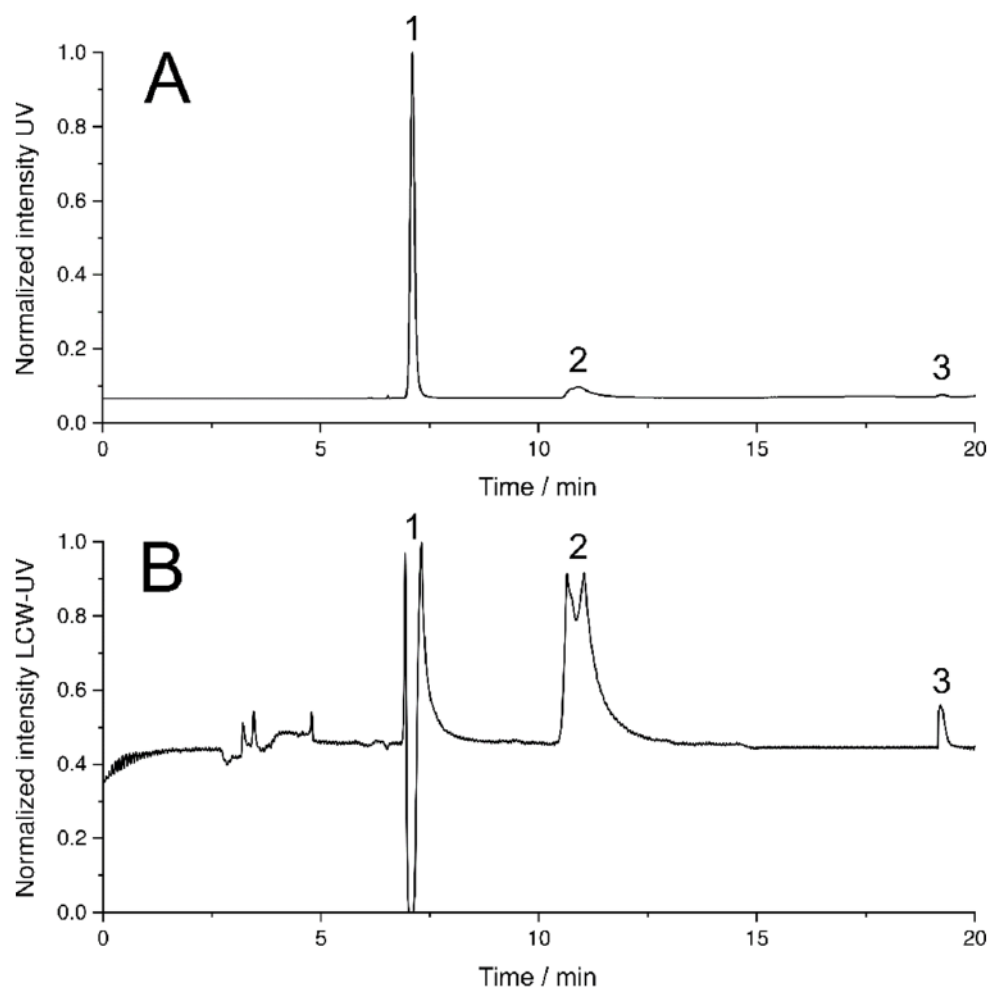


Figure 7. HPLC chromatogram using UV detection (A) and LCW-UV detection (B) of released levodopa (1), benserazide (2) and pramipexole (3) during dissolution study.

The extended flow line of the LCW-UV did not result in an additional measurable dead time (Figure 7B), but the peak widths increased greatly due to the long light path, particularly for levodopa and benserazide, which emphasizes the importance of the separation of both substances from pramipexole by more than 5 min. In the chromatogram of the HPLC run obtained by UV detection, the peak of levodopa shows a narrow peak width. In the chromatogram resulting from LCW-UV measurements, the elution of levodopa is shown as a peak splitting signal. The peak shown negatively in the chromatogram indicates that for a short time more light is detected, but this is caused by saturation of the signal between 262 and 268 nm. Quantitative evaluation of levodopa is not possible using the LCW-UV method but is performed using the UV detector integrated with the HPLC. For the quantita-

tive evaluation of benserazide, the UV detector is more suitable than the new implemented detector. The calculation of the LLOQ of pramipexole is involved the measurements of the UV and LCW-UV detector. By calculating the S/N, the LLOQ (S/N = 10) resulted in a concentration of 20 ng/mL (UV) and 1 ng/mL (LCW-UV). Compared to the first HPLC method, the LLOQ was subsequently lower for both LCW-UV and UV detection due to the focusing of pramipexole by the stepwise gradient of the second HPLC method. Again, an improvement of the quantification limit of the LCW-UV detection compared to UV detection after applying HPLC method 2 was achieved by a factor of 20. Calibration curves were also successfully established for LD (0.01–0.12 mg/mL) and BZ (0.005–0.03 mg/mL) by UV measurements. Figure 8 shows the resulting linear ranges of the three APIs.

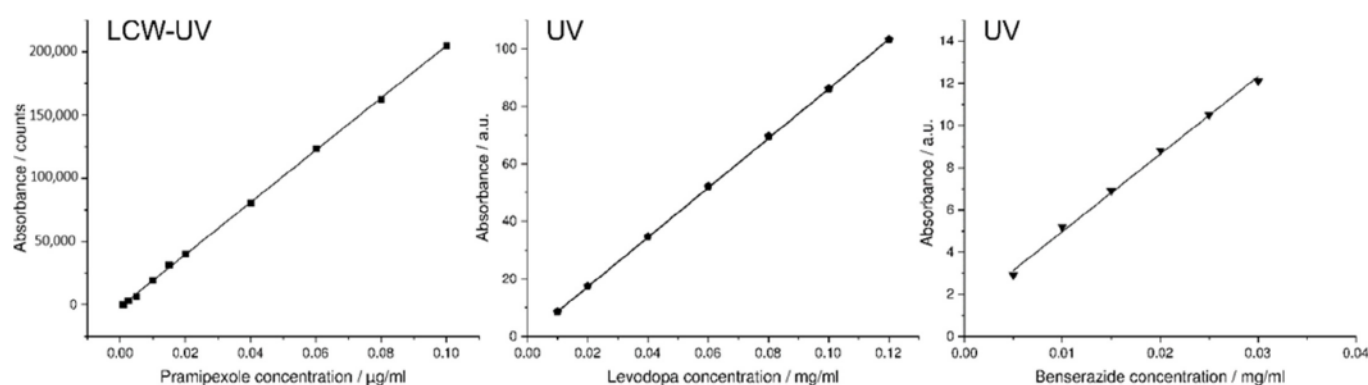


Figure 8. Calibration curve of pramipexole measured with the help of the LCW-UV detection system (1–100 ng/mL); calibration curves of benserazide (5–30 µg/mL), and levodopa (10–1200 µg/mL) both examined by UV detection.

After the identification of the calibration curves, a second drug release study was performed as described in Section 2.2. Attempts were again made to represent the real dose for pharmacotherapy of the respect API, so the filament amount was taken to examine 88 µg of pramipexole, 25 mg of benserazide and 100 mg of levodopa. Since the filament length of the EVA-LD-BZ filament exceeded the size of the basket, the filament was cut into four shorter pieces. Thus, five filaments (one PVA-P filament stick, four EVA-LD-BZ filament sticks) were placed in the baskets. The dissolution profile of 0.5% (*w/w*) pramipexole filaments and filaments containing 40% (*w/w*) levodopa and 10% (*w/w*) benserazide are shown in Figure 9. Both the drug release of pramipexole and benserazide can be described according to first order kinetics. Within 80 min, 100% of the pramipexole was released from the PVA matrix and could be categorized as unmodified drug release. For benserazide, 100% of the drug was released from the insoluble EVA matrix after 180 min. For the third API, levodopa, the drug release from the EVA matrix can be described by Higuchi (square root) kinetics since the diffusion distance to be passed by the API through the matrix does not remain constant but increases steadily. The authors assume that levodopa and benserazide are not homogeneously distributed in the matrix consisting of VA and EVA, leading to the different drug release behaviors of LD and BZ. It is further speculated that the pore former VA might be the reason that the affinity of the distribution differs for the two API. This assumption would lead to the conclusion, that benserazide would have a higher affinity for VA than for EVA. In addition, the slightly better water solubility of BZ may also lead to the faster release. Further dissolution studies and formulation development will be performed as part of an ongoing study to obtain the required release kinetics. However, this study showed that all three APIs can be detected during drug release.

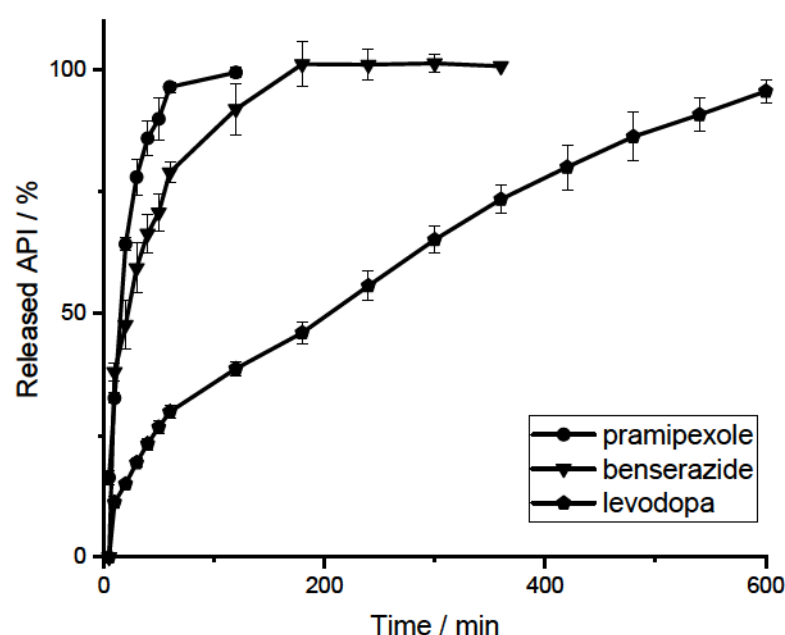


Figure 9. Release curve of 0.5% (*w/w*) pramipexole filaments ($\bar{m} = 17.51$ mg) and levodopa/ benserazide (40/10% (*w/w*)) filaments ($\bar{m} = 250.7$ mg) determined with LCW-UV (P) and UV (LD, BZ) measurement ($n = 6$, $\bar{x} \pm SD$).

4. Conclusions

In this study, an LCW was applied as a flow cell to increase the light path using total internal reflection. For pramipexole, the LLOQ was improved by a factor of 20 with LCW-UV detection compared to conventional UV detection. With the help of this method, concentrations of 1–100 ng/mL, which occur during drug release of low-dosed pramipexole preparations, were detected simultaneously with two other released higher-dose APIs by UV detection. The calculated f_2 -value for comparison of LCW-UV vs. LC-MS/MS was >90 , indicating that similar results for both technologies were obtained. The MDT was comparable for both methods (20 ± 0.4 min). The new method offers a promising alternative to expensive and time-consuming analytical technologies and can be easily integrated into existing HPLC systems. Especially during the development phase of individualized drug preparations and drug products of levodopa, benserazide and pramipexole, this analytical method can provide fast results after dissolution studies. The integration of the LCW-UV detection system can be used for various formulated API–polymer combinations and also drug products, e.g., 3D printed tablets, where the API dosing differs substantially regarding therapeutic regimens.

Author Contributions: Conceptualization, R.C., B.F.; Formal analysis, R.C.; Funding acquisition, J.B.; Investigation, R.C.; Methodology, R.C., H.W. and B.B.B.; Project administration, J.B.; Supervision, B.F.; Validation, R.C.; Visualization, R.C.; Writing—original draft, R.C., B.B.B.; Writing—review and editing, H.W., B.B.B., J.B. and B.F. All authors have read and agreed to the published version of the manuscript.

Funding: This research was funded by the German Federal Ministry of Education and Research—project ‘ProMat Leben-Polymere-PolyPrint’ project no.: 13XP5064B.

Institutional Review Board Statement: Not applicable.

Informed Consent Statement: Not applicable.

Data Availability Statement: The data presented in this study are available upon request from the corresponding author.

Acknowledgments: The authors want to thank Merck KGaA and TER Chemicals for supplying polymers. They are also very grateful for Andrea Michel's help during extrusion runs. This work is associated with the German Federal Ministry of Education and Research—project 'ProMat Leben-Polymere-PolyPrint' (project no.: 13XP5064B).

Conflicts of Interest: The authors declare no conflict of interest. Merck KGaA and TER Chemicals had no role in the design of the study; in the collection, analyses or interpretation of data; in the writing of the manuscript or in the decision to publish the results.

Abbreviations

API	active pharmaceutical ingredient
BZ	benserazide
EVA	poly (ethylene-vinyl acetate)-copolymer
DAD	diode array detection
HME	hot melt extrusion
HPLC	high-performance liquid chromatography
LCW	liquid-core waveguide
LD	levodopa
LLOQ	lower limit of quantification
MDT	mean dissolution time
MS	mass spectrometry
P	pramipexole
PVA	polyvinyl alcohol
SD	standard deviation
S/N	signal-to-noise ratio
UV	ultraviolet
VA	poly (vinylpyrrolidone-vinyl acetate)-copolymer

References

- Williams, B.; Mancia, G.; Spiering, W.; Agabiti Rosei, E.; Azizi, M.; Burnier, M.; Clement, D.L.; Coca, A.; de Simone, G.; Dominiczak, A.; et al. 2018 ESC/ESH Guidelines for the management of arterial hypertension. *Eur. Heart J.* **2018**, *39*, 3021–3104. [CrossRef]
- Guglietta, A.; Guerrero, M. Issues to consider in the pharmaceutical development of a cardiovascular polypill. *Nat. Clin. Pract. Cardiovasc. Med.* **2009**, *6*, 112–119. [CrossRef] [PubMed]
- Combination Products. Available online: <https://www.fda.gov/combination-products/about-combination-products> (accessed on 7 February 2022).
- Vaz, V.M.; Kumar, L. 3D Printing as a Promising Tool in Personalized Medicine. *AAPS PharmSciTech* **2021**, *22*, 49. [CrossRef] [PubMed]
- Goyanes, A.; Robles Martinez, P.; Buanz, A.; Basit, A.W.; Gaisford, S. Effect of geometry on drug release from 3D printed tablets. *Int. J. Pharm.* **2015**, *494*, 657–663. [CrossRef] [PubMed]
- Khaled, S.A.; Burley, J.C.; Alexander, M.R.; Roberts, C.J. Desktop 3D printing of controlled release pharmaceutical bilayer tablets. *Int. J. Pharm.* **2014**, *461*, 105–111. [CrossRef]
- Khaled, S.A.; Burley, J.C.; Alexander, M.R.; Yang, J.; Roberts, C.J. 3D printing of tablets containing multiple drugs with defined release profiles. *Int. J. Pharm.* **2015**, *494*, 643–650. [CrossRef]
- Melocchi, A.; Uboldi, M.; Maroni, A.; Foppoli, A.; Palugan, L.; Zema, L.; Gazzaniga, A. 3D printing by fused deposition modeling of single-and multi-compartment hollow systems for oral delivery—A review. *Int. J. Pharm.* **2020**, *579*, 119155. [CrossRef]
- Windolf, H.; Chamberlain, R.; Quodbach, J. Dose-independent Drug Release from 3D Printed Oral Medicines for Patient-specific Dosing to Improve Therapy Safety. *Int. J. Pharm.* **2022**, *616*, 121555. [CrossRef]
- Scheubel, E.; Lindenberg, M.; Beyssac, E.; Cardot, J.M. Small volume dissolution testing as a powerful method during pharmaceutical development. *Pharmaceutics* **2010**, *2*, 351–363. [CrossRef]
- Timed-Release Tablets and Capsules—In Vitro Test Procedure. In *National Formulary XIV*; The United States Pharmacopeial Convention, Inc.: Rockville, MD, USA, 1975.
- Dissolution Methods for Drug Products Database, U.S. Department of Health and Human Services, Food and Drug Administration, Center for Drug Evaluation and Research (CDER). 2008. Available online: https://www.accessdata.fda.gov/scripts/cder/dissolution/dsp_SearchResults_Dissolutions.cfm?PrintAll=1 (accessed on 7 February 2022).
- European Pharmacopoeia Commission 5.17.1. Recommendations on Dissolution Testing. In *European Pharmacopoeia*; EDQM: Strasbourg, France, 2020; Volume 10.2, pp. 801–807.
- Pedersen, B.L.; Brøndsted, H.; Lennernäs, H.; Christensen, F.N.; Müllertz, A.; Kristensen, H.G. Dissolution of hydrocortisone in human and simulated intestinal fluids. *Pharm. Res.* **2000**, *17*, 183–189. [CrossRef]

15. Wang, B.; Armenante, P.M. Experimental and computational determination of the hydrodynamics of mini vessel dissolution testing systems. *Int. J. Pharm.* **2016**, *510*, 336–349. [[CrossRef](#)] [[PubMed](#)]
16. Klein, S. The Mini Paddle Apparatus—A Useful Tool in the Early Development Stage? Experiences with Immediate-Release Dosage Forms. *Dissolution Technol.* **2006**, *13*, 6–11. [[CrossRef](#)]
17. Gibaldi, M.; Feldman, S. Establishment of sink conditions in dissolution rate determinations. Theoretical considerations and application to nondisintegrating dosage forms. *J. Pharm. Sci.* **1967**, *56*, 1238–1242. [[CrossRef](#)] [[PubMed](#)]
18. Abdel-Hamid, M.E. Comparative LC–MS and HPLC analyses of selected antiepileptics and beta-blocking drugs. *Il Farm.* **2000**, *55*, 136–145. [[CrossRef](#)]
19. Neilson, A.P.; Green, R.J.; Wood, K.V.; Ferruzzi, M.G. High-throughput analysis of catechins and theaflavins by high performance liquid chromatography with diode array detection. *J. Chromatogr.* **2006**, *1132*, 132–140. [[CrossRef](#)]
20. Li, Q.; Morris, K.J.; Dasgupta, P.K.; Raimundo, I.M., Jr.; Temkin, H. Portable flow-injection analyzer with liquid-core waveguide based fluorescence, luminescence, and long path length absorbance detector. *Anal. Chim. Acta* **2003**, *479*, 151–165. [[CrossRef](#)]
21. Kottke, D.; Burckhardt, B.B.; Breitzkreutz, J.; Fischer, B. Application and validation of a coaxial liquid core waveguide fluorescence detector for the permeation analysis of desmopressin acetate. *Talanta* **2021**, *226*, 122145. [[CrossRef](#)]
22. LeWitt, P.A. Levodopa therapy for Parkinson’s disease: Pharmacokinetics and pharmacodynamics. *Mov. Disord.* **2015**, *30*, 64–72. [[CrossRef](#)]
23. Rinne, U.K.; Mölsä, P. Levodopa with benserazide or carbidopa in Parkinson disease. *Neurology* **1979**, *29*, 1584–1589. [[CrossRef](#)]
24. Bennett, J.P., Jr.; Piercey, M.F. Pramipexole—A new dopamine agonist for the treatment of Parkinson’s disease. *J. Neurol. Sci.* **1999**, *163*, 25–31. [[CrossRef](#)]
25. Dasgupta, P.K.; Shelor, C.P.; Kadio, A.F.; Kraiczek, K.G. Flow-Cell-Induced Dispersion in Flow-through Absorbance Detection Systems: True Column Effluent Peak Variance. *Anal. Chem.* **2018**, *90*, 2063–2069. [[CrossRef](#)] [[PubMed](#)]
26. Le, T.; Tao, S. Intrinsic UV absorption spectrometry observed with a liquid core waveguide as a sensor technique for monitoring ozone in water. *Analyst* **2011**, *136*, 3335–3342. [[CrossRef](#)]
27. Pan, J.-Z.; Yao, B.; Fang, Q. Hand-held Photometer Based on Liquid-Core Waveguide Absorption Detection for Nanoliter-scale Samples. *Anal. Chem.* **2010**, *82*, 3394–3398. [[CrossRef](#)] [[PubMed](#)]
28. Robles, T.; Paige, D.; Anastasio, C. Lens-coupled liquid core waveguide for ultraviolet-visible absorption spectroscopy. *Rev. Sci. Instrum.* **2006**, *77*, 073103. [[CrossRef](#)]
29. Li, J.; Dasgupta, P.K. Selective Measurement of Gaseous Hydrogen Peroxide with Light Emitting Diode-Based Liquid-Core Waveguide Absorbance Detector. *Anal. Sci.* **2003**, *19*, 517–523. [[CrossRef](#)]
30. Byrne, R.H.; Kaltenbacher, E. Use of liquid core waveguides for long pathlength absorbance spectroscopy: Principles and practice. *Limnol. Oceanogr.* **2001**, *46*, 740–742. [[CrossRef](#)]
31. D’Sa, E.J.; Steward, R.G.; Vodacek, A.; Blough, N.V.; Phinney, D. Determining optical absorption of colored dissolved organic matter in seawater with a liquid capillary waveguide. *Limnol. Oceanogr.* **1999**, *44*, 1142–1148. [[CrossRef](#)]
32. Fujiwara, K.; Ito, S. Application of waveguiding in solutions for absorption and fluorescence spectrometry. *Trends Anal. Chem.* **1991**, *10*, 184–190. [[CrossRef](#)]
33. Quodbach, J.; Bogdahn, M.; Breitzkreutz, J.; Chamberlain, R.; Eggenreich, K.; Elia, A.G.; Gottschalk, N.; Gunkel-Grabole, G.; Hoffmann, L.; Kapote, D.; et al. Quality of FDM 3D Printed Medicines for Pediatrics: Considerations for Formulation Development, Filament Extrusion, Printing Process and Printer Design. *Ther. Innov. Regul. Sci.* **2021**, 1–19. [[CrossRef](#)]
34. European Pharmacopoeia Commission 2.9.3. Dissolution Test for Solid Dosage Forms. In *European Pharmacopoeia*; EDQM: Strasbourg, France, 2020; Volume 10.2, pp. 326–333.
35. Windolf, H.; Chamberlain, R.; Quodbach, J. Predicting Drug Release from 3D Printed Oral Medicines Based on the Surface Area to Volume Ratio of Tablet Geometry. *Pharmaceutics* **2021**, *13*, 1453. [[CrossRef](#)]
36. Tzankov, B.; Voycheva, C.; Yordanov, Y.; Aluani, D.; Spassova, I.; Kovacheva, D. Development and In Vitro safety evaluation of pramipexole-loaded Hollow Mesoporous Silica (HMS) particles. *Biotechnol. Equip.* **2019**, *33*, 1204–1215. [[CrossRef](#)]
37. Dinç, E.; Kaya, S.; Doganay, T.; Baleanu, D. Continuous wavelet and derivative transforms for the simultaneous quantitative analysis and dissolution test of levodopa-benserazide tablets. *J. Pharm. Biomed. Anal.* **2007**, *44*, 991–995. [[CrossRef](#)] [[PubMed](#)]
38. Krisai, K.; Charnvanich, D.; Chongcharoen, W. Increasing the solubility of levodopa and carbidopa using ionization approach. *Thai. J. Pharm. Sci.* **2020**, *44*, 251–255.
39. Wang, W.; He, Q.; Wang, T.; Fen, M.; Liao, Y.; Ran, G. Absorbance study of liquid-core optical fibers in spectrophotometry. *Anal. Chem.* **1992**, *64*, 22–25. [[CrossRef](#)]
40. Costa, P.; Lobo, J.M.S. Modeling and comparison of dissolution profiles. *Eur. J. Pharm. Sci.* **2001**, *13*, 123–133. [[CrossRef](#)]
41. U.S. Food and Drug Administration (FDA). *FDA Guidance for Industry—Dissolution Testing of Immediate Release Solid Oral Dosage Forms*; FDA Center for Drug Evaluation and Research: Silver Spring, MD, USA, 1997; Volume 1, pp. 1–17.
42. Chamberlain, R.; Windolf, H.; Geissler, S.; Quodbach, J.; Breitzkreutz, J. Precise Dosing of Pramipexole for Low-Dosed Filament Production by Hot Melt Extrusion Applying Various Feeding Methods. *Pharmaceutics* **2022**, *14*, 216. [[CrossRef](#)]
43. Wollmer, E.; Klein, S. Development and validation of a robust and efficient HPLC method for the simultaneous quantification of levodopa, carbidopa, benserazide and entacapone in complex matrices. *Int. J. Pharm. Sci.* **2017**, *20*, 258–269. [[CrossRef](#)]

4.3 3d Printed Mini-Floating-Polypill for Parkinson's Disease: Combination of Levodopa, Benserazide, and Pramipexole in Various Dosing for Personalized Therapy

Evaluation of authorship

author	idea [%]	study design [%]	experimental [%]	evaluation [%]	manuscript [%]
Hellen Windolf	60	60	60	50	50
Rebecca Chamberlain	30	40	40	35	35
Jörg Breitzkreutz	10	-	-	5	5
Julian Quodbach	-	-	-	10	10

Evaluation of Copyright permission:

The research paper was published under a Creative Commons license (Open Access) and is free to share and adapt (MDPI | Open Access Information; accessed on 18.05.2022).

3d Printed Mini-Floating-Polypill for Parkinson's Disease: Combination of Levodopa, Benserazide, and Pramipexole in Various Dosing for Personalized Therapy

Hellen Windolf¹, Rebecca Chamberlain¹, Jörg Breitzkreutz¹, Julian Quodbach²

¹ *Institute of Pharmaceutics and Biopharmaceutics, Heinrich Heine University, Universitätsstrasse 1, 40225 Duesseldorf, Germany*

² *Department of Pharmaceutics, Utrecht Institute for Pharmaceutical Sciences, Utrecht University, Universiteitsweg 99, 3584 CG Utrecht, The Netherlands*

Pharmaceutics

<https://doi.org/10.3390/pharmaceutics14050931>

Article

3D Printed Mini-Floating-Polypill for Parkinson's Disease: Combination of Levodopa, Benserazide, and Pramipexole in Various Dosing for Personalized Therapy

Hellen Windolf ¹, Rebecca Chamberlain ¹, Jörg Breitzkreutz ¹ and Julian Quodbach ^{1,2,*}

- ¹ Institute of Pharmaceutics and Biopharmaceutics, Heinrich Heine University, Universitätsstr. 1, 40225 Düsseldorf, Germany; hellen.windolf@hhu.de (H.W.); rebecca.chamberlain@hhu.de (R.C.); joerg.breitzkreutz@hhu.de (J.B.)
- ² Department of Pharmaceutics, Utrecht Institute for Pharmaceutical Sciences, Utrecht University, Universiteitsweg 99, 3584 CG Utrecht, The Netherlands
- * Correspondence: j.h.j.quodbach@uu.nl

Abstract: Therapy for Parkinson's disease is quite challenging. Numerous drugs are available for symptomatic treatment, and levodopa (LD), in combination with a dopa decarboxylase inhibitor (e.g., benserazide (BZ)), has been the drug of choice for years. As the disease progresses, therapy must be supplemented with a dopamine agonist (e.g., pramipexole (PDM)). Side effects increase, as do the required dose and dosing intervals. For these specific requirements of drug therapy, the 3D printing method fused deposition modelling (FDM) was applied in this study for personalized therapy. Hot melt extrusion was utilized to produce two different compositions into filaments: PDM and polyvinyl alcohol for rapid drug release and a fixed combination of LD/BZ (4:1) in an ethylene-vinyl acetate copolymer matrix for prolonged drug release. Since LD is absorbed in the upper gastrointestinal tract, a formulation that floats in gastric fluid was desired to prolong API absorption. Using the FDM 3D printing process, different polypill geometries were printed from both filaments, with variable dosages. Dosage forms with 15–180 mg LD could be printed, showing similar release rates ($f_2 > 50$). In addition, a mini drug delivery dosage form was printed that released 75% LD/BZ within 750 min and could be used as a gastric retentive drug delivery system due to the floating properties of the composition. The floating mini-polypill was designed to accommodate patients' swallowing difficulties and to allow for individualized dosing with an API release over a longer period of time.

Keywords: FDM 3D printing; polypill; Morbus Parkinson; personalized medicine; additive manufacturing; gastro retentive drug delivery



Citation: Windolf, H.; Chamberlain, R.; Breitzkreutz, J.; Quodbach, J. 3D Printed Mini-Floating-Polypill for Parkinson's Disease: Combination of Levodopa, Benserazide, and Pramipexole in Various Dosing for Personalized Therapy. *Pharmaceutics* **2022**, *14*, 931. <https://doi.org/10.3390/pharmaceutics14050931>

Academic Editors: Mateusz Kurek and Witold Jamróz

Received: 25 March 2022

Accepted: 22 April 2022

Published: 25 April 2022

Publisher's Note: MDPI stays neutral with regard to jurisdictional claims in published maps and institutional affiliations.



Copyright: © 2022 by the authors. Licensee MDPI, Basel, Switzerland. This article is an open access article distributed under the terms and conditions of the Creative Commons Attribution (CC BY) license (<https://creativecommons.org/licenses/by/4.0/>).

1. Introduction

Worldwide, about 9% of the world's population is older than 65 years. Over the next few decades, the UN expects the proportion of older people to continue to rise significantly, so that by 2100 almost 23% of the population will be at least 65. In the EU, the aging process is already more advanced; in 2020, more than 20% of the EU population was 65 years and older [1–3]. Due to the increase in susceptibility to disease with age, approximately 50% of Rx-medications are prescribed to patients older than 65 years [4–8]. The average geriatric patient (≥ 65 years) takes 8.5 tablets per day at different times [3]. This can lead to complications between the different drugs with potential interactions, but also to a decrease in medication adherence, as certain dosing times and intervals are not adhered to or administration is forgotten [9,10]. To promote patient adherence, community pharmacies frequently offer to blister tablets in pouches or place them in medication boxes for daily use [7]. Also, pharmaceutical manufacturers are trying to produce tablets that contain multiple active pharmaceutical ingredients (APIs) in fixed dosages that are often prescribed together [11,12]. For example, several APIs are prescribed for high blood pressure or

cardiovascular diseases, and these are now in just one tablet for ingestion (e.g., Vocado[®] HCT, Berlin-Chemie AG, with olmesartan, amlodipine and hydrochlorothiazide). Another disease that requires the administration of multiple tablets is Parkinson's disease. So far, the disease can only be treated symptomatically and must be tailored very precisely to the patient, since here effect and side effect go hand in hand, as both too low and too high dopamine levels can lead to symptoms [13–15]. Parkinson's disease is the second most common neurodegenerative disease. On average, patients are diagnosed with Parkinson's at around 60 years of age. However, the onset is probably preceded by decades of changes in the body. The number of patients worldwide has increased from 2.5 million in 1990 to 6.1 million in 2016. The main cause is the increasing aging of the population. However, the incidence of the disease has also increased by more than 20% within individual age groups during this time [16,17]. Parkinson's disease is characterized by progressive degeneration of dopaminergic neurons in the substantia nigra [18–22]. This results in an imbalance in the transmitter system with disinhibition of cholinergic neurons and increased glutamatergic activity (dopamine deficiency and excess of acetylcholine). This results in inhibition of movement. Due to the lack of dopamine, akinesia and bradyphrenia develop, rigor and tremor are consequences of the disinhibited cholinergic system. The disease advances in a progressive manner, showing a stepwise course associated with various motor, behavioral, and psychological disabilities. Therapy begins early with the diagnosis. Suitable APIs and API-classes are: levodopa (LD) (always in combination with dopa decarboxylase inhibitors (DDI, e.g., benserazide, carbidopa)), dopamine agonists (DA, e.g., pramipexole, ropinirole), monoamine oxidase B (MAO-B) inhibitors (selegiline, rasagiline), catechol-O-methyl transferase (COMT, entacapone, tolcapone) inhibitors, N-methyl-D-aspartate (NMDA) agonists (e.g., amantadine), and anticholinergics (biperidine). For patients <70 years of age (biological age), DA are the drug of choice. In patients >70 years, LD combined with DDI is the preferred therapy [23,24]. As the disease progresses, however, it becomes more difficult to control symptoms by taking tablets alone [21,25–28]. The effect of the medication then sets in increasingly later and does not last as long: The optimal range of action in which a drug is available in the desired concentration in the body and has the intended effect decreases. Phases with good mobility (ON phases) and with under-mobility (OFF phases) thus become more and more prominent. Non-motor symptoms such as behavioral changes or depression may also become more apparent [24,29,30]. That is why the therapy of Parkinson's patients is constantly adapted and rarely remains a monotherapy. In the later course, DA and LD are often combined. As patient suffering increases, pharmaceutical manufacturers are trying to develop dosage forms that can alleviate suffering. Thus, there are intestinal pumps (Duodopa[®], Lecigon[®], [31–33]), transdermal therapeutic systems (TTS, Neupro[®]), orodispersible films and tablets (ODF, ODT [34,35]), tablets, capsules, and floating dosage forms (Madopar[®] HBS [36,37]) for therapy on the market or in clinical trials. Various research groups are also working on improved therapy [38]. Accordion Pill[®] is one of the new innovative dosage forms [39]. It contains LD and carbidopa (DDI) in a novel drug delivery system with combined immediate release (IR) and sustained release (SR) kinetics. The design allows gastric retention and thus improved API uptake for Parkinson's patients. In another approach, nanoparticles are being investigated as oral and nasal dosage forms, as well as a LD powder inhaler [40–44]. Other research groups test microspheres, liposome nanocapsules, and niosomes loaded with DA for the treatment of Parkinson's disease. The lipophilic formulation is expected to improve transport through the blood-brain barrier to achieve dose reduction, thereby reducing side effects [45–47].

As Fused Deposition Modelling (FDM) 3D printing is currently being investigated for many drugs for personalized medicine [48–59], some research groups are also interested in printing individual drug dosage forms for Parkinson's patients with tailored dosages and release profiles [48,49,60–63]. The layered structure of the geometries from FDM 3D printing and semi-solid 3D printing allows very precise dosage and adjustment of the dose. This allows the required dose to be administered without triggering side effects, even for APIs with a small therapeutic range [63,64]. FDM 3D printing, also called fused filament

fabrication, requires a filament, which is previously produced by hot-melt extrusion (HME) from a mixture of API and polymer as matrix. By simply changing the filament during printing, FDM 3D printing enables the use of multiple APIs and polymer matrices in one tablet during one manufacturing step. This offers the advantage of also being able to combine APIs that are incompatible with each other in a combined formulation, as well as being able to individually adjust the release properties of the APIs due to the polymer matrix and surface area to volume (SA/V) ratio [65,66]. For example, Khaled et al. developed a 3D printed polypill with five different drugs in various compartments and two different release profiles for cardiovascular therapy [67].

In our study, we aimed to develop a 3D printed polypill-dosage form containing three APIs with different release kinetics for the therapy of Parkinson's disease: pramipexole (PDM), levodopa (LD), and benserazide (BZ). In addition, the dosage form should be adapted to the requirements of Parkinson's patients and thus be easy to swallow, individually dosed, and have the longest possible gastric residence time (GRT) to saturate the transporters in the upper small intestine section with LD over a long period of time to reduce side effects and ON-OFF fluctuations. Levodopa is a precursor of dopamine and is used in the treatment of movement disorders in Parkinson's disease and restless legs syndrome. The initial dose is 100 mg LD once or twice daily combined with 25 mg BZ. A dose increase should be made every 3rd–7th day, until a maximum daily dose of 800 mg LD is reached. LD and BZ are dosed in a 4:1 combination. PDM is a dopamine agonist. The initial dose is 0.26 mg pramipexole per day (corresponds to 0.375 mg PDM), the lowest dose of one tablet is 0.088 mg. The daily dose may be increased by 0.52 mg at weekly intervals, to a maximum dose of 3.15 mg per day (corresponds to 4.5 mg PDM) [23]. For individual dosage and adjusted release rate, the FDM 3D printing process was used. The DA PDM should have a fast release and the combination LD/BZ should display sustained release from the dosage form. Therefore, PDM was processed by HME in a polyvinyl alcohol (PVA)-filament and the combination LD/BZ in an ethylene-vinyl acetate-copolymer (EVA)-filament. The dosage form design should be adjusted for the release rate with respect to the absorption window in the upper jejunum via the SA/V ratio.

2. Materials and Methods

2.1. Materials

For formulation development, various sustained release (SR) polymers were first screened using the vacuum compression molding (VCM) method (Table 1).

Table 1. SR-polymers used for VCM-formulation development (MW, molecular weight; MFI, melt flow index).

	Polyvinyl Alcohol (PVA)	Hydroxypropyl Cellulose (HPC H)	Hydroxypropyl Cellulose (HPC SSL)	Ethylene Vinyl Acetate (EVA) (72:28)	Hydroxypropyl Methylcellulose Acetate Succinate (HPMC-AS)
Manufacturer	Parateck MXP [®] , 87–89% hydrolysis grade, MW: approx. 32,000 Da, Merck, Darmstadt, Germany	MW: 1,000,000 Da, Nisso Chemical Europe, Düsseldorf, Germany	MW: 40,000 Da, Nisso Chemical Europe, Düsseldorf, Germany	Escorene UL 02528 [®] , MFI: 25 g/10 min, TER Chemicals, Hamburg, Germany	Aquasolve [®] , MW: 75,100 Da, Ashland, Wilmington, DE, USA

After formulation development, the polypill was printed with two different filaments, manufactured by hot-melt extrusion (HME). The composition of the filaments is shown in Table 2.

Table 2. Formulations used for the polypill.

Filament 1			
API and Excipients	%	Function	Manufacturer/Source
Pramipexole 2 HCl * H ₂ O (PDM)	5.0	API	99.5%, Chr. Olesen, Gentofte, Denmark
Mannitol	10.0	plasticizer	Parteck M [®] , Merck, Darmstadt, Germany
Polyvinyl alcohol (PVA)	84.0	polymer	Parteck MXP [®] , Merck, Darmstadt, Germany
Fumed silica	1.0	glidant	Aerosil [®] 200 VV Pharma, Evonik, Essen, Germany
Filament 2			
APIs and Excipients	%	Function	Manufacturer/Source
Levodopa (LD)	40.0	API	99.6%, Zhejiang Wild Wind Pharmaceutical, Dongyang, Zhejiang Prov., China
Benserazide (BZ)	10.0	API	99.8%, BioPharma Synergies, Barcelona, Spain
Vinylpyrrolidone-vinyl acetate copolymer 60:40 (PVP-VA)	15.0	polymer	Kollidon VA 64 [®] , MW: 40,000 Da, BASF, Ludwigshafen, Germany
Ethylene-vinyl acetate copolymer 82:18 (EVA)	34.5	polymer	Escorene [®] FL01418, MFI: 14 g/10 min, TER Chemicals, Hamburg, Germany
Fumed silica	0.5	glidant	Aerosil [®] 200 VV Pharma, Evonik, Essen, Germany

LD, BZ and PDM exhibit good water solubility (c_s (LD) ≥ 12 mg/mL, c_s (BZ) ≥ 10 mg/mL, c_s (PDM) ≥ 200 mg/mL [68–70]) and thus belong to the biopharmaceutical classification system (BCS) class I. As HME and FDM 3D printing are heat intensive processes, care was also taken to ensure that the process temperatures were below the decomposition temperatures (260–330 °C) [62,71–74]. Due to the high water solubility of the drug substances, the dissolution is governed solely by the polymer properties and not by their solid-state properties.

2.2. Methods

2.2.1. Vacuum Compression Molding

To compare the release profiles of different sustained release (SR) polymers under the same conditions, molten platelets were prepared with vacuum compression molding (VCM, MeltPrep GmbH, Graz, Austria) technology [75]. The resulting platelets had the same surface area (SA) and volume (V), so that the SA/V ratio did not influence the release profile. For this purpose, powder mixtures of different SR polymers with 33% LD each were prepared so that there was 100 mg LD in each VCM-sample (300 mg). The physical mixture of SR polymer and LD was filled into the sample holder, which was connected to a vacuum source. A piston was pressed onto the sample, which was melted on the hot plate until the sample was homogeneously mixed. The process settings used are shown in Table 3. Afterwards, the VCM-platelet was cooled and removed from the holder. The dimensions of the resulting VCM-platelet were 20 mm in diameter and 1.5 mm in height (Figure 1).

Table 3. VCM-Process settings for different SR-polymers.

	PVA	HPC H	HPC SSL	EVA (72:28)	HPMC-AS
Heating temperature/°C	210	170	170	120	210
Heating time/min	7	7	8	7	7
Mass/mg (MV)	307	310	308	311	310
SA/V ratio/mm ^{−1}	1.5	1.5	1.5	1.5	1.5



Figure 1. VCM platelets of different SR polymers.

2.2.2. Hot-Melt Extrusion for Filament Fabrication

All filaments were prepared by HME with a co-rotating twin-screw extruder (Pharmalab HME 16, Thermo Fisher Scientific, Rockford, IL, USA). A gravimetric feeder (K-SFS-24/6, Coperion K-Tron, Stuttgart, Germany) was used for all experiments. An in-house manufactured die with a diameter of 1.85 mm was used. The desired filament diameter was achieved using a belt haul-off unit of a winder (Model 846700, Brabender, Duisburg, Germany) with a belt speed of 0.8 m/min and the filament was transported through a roller system with four 360°—air flow ring nozzles (Super Air Wipe™, Exair®, Cincinnati, OH, USA). With the help of a laser-based diameter measurement module (Laser 2025 T, Sikora, Bremen, Germany), the filament diameter was detected and logged during the process with a readout rate of 1 Hz to ensure the production of filaments with low diameter fluctuations. For extrusions with EVA, the screw speed was set to 20 rpm and powder feed rate was set to 2 g/min. The screw configurations and the temperatures of the heating zones are summarized in Table 4 and also described in previous publications [60,61,76].

Table 4. Extrusion parameters with adjusted temperatures during extrusion and screw configuration of performed extrusions.

	Temperature Profile in Zone 2–10 [°C]								
	2	3	4	5	6	7	8	9	10
PDM-PVA filament	20	20	100	180	180	180	180	195	195
LD/BZ-EVA filament	20	20	100	100	100	100	100	100	100
	Screw Configuration (Die-Gear)								
	die-10 CE 1 L/D-KZ 1: 5 × 60°–3 × 30°–5 CE 1 L/D-KZ 2: 4 × 90°–5 × 60°–3 × 30°–16 CE 1 L/D–2 CE 3/2 L/D–1 L/D adapter-gear								
PVA/EVA filaments	CE = conveying element, KZ = kneading zone								

2.2.3. 3D Printing Process of the Polypill-Geometries

To achieve various dosages and release profiles, the geometries were designed with the computer-aided design (CAD) program Fusion360® (Autodesk, San Rafael, CA, USA) with focus on the volume and surface area to volume (SA/V) ratio. Afterwards, the generated stl-files were transferred to the slicing program PrusaSlicer® (Prusa research, Prague, Czech Republic). The individual parts of the geometries were assigned to the respective filament. The layer height and extrusion width were adjusted to generate the

desired height and width of the geometry. The G-code was sent to a Prusa 3D printer (Prusa i3 Mk3, Prusa research, Prague, Czech Republic), which printed the objects defined in the data file (Figure 2). The multi material unit (MMU) from Prusa® was used for printing the polypill. A cleaning tower was printed between filament changes so that the previous filament could be washed out of the nozzle and the following used filament was not contaminated. The best results were obtained with the following temperatures: PDM-PVA filament: 185 °C print temperature and 70 °C bed temperature, LD/BZ-EVA-filament: 220 °C print temperature and 70 °C bed temperature. Cooling during printing was turned off, otherwise the layers would not adhere to each other. The objects were printed one by one. The printing speed was set to 10 mm/s because the geometries had little contact area with the print bed due to their small size and quickly detached, interrupting the printing process.



Figure 2. Printed polypills in various designs.

2.2.4. Dissolution Tests of the Polypills

The dissolution tests for the polypill ($n = 3$) were performed according to European Pharmacopoeia monographs 2.9.3 and 5.17.1 [77,78]. A modified basket apparatus was used for the dissolution apparatus (DT 700, Erweka, Langen, Germany) [61,63]. Adapted baskets were 3D printed with water insoluble polylactide acid filament (PLA, Bavaria-Filaments, Freilassing, Germany) with a mesh size of 3 mm and the same outer dimensions as the regular baskets described in the European Pharmacopoeia. This adjustment was necessary because the 3D printed tablets clogged the small meshes of the original Erweka baskets (0.36–0.44 mm) with swollen polymer, affecting the hydrodynamics around the printed tablet. The use of the modified baskets prevented this blockage. In addition, a 3D printed PLA-plate with a mesh size of 3 mm was clipped into the basket above the floating dosage form so that it could not stick to the stirrer and thus distort the release profiles. As dissolution medium degassed 0.1 N hydrochloric acid (HCl) was used. The volume was 1000 mL, the stirring speed was set to 50 rpm and the temperature was set to 37 ± 0.5 °C. The dissolution tests were performed under sink conditions [63,76]. Samples were drawn using an autosampler (Vision® AutoFill™ + AutoPlus™, Teledyne Hanson Research, Chatsworth, CA, USA). At the set time point, 5 mL were withdrawn from the vessel, 3.5 mL were used to wash the tubes before sampling, and 1.5 mL were transferred directly to a HPLC vial. For polypill design (PP) 1-PP3, the first sample was drawn after 15 min, then after 30 min, and subsequently every 30 min until 180 min. Afterwards, a sample was taken every hour until 360 min, then every 2 h until 600 min. For PP3 additional samples were taken after 600 min every 5 h until 50 h. For the mini tablet designs *MiniTab* and *MiniHC*, the first sample was taken after 10 min, then every 10 min until 60 min, followed by every 30 min to 120 min, then after 1 h to 240 min, and every 2 h to 600 min. Subsequently, samples were taken every 5 h to 1500 min.

2.2.5. HPLC Method: Chromatographic Conditions for Simultaneous Quantification of Levodopa, Benserazide and Pramipexole

The following method is described in more detail in [76]. High performance liquid chromatography (HPLC) analysis was used to separate all three APIs (PDM, LD, BZ). The HPLC (Dionex, Sunnyvale, CA, USA) was equipped with a quaternary pump (P 580 A, Dionex, Sunnyvale, CA, USA) and an autosampler (ASI-100, Dionex, Sunnyvale, CA, USA).

For the HPLC method, a C18-column (Eurospher II 100-5, Knauer, Berlin, Germany) with integrated precolumn was used. The eluent consisted of methanol (mobile phase B) and ammonium acetate buffer (0.05 M, pH 4). The flow rate was set to 1 mL/min and the oven temperature for tempering the column to 40 °C. The gradient was as follows: mobile phase B was increased from 1 to 5% (v/v), within the first min, held at 5% (v/v) for 4 min, increased from 5 to 10% (v/v) within 1 min, held at 10% (v/v) for 4 min, increased again from 10 to 20% (v/v) within 1 min, held for 4 min at 20% (v/v), increased again from 20 to 99% (v/v) within 5 min, held for 2 min at 99% (v/v) and decreased to 1% (v/v) within 0.5 min, again until 22.5 min after sample injection. An equilibration time of 3.5 min per run was allowed to pass before the next sample was injected. An injection volume of 200 µL was chosen to analyze the APIs. Detection was achieved by measuring the UV absorption of the sample at 264 nm with the help of the HPLC UV-detector [77].

2.2.6. Density Measurements with Helium Pycnometer

To determine the true density of the filaments and printed tablets, measurements were made using a helium pycnometer (AccuPyk 1330, Model 133/00010/10, Micromeritics, Norcross, GA, USA). The analysis conditions were 10 cycles with a purging filling pressure of 134.55 kPa with Helium. 5 measurements per sample were performed in a 1 cm³ chamber.

2.2.7. Comparison of Release Profiles

Mean Dissolution Time

The *Mean Dissolution Time (MDT)*, expressed in units of time, was used to compare the curves and to categorize them [61,79,80]. The *MDT* was calculated according to Equation (1).

$$MDT = \frac{ABC}{c_{\infty}} = \frac{\sum_{i=0}^{\infty} [(c_{i+1} - c_i) \times \frac{(t_i + t_{i+1})}{2}]}{c_{\infty}} \quad (1)$$

The quotient of the *ABC (area between the curves)* and c_{∞} , the initial drug load of the dosage form results in the *MDT*. Via the trapezoidal equation, *ABC* is calculated with c_i as the concentration of the API released over time t . Values up to 100% API release were used, since the *ABC* does not change afterwards.

Similarity Factor

In addition, the similarity factor was used to compare the release curves. Equation (2) was used to perform the calculation [61,79,81,82].

$$f_2 = 50 \times \log \left\{ \left[1 + \frac{1}{n} \sum_{t=1}^n (R_t - T_t)^2 \right]^{-0.5} \times 100 \right\} \quad (2)$$

R_t represents the API in % at time point t for the reference and T_t the API in % at time point t for the test product. The factor n summarizes the considered number of time points. Since the f_2 value is sensitive to the number of measurement points, the number of the considered values was constantly limited to 12 time points. An f_2 value of 100 results if the dissolution curve of the test product is completely identical to the reference curve. The measured values may deviate from the reference by a maximum of 10%, resulting in f_2 values between 50–100. If the achieved f_2 value is below 50, the dissolution profiles differ strongly, and they are not considered similar.

3. Results and Discussion

3.1. Polymer Selection for Levodopa

To increase Parkinson's patients' adherence to their therapy, the LD/BZ combination should be released slowly over 12–24 h so that dosing intervals increase, and ON-OFF fluctuations decrease. The PVA-formulation with PDM has already been developed for previous studies [60,61,63]. To find a suitable SR polymer for the LD/BZ combination,

VCM-platelets were prepared with a drug loading of 33% (*w/w*) LD and established SR polymers: PVA, HPC H, HPC SSL, EVA and HPMC-AS. All VCM-platelets had the same SA/V ratio and could thus be compared based on their dissolution properties (Figure 3).

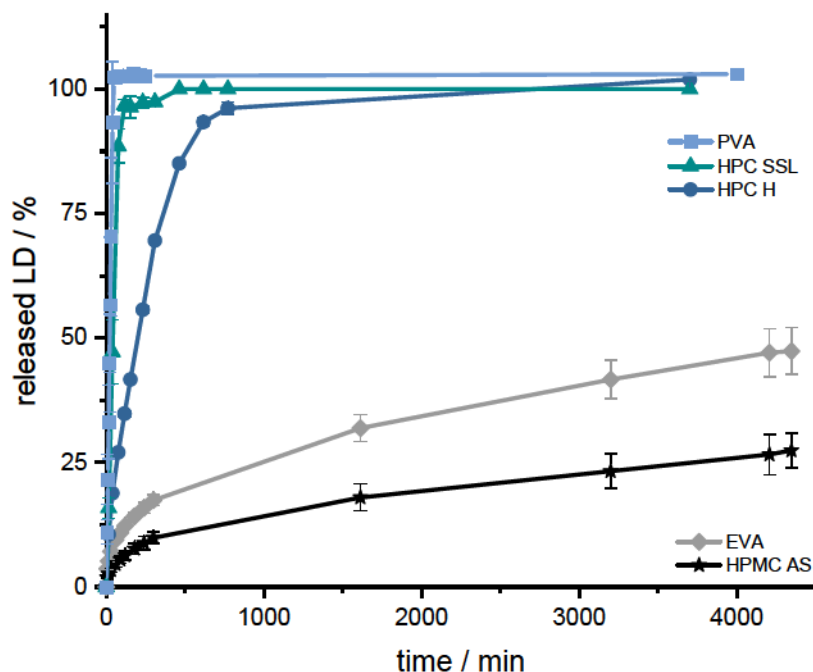


Figure 3. Dissolution profiles of LD from SR-polymer-VCM platelets (33% (*w/w*) LD-loading); modified basket apparatus, 1000 mL 0.1 N HCl, 50 rpm, 37.0 ± 0.5 °C. $\bar{x} \pm s$; $n = 3$.

The aim was to achieve prolonged release with a constant dissolution rate of the API. This target was set regarding the prolonged gastrointestinal passage in Parkinson's patients [83,84] and the resorption window of levodopa in the small intestinal tract via large neutral amino acid (LNAA) transport carrier [85,86]. To achieve continuous availability of LD/BZ in the body, the dosage form should release a constant amount of LD/BZ and saturate the transporters for as long as possible so the "wearing off" phenomenon at the end of dose interval is decreased [87–89]. To ensure a constant release, the tablet should release 75% within 12 h, so that a constant API exposition is realized within the desired time frame. Using the VCM-platelets, it was determined that PVA, HPC H and HPC SSL would not be considered because they released the API too fast (HPC SSL 75% LD in 25 min, PVA: 75% LD in 33 min, and HPC H 75% LD in 133 min) based on their high hydrophilicity, the formation of a hydrocolloid matrix, and swelling, as well as eroding properties of the matrix so that the API can be solubilized faster. The final formulation including BZ should have 50% drug-loading and thus become even more hydrophilic, so that the API release will be faster than the VCM-API release. The API release of HPMC-AS, on the other hand, was too slow (25% LD in 63 h), so the decision was made for the SR polymer EVA (50% API in 75 h). In addition, EVA has a lower density (0.95 g/cm^3) than water and 0.1 N HCl (gastric fluid), so this property can be exploited for a floating, gastro-retentive drug delivery dosage form [86].

3.2. Formulation Development with EVA

First, a formulation containing 40% LD and 60% EVA was extruded (F1, Table 5). However, the API release was too slow, even with a high SA/V ratio of 3 mm^{-1} (Figure 4), and the printing process of the filament was difficult, because of the high flexibility of the filament. Therefore, the formulation was changed. PVA was added in equal parts with EVA as hydrophilic polymer (F2). Nevertheless, the flexibility of EVA with a VA content of 28% was too high, so that the printability was poor, the printed objects were not reproducible, and the printing process repeatedly stopped because the filament clogged the nozzle. Drug

release was faster than in F1, but still not suitable. Therefore, the EVA polymer with a VA content of 28% was replaced by EVA with a VA content of 18% (F3). The same excipient combination with other quantification was now extruded and printed with EVA (18% VA). Drug release was much faster than with formulation F2, but the dosage form disintegrated within a few minutes, so no gastro-retentive drug delivery form can be developed with this composition. Therefore, the EVA content was increased, PVA was replaced by PVP-VA, and mannitol was added, as the filament otherwise became too brittle (F4).

Table 5. Formulation development of SR LD-EVA formulation.

	F1	F2	F3	F4
LD/%	40	10	10	10
EVA (72:28)/%	60	44.5	-	-
EVA (82:18)/%	-	-	25	39.5
PVA/%	-	44.5	64	-
Mannitol/%	-	-	-	10
PVP-VA/%	-	-	-	39.5
Fumed Silica/%	-	1	1	1

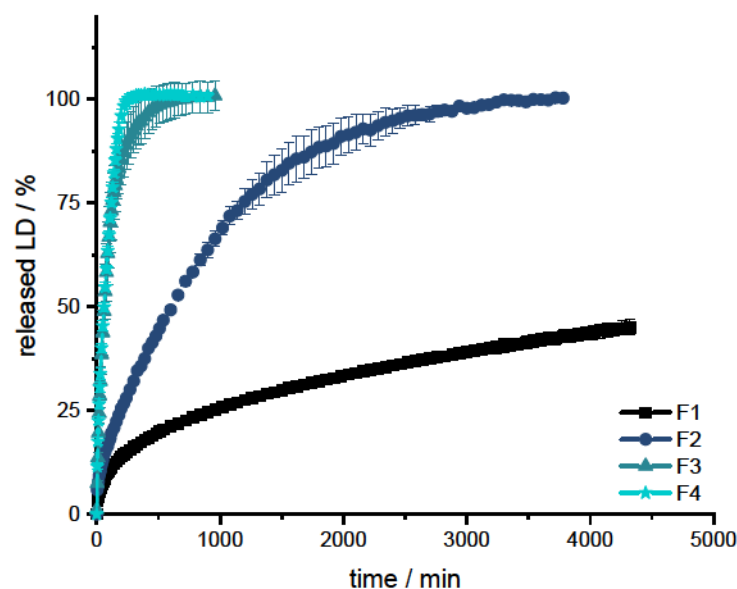


Figure 4. Dissolution of LD from F1, F2, F3 and F4; modified basket apparatus, 1000 mL 0.1 N HCl, 50 rpm, 37.0 ± 0.5 °C. $\bar{x} \pm s$; $n = 3$.

All formulations show a burst in the first few minutes. Subsequently, the API is released constantly over time until approximately 80% of LD has been released. Thereafter, the release of LD is slower and results in a plateau. The release profile can be described with Higuchi's square root-of-time kinetics [90–92]. First, the API, which is on the surface of the dosage form, is dissolved. The larger the surface, the more API goes directly into the solution. This results in what is known as a burst. The API is then released from the matrix. In the inert matrix, depending on the diffusion path, the amount of dissolved API remains constant over time. After a certain time, the diffusion paths for the API become longer and longer and less API is released over time until the plateau at 100% is reached.

The formulations F3 and F4 result in a fast release profile (50% released API in 60 min, 75% released API in 125 min), which may be advantageous when the dosage form is not gastro retentive, and the API must be fully released prior to small intestinal passage. However, since F3 dissolves and does not retain an inert matrix, F4 was used as orientation for the fixed-combination formulation. Formulations F1 and F2 released the API much more slowly (F1: 25% released API in 960 min; F2: 75% released API in 1200 min) and were thus not developed further.

From the obtained results, it could be concluded that the fixed-combination formulation should contain more than 25% EVA for the tablet to remain durable. In addition, PVP-VA was identified as a good pore former and stiffness enhancer for better printability. Since the desired release profile of the fixed combination should still be slower than displayed by F4, the amount of EVA could be increased.

3.3. Formulation Development for Fixed Combination LD/BZ

Based on the previously found formulation with 10% LD, different fixed combinations (FC) were now extruded. The EVA content was set above 30% to produce an inert, non-disintegrating matrix (Table 6). The API proportions were fixed, as they are dosed in a 4:1 ratio (LD:BZ). The maximum dose is 200 mg LD per tablet, which is equivalent to a 500 mg tablet at 40% content, which should be swallowable by patients and designable so that the dimensions of the dosage form are similar to those of tablets on the market. The PVP-VA content varied from 5–20%. The filaments with 20% PVP-VA (FC4) were too brittle and broke directly during cooling after HME, so that they could not be used for printing. The density measurements also reflect the EVA content. The higher the content of EVA in the filament, the lower the density.

Table 6. Formulation development of LD/BZ fixed combination (FC) formulation.

	FC1	FC2	FC3	FC4
LD/%	40	40	40	40
BZ/%	10	10	10	10
EVA (82:18)/%	44.5	39.5	34.5	29.5
PVP-VA/%	5	10	15	20
Fumed Silica/%	0.5	0.5	0.5	0.5
Density/g/cm ³	1.15	1.16	1.17	-

After extrusion, parts of the filaments were used for dissolution tests to assess which formulation was most likely to reproduce the desired release profile (SA/V : 2.3 mm^{-1}). Parallel quantification of LD and BZ is challenging, and the development of a suitable analytical method to quantify the APIs simultaneous in the presence of PDM is described in another publication [76]. As other publications have already shown, the release profiles of BZ and LD are comparable [93–97]. To simplify the analyses in the present study, the release profile of LD is also used as a surrogate for BZ release (Figure 5).

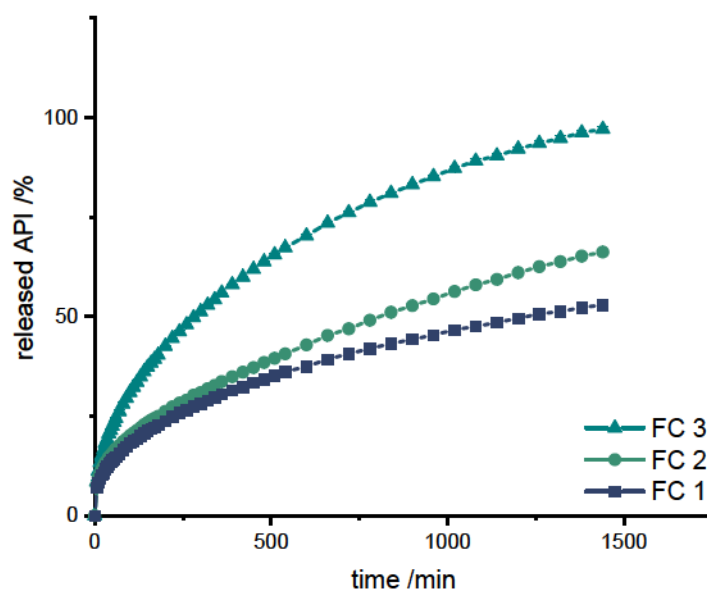


Figure 5. Dissolution of LD/BZ from FC1, FC2, and FC3; modified basket apparatus, 1000 mL 0.1 N HCl, 50 rpm, 37.0 ± 0.5 °C. $\bar{x} \pm s$; $n = 3$.

Also with these formulations, the release starts with a burst effect. Subsequently, the release of the APIs is more uniform. The diffusion paths within the filament strand are very short (\varnothing 1.75 mm), so that the decrease in the release rate towards the end is small.

The formulations FC 1+2 release the APIs too slow (FC 1: 50% API in 1260 min, FC 2: 50% API in 780 min), whereas FC 3 shows the fastest release course and displays the desired course (50% API in 290 min, 75% API in 720 min, 100% API in 1440 min).

3.4. Design and Dissolution of Polypill Tablet Variations

With the final LD-EVA filament formulation (FC3), and the beforehand developed PDM-PVA filament, different geometries with various PDM and LD/BZ contents were printed and released. The selected doses were adjusted to the dosages in available market preparations.

First, a simple polypill design was chosen (PP1) to observe the release behavior of the printed formulation (Figure 6 left). A cylinder with a diameter of 10 mm was selected as geometry, which should therefore also be easy to swallow (Figure 6 right). A LD/BZ dose of 50/12.5 mg was targeted, which corresponds to the lowest dose of tablets available on the market, as well as a PDM dose of 3.5 mg (Table 7). The release rate was calculated for the linear section of the profiles, after the burst until the end of the measurement (LD/BZ), or until the plateau was reached (PDM).

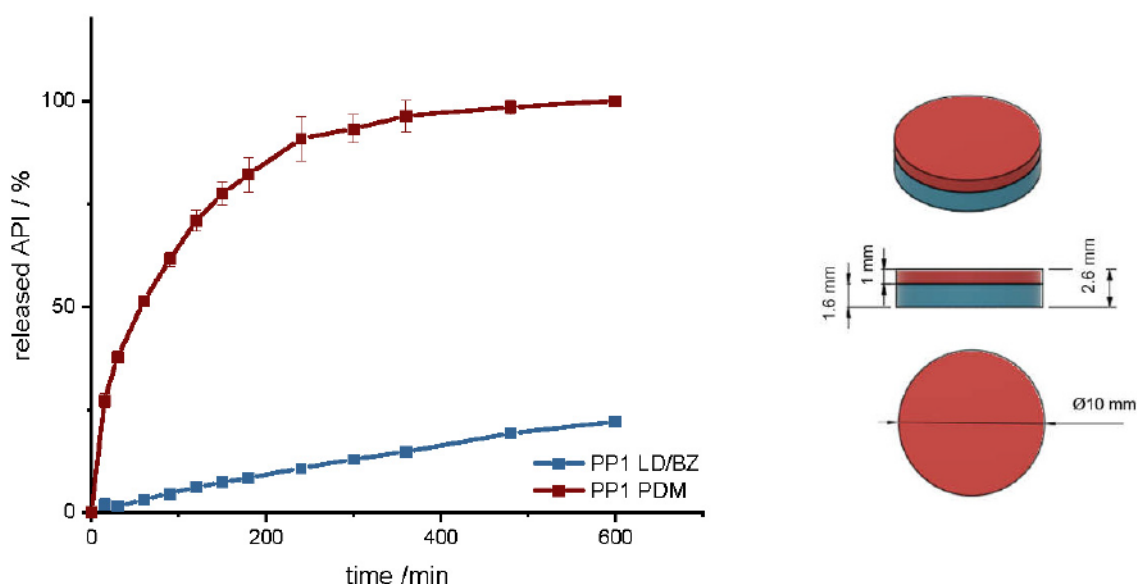


Figure 6. (Left): release profile of PP1; modified basket apparatus, 1000 mL 0.1 N HCl, 50 rpm, 37.0 ± 0.5 °C, $x \pm s$; $n = 3$. (Right): Image of PP1: red: PDM-PVA, blue: LD/BZ-EVA.

Table 7. Structure and release properties of PP1.

	LD/BZ	PDM
SA/V total/mm ⁻¹	1.2	
SA/V/mm ⁻¹	1.6	2.4
mg API/mg	50.0/12.5	3.5
% API in 600 min	22	100
t _{75%} /min	n.d.	140
MDT/min	n.d.	97
release rate/%/min	0.03	0.33

The geometry has a total SA/V ratio of 1.17 mm^{-1} . As the PDM-PVA formulation dissolves over time, the SA of the insoluble LD/BZ formulation increases to 1.65 mm^{-1} . The release of PDM can be described by the Peppas Sahlin equation [61]. The formulation releases the API by diffusion and erosion due to the formation of a hydrocolloid matrix [98].

Due to the layered structure of the FDM printed geometry, the medium can easily penetrate the cylinder and release the API from the individual strands. The formulation begins to swell and dissolve over time. The API can release through the layers and dissolve directly due to its good solubility. After 140 min, 75% PDM was released, and thus the dissolution profile can be categorized as prolonged release. The combination of LD/BZ is released very slowly from the SR polymer. The matrix is inert, and the APIs can only enter solution by diffusion. After 600 min, just 22% LD/BZ is released. The density of the entire PP1 is 1.18 g/cm^3 . Due to the low EVA density and most probably included pores, the buoyancy of the polypill is maintained (Figure 7). While the PDM-PVA layer (density 1.3 g/cm^3) dissolves over time, the remaining EVA-based part retains the floating property.



Figure 7. Floating properties of PP1 in 300 mL 0.1 N HCl, $37 \pm 0.5 \text{ }^\circ\text{C}$.

To increase the dose, a hollow cylinder-geometry (PP2) was designed that is built up in three layers, with a total SA/V ratio of 0.9 mm^{-1} (Table 8). The SA/V ratio was kept similar to PP1 to see if it is possible to increase the dose without strongly affecting the overall release. This is of particular importance for personalized therapy [63]. The PDM filament was printed between two LD/BZ-EVA hollow cylinder layers, so that these two hollow cylinders can detach from each other after a while due to the solubility of PDM-PVA-compartment and further increase the SA of the geometry during release to a SA/V ratio of 1.3 mm^{-1} (Figure 8).

Table 8. Structure and release properties of PP2.

	LD/BZ	PDM
SA/V total/ mm^{-1}	0.9	
SA/V/ mm^{-1}	1.3	2.6
mg API/mg	83/20.75	3.5
SA/V/ mm^{-1}	1.2	-
mg API/mg	97/24.25	-
%API in 600 min	21	100
$t_{75\%}/\text{min}$	n.d.	310
MDT/min	n.d.	187
release rate/%/min	0.02	0.20

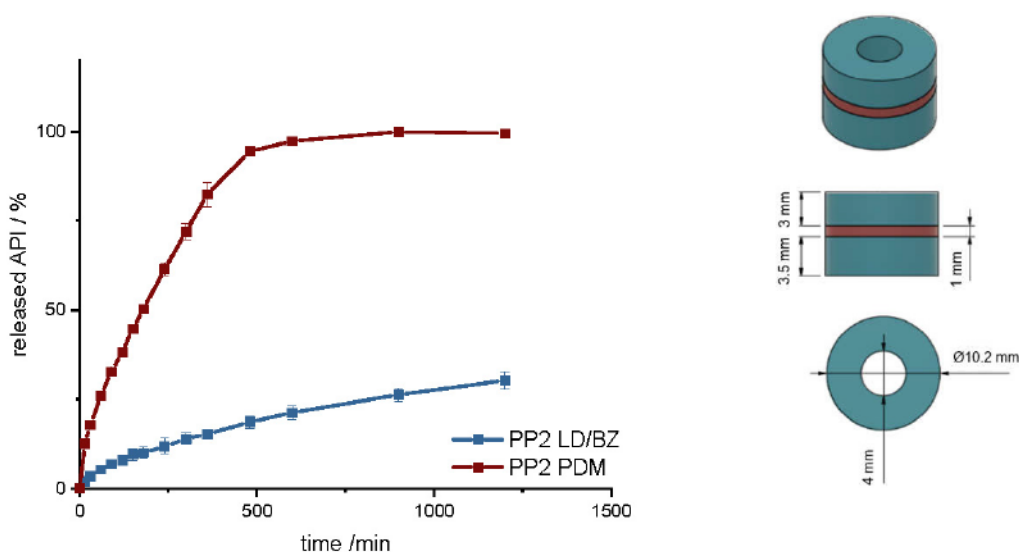


Figure 8. (Left): release profile of PP2; modified basket apparatus, 1000 mL 0.1 N HCl, 50 rpm, 37.0 ± 0.5 °C, $x \pm s$; $n = 3$. (Right): Image of PP2: red: PDM-PVA, blue: LD/BZ-EVA.

Compared to PP1, PDM is released more slowly here. This is due to the enclosed SA of the two LD/BZ hollow cylinders. The LD/BZ release curve is very similar to PP1 (f_2 : 87.5). Here, 21% API is also released in 600 min. Due to the small outer SA of the PVA formulation in contact with the medium (24% of the SA), the separation of the layers could not proceed as quickly as desired, so that the increase in SA due to the separation of the hollow cylinders occurred late and thus did not lead to a faster API dissolution. In addition, it was observed that during printing of the PVA layer, EVA residues were still present in the print head, which were rinsed out despite the intermediate cleaning step and thus contaminated the PVA layer with EVA. The total density of the PP2 is 1.1 g/cm^3 . Despite the large shape, the dosage form floats on the medium, again most likely because of air entrapped in the structure (Figure 9). If the PDM-PVA layer between the LD/BZ-EVA-hollow cylinders dissolves, both parts (hollow cylinders with LD/BZ-EVA) float on the surface of the medium.



Figure 9. Floating properties of PP2 in 300 mL 0.1 N HCl, 37 ± 0.5 °C.

In another polypill design (PP3), the PDM dose was changed. The total SA/V ratio was kept similar to PP1 and PP2. PP3 design was a hollow cylinder, this time with a small cylinder as inlay printed with the PDM-PVA filament (Figure 10). PDM-PVA was low-dosed with 1.5 mg and LD/BZ-EVA had a content of 50/12.5 mg (Table 9).

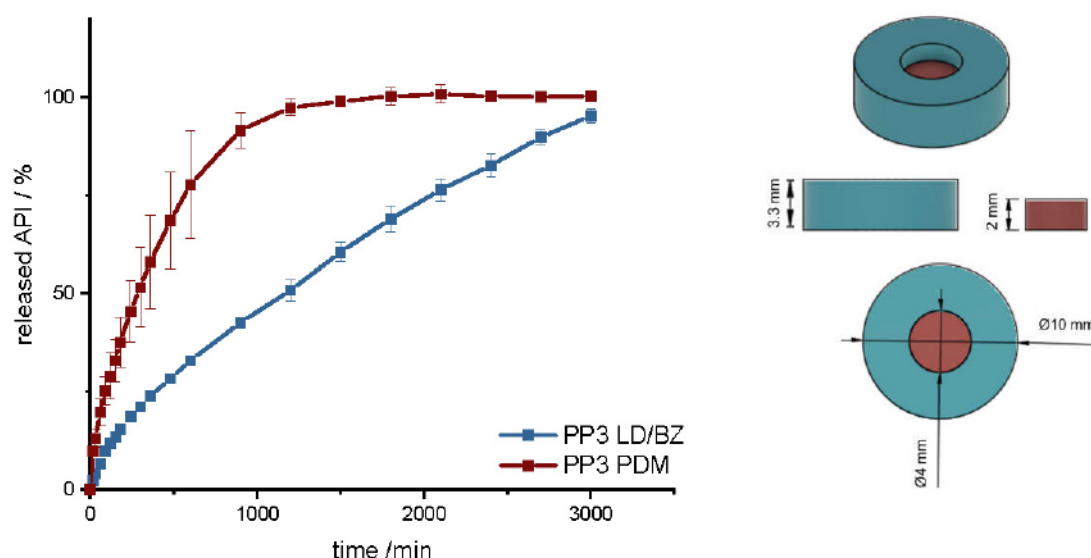


Figure 10. (Left): release profile of PP3; modified basket apparatus, 1000 mL 0.1 N HCl, 50 rpm, 37.0 ± 0.5 °C, $x \pm s$; $n = 3$. (Right): Image of PP3: red: PDM-PVA, blue: LD/BZ-EVA.

Table 9. Structure and release properties of PP3.

	LD/BZ	PDM
SA/V total/mm ⁻¹	1.1	
SA/V/mm ⁻¹	1.3	2.0
mg API/mg	50.0 / 12.5	1.5
% API in 600 min	33	75
t _{75%} /min	2100	600
MDT/min	1130	360
release rate/%/min	0.03	0.11

To represent the complete release profile, the time of the dissolution test was extended to 3000 min. In this design, PDM was released very slowly. Despite a comparable SA/V ratio to PP1 and PP2, only 75% PDM was released within 600 min. The SA in contact with the medium was limited to 50%, so the SA in the complete design was reduced by the hollow cylinder from the EVA formulation. In addition, a filament change had to be performed for every single layer in this geometry, which again resulted in carryover of EVA into the PVA layers. For the LD/BZ-EVA formulation, a constant drug release after the burst could be realized with this design. With a release rate of 0.03% API/min, the release profile is comparable to PP1 and PP2, which was desired with the choice of SA/V ratio (f_2 : 60.1). The total density of the PP3 is 1.1 g/cm³. It also floats on the surface of the medium and maintains this property over the time of release.

With these geometries, it is possible to achieve a prolonged gastro-retentive API release for various dosages, which allows a larger time interval for drug absorption. In addition, due to the different geometric forms but comparable SA/V ratios, it is possible to vary the dosages from 50/12.5 mg–200/50 mg LD/BZ but keep the release profile similar ($f_2 > 50$). However, the release profile of the LD/BZ combination is very slow (75% LD/BZ in 2100 min). For patients who need to respond more specifically to LD/BZ spikes, a 24 h ingestion-interval is not an option. In addition, the selected tablet sizes are not advantageous for patients with swallowing difficulties. Therefore, the possibility of printing mini tablets was also investigated in this study.

3.5. Design and Dissolution of Polypill Mini Tablet Variations

With mini tablets, the dose can be finely adjusted by the patient himself by the selected number of mini tablets. Since the diameter is ≤ 5 mm, these dosage forms are easy to swallow [99,100].

First, a mini tablet (MiniTab) was printed with the dimensions of 4 mm in diameter and 3.6 mm in height (Figure 11 and Figure S1, Supplementary Material). The dose of LD/BZ was reduced to 15/3.75 mg per mini tablet, so the patient can adjust the desired LD/BZ dose in 15/3.75 mg steps by the number of tablets (Table 10). The dose of PDM was set to 0.375 mg, which represents the smallest dose in market preparations for SR. Therefore, the therapy can be adapted in small discreet steps.

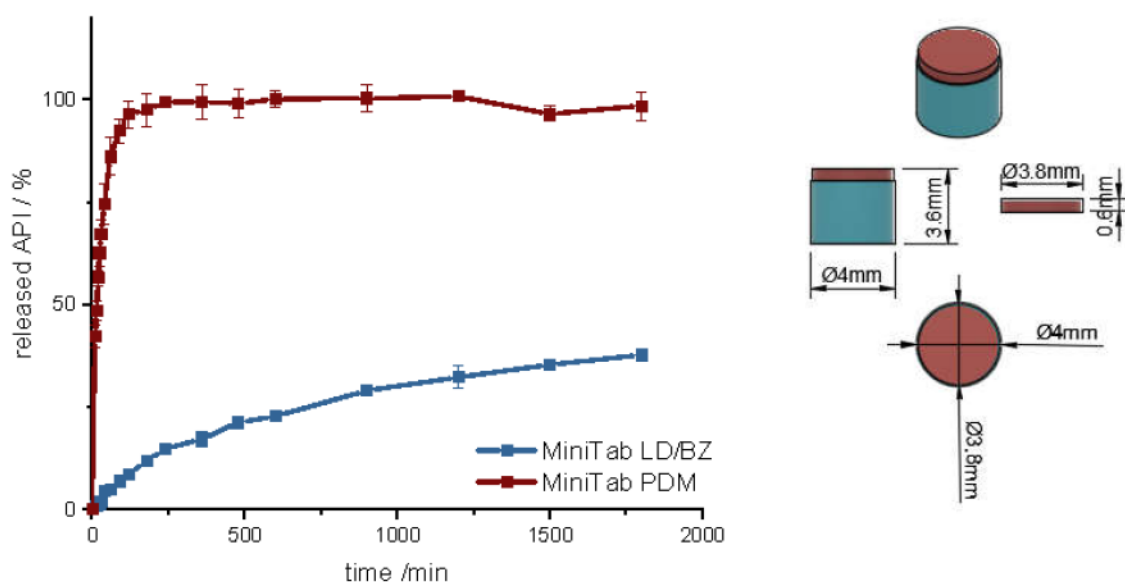


Figure 11. (Left): release profile of polypill design MiniTab; modified basket apparatus, 1000 mL 0.1 N HCl, 50 rpm, 37.0 ± 0.5 °C, $\bar{x} \pm s$; $n = 3$. (Right): Image of MiniTab: red: PDM-PVA, blue: LD/BZ-EVA.

Table 10. Structure and release properties of MiniTab.

	LD/BZ	PDM
SA/V total/mm ⁻¹	2.1	
SA/V/mm ⁻¹	1.6	4.4
mg API/mg	15/3.75	0.375
% API in 600 min	22.7	100
t _{75%} /min	n.d.	40
MDT/min	n.d.	26
release rate/%/min	0.02	0.80

The release of PDM is fast (100% PDM in 60 min). The small cylinder can be well covered by the medium, so that the API is quickly released from the matrix and the PDM-PVA cylinder can be well dissolved. The release of LD/BZ is again comparable to PP1-PP3 (f_2 : 80.3). 23% API was released in 600 min, and the release rate is 0.02% API/ min. With the MiniTab design, it would therefore be possible to reproduce the same release rate as with PP1-PP3, but the dose can be individually adjusted in small steps. In addition, PDM is released much faster with this form, so that any OFF phases of the patient can be treated quickly. Due to the low density (1.1 g/cm³), as well as the low volume likely in combination with entrapped air, this dosage form also floats on the surface of the medium and can thus be used as a gastro-retentive dosage form.

To increase the release rate of the LD/BZ combination, a SA/V ratio of 4.7 mm⁻¹ was targeted with the next design. Therefore, a mini-hollow cylinder (MiniHC) with a dose of 10 mg LD and the appropriate SA/V ratio was printed. The interior was filled with a cross of PDM-PVA (Figure 12, Figures S2 and S3). This design allows for maximum circulation of the medium around both formulations. In addition, the dose of PDM can be varied by the height of the cross, or with a different design, which can be inserted into the hollow

cylinder. The variation in height was tested with two different PDM-doses (Table 11). Figure 12 shows the release of MiniHC with cross with 0.4 mg PDM (MiniHCwC1, Top) and bottom shows the release of MiniHCwC2 with 1.5 mg PDM.

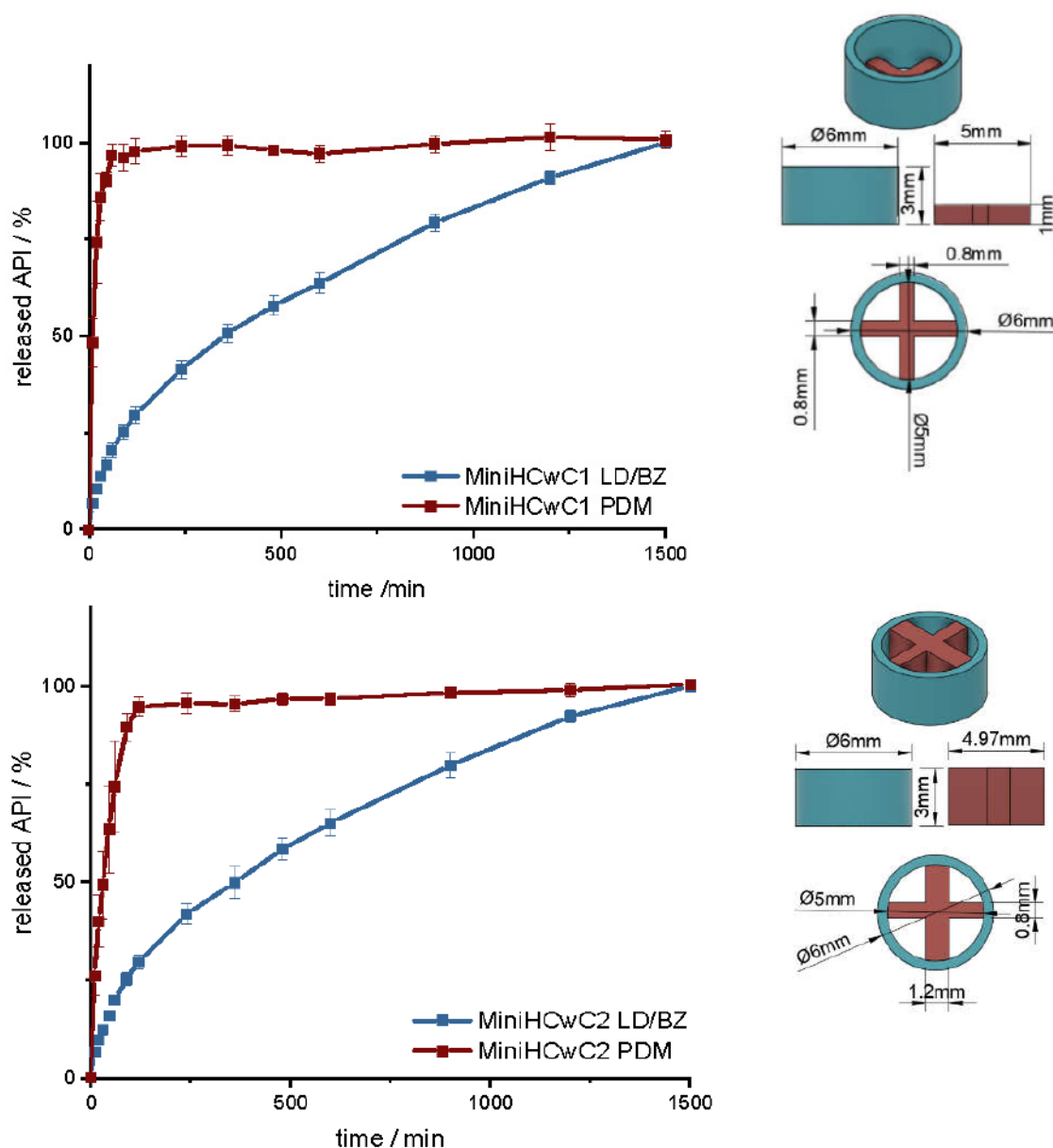


Figure 12. (Left): release profile of MiniHCwC 1 (top) and 2 (bottom); modified basket apparatus, 1000 mL 0.1 N HCl, 50 rpm, 37.0 ± 0.5 °C, $x \pm s$; $n = 3$. (Right): Image of MiniHCwC1 + 2: red: PDM-PVA, blue: LD/BZ-EVA.

Table 11. Structure and release properties of MiniHC with a cross.

	LD/BZ 1 + 2	PDM 1	PDM 2
SA/V total/mm ⁻¹	-	4.7 with LD/BZ	3.7 with LD/BZ
SA/V/mm ⁻¹	4.7	4.6	2.9
mg API/mg	10/2.5	0.4	1.5
% API in 600 min	65	100	100
t _{75%} /min	750	20	60
MDT/min	363	14	28
release rate/%/min	0.07	1.88	0.95

The LD/BZ release shows the same dissolution profile in both MiniHC versions. First, a burst is seen; then, the API is released continuously over time at a rate of 0.07% API/min. Due to the low wall thickness of the HC (1 mm) and the resulting short diffusion pathways for the APIs, the release profile remains constant over a long time and the release rate hardly decreases towards the end. With a released API fraction of 75% LD/BZ in 750 min, this release profile corresponds to the initially desired course. The PDM release is faster and differs in both variations. This was expected due to the various SA/V ratios. The printed cross with 0.4 mg PDM (PDM1, Table 11) has almost twice the SA/V ratio than the cross with 1.5 mg PDM (PDM2). Thus, the MDT is half as big, and the drug is released faster. This design makes it possible to insert various designs of other filaments, various SA/V ratios, and APIs, and to combine different release profiles. The inserted geometries can also be printed and inserted individually, independently of the outer hollow cylinder, so that there is no cross-contamination or mixing of the filaments. The floating property of the formulation allows prolongation of the GRT, a continuous release of the API and thus a saturation of the amino acid transporters in the upper small intestine section with LD (Figure 13). The small diameter and height, as well as the flexibility of the structure facilitate the swallowing of the 3D printed form for the Parkinson's patients. This allows the therapy to be individually adapted to the patient.

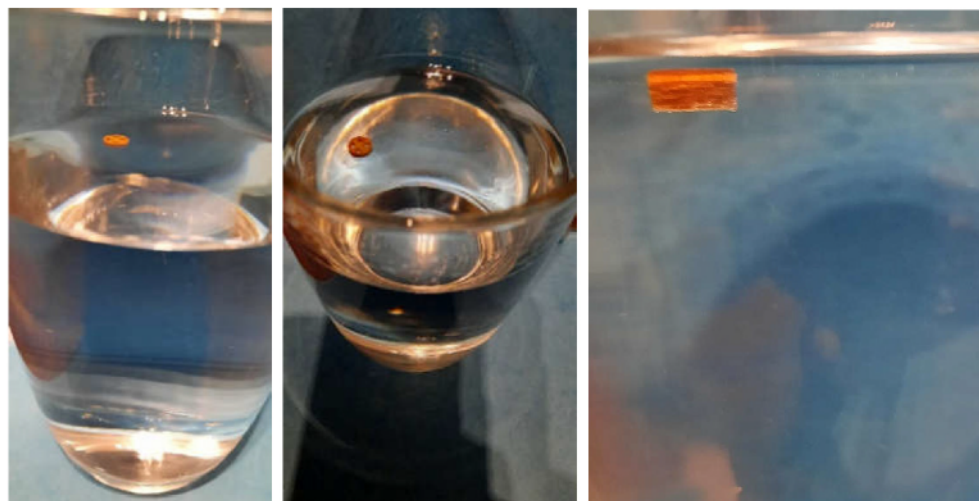


Figure 13. Floating properties of MiniHCwC in 300 mL 0.1 N HCl, 37 ± 0.5 °C.

4. Conclusions

In this study, the first printed oral dosage form with PDM/LD/BZ was developed. VCM was used as another new technology that is very useful to study the release properties of polymers without the influence of SA/V ratio. HME was used to prepare a fixed-combination of two drugs, and the FDM 3D printing process allowed the filament with the fixed-combination to be combined with another drug-loaded filament in variable dosages. In addition, the FDM 3D printing process enables variation of the SA/V ratio through the variety of possible geometries, as well as the incorporation of different layers and pores, all of which have an impact on the drug release process. Thus, not only the dose but also the onset and duration of the effect can be influenced. This approach makes it possible to address the individual needs of Parkinson's patients, titrating the dose and increasing or decreasing it in small steps as needed. In this study, it was possible to increase the LD/BZ dose from 15–180 mg LD (3.75–107 mg BZ) and achieve a similar release profile ($f_2 > 50$). In addition, mini tablets and mini hollow cylinders were printed, which might be easier for Parkinson's patients to swallow and can be varied in number for ingestion so that the dose can be adjusted to the situation and the daily dose, to respond to ON-OFF-phenomena. Furthermore, the formulation has a low density, resulting in a floating property, which was used to prolong GRT. For drugs that are absorbed in the upper part of the small intestine,

this increases the time of API absorption, and thus the medicine intake interval is increased. This improves patient adherence to their therapy.

The choice of polymer resulted in a very slow release; further studies may test whether the results can be achieved with other polymers. In addition, the polypill was prepared only with well water-soluble APIs. It would also be interesting to see how such a combination behaves with APIs of different BCS classes.

Supplementary Materials: The following supporting information can be downloaded at: <https://www.mdpi.com/article/10.3390/pharmaceutics14050931/s1>, Figure S1: Dimensions of *MiniTab*: 4.93 mm in diameter, deviation of 0.07 mm to the CAD model; Figure S2: Dimensions of *MiniHCwC*: 6.03 mm in diameter, deviation of 0.03 mm to the CAD model; Figure S3: Images of *MiniHCwC1* (left) and *MiniHCwC2* (right).

Author Contributions: H.W.: conceptualization, data curation, methodology, investigation, visualization, formal analysis, writing—original draft preparation; R.C.: resources, validation, methodology, writing—review and editing; J.B.: conceptualization, writing—review and editing; J.Q.: supervision, project administration, writing—review and editing. All authors have read and agreed to the published version of the manuscript.

Funding: This research was funded by Bundesministerium für Bildung und Forschung—Project ‘ProMat Leben—Polymere’ ‘PolyPrint’, Project no.: 13XP5064B.

Institutional Review Board Statement: Not applicable.

Informed Consent Statement: Not applicable.

Acknowledgments: The authors want to thank Alessandro Guiseppe Elia and Thomas Kipping for the VCM platelet preparation and Andrea Michel for density measurements. We also thank Merck KGaA and TER Chemicals for providing large quantities of PVA and EVA. This work is associated and funded by the Bundesministerium für Bildung und Forschung—Projekt ‘ProMat Leben—Polymere’ ‘PolyPrint’ (Project no.: 13XP5064B).

Conflicts of Interest: The authors declare no conflict of interest. The funders had no role in the design of the study; in the collection, analyses, or interpretation of data; in the writing of the manuscript, or in the decision to publish the results.

References

1. The World Bank. Population Ages 65 and above (% of Total Population). Available online: <https://data.worldbank.org/indicator/SP.POP.65UP.TO.ZS> (accessed on 6 February 2022).
2. BiB-Fakten. Anteil Junger Und Älterer Menschen an Der Bevölkerung, Welt (1950–2020). Available online: <https://www.bib.bund.de/DE/Fakten/Fakt/W04-Junge-aeltere-Menschen-Welt-ab-1950.html> (accessed on 6 February 2022).
3. Rochon, P.A.; Petrovic, M.; Cherubini, A.; Onder, G.; O’Mahony, D.; Sternberg, S.A.; Stall, N.M.; Gurwitz, J.H. Polypharmacy, Inappropriate Prescribing and Deprescribing in Older People: Through a Sex and Gender Lens. *Lancet Healthy Longev.* **2021**, *2*, e290–e300. [CrossRef]
4. Ludwig, W.-D.; Mühlbauer, B.; Seifert, R. *Arzneiverordnungs-Report 2021*; Springer: Berlin/Heidelberg, Germany, 2021; Volume 1, ISBN 978-3-662-63825-5.
5. Vrdoljak, D.; Borovac, J.A. Medication in the Elderly—Considerations and Therapy Prescription Guidelines. *Acta Med. Acad.* **2015**, *44*, 159–168. [CrossRef] [PubMed]
6. Milton, J.C.; Hill-Smith, I.; Jackson, S.H.D. Prescribing for Older People. *BMJ Br. Med. J.* **2008**, *336*, 606–609. [CrossRef] [PubMed]
7. Mehta, R.S.; Kochar, B.D.; Kennelty, K.; Ernst, M.E.; Chan, A.T. Emerging Approaches to Polypharmacy among Older Adults. *Nat. Aging* **2021**, *1*, 347–356. [CrossRef]
8. Drenth-van Maanen, A.C.; Wilting, I.; Jansen, P.A.F. Prescribing Medicines to Older People—How to Consider the Impact of Ageing on Human Organ and Body Functions. *Br. J. Clin. Pharmacol.* **2020**, *86*, 1921–1930. [CrossRef] [PubMed]
9. Barat, I.; Andreassen, F.; Damsgaard, E.M.S. Drug Therapy in the Elderly: What Doctors Believe and Patients Actually Do. *Br. J. Clin. Pharmacol.* **2001**, *51*, 615–622. [CrossRef]
10. Chang, T.I.; Park, H.; Kim, D.W.; Jeon, E.K.; Rhee, C.M.; Kalantar-Zadeh, K.; Kang, E.W.; Kang, S.W.; Han, S.H. Polypharmacy, Hospitalization, and Mortality Risk: A Nationwide Cohort Study. *Sci. Rep.* **2020**, *10*, 18964. [CrossRef]
11. Fuster, V.; Gambús, F.; Patriciello, A.; Hamrin, M.; Grobbee, D.E. The Polypill Approach—An Innovative Strategy to Improve Cardiovascular Health in Europe. *BMC Pharmacol. Toxicol.* **2017**, *18*, 10. [CrossRef]
12. Sleight, P.; Pouleur, H.; Zannad, F. Benefits, Challenges, and Registerability of the Polypill. *Eur. Heart J.* **2006**, *27*, 1651–1656. [CrossRef]

13. Obeso, J.A.; Stamelou, M.; Goetz, C.G.; Poewe, W.; Lang, A.E.; Weintraub, D.; Burn, D.; Halliday, G.M.; Bezzard, E.; Przedborski, S.; et al. Past, Present, and Future of Parkinson's Disease: A Special Essay on the 200th Anniversary of the Shaking Palsy. *Mov. Disord.* **2017**, *32*, 1264–1310. [\[CrossRef\]](#)
14. Poewe, W.; Seppi, K.; Tanner, C.M.; Halliday, G.M.; Brundin, P.; Volkmann, J.; Schrag, A.E.; Lang, A.E. Parkinson Disease. *Nat. Rev. Dis. Primers* **2017**, *3*, 17013. [\[CrossRef\]](#)
15. Charvin, D.; Medori, R.; Hauser, R.A.; Rascol, O. Therapeutic Strategies for Parkinson Disease: Beyond Dopaminergic Drugs. *Nat. Rev. Drug Discov.* **2018**, *17*, 804–822. [\[CrossRef\]](#) [\[PubMed\]](#)
16. Heinzel, S.; Berg, D.; Binder, S.; Ebersbach, G.; Hickstein, L.; Herbst, H.; Lorrain, M.; Wellach, I.; Mätzler, W.; Petersen, G.; et al. Do We Need to Rethink the Epidemiology and Healthcare Utilization of Parkinson's Disease in Germany? *Front. Neurol.* **2018**, *9*, 500. [\[CrossRef\]](#) [\[PubMed\]](#)
17. Dorsey, E.R.; Elbaz, A.; Nichols, E.; Abd-Allah, F.; Abdelalim, A.; Adsuar, J.C.; Ansha, M.; Brayne, C.; Choi, J.-Y.; Collado-Mateo, D.; et al. Global, Regional, and National Burden of Parkinson's Disease, 1990–2016: A Systematic Analysis for the Global Burden of Disease Study 2016. *Lancet Neurol.* **2018**, *17*, 939–953. [\[CrossRef\]](#)
18. Hornykiewicz, O. The Discovery of Dopamine Deficiency in the Parkinsonian Brain. *J. Neural Transm. Suppl.* **2006**, *70*, 9–15. [\[CrossRef\]](#)
19. Jankovic, J. Parkinson's Disease: Clinical Features and Diagnosis. *J. Neurol. Neurosurg. Psychiatry* **2008**, *79*, 368–376. [\[CrossRef\]](#)
20. Dauer, W.; Przedborski, S. Parkinson's Disease: Mechanisms and Models. *Neuron* **2003**, *39*, 889–909. [\[CrossRef\]](#)
21. Lees, A.J.; Hardy, J.; Revesz, T. Parkinson's Disease. *Lancet* **2009**, *373*, 2055–2066. [\[CrossRef\]](#)
22. Parkinson, J. An Essay on the Shaking Palsy. 1817. *J. Neuropsychiatry Clin. Neurosci.* **2002**, *14*, 223–236. [\[CrossRef\]](#)
23. Deutsche Gesellschaft für Neurologie (DGN). S3 Leitlinie Idiopathisches Parkinson-Syndrom. *AWMF-Regist. Nr.* **2016**, *1*, 1–77.
24. Cotzias, G.C.; Papavasiliou, P.S.; Gellene, R. Modification of Parkinsonism—Chronic Treatment with L-Dopa. *N. Engl. J. Med.* **1969**, *280*, 337–345. [\[CrossRef\]](#)
25. Olanow, C.W.; Koller, W.C. An Algorithm (Decision Tree) for the Management of Parkinson's Disease: Treatment Guidelines. *Neurology* **1998**, *50* (Suppl. S3), S1–S88. [\[CrossRef\]](#) [\[PubMed\]](#)
26. Poewe, W. Should Treatment of Parkinson's Disease Be Started with a Dopamine Agonist? *Neurology* **1998**, *51*, S21–S24. [\[CrossRef\]](#) [\[PubMed\]](#)
27. Rascol, O.; Brooks, D.J.; Korczyn, A.D.; de Deyn, P.P.; Clarke, C.E.; Lang, A.E. A Five-Year Study of the Incidence of Dyskinesia in Patients with Early Parkinson's Disease Who Were Treated with Ropinirole or Levodopa. *N. Engl. J. Med.* **2000**, *342*, 1484–1491. [\[CrossRef\]](#) [\[PubMed\]](#)
28. Hauser, R.A. Levodopa: Past, Present, and Future. *Eur. Neurol.* **2009**, *62*, 1–8. [\[CrossRef\]](#) [\[PubMed\]](#)
29. Fahn, S. Levodopa-Induced Neurotoxicity: Does It Represent a Problem for the Treatment of Parkinson's Disease? *CNS Drugs* **1997**, *8*, 376–393. [\[CrossRef\]](#)
30. Ahlskog, J.E.; Muenter, M.D. Frequency of Levodopa-Related Dyskinesias and Motor Fluctuations as Estimated from the Cumulative Literature. *Mov. Disord.* **2001**, *16*, 448–458. [\[CrossRef\]](#)
31. Olanow, C.W.; Kieburtz, K.; Odin, P.; Espay, A.J.; Standaert, D.G.; Fernandez, H.H.; Vanaganas, A.; Othman, A.A.; Widnell, K.L.; Robieson, W.Z.; et al. Continuous Intrajejunal Infusion of Levodopa-Carbidopa Intestinal Gel for Patients with Advanced Parkinson's Disease: A Randomised, Controlled, Double-Blind, Double-Dummy Study. *Lancet Neurol.* **2014**, *13*, 141–149. [\[CrossRef\]](#)
32. Senek, M.; Nielsen, E.I.; Nyholm, D. Levodopa-Entacapone-Carbidopa Intestinal Gel in Parkinson's Disease: A Randomized Crossover Study. *Mov. Disord.* **2017**, *32*, 283–286. [\[CrossRef\]](#)
33. Pålhagen, S.E.; Sydow, O.; Johansson, A.; Nyholm, D.; Holmberg, B.; Widner, H.; Dizdar, N.; Linder, J.; Hauge, T.; Jansson, R.; et al. Levodopa-Carbidopa Intestinal Gel (LCIG) Treatment in Routine Care of Patients with Advanced Parkinson's Disease: An Open-Label Prospective Observational Study of Effectiveness, Tolerability and Healthcare Costs. *Parkinsonism Relat. Disord.* **2016**, *29*, 17–23. [\[CrossRef\]](#)
34. Rascol, O.; Azulay, J.P.; Blin, O.; Bonnet, A.-M.; Brefel-Courbon, C.; Césaro, P.; Damier, P.; Debilly, B.; Durif, F.; Galitzky, M.; et al. Orodispersible Sublingual Piribedil to Abort OFF Episodes: A Single Dose Placebo-Controlled, Randomized, Double-Blind, Cross-over Study. *Mov. Disord.* **2010**, *25*, 368–376. [\[CrossRef\]](#) [\[PubMed\]](#)
35. Lai, K.L.; Fang, Y.; Han, H.; Li, Q.; Zhang, S.; Li, H.Y.; Chow, S.F.; Lam, T.N.; Lee, W.Y.T. Orally-Dissolving Film for Sublingual and Buccal Delivery of Ropinirole. *Colloids Surf. B Biointerfaces* **2018**, *163*, 9–18. [\[CrossRef\]](#) [\[PubMed\]](#)
36. Arora, S.; Ali, J.; Ahuja, A.; Khar, R.K.; Baboota, S. Floating Drug Delivery Systems: A Review. *AAPS PharmSciTech* **2005**, *6*, E372–E390. [\[CrossRef\]](#) [\[PubMed\]](#)
37. Jansen, E.N.H.; Meerwaldt, J.D. Madopar HBS in Parkinson Patients with Nocturnal Akinesia. *Clin. Neurol. Neurosurg.* **1988**, *90*, 35–39. [\[CrossRef\]](#)
38. Schapira, A.H.V.; Bezzard, E.; Brotchie, J.; Calon, F.; Collingridge, G.L.; Ferger, B.; Hengerer, B.; Hirsch, E.; Jenner, P.; Le Novère, N.; et al. Novel Pharmacological Targets for the Treatment of Parkinson's Disease. *Nat. Rev. Drug Discov.* **2006**, *5*, 845–854. [\[CrossRef\]](#)
39. LeWitt, P.A.; Giladi, N.; Navon, N. Pharmacokinetics and Efficacy of a Novel Formulation of Carbidopa-Levodopa (Accordion Pill®) in Parkinson's Disease. *Parkinsonism Relat. Disord.* **2019**, *65*, 131–138. [\[CrossRef\]](#)

40. Sharma, S.; Lohan, S.; Murthy, R.S.R. Formulation and Characterization of Intranasal Mucoadhesive Nanoparticulates and Thermo-Reversible Gel of Levodopa for Brain Delivery. *Drug Dev. Ind. Pharm.* **2014**, *40*, 869–878. [\[CrossRef\]](#)
41. Bartus, R.T.; Emerich, D.; Snodgrass-Belt, P.; Fu, K.; Salzberg-Brenhouse, H.; Lafreniere, D.; Novak, L.; Lo, E.S.; Cooper, T.; Basile, A.S. A Pulmonary Formulation of L-Dopa Enhances Its Effectiveness in a Rat Model of Parkinson's Disease. *J. Pharmacol. Exp. Ther.* **2004**, *310*, 828–835. [\[CrossRef\]](#)
42. Bahrainian, S.; Mirmoeini, M.S.; Gilani, Z.; Gilani, K. Engineering of Levodopa Inhalable Microparticles in Combination with Leucine and Dipalmitoylphosphatidylcholine by Spray Drying Technique. *Eur. J. Pharm. Sci.* **2021**, *167*, 106008. [\[CrossRef\]](#)
43. Shankar, J.K.M.G.; Wilson, B. Potential Applications of Nanomedicine for Treating Parkinson's Disease. *J. Drug Deliv. Sci. Technol.* **2021**, *66*, 102793. [\[CrossRef\]](#)
44. Ahmad, J.; Haider, N.; Khan, M.A.; Md, S.; Alhakamy, N.A.; Ghoneim, M.M.; Alshehri, S.; Imam, S.S.; Ahmad, M.Z.; Mishra, A. Novel Therapeutic Interventions for Combating Parkinson's Disease and Prospects of Nose-to-Brain Drug Delivery. *Biochem. Pharmacol.* **2022**, *195*, 114849. [\[CrossRef\]](#) [\[PubMed\]](#)
45. Kar, K.; Pal, R.N.; Bala, N.N.; Nandi, G. Evaluation of Stability of Ropinirole Hydrochloride and Pramipexole Dihydrochloride Microspheres at Accelerated Condition. *Int. J. Appl. Pharm.* **2018**, *10*, 82–86. [\[CrossRef\]](#)
46. Li, S.; Liu, J.; Zhang, X.; Li, G. Near-Infrared Light-Responsive, Pramipexole-Loaded Biodegradable PLGA Microspheres for Therapeutic Use in Parkinson's Disease. *Eur. J. Pharm. Biopharm.* **2019**, *141*, 1–11. [\[CrossRef\]](#) [\[PubMed\]](#)
47. Subbarao, K.; Suresh, G. Preparation and Evaluation of Floating Microspheres of Pramipexole HCL-Review Article. *Am. J. Pharm. Tech. Res.* **2018**, *8*, 44–58. [\[CrossRef\]](#)
48. Skowrya, J.; Pietrzak, K.; Alhnan, M.A. Fabrication of Extended-Release Patient-Tailored Prednisolone Tablets via Fused Deposition Modelling (FDM) 3D Printing. *Eur. J. Pharm. Sci.* **2015**, *68*, 11–17. [\[CrossRef\]](#) [\[PubMed\]](#)
49. Goyanes, A.; Robles Martinez, P.; Buanz, A.; Basit, A.W.; Gaisford, S. Effect of Geometry on Drug Release from 3D Printed Tablets. *Int. J. Pharm.* **2015**, *494*, 657–663. [\[CrossRef\]](#)
50. Sadia, M.; Arafat, B.; Ahmed, W.; Forbes, R.T.; Alhnan, M.A. Channelled Tablets: An Innovative Approach to Accelerating Drug Release from 3D Printed Tablets. *J. Control. Release* **2018**, *269*, 355–363. [\[CrossRef\]](#)
51. Sun, Y.; Soh, S. Printing Tablets with Fully Customizable Release Profiles for Personalized Medicine. *Adv. Mater.* **2015**, *27*, 7847–7853. [\[CrossRef\]](#)
52. Than, Y.M.; Titapiwatanakun, V. Tailoring Immediate Release FDM 3D Printed Tablets Using a Quality by Design (QbD) Approach. *Int. J. Pharm.* **2021**, *599*, 120402. [\[CrossRef\]](#)
53. Duranović, M.; Obeid, S.; Madžarević, M.; Cvijić, S.; Ibrić, S. Paracetamol Extended Release FDM 3D Printlets: Evaluation of Formulation Variables on Printability and Drug Release. *Int. J. Pharm.* **2021**, *592*, 120053. [\[CrossRef\]](#)
54. Okwuosa, T.C.; Pereira, B.C.; Arafat, B.; Cieszyńska, M.; Isreb, A.; Alhnan, M.A. Fabricating a Shell-Core Delayed Release Tablet Using Dual FDM 3D Printing for Patient-Centred Therapy. *Pharm. Res.* **2017**, *34*, 427–437. [\[CrossRef\]](#) [\[PubMed\]](#)
55. Quodbach, J.; Bogdahn, M.; Breitzkreutz, J.; Chamberlain, R.; Eggenreich, K.; Elia, A.G.; Gottschalk, N.; Gunkel-Grabole, G.; Hoffmann, L.; Kapote, D.; et al. Quality of FDM 3D Printed Medicines for Pediatrics: Considerations for Formulation Development, Filament Extrusion, Printing Process and Printer Design. *Ther. Innov. Regul. Sci.* **2021**, *1*, 1–19. [\[CrossRef\]](#) [\[PubMed\]](#)
56. Schneider, C.; Langer, R.; Loveday, D.; Hair, D. Applications of Ethylene Vinyl Acetate Copolymers (EVA) in Drug Delivery Systems. *J. Control. Release* **2017**, *262*, 284–295. [\[CrossRef\]](#) [\[PubMed\]](#)
57. Genina, N.; Holländer, J.; Jukarainen, H.; Mäkilä, E.; Salonen, J.; Sandler, N. Ethylene Vinyl Acetate (EVA) as a New Drug Carrier for 3D Printed Medical Drug Delivery Devices. *Eur. J. Pharm. Sci.* **2016**, *90*, 53–63. [\[CrossRef\]](#) [\[PubMed\]](#)
58. Goyanes, A.; Kobayashi, M.; Martínez-Pacheco, R.; Gaisford, S.; Basit, A.W. Fused-Filament 3D Printing of Drug Products: Microstructure Analysis and Drug Release Characteristics of PVA-Based Caplets. *Int. J. Pharm.* **2016**, *514*, 290–295. [\[CrossRef\]](#)
59. Ibrahim, M.; Barnes, M.; McMillin, R.; Cook, D.W.; Smith, S.; Halquist, M.; Wijesinghe, D.; Roper, T.D. 3D Printing of Metformin HCl PVA Tablets by Fused Deposition Modeling: Drug Loading, Tablet Design, and Dissolution Studies. *AAPS PharmSciTech* **2019**, *20*, 195. [\[CrossRef\]](#)
60. Chamberlain, R.; Windolf, H.; Geissler, S.; Quodbach, J.; Breitzkreutz, J. Precise Dosing of Pramipexole for Low-Dosed Filament Production by Hot Melt Extrusion Applying Various Feeding Methods. *Pharmaceutics* **2022**, *14*, 216. [\[CrossRef\]](#)
61. Windolf, H.; Chamberlain, R.; Quodbach, J. Predicting Drug Release from 3D Printed Oral Medicines Based on the Surface Area to Volume Ratio of Tablet Geometry. *Pharmaceutics* **2021**, *13*, 1453. [\[CrossRef\]](#)
62. Gültekin, H.E.; Tort, S.; Acartürk, F. An Effective Technology for the Development of Immediate Release Solid Dosage Forms Containing Low-Dose Drug: Fused Deposition Modeling 3D Printing. *Pharm. Res.* **2019**, *36*, 128. [\[CrossRef\]](#)
63. Windolf, H.; Chamberlain, R.; Quodbach, J. Dose-Independent Drug Release from 3D Printed Oral Medicines for Patient-Specific Dosing to Improve Therapy Safety. *Int. J. Pharm.* **2022**, *616*, 121555. [\[CrossRef\]](#)
64. El Aita, I.; Rahman, J.; Breitzkreutz, J.; Quodbach, J. 3D-Printing with Precise Layer-Wise Dose Adjustments for Paediatric Use via Pressure-Assisted Microsyringe Printing. *Eur. J. Pharm. Biopharm.* **2020**, *157*, 59–65. [\[CrossRef\]](#) [\[PubMed\]](#)
65. Goyanes, A.; Wang, J.; Buanz, A.; Martínez-Pacheco, R.; Telford, R.; Gaisford, S.; Basit, A.W. 3D Printing of Medicines: Engineering Novel Oral Devices with Unique Design and Drug Release Characteristics. *Mol. Pharm.* **2015**, *12*, 4077–4084. [\[CrossRef\]](#) [\[PubMed\]](#)
66. Gioumouxouzis, C.I.; Baklavaridis, A.; Katsamenis, O.L.; Markopoulou, C.K.; Bouropoulos, N.; Tzetzis, D.; Fatouros, D.G. A 3D Printed Bilayer Oral Solid Dosage Form Combining Metformin for Prolonged and Glimepiride for Immediate Drug Delivery. *Eur. J. Pharm. Sci.* **2018**, *120*, 40–52. [\[CrossRef\]](#) [\[PubMed\]](#)

67. Khaled, S.A.; Burley, J.C.; Alexander, M.R.; Yang, J.; Roberts, C.J. 3D Printing of Five-in-One Dose Combination Polypill with Defined Immediate and Sustained Release Profiles. *J. Control Release* **2015**, *217*, 308–314. [\[CrossRef\]](#) [\[PubMed\]](#)
68. Komal, C.; Dhara, B.; Sandeep, S.; Shantanu, D.; Priti, M.J. Dissolution-Controlled Salt of Pramipexole for Parenteral Administration: In Vitro Assessment and Mathematical Modeling. *Dissolution Technol.* **2019**, *26*, 28–36. [\[CrossRef\]](#)
69. Tzankov, B.; Voycheva, C.; Yordanov, Y.; Aluani, D.; Spassova, I.; Kovacheva, D. Development and In Vitro Safety Evaluation of Pramipexole-Loaded Hollow Mesoporous Silica (HMS) Particles. *Biotechnol. Biotechnol. Equip.* **2019**, *33*, 1204–1215. [\[CrossRef\]](#)
70. Krisai, K.; Charnvanich, D.; Chongcharoen, W. Increasing the Solubility of Levodopa and Carbidopa Using Ionization Approach. *Thai J. Pharm. Sci.* **2020**, *44*, 251–255.
71. Łaszcz, M.; Trzcńska, K.; Kubiszewski, M.; Kosmacńska, B.; Glice, M. Stability Studies and Structural Characterization of Pramipexole. *J. Pharm. Biomed. Anal.* **2010**, *53*, 1033–1036. [\[CrossRef\]](#)
72. Pawar, S.M.; Khatal, L.D.; Gabhe, S.Y.; Dhaneshwar, S.R. Establishment of Inherent Stability of Pramipexole and Development of Validated Stability Indicating LC–UV and LC–MS Method. *J. Pharm. Anal.* **2013**, *3*, 109–117. [\[CrossRef\]](#)
73. Panditrao, V.M.; Sarkate, A.P.; Sangshetti, J.N.; Wakte, P.S.; Shinde, D.B. Stability-Indicating HPLC Determination of Pramipexole Dihydrochloride in Bulk Drug and Pharmaceutical Dosage Form. *J. Braz. Chem. Soc.* **2011**, *22*, 1253–1258. [\[CrossRef\]](#)
74. Ledeti, A.; Olariu, T.; Caunii, A.; Vlase, G.; Circioban, D.; Baul, B.; Ledeti, I.; Vlase, T.; Murariu, M. Evaluation of Thermal Stability and Kinetic of Degradation for Levodopa in Non-Isothermal Conditions. *J. Anal. Calorim.* **2017**, *131*, 1881–1888. [\[CrossRef\]](#)
75. Shadambikar, G.; Kipping, T.; Di-Gallo, N.; Elia, A.G.; Knüttel, A.N.; Treffer, D.; Repka, M.A. Vacuum Compression Molding as a Screening Tool to Investigate Carrier Suitability for Hot-Melt Extrusion Formulations. *Pharmaceutics* **2020**, *12*, 1019. [\[CrossRef\]](#)
76. Chamberlain, R.; Windolf, H.; Burckhardt, B.B.; Breitzkreutz, J.; Fischer, B. Embedding a Sensitive Liquid-Core Waveguide UV Detector into an HPLC-UV System for Simultaneous Quantification of Differently Dosed Active Ingredients during Drug Release. *Pharmaceutics* **2022**, *14*, 639. [\[CrossRef\]](#)
77. European Pharmacopoeia Commission 2.9.3. Dissolution Test for Solid Dosage Forms. In *European Pharmacopoeia*; EDQM: Strasbourg, France, 2020; Volume 10.2, pp. 326–333.
78. European Pharmacopoeia Commission 5.17.1. Recommendations on Dissolution Testing. In *European Pharmacopoeia*; EDQM: Strasbourg, France, 2020; Volume 10.2, pp. 801–807.
79. Costa, P.; Sousa Lobo, J.M. Modeling and Comparison of Dissolution Profiles. *Eur. J. Pharm. Sci.* **2001**, *13*, 123–133. [\[CrossRef\]](#)
80. Tanigawara, Y.; Yamaoka, K.; Nakagawa, T.; Uno, T. New Method for the Evaluation of in Vitro Dissolution Time and Disintegration Time. *Chem. Pharm. Bull.* **1982**, *30*, 1088–1090. [\[CrossRef\]](#)
81. U.S. Department of Health and Human Services. FDA Guidance for Industry: Dissolution Testing of Immediate Release Solid Oral Dosage Forms. *Academy* **1997**, *1*, 15–22.
82. Shah, V.P.; Tsong, Y.; Sathe, P.; Liu, J.-P. In Vitro Dissolution Profile Comparison—Statistics and Analysis of the Similarity Factor, F2. *Pharm. Res.* **1998**, *15*, 889–896. [\[CrossRef\]](#)
83. Nyholm, D.; Lennernäs, H. Irregular Gastrointestinal Drug Absorption in Parkinson's Disease. *Expert Opin. Drug Metab. Toxicol.* **2008**, *4*, 193–203. [\[CrossRef\]](#)
84. Doi, H.; Sakakibara, R.; Sato, M.; Masaka, T.; Kishi, M.; Tateno, A.; Tateno, F.; Tsuyusaki, Y.; Takahashi, O. Plasma Levodopa Peak Delay and Impaired Gastric Emptying in Parkinson's Disease. *J. Neurol. Sci.* **2012**, *319*, 86–88. [\[CrossRef\]](#)
85. Gundert-Remy, U.; Hildebrandt, R.; Stiehl, A.; Weber, E.; Zürcher, G.; da Prada, M. Intestinal Absorption of Levodopa in Man. *Eur. J. Clin. Pharmacol.* **1983**, *25*, 69–72. [\[CrossRef\]](#)
86. Awasthi, R.; Kulkarni, G.T. Decades of Research in Drug Targeting to the Upper Gastrointestinal Tract Using Gastroretention Technologies: Where Do We Stand? *Drug Deliv.* **2014**, *23*, 378–394. [\[CrossRef\]](#) [\[PubMed\]](#)
87. Klausner, E.A.; Lavy, E.; Barta, M.; Cserepes, E.; Friedman, M.; Hoffman, A. Novel Gastroretentive Dosage Forms: Evaluation of Gastroretentivity and Its Effect on Levodopa Absorption in Humans. *Pharm. Res.* **2003**, *20*, 1466–1473. [\[CrossRef\]](#) [\[PubMed\]](#)
88. Hoffman, A. Pharmacodynamic Aspects of Sustained Release Preparations. *Adv. Drug Deliv. Rev.* **1998**, *33*, 185–199. [\[CrossRef\]](#)
89. Nutt, J.G.; Holford, N.H.G. The Response to Levodopa in Parkinson's Disease: Imposing Pharmacological Law and Order. *Ann. Neurol.* **1996**, *39*, 561–573. [\[CrossRef\]](#) [\[PubMed\]](#)
90. Siepmann, J.; Peppas, N.A. Higuchi Equation: Derivation, Applications, Use and Misuse. *Int. J. Pharm.* **2011**, *418*, 6–12. [\[CrossRef\]](#) [\[PubMed\]](#)
91. Petropoulos, J.H.; Papadokostaki, K.G.; Sanopoulou, M. Higuchi's Equation and beyond: Overview of the Formulation and Application of a Generalized Model of Drug Release from Polymeric Matrices. *Int. J. Pharm.* **2012**, *437*, 178–191. [\[CrossRef\]](#)
92. Higuchi, T. Mechanism of Sustained-action Medication. Theoretical Analysis of Rate of Release of Solid Drugs Dispersed in Solid Matrices. *J. Pharm. Sci.* **1963**, *52*, 1145–1149. [\[CrossRef\]](#)
93. Erni, W.; Held, K. The Hydrodynamically Balanced System: A Novel Principle of Controlled Drug Release: (With 2 Color Plates). *Eur. Neurol.* **1987**, *27*, 21–27. [\[CrossRef\]](#)
94. Schneider, F.; Hoppe, M.; Koziol, M.; Weitschies, W. Influence of Postprandial Intra-gastric Pressures on Drug Release from Gastroretentive Dosage Forms. *AAPS PharmSciTech* **2018**, *19*, 2843–2850. [\[CrossRef\]](#)
95. Qu, Y.; Lai, W.L.; Xin, Y.R.; Zhu, F.Q.; Zhu, Y.; Wang, L.; Ding, Y.-P.; Xu, Y.; Liu, H.F. Development, Optimization, and Evaluation In Vitro/In Vivo of Oral Liquid System for Synchronized Sustained Release of Levodopa/Benserazide. *AAPS PharmSciTech* **2019**, *20*, 312. [\[CrossRef\]](#)

-
96. Dinç, E.; Kaya, S.; Doganay, T.; Baleanu, D. Continuous Wavelet and Derivative Transforms for the Simultaneous Quantitative Analysis and Dissolution Test of Levodopa-Benserazide Tablets. *J. Pharm. Biomed. Anal.* **2007**, *44*, 991–995. [[CrossRef](#)] [[PubMed](#)]
 97. Iravani, M.; Ferraro, L.; Xie, C.-L. Levodopa/Benserazide PLGA Microsphere Prevents L-Dopa-Induced Dyskinesia via Lower β -Arrestin2 in 6-Hydroxydopamine Parkinson's Rats. *Front. Pharmacol.* **2019**, *10*, 660. [[CrossRef](#)]
 98. Freichel, O.L. Hydrokolloidretardarzneiformen Mit Endbeschleunigter Freisetzung. Ph.D. Thesis, Heinrich-Heine-Universität, Düsseldorf, Germany, 2002.
 99. Goole, J.; Vanderbist, F.; Amighi, K. Development and Evaluation of New Multiple-Unit Levodopa Sustained-Release Floating Dosage Forms. *Int. J. Pharm.* **2007**, *334*, 35–41. [[CrossRef](#)] [[PubMed](#)]
 100. Keerthi, M.L.; Kiran, S.; Rao, U.M.; Sannapu, A.; Dutt, A.G.; Krishna, K.S. Pharmaceutical Mini-Tablets, Its Advantages, Formulation Possibilities and General Evaluation Aspects: A Review. *Int. J. Pharm. Sci. Rev. Res.* **2014**, *28*, 214–221.

5 Summary and Outlook

The respective research work provides important quality attributes in the manufacturing and their specifications for quality control of intermediate filaments. The results have been presented and put into a scientific context.

In order to describe the homogeneity of the filament diameter, the percentage of the diameter measurements within defined limits of ± 0.02 mm and ± 0.05 mm was calculated. The influence of the process parameters such as temperature and screw configuration on the CQA “filament diameter” could be observed by this correlation. A continuous melt flow was prevented by the introduction of two kneading zones in screw configuration, which leads to a fluctuation in the diameter of PVA filaments. Furthermore, it was demonstrated that the filament diameter was not strongly affected by barrel temperatures $\geq 185^\circ\text{C}$, since a continuous melt flow in the barrel and through the die could be ensured if a venting port was present in the barrel. This characterization was not previously described in the literature and the dependence of screw configuration and extrusion temperature on the diameter homogeneity of PVA filaments was demonstrated for the first time in this work. For the further development of filaments, care was taken during optimization to ensure a continuous flow of material by optimizing the screw- or barrel configuration.

The hot melt extruded strands were manually cut into long filaments so that a dosage form was 3d printed by using only one filament avoiding air entrapments while reloading of an additional filament. The unused material was often discarded. A cutting device was invented enabling cuts into filament sticks of any length, regardless of the mechanical properties. This invention was described in detail in the patent application DE 10 2022 002 368.7. With the help of this novel device, it was possible to cut the variously thick and mechanical indifferent filament strands into filament sticks with straight cutting ends by sharp edges of elongated holes located on two counter-rotating discs. The filament strand can be cut in filaments with a desired length by controlling the timepoint of cutting cycle. The integration into a continuous extrusion process is still under investigation.

For the manufacturing of low-dosed filaments, a suitable feeding method was found to obtain the target concentration of 0.1 w% pramipexole. With the help of preliminary dry granulation and a preblend consisting of pramipexole granules with a drug load of 1 w% and granules without API (1:10 ratio), homogenous filaments (0.101 ± 0.006 w% acc. to the established API assay) were obtained. The largest variations from target drug loading

were found for the extrusion runs, wherein the physical preblend of API and excipients was fed by one feeder and where the API was fed with the help of a second gravimetric feeder (extrusion run “split feeding”) due to material loss and the additive variation of dosing from the second feeder (0.091 ± 0.010 w% API assay). Furthermore, limitations of deviations were found by calculating the smallest possible deviation of the target concentration due to the sample quantity and the properties of the starting materials. When analyzing the drug content of pramipexole filaments with a weight of 50 mg and a drug load of 0.1 w%, a deviation of 6 w% from the target concentration is to be expected. This was successfully accomplished during extrusion with pre-granulated material with a deviation of 6 w% representing the calculated deviation from the target drug load.

To determine the drug content of low-dosed filaments during the manufacturing process, a method has been developed, which can be integrated as an in-line process control methodology. Since the drug content of only 0.1 w% implicit that the signal results by 99.9 w% of the polymer, the API is hardly visible. The experimental setup was first optimized so that the signal was always in focus of the laser by installing a mechanism, which moved the filament surface always to the same distance from the laser. In the extrusion of 0.1 w% praziquantel filaments, the effect was exploited after excitation of the API by a laser. Not only the Raman effect occurs, but also fluorescence is emitted. This signal was overlapping the Raman signals of the matrix and the intensity of the fluorescence could be correlated with the drug concentration. An integration into the extrusion process is still lacking.

When determining the drug content of API, clinically relevant methods should be used. Since the production of filaments for 3d printing enables personalized therapy of individual patients, the color of the filaments was characterized using simple detection methods. Filaments with a drug load of 1, 5, and 10 w% pramipexole could be distinguished based on the introduced colorimetric CIELAB values. For filaments that did not change color due to variation in drug content, the addition of low concentrations of pharmaceutical coloring agents could generate a change in CIELAB values of the filaments and thus realizing discriminability. Thus, indirect identification of the filament composition was achieved through the addition of low concentrations of coloring agents. However, it must be clarified whether other combinations of polymers, APIs and coloring agents can lead to one and the same color and thus limit the differentiation of filaments.

When varying the dose in the titration phase at the beginning of therapy or when the dose must be increased or decreased at later stage of the pharmacotherapy, it must be ensured that the release of the APIs from the polymer matrix is unchanged so that the absorption of the APIs is guaranteed. Adapting the dose but keeping the SA/V ratio, the release was unaffected as the diffusion pathway remained unchanged for the API when the matrix was not eroding, and the diffusion layer was not changed when the matrix was eroding. Considering the limitation that hollow structures must have a minimum hole size, the release profile of the API can be maintained by changing the geometry but ensuring that the SA/V remains constant.

Towards the goal of manufacturing a combination drug product for the treatment of Parkinson's disease, another filament with a fixed combination of levodopa and benserazide was formulated. Since the resorption and therapeutic range of the low-dosed pramipexole differ from the high-dosed APIs, the preparation of the combination drug required care to ensure that the release profiles met defined requirements. An analytical method had to be evaluated that would allow the determination of the APIs despite the different concentration ranges. By connecting a liquid-core waveguide to a conventional HPLC system, all three API were detected with one single analytical method within 21 min. The high concentrations of levodopa and benserazide were detected by an UV/Vis detector of a conventional HPLC and the low concentrations of pramipexole were analyzed by an in-house built highly sensitive liquid-core waveguide UV detector. After method optimization, 1% of the released amount of the lowest dose of pramipexole could be detected. The results were confirmed by a sensitive MS-method.

A combination drug product has been developed for three APIs for the treatment of Parkinson's patients and suitable analytical methods were established. The use of FDM 3d printing enables a small-step dose increase and the combination of differently dosed APIs with tailored release kinetics.

In subsequent in vivo studies it has to be demonstrated whether these approaches show clinical superiority over existing pharmacotherapy. To demonstrate clinical superiority, the conventional standard therapy needs to be either tested against an optimized therapy or bioindicators can be consulted to determine whether an adapted therapy is more appropriate.

The transfer from mass production to patient-specific production of DDS means rethinking the cost structure of pharmaceutical products. The high development costs of dosage forms formulated and designed for individual patients would have to be paid either by the health insurance companies or by the patients themselves. As long as submission to the FDA is possible using the existing 505b(2) regulatory pathway of the Federal Food, Drug, and Cosmetic Act, the pharmaceutical company can obtain approval for a 3d printed drug product. However, once this approval pathway and its requirements are no longer applicable due to the challenges and processing risks associated with 3d printing technology, new approval guidelines will need to be established prior to the approval of novel 3d printed DDS.

In addition to company regulations for the consideration of 3d printing technologies in local pharmacies, regulatory aspects, including batch release responsibilities, still need to be clarified before 3d printed medicines are available for on-demand manufacturing. If the pharmacy has to test the starting materials and the manufactured preparation according to the pharmacopoeia, this would mean an extensive investment in equipment and personnel. If the 3d printer and the required analyses can be adapted to the capabilities of local pharmacies, it may be possible to carry out small-scale production for on-demand manufacturing.

6 Acknowledgements / Danksagung

Herrn Prof. Dr. Breitzkreutz möchte ich zuallererst für die Möglichkeit danken in seinem Arbeitskreis diese Promotionsarbeit anzufertigen. Mit einer unermüdlichen Geduld unterstütze er mich während meiner Promotionszeit und wies mir den Weg, wenn ich über Steine stolperte oder vom Weg abkam. Er ermöglichte mir in der Zeit nicht nur fachlich, sondern auch persönlich von ihm außerordentlich viel zu lernen, ließ mir allerdings gleichzeitig uneingeschränkt Raum, mich selbst zu entfalten. Ich hoffe, dass sich unsere Wege noch oft kreuzen werden.

Ich danke Herrn Jun.-Prof. Dr. Michael Hacker für die Übernahme des Koreferats und der hilfreichen Unterstützung insbesondere in der Polymeranalytik.

Dem BMBF möchte ich mich für die Finanzierung danken, welche mir die Promotion ermöglicht hat.

Meiner „besseren Promotionshälfte“ Dr. Hellen Mazur danke ich für ihre wunderbare Persönlichkeit, ihrer Kreativität, ihrer Beharrlichkeit, ihrem Durchhaltevermögen, ihrer Teamfähigkeit und ihrer Freundschaft.

Dr. Björn Fischer danke ich für den fachlichen Rat während meiner gesamten Promotion und für die unermüdliche, geduldige Hilfe. Ich durfte viel von ihm lernen und habe durch ihn Spaß an der Analytik gewonnen.

Dr. Björn Burckhard danke ich für die hilfreiche Unterstützung nicht nur bei der MS-Analytik. Außerdem durfte ich Einblicke in Führungsqualitäten erhalten.

Dr. Simon Geissler danke ich für das Interesse an meiner Arbeit und die Möglichkeit bei der Merck KGaA Versuche durchführen zu können. Außerdem bedanke ich mich vielmals dafür, dass in BMBF-Meetings oft kritisch nachgefragt wurde und ich so viele hilfreiche Hinweise erhalten haben, die diese Arbeit vorangetrieben haben.

Nadine Gottschalk danke ich für diverse Fachgespräche über den 3d Druck und der Möglichkeit in Darmstadt ein kleines Zuhause zu haben.

Dr. Katharina Seel danke stellvertretend für die Unterstützung seitens der GenPlus besonders für die Unterstützung der Analytik der Filamente und 3d gedruckten Geometrien.

Stefan Stich danke ich für seine Mitwirkung und Ideeneinbringung bezüglich der Schneideeinheit.

Kathrin Morawietz und Julia Bedkowski danke ich für ihren Einsatz, den sie im Rahmen ihres WPPs gezeigt haben. Mit großer Begeisterung wurden unzählige Schneideversuche durchgeführt und etliche Male die Prusa Drucker von Filamentresten befreit.

Der Erasmus-Studentin Eirini Mangiorou danke ich für ihre Geduld mit (mir und) farbigen Filamenten. Innerhalb von kürzester Zeit wurden unzählige Messungen durchgeführt und wertvolle Daten gesammelt.

Dr. Laura Falkenstein und Dr. Jhinuk Rahman-Yildir danke ich für die gemeinsame Zeit, die ich mit euch teilen durfte. Ich werde hier nicht ins Details gehen, aber ohne euch wäre ich untergegangen.

Dr. Annika Wilms danke ich für die Einführung in die Trockengranulat-Welt. Außerdem durfte ich in dir ein Vorbild sehen, wie besonnen und ruhig Wissen übermittelt werden kann.

Meiner Familie danke ich für die bedingungslose Unterstützung insbesondere während meiner Promotionszeit. Besonders danke ich meinen Brüdern, die mich gelehrt haben nie aufzugeben, egal wie sehr ich getestet wurde. Meinen Großeltern möchte ich für ihre hohe Präsenz in meinem Leben danken und für die Weitergabe von wichtigen Werten und Pflichten. Meinem Papa danke ich für die Vermittlung seiner Liebe zu Mitmenschen, seiner Empathie und seinem Lebensmotto. Meiner Mama und meinem liebsten Rick danke ich für ihre starken Schultern, an die ich mich oft lehnen musste. Ich danke den beiden für ihre Kraft, die mich mitgerissen hat und schließlich dazu geführt hat, dass diese Arbeit wirklich zum Abschluss kommt.

7 Eidesstattliche Erklärung

Ich versichere an Eides Statt, dass die Dissertation von mir selbständig und ohne unzulässige fremde Hilfe unter Beachtung der „Grundsätze zur Sicherung guter wissenschaftlicher Praxis an der Heinrich-Heine-Universität Düsseldorf“ erstellt worden ist.



Rebecca Chamberlain